



UNIVERSITÄT
BAYREUTH



Reusable Ni-Catalysts for the Highly Chemoselective Synthesis of Primary Amines

DISSERTATION

zur Erlangung des akademischen Grades eines
Doktors der Naturwissenschaften (Dr. rer. nat.)
an der Fakultät für Biologie, Chemie und Geowissenschaften
der Universität Bayreuth

vorgelegt von

M. Sc. Gabriela Hahn

geb. Wietzel; in Münchberg

Bayreuth, 2018

Die vorliegende Arbeit wurde in der Zeit von Januar 2016 bis Dezember 2018 in Bayreuth am Lehrstuhl Anorganische Chemie II unter Betreuung von Herrn Professor Dr. Rhet Kempe angefertigt.

Dissertation eingereicht am: 19.12.2018

Zulassung durch Promotionskommission: 09.01.2019

Wissenschaftliches Kolloquium: 18.04.2019

Amtierender Dekan: Prof. Dr. Stefan Peiffer

Prüfungsausschuss:

Prof. Dr. Rhet Kempe (Gutachter)

Dr. habil. Günter Motz (Gutachter)

Prof. Dr. Peter Strohriegl (Vorsitz)

Prof. Dr. Roland Marschall

Meiner Familie in Dankbarkeit gewidmet.

Table of Contents

Abbreviations.....	VII
1 Summary/Zusammenfassung	1
1.1 Summary	1
1.2 Zusammenfassung.....	4
2 Introduction	7
2.1 Earth-abundant metal catalysts for complex organic synthesis	7
2.2 Primary amines	8
2.3 Ceramic catalyst supports	11
2.4 References.....	13
3 Overview of Thesis Results	17
3.1 Synopsis	17
3.2 Individual contributions to joint publications	26
4 A Reusable Mesoporous Nickel Nanocomposite Catalyst for the Selective Hydrogenation of Nitroarenes in the Presence of Sensitive Functional Groups	29
4.1 Introduction.....	29
4.2 Results and Discussion	30
4.3 Conclusion	36
4.4 References.....	37
4.5 Supporting Information.....	39
5 General synthesis of primary amines via reductive amination employing a reusable nickel catalyst.....	51
5.1 Introduction.....	51
5.2 Results.....	52
5.3 Discussion	59
5.4 Methods.....	59
5.5 References.....	61
5.6 Supporting Information.....	65

6	A Nanostructured Earth-abundant Metal Catalyst Can Mediate the Efficient Synthesis of Amino Acids from Ammonia Dissolved in Water under Very Mild Conditions	141
6.1	Introduction.....	141
6.2	Results and Discussion	143
6.3	Conclusion	146
6.4	References.....	148
6.5	Supporting information	152
7	List of Publications	163
8	Acknowledgements/Danksagung.....	165
9	Declaration/Erklärung	169

Abbreviations

ADME	adsorption, distribution, metabolism and excretion
a.u.	arbitrary units
BET	Brunauer Emmett Teller
BINAS	2,2'-bis(bis(3-sulfophenyl)phosphinomethyl-4,4,7,7-tetrasulfo-1,1'-binaphthyl octasodium salt
DABCO	1,4-diazabicyclo[2.2.2]octane
EDX	energy-dispersive X-ray spectroscopy
EELS	electron energy loss spectroscopy
FT-IR	fourier transform infrared spectroscopy
GC	gas chromatography
GC/MS	gas chromatography coupled with mass spectroscopy
HAADF-STEM	high-angle annular dark-field scanning TEM
HR-TEM	high resolution transmission electron microscopy
ICP-OES	inductively coupled plasma optical emission spectrometry
M@SiCN	metal supported on silicon carbo nitride
MOF	metal organic framework
nacnac	deprotonated (<i>E</i>)- <i>N</i> -[(<i>Z</i>)-4-(phenylamino)pent-3-en-2-ylidene]aniline
Ni@PS ₆₀ SiCN	nickel supported on silicon carbo nitride structured with PS ₆₀
NMR	nuclear magnetic resonance
ppm	parts per million
PS	polystyrene
PS _x	polystyrene with x nm diameter
SEM	scanning electron microscopy
SiCN	silicon carbo nitride
SSA	specific surface area
TEM	transmission electron microscopy
TGA	thermogravimetric analysis
TPA	terephthalic acid
TPPS	tris-/3-sulphophenyl)phosphine trisodium salt
XPS	X-ray photoelectron spectroscopy
XRD	X-ray diffraction

1 Summary/Zusammenfassung

1.1 Summary

This work focuses on the development of selective and reusable nickel catalysts and their application in the synthesis of primary amines. Primary amines are an important substance class due to their wide range of applications in pharmaceutical, agricultural and material chemistry. This makes it increasingly important to enable an efficient and atom-economic production of this compound class. Nickel, as an earth-abundant and, therefore, inexpensive metal, was used in early history in the form of Raney nickel in catalytic hydrogenation reactions. The synthesis of novel, heterogeneous nickel catalysts should compensate the highly decisive disadvantages, such as a difficult reusability and high demand of safety precautions. At the same time, the high activity of Raney nickel should be maintained. For this purpose, heterogeneous, reusable nickel catalysts were generated. They show a high porosity of the carrier material, a high hydrogenation activity and an enormous stability, resulting in easy handling (see Figure 1. 1).

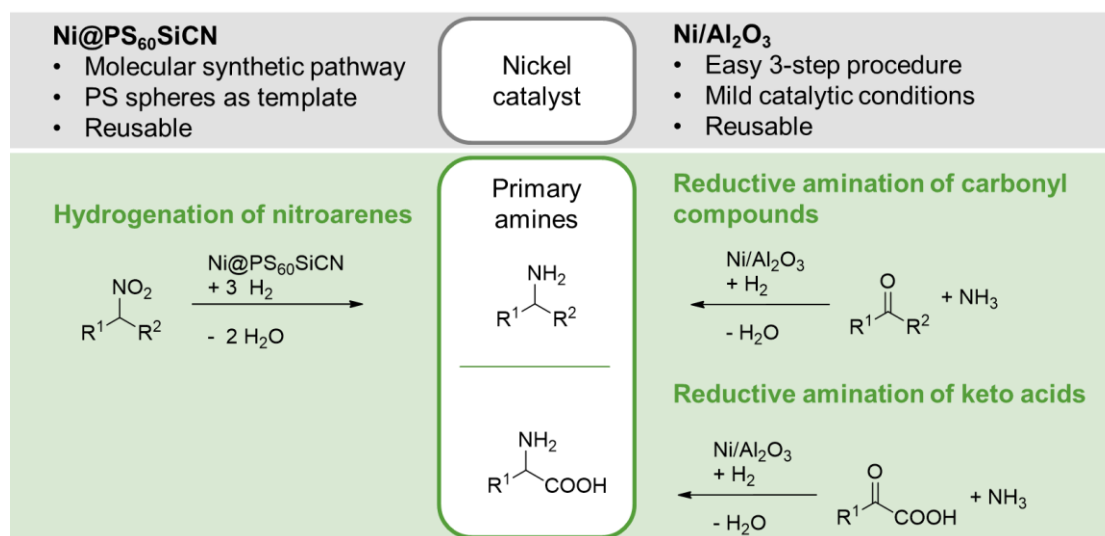


Figure 1. 1: Overview of the synthesized nickel catalysts (Ni@PS₆₀SiCN and Ni/Al₂O₃) and their applications in the selective synthesis of primary amines.

Ni@PS₆₀SiCN, a nanocomposite material of nickel nanoparticles embedded in a mesoporous SiCN matrix, was produced by a molecular synthetic pathway. The metal was selectively transferred from a [(nacnac)₂Ni] complex (nacnac = deprotonated (*E*)-*N*-[(*Z*)-4-(phenylamino)pent-3-en-2-ylidene]aniline) to the preceramic polymer (polysilazane HTT 1800) by transmetalation. Simultaneously, polystyrene spheres, produced by emulsion polymerization in a defined size of 60 nm, were introduced into the green body as templates. Subsequent pyrolysis at 900 °C under inert gas (N₂) generated a porous nickel-doped ceramic (Ni@PS₆₀SiCN). The complex that was applied and the structuring of the surface had an

especially decisive influence on the particle size and the porosity of the composite material and, therefore, on the catalytic activity in the hydrogenation of nitroarenes. Characterization via transmission electron microscopy (TEM), scanning electron microscopy (SEM) and N₂-physisorption measurements provided evidence for the high accessibility of the nickel nanoparticles (5.5 nm) due to a specific surface area of 90 m²g⁻¹ and a mesopore content of > 95%. In catalytic studies, various nitroarenes were converted into the corresponding aniline derivatives within 20 h at 110 °C, 5.0 MPa H₂ and 1–3 mol% Ni@PS₆₀SiCN catalyst. The high chemoselectivity was impressive. A lot of hydrogenation-sensitive groups such as iodides, C-C double bonds, heteroaromatics, amides, ketones, aldehydes and nitriles, were tolerated and the corresponding amines were obtained in very good yields (≥ 81%) and selectivities (≥ 86%). In addition to the easy handling under ambient conditions, the robustness of the catalyst system described is another special feature which was demonstrated by recycling studies. No decrease in catalytic activity was observed after five consecutive catalytic runs.

Another possibility to synthesize primary amines is the reductive amination of carbonyl compounds. Ammonia, in gaseous, liquid or aqueous form, generally acts as a nitrogen source and forms a Schiff base with a carbonyl compound, followed by reduction to the amine. The main challenge here is the high selectivity of the primary amine. The catalyst has to provide a rapid formation of the imine and its hydrogenation to the amine. At the same time, the formation of secondary or tertiary amines must be inhibited. A catalyst was generated during this work which meets these requirements. The active Ni/Al₂O₃ catalyst was obtained by wet impregnation of the commercial support γ-Al₂O₃ with a solution of a specific nickel complex, followed by pyrolysis under nitrogen and reduction under forming gas. A detailed characterization was carried out using TEM, high-angle annular dark field scanning transmission electron microscopy (HAADF-STEM), energy-dispersed X-ray (EDX) and electron energy loss spectroscopy (EELS), among others. This displayed the formation of nickel particles (8 nm) in a nitrogen-doped carbon layer on the surface of the γ-Al₂O₃. N₂-physisorption measurements and the pore size distributions calculated showed no significant difference between the pure γ-Al₂O₃ support and the Ni/Al₂O₃ catalyst. The pore structure, with a mesopore content of > 95% and the surface area of 210 m²g⁻¹, was preserved. The acidic centers, located on the surface of γ-Al₂O₃, have a beneficial effect on the catalytic activity. They permit the activation of the carbonyl compound and the formation of the imine. The subsequent hydrogenation to an amine was mediated by the catalytically active nickel nanoparticles. More than 50 different aromatic and aliphatic carbonyl compounds were converted to the corresponding primary amines under mild conditions (1.0 MPa H₂, 80 °C, 20 h, 1.4–5.6 mol% Ni/Al₂O₃) in aqueous ammonia. A variety of functional groups, especially hydrogenation-sensitive groups such as amides, iodides or olefins, were tolerated. Even challenging substrates, such as pharmaceuticals or steroids, were reductively aminated in high selectivities and isolated yields. Reusability and upscaling studies were carried out to evaluate the high potential of this catalyst system regarding a possible industrial application.

Amino acids, a subclass of primary amines, are the basic building block in proteins and of considerable economic interest. They are used in the food and feed processing industry and have found applications in human nutrition and health and materials, such as biodegradable plastics. Furthermore, they play a decisive role in the discussion about the origin of life. Many different concepts dealing with the prebiotic synthesis were introduced. It is conceivable that Nickel acted as a catalyst in the prebiotic synthesis of amino acids due to its high abundance in the earth's crust. Furthermore, amino acids, such as glutamate and glutamine, are synthesized biochemically by reductive amination of α -ketoglutarate. The high activity and selectivity of our nanostructured Ni/Al₂O₃ catalysts described above motivated us to introduce it for the synthesis of amino acids under early earth conditions. After optimization of the reaction conditions, keto acids could be converted to the corresponding amino acids in the presence of the Ni/Al₂O₃ catalyst at hydrogen pressures of 0.1–0.5 MPa and a temperature of 85 °C, similar to processes in the human body. It should be emphasized that no by-products were observed, even under very mild conditions (0.1 MPa H₂). In addition to essential amino acids, such as phenylalanine and leucine, non-essential amino acids, such as tyrosine or alanine and the non-biological synthetic amino acid phenylglycine were also produced.

1.2 Zusammenfassung

Im Fokus dieser Arbeit steht die Entwicklung von selektiven und wiederverwendbaren Nickelkatalysatoren und deren Anwendung in der Synthese von primären Aminen. Diese sind aufgrund ihres großen Anwendungsspektrums in der Pharma-, Agrar- und Materialchemie eine bedeutende Stoffklasse. Umso wichtiger ist es, eine effiziente und atomökonomische Herstellung dieser Verbindungsklasse zu ermöglichen. Nickel, als ein gut zugängliches und daher preiswertes Metall, fand schon früh in der Geschichte in Form von Raney-Nickel Anwendung in katalytischen Hydrierreaktionen. Durch die Synthese neuartiger, heterogener Nickelkatalysatoren sollen die hohen Aktivitäten von Raney-Nickel erhalten bleiben, gleichzeitig jedoch die entscheidenden Nachteile, wie eine schwere Wiederverwendbarkeit und hohe Anforderungen an Sicherheitsvorkehrungen, ausgeglichen werden. Dazu wurden heterogene, wiederverwendbare Nickelkatalysatoren generiert. Gemein haben sie eine hohe Porosität des Trägermaterials, eine hohe Hydrieraktivität und eine enorme Stabilität, sodass eine einfache Handhabung resultiert (siehe Abbildung 1. 1).

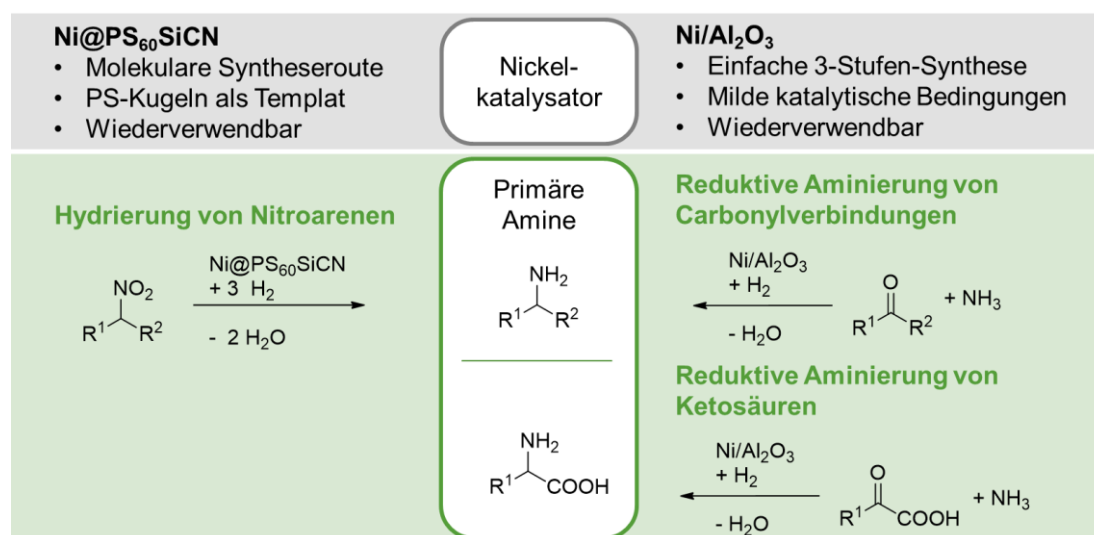


Abbildung 1. 1: Überblick über die hergestellten Nickelkatalysatoren (Ni@PS₆₀SiCN und Ni/Al₂O₃), sowie deren Anwendungen in der selektiven Synthese von primären Aminen

Ni@PS₆₀SiCN, ein Nanokompositmaterial aus Nickel-Nanopartikeln eingebettet in einer mesoporösen SiCN Matrix, wurde durch einen molekularen Syntheseweg hergestellt. Das Metall wurde gezielt durch einen [(nacnac)₂Ni] Komplex (nacnac = deprotoniertes (*E*)-*N*-[(*Z*)-4-(Phenylamino)pent-3-en-2-ylidene]anilin) mittels Transmetallierung auf das präkeramische Polymer (Polysilazan HTT 1800) übertragen. Parallel dazu wurden Polystyrolkugeln, welche in definierten Größe von 60 nm mittels Emulsionspolymerisation hergestellt wurden, als Template in den Grünkörper eingebracht. Anschließende Pyrolyse bei 900 °C unter Inertgas (N₂) generierte eine poröse, mit Nickel dotierte Keramik (Ni@PS₆₀SiCN). Besonders die Wahl des verwendeten Komplexes und die Strukturierung hatten einen entscheidenden Einfluss auf die Partikelgröße und die Porosität des Kompositwerkstoffs und somit auf

die katalytische Aktivität in der Hydrierung von Nitroaromaten. Mittels TEM, REM und N_2 -Physisorptionsmessungen wurde die gute Zugänglichkeit der etwa 5.5 nm großen Nickelnanopartikel durch eine spezifische Oberfläche von $90 \text{ m}^2\text{g}^{-1}$ und einem Mesoporenanteil von $> 95 \%$ belegt. In den katalytischen Studien wurden verschiedene Nitroaromaten bei $110 \text{ }^\circ\text{C}$, 5.0 MPa H_2 und $1 \text{ mol}\%$ des $\text{Ni@PS}_{60}\text{SiCN}$ Katalysators innerhalb von 20 Stunden zu den entsprechenden Anilinderivaten umgesetzt. Beeindruckend hierbei ist die hohe Chemoselektivität. Es wurden eine Vielzahl an hydrierempfindlichen Gruppen, wie etwa Iodide, C-C Doppelbindungen, Heteroaromaten, Amide, Ketone, Aldehyde und Nitrile toleriert und die entsprechenden Amine in sehr guten Ausbeuten ($\geq 81 \%$) und Selektivitäten ($\geq 86 \%$) erhalten. Neben der einfachen Handhabung unter Normalbedingungen ist die Robustheit des beschriebenen Katalysatorsystems eine weitere Besonderheit. Diese wurde an Hand von Wiederverwendbarkeitsstudien gezeigt. So war nach fünf aufeinander folgenden Katalysezyklen keinen Einbruch in der Aktivität des Katalysators zu verzeichnen.

Eine andere Möglichkeit primäre Amine zu synthetisieren, stellt die reduktive Aminierung von Carbonylverbindungen dar. Als Stickstoffquelle dient hierbei Ammoniak in gasförmiger, flüssiger oder wässriger Form, welcher mit einer Carbonylverbindung eine Schiff'sche Base bildet, die dann durch Reduktion ins Amin überführt wird. Herausforderung hierbei ist die hohe Selektivität zum primären Amin. Der Katalysator muss eine schnelle Bildung des Imins und dessen Hydrierung zum Amin gewährleisten und zugleich die Bildung von sekundären oder tertiären Aminen unterbinden. Im Rahmen dieser Arbeit wurde ein Katalysator, der diesen Anforderungen gerecht wird, generiert. Durch Nasimprägnierung des kommerziellen Trägers $\gamma\text{-Al}_2\text{O}_3$ mit einer Lösung eines Nickelsalenkomplexes, sowie anschließende Pyrolyse unter Stickstoff und Reduktion unter Formiergas wird der aktive $\text{Ni/Al}_2\text{O}_3$ Katalysator erhalten. Eine ausführliche Charakterisierung erfolgte unter anderem mittels TEM, HAADF-STEM, EDX und EELS. Hierbei wurde deutlich, dass sich die etwa 8 nm großen Nickelpartikel in einer Stickstoff dotierten Kohlenstoffschicht auf der Oberfläche des $\gamma\text{-Al}_2\text{O}_3$ bilden. N_2 -Physisorptionsmessungen und die daraus kalkulierten Porenverteilungen zeigen, dass kaum Unterschied zwischen dem reinen $\gamma\text{-Al}_2\text{O}_3$ Träger und dem $\text{Ni/Al}_2\text{O}_3$ Katalysator zu erkennen sind. Die Porenstruktur, mit einem Anteil von $> 95 \%$ Mesoporen, und die Oberfläche von $210 \text{ m}^2\text{g}^{-1}$ bleiben erhalten. Die sauren Zentren, die auf der Oberfläche von $\gamma\text{-Al}_2\text{O}_3$ zu finden sind, wirken sich positiv auf die katalytische Aktivität aus. Sie ermöglichen eine Aktivierung der Carbonylverbindung und eine schnelle Bildung des Imins. Die anschließende Hydrierung zum Amin erfolgt an den katalytisch aktiven Nickelnanopartikeln. Es konnten über 50 verschiedene aromatische und aliphatische Carbonylverbindungen unter milden Bedingungen (1.0 MPa H_2 , $80 \text{ }^\circ\text{C}$, 20 h , $1.4\text{--}5.6 \text{ mol}\%$ $\text{Ni/Al}_2\text{O}_3$) in wässrigem Ammoniak zu den entsprechenden primären Aminen umgesetzt werden. Neben einfachen funktionellen Gruppen wurden insbesondere hydrierempfindliche Gruppen wie Amide, Iodide oder Olefine toleriert. Auch anspruchsvolle Substrate wie Pharmazeutika oder Steroide wurden in hohen isolierten Ausbeuten und Selektivitäten reduktiv aminiert. Um das hohe Potenzial dieses Katalysatorsystems im Hinblick auf eine mögliche

industrielle Anwendung zu verdeutlichen, wurden Wiederverwendbarkeitsstudien durchgeführt und Reaktionsansätze um den Faktor 20 hochskaliert.

Aminosäuren, als Unterklasse der primären Amine, sind die Grundbausteine von Proteinen und zudem von ökonomischem Interesse. Sie finden Anwendung in der Lebensmittel- und Futtermittelindustrie, in der Gesundheitsbranche sowie in Materialien, wie bioabbaubaren Kunststoffen. Außerdem nehmen sie bei Diskussionen über die Entstehung des Lebens eine wichtige Rolle ein. Biochemisch werden Aminosäuren wie Glutamat und Glutamin durch reduktive Aminierung von α -Ketoglutarat synthetisiert. Es wurden viele Konzepte erarbeitet, die sich mit der prebiotischen Synthese von Aminosäuren beschäftigen. Denkbar ist es, dass Nickel als ein auf der Erde häufig vorkommendes Metall diese Reaktion katalysierte. Die hohe Aktivität und Selektivität des oben beschriebenen nanostrukturierten Ni/Al₂O₃ Katalysators motivierte uns, diesen für die Synthese von Aminosäuren unter *early earth conditions* zu untersuchen. Nach Optimierung der Reaktionsbedingungen konnten Ketosäuren, ähnlich wie im menschlichen Körper, unter Anwesenheit des Ni/Al₂O₃ Katalysators bei Wasserstoffdrücken von 0.1–0.5 MPa und einer Temperatur von 85 °C zu den entsprechenden Aminosäuren umgewandelt werden. Hierbei ist besonders hervorzuheben, dass auch bei sehr milden Bedingungen (0.1 MPa H₂) keine Nebenprodukte beobachtet werden konnten. Neben essenziellen Aminosäuren wie Phenylalanin und Leucin wurden auch nicht-essentielle Aminosäuren wie Tyrosin oder Alanin sowie die nicht-biologische, synthetische Aminosäure Phenylglycin hergestellt.

2 Introduction

2.1 Earth-abundant metal catalysts for complex organic synthesis

The use of substrates derived from biomass for the production of fine chemicals, the reversible storage of hydrogen as an energy source or the conservation of resources on our planet are important issues regarding sustainability. All these topics guarantee our existence and ensure a high standard of living for future generations. Rare noble metals, such as ruthenium, iridium and rhodium, are commonly used in key technologies and their replacement by earth-abundant base metals, such as manganese, iron, cobalt or nickel, is a central challenge and a potential strategy for their conservation. Figure 2. 1 shows the abundance of different metals in the solar system. Base metals, such as manganese, iron, cobalt or nickel, are very common in contrast to precious metals, such as ruthenium, rhodium, palladium, iridium or platinum.^[1]

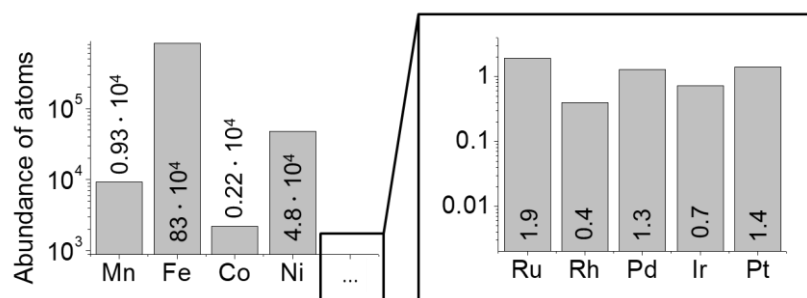


Figure 2. 1: Abundance of atoms normalized to Si = 10⁶.

This is also reflected in their prices. A gram of nickel, for example, currently costs around 0,02 US\$ and 1 g iridium costs 50 US\$. However, the price for 1 mol are essential since the amount of active species is crucial in catalysis. Therefore, 1 US\$/mol for nickel and 9500 US\$/mol for iridium result.^[2] Replacing precious metals with base metals is desirable not only for cost reasons. A further advantage is that base metal catalysts show totally different selectivity patterns compared to known systems based on precious metals. Reactions that are not possible with precious metal catalysts are now conceivable and the scope of reactions can be extended.

Homogeneous catalysts based on base metals for complex organic synthesis have been disclosed in the last few years.^[3] Iron and cobalt especially were introduced for different hydrogenation reactions. *Morris and coworkers* explored an amine(imine)diphosphine iron catalyst for the asymmetric, enantiopure transfer hydrogenation of ketones and imines.^[4] *Chirik and coworkers* used a simple cobalt precursor (CoCl₂) and chiral phosphine ligands for the asymmetric hydrogenation of functionalized and unfunctionalized olefins.^[5] The hydrogenation of carboxylic acids to alcohols with a Co(BF₄)₂·6H₂O combined

with a tridentate phosphine ligand was disclosed by *de Bruin and coworkers*.^[6] Furthermore, iron catalysts ($\text{Fe}(\text{BF}_4)_2 \cdot 6\text{H}_2\text{O}$ and phosphine ligand) can promote the dehydrogenation of formic acid. *Beller and coworkers* demonstrate that formic acid can be used here as an energy storage material.^[7] *Chirik and coworkers* employed a bis(imino)pyridine iron complex for anti-Markovnikov alkene hydrosilylation.^[8] A regio- and stereoselective route to cyclobutanes via intramolecular [2+2] cycloaddition of unactivated alkenes or cross-coupling of alkenes and dienes were mediated by a homogeneous iron catalyst introduced by *Chirik and coworkers*.^[9] They also made an important contribution to the direct tracing of the drug molecule without altering its structure or function substantially. They describe an iron-catalyzed method for the direct ^3H labelling of pharmaceuticals by hydrogen isotope exchange and enable an ADME (absorption, distribution, metabolism and excretion) study early in the drug development process.^[10]

Parallel to the transformations in selective organic synthesis described above, the development of similar heterogeneous catalysts with comparable selectivity patterns and activity is highly desirable and of great interest. However, reusable nanostructured earth-abundant 3d metal catalysts for a broad applicability in complex organic synthesis has been disclosed only rarely. *Beller and coworkers* introduced iron and cobalt catalysts for the selective hydrogenation of nitroarenes. Both catalysts were generated by pyrolysis of a metal (Co or Ir) phenanthroline complex on a commercial carbon support. Additionally, a defined Co-MOF was impregnated on carbon and pyrolyzed to generate cobalt nanoparticles, catalytically active in the synthesis of various amines via reductive amination (combined with hydrogenation of nitroarenes).^[11]

2.2 Primary amines

Amines represent an important substrate class. They are widely used industrially as pharmaceuticals, polymers, agrochemicals, dyes, surfactants or fine chemicals. Primary amines are of particularly great significance and play an essential role as intermediates in chemical synthesis. Name reactions, such as *Gabriel synthesis* (synthesis of primary amines from alkylhalogenides and phthalimide potassium), *Hoffmann degradation* (conversion of carboxylic acid amides into primary amines), *Leuckart-Wallach reaction* (reductive alkylation of carbonyl compounds with formic acid to amines) or *Staudinger reaction* (synthesis of amines from azides), enabled the production of primary amines more or less selectively. In addition, amination of alcohols, hydroamination, hydrogenation of nitro or cyano groups or reductive amination permit their chemical production. Under all these variants, efficient, catalytic and atom-economic synthesis routes with few by-products are of increased interest.^[12]

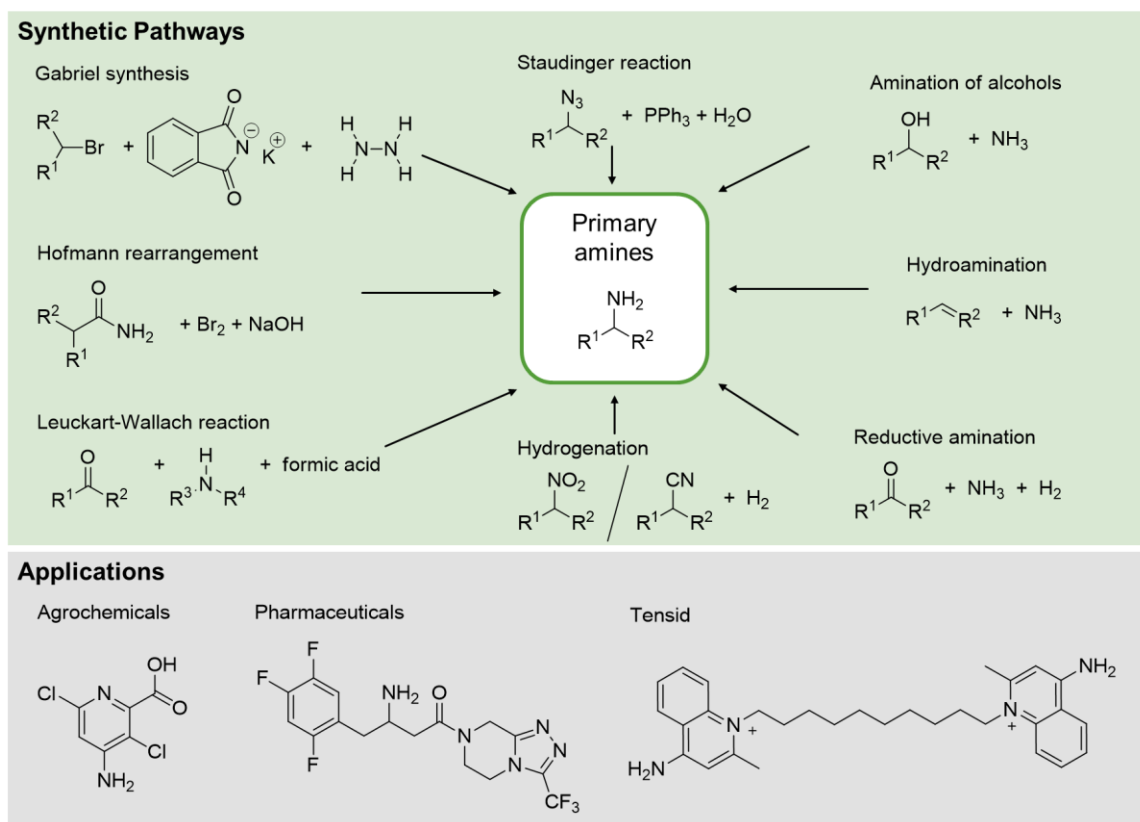


Figure 2. 2: Synthetic pathway and applications of primary amines.

2.2.1 Hydrogenation of nitroarenes

The heterogeneous catalytic hydrogenation of nitroarenes to the corresponding anilines is one of these atom-economic variants. The mechanism for the electrochemical reduction of nitroarenes was first described 100 years ago by *Haber* and later accepted as a general mechanism for hydrogenation.^[13] Starting from the aromatic nitro compound, the corresponding aniline derivative can be formed by the direct or condensation route via various intermediates, such as hydroxylamine or azo compounds. This results in the requirement for the catalyst to catalyze all these partial steps in the reduction of NO_2 to NH_2 . The tolerance of functional groups, such as C-C double bonds or halogens, is crucial here. Parallel to the reduction of the nitro group, unwanted reduction or cleavage of hydrogenation-sensitive groups may occur.^[14] Modified noble metal catalysts, such as Pt-Pb- $CaCO_3$ or Pt/C- H_3PO_2 , were often used for this task.^[15] An important contribution to the selective hydrogenation of nitroarenes was achieved by *Corma* and *Serna* in 2006. They investigated the selective hydration of 3-nitrostyrene, 4-nitrobenzaldehyde, 4-nitrobenzotrile, 4-nitrobenzamide and 1-nitro-1-cyclohexene (selectivities > 95%) under mild conditions (100–140 °C, 0.9–1.5 MPa H_2 , 0.23–4.3 mol% Au) with Au/ TiO_2 and Au/ Fe_2O_3 .^[16] Further studies followed with ruthenium-,^[17] rhodium-,^[18] palladium-,^[19] platinum-^[17,18] or gold-based^[20] catalyst systems.

The conservation of the elemental resources of our planet is a global challenge, and the replacement of noble metals by abundantly available transition (base) metals is an appealing strategy to conserve noble

metals.^[21] In this context, *Beller and coworkers* introduced a cobalt catalyst^[22] and related iron^[23] catalysts with impressive selectivity and scope for the hydrogenation of nitroarenes. However, other examples for cobalt^[24] and iron^[25] catalysts have also been described. Heterogeneous nickel catalysts,^[18,26] as an alternative to noble metal catalysts, have been introduced by several groups. However, none of these catalysts is reusable and tolerates a variety of functional groups.

2.2.2 Reductive amination of carbonyl compounds

Reductive amination of carbonyl compounds with ammonia or an amine is another attractive way to synthesize amines. In 1921, *Mignonac* showed that a reductive amination can take place in the presence of nickel powder and dry ammonia.^[27] Ketones and aldehydes generally react with ammonia or amines under condensation and form a hemiaminal (carbinolamine). Further elimination of H₂O gives a Schiff base (imine). The subsequent reduction takes place to the amine in the presence of a reducing agent (e.g. formic acid, metal hydrides and molecular hydrogen) and/or a catalyst. The imine, as a reactive intermediate, or the primary amine, due to its increased nucleophilicity, can act as amination agents and secondary and tertiary amines are often generated parallel to the primary amine. Hence, the greatest challenge in the synthesis of primary amines is the control of selectivity.^[28]

In order to enable atom-economic reductive amination with fewer by-products, the selectivity of the primary amine has not only to be high, but also the use of molecular hydrogen as a reducing agent is required. Most of the catalysts described for this reaction are based on noble metals. The work of *Beller's* group^[29] and *Kadyrov's* group^[30], which introduced parallel the first homogeneous catalyst tolerating aqueous ammonia, is to be highlighted. Both research groups apply [Rh(COD)Cl]₂ as a precatalyst and a water-soluble phosphine ligand (TPPS = tris-/3-sulphophenyl)phosphine trisodium salt; BINAS = 2,2'-bis(bis(3-sulphophenyl)phosphinomethyl-4,4,7,7-tetrasulfo-1,1'-binaphthyl octasodium salt). These soluble transition metal complexes facilitate the smooth reductive amination of aldehydes^[29] and ketones^[30] with aqueous ammonia. A bimetallic catalyst based on Rh and Ir had to be used for the reductive amination of aliphatic aldehydes to produce high yields and selectivities.^[29]

In addition, heterogeneous noble metal catalysts, such as Ru/ZrO₂^[31], Rh/Al₂O₃^[32] or Ru/Nb₂O₅^[33], have been described for this reaction. Similar to very early work^[34] involving Raney nickel^[35], the catalyst systems exhibit no tolerance of hydrogenation-sensitive functional groups and, therefore, only a small substrate scope.

As has already been mentioned, the scope of reactions can be extended if base metal catalysts with totally different selectivity patterns compared to known systems based on precious metals are employed. *Beller and coworkers* disclosed a Co catalyst for the synthesis of various amines. A Co-metal organic framework (Co-MOF = Co-DABCO-TPA MOF) was used as a template and supported on commercial carbon. Further pyrolysis under inert atmosphere (argon) generated cobalt nanoparticles encapsulated by a graphitic shell on carbon. In addition to secondary and tertiary amines, primary amines bearing hydrogenation-sensitive groups, such as C-C double bonds or even a C-C triple bond, were generated in

high yields and selectivities, though high pressures of H₂ (4 MPa) and temperatures (120 °C) were required.^[11]

Amino acids, a subclass of primary amines, are the basic building block in proteins, are used in the food and feed processing industry and are discussed as a decisive intermediate in the origin of life. It is conceivable, that nickel, as an earth-abundant metal, mediated the formation of such small but relevant molecules. Regarding the origin of life (abiogenesis), demonstrating the production of amino acids under early earth conditions is of great interest. However, reductive amination of ketones and aldehydes are known, no efficient catalyst system for the reductive amination of keto acids has emerged.

Firstly, *Miller* demonstrated that amino acids can be produced in an atmosphere of methane, ammonia, water and hydrogen.^[36] He used as an electric discharge as energy source and provided evidence for the primordial soup theory by *Oparin*^[37] and *Haldane*^[38]. The following experiments were performed with various energy sources. New concepts were developed for the synthesis of amino acids under hydrothermal conditions by the discovery of hydrothermal vents. Furthermore, amino acids were generated in a neutral atmosphere consisting of CO₂ and N₂ applying electric discharges and a Cu-electrode. Mechanochemical activation (ball mill) was introduced in 2018. Benzaldehyde was milled with benzylamine, a CN⁻ source and SiO₂ as an additive to synthesize aminonitriles. Further transformation by hydrolysis generated the amino acids. Catalytic research in the last few years has focused on the development of base metal catalysts. The development of such an active, heterogeneous base metal catalyst that operates under very mild conditions (comparable with early earth conditions) represents a highly desirable strategy for the synthesis of amino acids via reductive amination.

2.3 Ceramic catalyst supports

In principle, ceramics can be divided into two groups. Non-oxidic ceramics, such as silicon carbonitride (SiCN), silicon carbide (SiC), silicon nitride (Si₃N₄) or aluminum nitride (AlN), are available in addition to oxide ceramics such as aluminum oxide (Al₂O₃), aluminum titanate (Al₂TiO₅) or zirconium oxide (ZrO₂). Due to their unique mechanical, thermal, biological-chemical and electrical properties, they are used in vehicle and automobile construction, electronics, energy and the environment, device and mechanical engineering, and in medical technology. Ceramics are, by definition, thermostable, chemically resistant and hard. These properties make them especially suitable for use as catalyst supports.^[39]

Polymer-derived ceramics have attracted increased interest in recent years, especially in the area of material sciences and as catalyst supports. The preceramic polymer can be easily modified and permits the production of a wide variety of nanocomposites. Nanoparticles can be introduced into the SiCN matrix via a molecular synthesis pathway, first demonstrated on the example of copper.^[40]

Surface area can be generated by the following two methods (template method/sacrificial filler method and block copolymer method). Activated carbon^[41], silicates^[42,43], polyethylene^[44] or polystyrene spheres^[42,45], for example, can be used as sacrificial fillers. These templates are generally suspended or

infiltrated with the preceramic polymer and removed after cross-linking by pyrolysis, oxidation or etching to obtain a porous ceramic. Furthermore, a block copolymer existing of an organic and inorganic block gave a structured green body via microphase separation. The following pyrolysis removes the organic polymer block and generates the porous ceramic.^[46] All these methods require a high stability of the pores to prevent collapse. Generation of pores with a diameter of 2–50 nm is particularly attractive but challenging. These concepts could be extended to Pt@PE-SiCN^[47], Rh@PE-SiCN^[48], Pd@C-SiCN^[49] and Ni@PE-SiC^[50].

In chapter 4, the combination of the PS soft template method is extended and the generation of a Ni@PS₆₀SiCN₉₀₀^[51] nanocomposite is demonstrated. The catalyst is employed for the selective hydrogenation of nitroarenes. Furthermore, Al₂O₃ was impregnated with a special nickel complex and pyrolysis generated nickel nanoparticles embedded in a nitrogen doped carbon layer on this ceramic support. This nanoparticles show high activity in the selective synthesis of primary amines^[52] (see chapter 5) and amino acids (see chapter 6) via reductive amination.

2.4 References

- [1] A. G. W. Cameron, *Space Science Review* **1970**, *15*, 121.
- [2] Stock market prices for metals from 18.12.2017 available at <http://www.infomine.com>.
- [3] a) F. Kallmeier, R. Kempe, *Angew. Chem. Int. Ed.* **2018**, *57*, 46; b) F. Kallmeier, R. Kempe, *Angew. Chem.* **2018**, *130*, 48; c) G. A. Filonenko, R. van Putten, E. J. M. Hensen, E. A. Pidko, *Chem. Soc. Rev.* **2018**, *47*, 1459.
- [4] Zuo, Weiwei, Lough, Alan J., Y. F. Li, R. H. Morris, *Science* **2013**, *342*, 1080.
- [5] a) M. R. Friedfeld, M. Shevlin, J. M. Hoyt, S. W. Krska, M. T. Tudge, P. J. Chirik, *Science* **2013**, *342*, 1076; b) M. R. Friedfeld, H. Zhong, R. T. Ruck, M. Shevlin, P. J. Chirik, *Science* **2018**, *360*, 888.
- [6] T. J. Korstanje, van der Vlugt, Jarl Ivar, C. J. Elsevier, B. de Bruin, *Science* **2015**, *350*, 298.
- [7] A. Boddien, D. Mellmann, F. Gärtner, R. Jackstell, H. Junge, P. J. Dyson, G. Laurenczy, R. Ludwig, M. Beller, *Science* **2011**, *333*, 1733.
- [8] A. M. Tondreau, C. C. H. Atienza, K. J. Weller, S. A. Nye, K. M. Lewis, J. G. P. Delis, P. J. Chirik, *Science* **2012**, *335*.
- [9] J. M. Hoyt, V. A. Schmidt, A. M. Tondreau, P. J. Chirik, *Science* **2015**, *349*, 960.
- [10] R. P. Yu, D. Hesk, N. Rivera, I. Pelczer, P. J. Chirik, *Nature* **2016**, *529*, 195.
- [11] R. V. Jagadeesh, K. Murugesan, A. S. Alshammari, H. Neumann, M.-M. Pohl, J. Radnik, M. Beller, *Science* **2017**, *358*, 326.
- [12] L. Legnani, B. Bhawal, B. Morandi, *Synthesis* **2017**, *49*, 776.
- [13] a) F. Haber, *Z. Elektrotech. Elektrochem.* **1898**, *4*, 506; b) F. Haber, *Angew. Chem.* **1900**, *13*, 433.
- [14] H.-U. Blaser, *Science* **2006**, *313*, 312.
- [15] a) H.-U. Blaser, H. Steiner, M. Studer, *ChemCatChem* **2009**, *1*, 210; b) U. Siegrist, P. Baumeister, H. U. Blaser, *Chem. Ind.* **1998**, *75*, 207.
- [16] A. Corma, P. Serna, *Science* **2006**, *313*, 332.
- [17] H. Wei, X. Liu, A. Wang, L. Zhang, B. Qiao, X. Yang, Y. Huang, S. Miao, J. Liu, T. Zhang, *Nat. Commun.* **2014**, *5*, 5634.
- [18] A. Corma, P. Serna, P. Concepción, J. J. Calvino, *J. Am. Chem. Soc.* **2008**, *130*, 8748.
- [19] J. Li, X.-Y. Shi, Y.-Y. Bi, J.-F. Wei, Z.-G. Chen, *ACS Catal.* **2011**, *1*, 657.
- [20] S. Fountoulaki, V. Daikopoulou, P. L. Gkizis, I. Tamiolakis, G. S. Armatas, I. N. Lykakis, *ACS Catal.* **2014**, *4*, 3504.
- [21] R. M. Bullock, *Science* **2013**, *342*, 1054.
- [22] a) F. A. Westerhaus, R. V. Jagadeesh, G. Wienhöfer, M.-M. Pohl, J. Radnik, A.-E. Surkus, J. Raebach, K. Junge, H. Junge, M. Nielsen et al., *Nat. Chem.* **2013**, *5*, 537; b) R. V. Jagadeesh, T. Stemmler, A.-E. Surkus, M. Bauer, M.-M. Pohl, J. Radnik, K. Junge, H. Junge, A. Brückner, M. Beller, *Nat. Protoc.* **2015**, *10*, 916 EP -.

- [23] R. V. Jagadeesh, A.-E. Surkus, H. Junge, M.-M. Pohl, J. Radnik, J. Rabeah, H. Huan, V. Schüenemann, A. Brückner, M. Beller, *Science* **2013**, *342*, 1073.
- [24] a) Z. Zhao, H. Yang, Y. Li, X. Guo, *Green Chem.* **2014**, *16*, 1274; b) Z. Wei, J. Wang, S. Mao, D. Su, H. Jin, Y. Wang, F. Xu, H. Li, Y. Wang, *ACS Catal.* **2015**, *5*, 4783; c) T. Stemmler, F. A. Westerhaus, A.-E. Surkus, M.-M. Pohl, K. Junge, M. Beller, *Green Chem.* **2014**, *16*, 4535; d) T. Schwob, R. Kempe, *Angew. Chem. Int. Ed.* **2016**, *55*, 15175; e) M. Eckardt, M. Zaheer, R. Kempe, *Sci. Rep.* **2018**, *8*, 2567; f) B. Chen, F. Li, Z. Huang, G. Yuan, *ChemCatChem* **2016**, *8*, 1132; g) P. Ji, K. Manna, Z. Lin, X. Feng, A. Urban, Y. Song, W. Lin, *J. Am. Chem. Soc.* **2017**, *139*, 7004; h) P. Zhou, Z. Zhang, *ChemSusChem* **2017**, *10*, 1892; i) H. Alex, P. Loos, T. Baramov, J. Barry, T. Godiawala, J. Hassfeld, N. Steinfeldt, *ChemCatChem* **2017**, *9*, 3210; j) I. Sorribes, L. Liu, A. Corma, *ACS Catal.* **2017**, *7*, 2698; k) B. Sahoo, D. Formenti, C. Topf, S. Bachmann, M. Scalone, K. Junge, M. Beller, *ChemSusChem* **2017**, *10*, 3035; l) Z. Wei, S. Mao, F. Sun, J. Wang, B. Mei, Y. Chen, H. Li, Y. Wang, *Green Chem.* **2018**, *20*, 671; m) L. Liu, P. Concepción, A. Corma, *J. Catal.* **2016**, *340*, 1; n) L. Liu, F. Gao, P. Concepción, A. Corma, *J. Catal.* **2017**, *350*, 218; o) F. Zhang, C. Zhao, S. Chen, H. Li, H. Yang, X.-M. Zhang, *J. Catal.* **2017**, *348*, 212.
- [25] C. Bäumlner, R. Kempe, *Chem. Eur. J.* **2018**, *24*, 8989.
- [26] a) S. Pisiewicz, D. Formenti, A.-E. Surkus, M.-M. Pohl, J. Radnik, K. Junge, C. Topf, S. Bachmann, M. Scalone, M. Beller, *ChemCatChem* **2016**, *8*, 129; b) T. Fu, M. Wang, W. Cai, Y. Cui, F. Gao, L. Peng, W. Chen, W. Ding, *ACS Catal.* **2014**, *4*, 2536; c) P. Zhang, C. Yu, X. Fan, X. Wang, Z. Ling, Z. Wang, J. Qiu, *PCCP* **2015**, *17*, 145.
- [27] G. Mignonac, *Compt. Rend.* **1921**, *172*, 223.
- [28] a) S. Gomez, J. A. Peters, T. Maschmeyer, *Adv. Synth. Catal.* **2002**, *344*, 1037; b) J. L. Klinkenberg, J. F. Hartwig, *Angew. Chem. Int. Ed.* **2011**, *50*, 86; c) J. Kim, H. J. Kim, S. Chang, *Eur. J. Org. Chem.* **2013**, *2013*, 3201; d) H. Alinezhad, H. Yavari, F. Salehian, *Curr. Org. Chem.* **2015**, *19*, 1021.
- [29] T. Gross, A. M. Seayad, M. Ahmad, M. Beller, *Org. Lett.* **2002**, *4*, 2055.
- [30] T. Riermeier, K. Haack, U. Dingerdissen, A. Boerner, V. Tararov, R. Kadyrov, US 6,884,887 B1, **2005**.
- [31] G. Liang, A. Wang, L. Li, G. Xu, N. Yan, T. Zhang, *Angew. Chem. Int. Ed.* **2017**, *56*, 3050.
- [32] M. Chatterjee, T. Ishizaka, H. Kawanami, *Green Chem.* **2016**, *18*, 487.
- [33] T. Komanoya, T. Kinemura, Y. Kita, K. Kamata, M. Hara, *J. Am. Chem. Soc.* **2017**, *139*, 11493.
- [34] a) E. R. Alexander, A. L. Misegades, *J. Am. Chem. Soc.* **1948**, *70*, 1315; b) M. V. Klyuev, M. L. Khidekel', *Russ. Chem. Rev.* **1980**, *49*, 14.
- [35] a) C. F. Winans, *J. Am. Chem. Soc.* **1939**, *61*, 3566; b) A. S.C. Chan, C.-c. Chen, Y.-c. Lin, *Appl. Catal. A Ge.* **1994**, *119*, L1-L5; c) P. Dolezal, O. Machalický, M. Pavelek, P. Kubec, K. Hrádková, R. Hrdina, R. Suláková, *Appl. Catal., A* **2005**, *286*, 202.
- [36] S. L. Miller, *Science* **1953**, 528.

- [37] A. I. Oparin, *The origin of life*, Dover Publications, New York, **1965**.
- [38] J. B. S. Haldane, *Rationalist Annual* **1929**, 148.
- [39] K.-D. Linsmeier, *Technische Keramik. Werkstoffe für höchste Ansprüche*, Verl. Moderne Industrie, Lansberg/ Lech, **2010**.
- [40] G. Glatz, T. Schmalz, T. Kraus, F. Haarmann, G. Motz, R. Kempe, *Chem. Eur. J.* **2010**, *16*, 4231.
- [41] a) J. Yan, A. Wang, D.-P. Kim, *Microporous Mesoporous Mat.* **2007**, *100*, 128; b) Y. Shi, Y. Wan, Y. Zhai, R. Liu, Y. Meng, B. Tu, D. Zhao, *Chem. Mater.* **2007**, *19*, 1761.
- [42] I.-K. Sung, Christian, M. Mitchell, D.-P. Kim, Kenis, P. J. A., *Adv. Funct. Mater.* **2005**, *15*, 1336.
- [43] H. Wang, S.-Y. Zheng, X.-D. Lia, D.-P. Kim, *Microporous Mesoporous Mat.* **2005**, *80*, 357.
- [44] B. H. Jones, T. P. Lodge, *J. Am. Chem. Soc.* **2009**, *131*, 1676.
- [45] J.-K. Ewert, C. Denner, M. Friedrich, G. Motz, R. Kempe, *Nanomaterials* **2015**, *5*, 425.
- [46] a) Pillai, S. K. T., W. P. Kretschmer, M. Trebbin, S. Förster, R. Kempe, *Chem. Eur. J.* **2012**, *18*, 13974; b) Pillai, S. K. T., W. P. Kretschmer, C. Denner, G. Motz, M. Hund, A. Fery, M. Trebbin, S. Förster, R. Kempe, *Small* **2013**, *9*, 984; c) Q. D. Nghiem, D. J. Kim, D.-P. Kim, *Adv. Mater.* **2007**, *19*, 2351.
- [47] S. M. Sachau, M. Zaheer, A. Lale, M. Friedrich, C. E. Denner, U. B. Demirci, S. Bernard, G. Motz, R. Kempe, *Chem. Eur. J.* **2016**, *22*, 15508.
- [48] S. Fehn, M. Zaheer, C. E. Denner, M. Friedrich, R. Kempe, *New J. Chem.* **2016**, *40*, 9252.
- [49] S. Schwarz, M. Friedrich, G. Motz, R. Kempe, *Z. anorg. allg. Chem.* **2015**, *641*, 2266.
- [50] M. Zaheer, J. Hermannsdörfer, W. P. Kretschmer, G. Motz, R. Kempe, *ChemCatChem* **2014**, *6*, 91.
- [51] G. Hahn, J.-K. Ewert, C. Denner, D. Tilgner, R. Kempe, *ChemCatChem* **2016**, *8*, 2461.
- [52] G. Hahn, P. Kunnas, N. de Jonge, R. Kempe, *Nature Catalysis* **2019**, *2*, 71.

3 Overview of Thesis Results

This thesis contains three publications, presented in chapter 4–6. The first is published, the second has been accepted and the third is to be submitted. The results of the publications are summarized in chapter 1. Chapter 3.1 gives an overview of the main topics of the thesis and discusses the correlation between the different publications. Individual contributions to joint publications are pointed out in chapter 3.2.

3.1 Synopsis

In the last few years, *Kempe and coworkers* have focused on heterogeneous catalysis, a key technology of our century, which addresses sustainability in different aspects. In this context, a Ni@SiC catalyst for the hydrogenolysis of bio-based aryl ethers to platform chemicals, a Pd₂Ru@SiCN catalyst for the reversible storage of hydrogen, or other catalysts, such as Cu@SiCN, Fe@SiCN, Co@SiCN or Ni@SiCN were introduced in oxidation and hydrogenation reactions commonly accomplished by catalysts based on noble metals. This conservation strategy of rare elements and the fact that novel selectivity patterns could be observed with a base metal catalyst, motivated us to develop different reusable, heterogeneous and highly selective nickel catalysts for the production of amines.

Most of the SiC- or SiCN-based catalysts mentioned above have a very low surface area. Consequently, many of the metal nanoparticles are not accessible for substrates and catalytically inactive. *Ewert et al.* were able to provide an innovative synthesis route leading to mesoporous SiCN materials. In the first work (details see chapter 4), this route was extended and *in-situ* metal nanoparticles were generated (see Figure 3. 1).

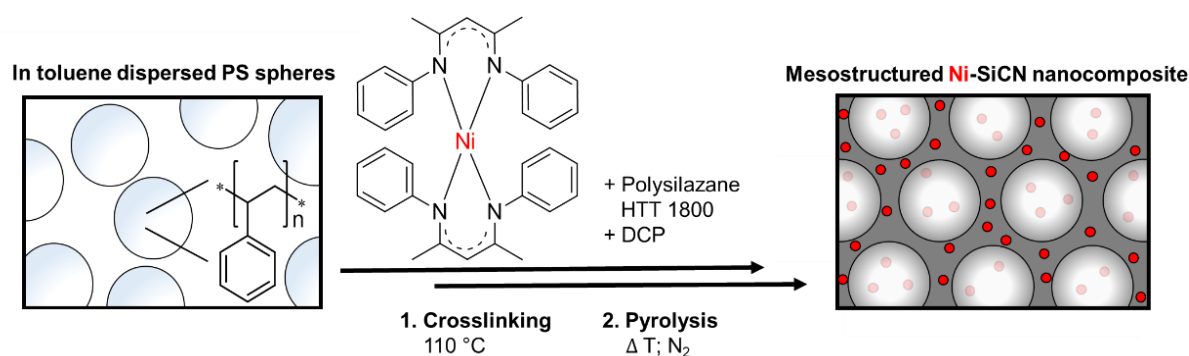


Figure 3. 1: General pathway to synthesize a mesoporous and metal-doped nanocomposite.

The polystyrene spheres, produced in a determined size by emulsion polymerization, are generally first suspended in toluene. After the addition of the polysilazane HTT 1800 and a specific nickel complex, transmetalation took place, i.e. the metal center of the complex was transferred to the preceramic polymer. Subsequent cross-linking, initiated by DCP, and pyrolysis of the green body, which had previously

been dried in vacuum, finally produced a mesoporous nanocomposite of nickel nanoparticles and the inorganic, amorphous SiCN carrier.

The applied metal complex is crucial for this synthesis. Using Ni@SiCN nanocomposites, *Zaheer et al.* showed that the metal itself influences the structure of the support and affects cross-linking and pyrolysis. This leads to several requirements from the nickel precursor. Firstly, the influence on cross-linking and pyrolysis should not be excessive and the structuring by polystyrene should not be inhibited. On the other hand, the complex must be stable under the conditions specified by the structure but, at the same time, reactive enough to accomplish the transmetalation and permit the formation of well-defined nickel nanoparticles during pyrolysis. It was shown that the [(nacnac)₂Ni] complex meets all these requirements and was suitable for this task.

The size of the polystyrene spheres and the maximal pyrolysis temperature have another significant effect on the structure of the material. Polystyrene spheres with various diameters (60 nm, 120 nm and 210 nm) in combination with different pyrolysis temperatures (700 °C, 900 °C and 1000 °C), were used as templates.

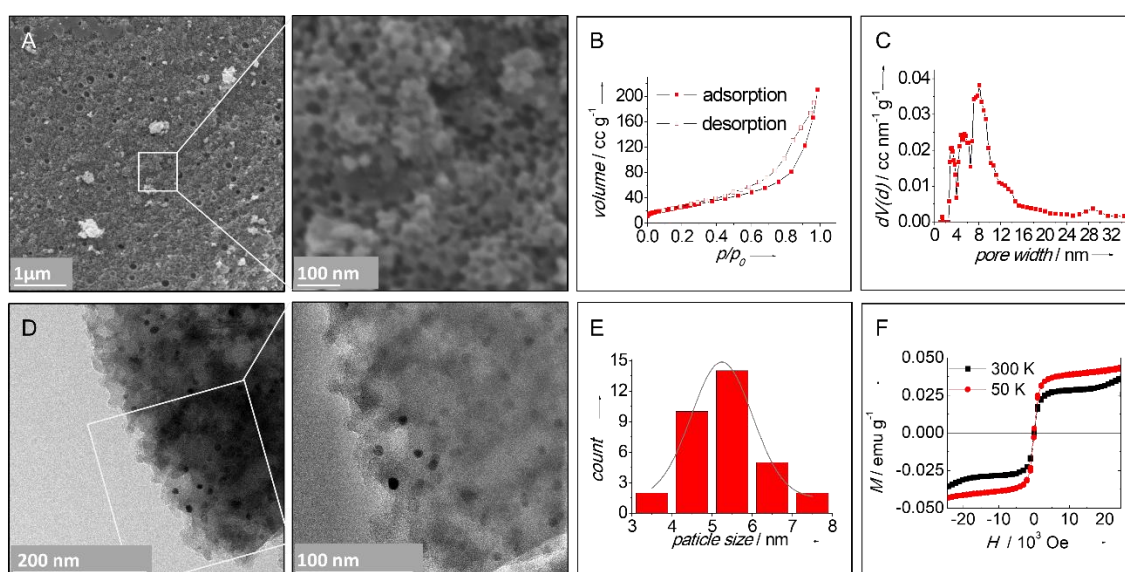


Figure 3. 2: Characterization of the Ni@PS₆₀SiCN₉₀₀ nanocomposite. A) SEM measurements; B) N₂-Physorption measurement with a type IV hysteresis; C) calculated pore size distribution; D) TEM measurements; E) particle size distribution; and F) magnetic measurements.

It could be shown by different characterization methods that a pyrolysis temperature of 900 °C and polystyrene spheres of 60 nm as a template provided the best surface areas. Figure 3. 2 A–C show the SEM images and N₂-physorption measurements of the Ni@PS₆₀SiCN₉₀₀ nanocomposite. A homogeneously distributed pore structure and a hysteresis of type IV in the isotherm, typical for mesoporous materials, can be observed. The specific surface calculated by the Brunauer–Emmett–Teller (BET) method was found to be 90 m²g⁻¹. The calculated pore size distribution displays mesopores with an average size of 8.2 nm and a total amount of > 95%. The TEM analysis (Figure 3. 2 D) of the

Ni@PS₆₀SiCN₉₀₀ nanocomposite indicates the generation of homogeneously distributed nickel nanoparticles with a diameter of 5.5 nm (Figure 3. 2 E). Magnetic measurements (Figure 3. 2 F) also provide evidence for the presence of small Ni-NPs, as superparamagnetism was observed. Metallic nickel nanoparticles were generated by the reducing atmosphere during pyrolysis. The XRD measurements show the typical reflections for a cubic Ni⁰ phase.

Compared to a non-structured Ni@SiCN₇₀₀ hybrid material, the Ni@PS₆₀SiCN catalyst showed a higher activity in the hydrogenation of nitroarenes to the corresponding aniline derivatives. After screening of different reaction parameters, to our delight, the catalyst exhibits a very high chemoselectivity. Different functional groups were tolerated. Nitroarenes, for example, containing halogenides (bromides, chlorides and iodides), nitrile, keto, aldehyde, amide and even vinyl groups were smoothly hydrogenated to the aniline derivatives. Recyclability studies and leaching experiments were carried out to prove the long-term stability of the catalyst. No decrease in the activity could be detected after five consecutive runs.

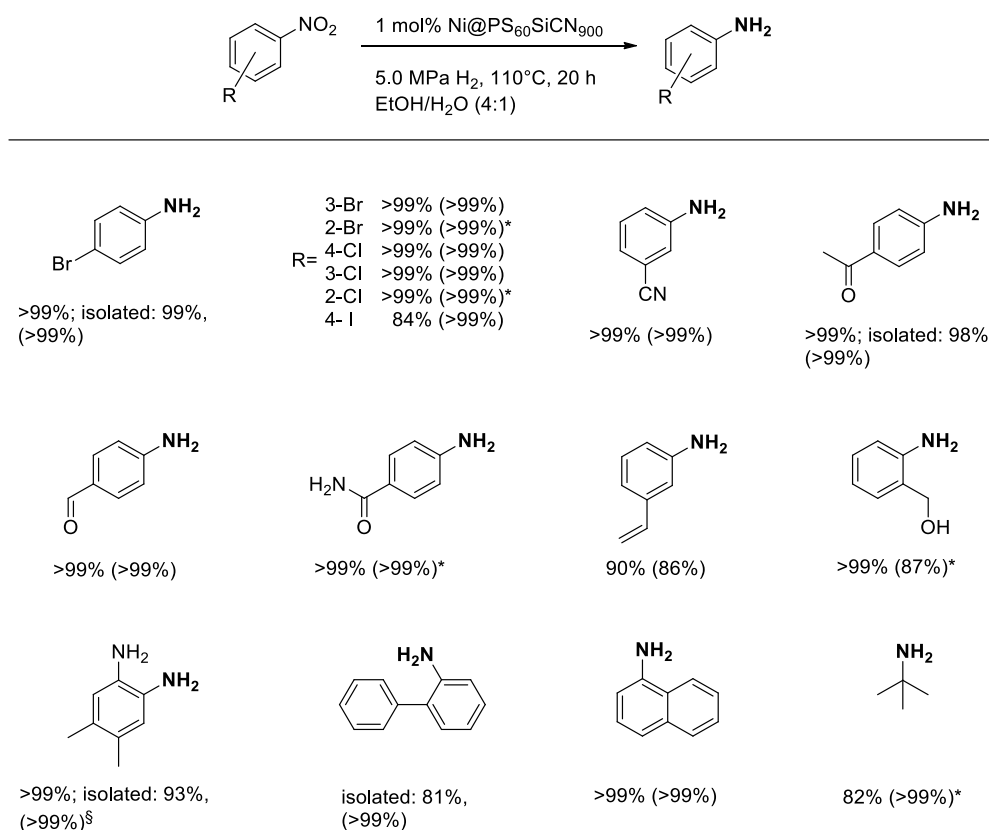


Figure 3. 3: Substrate scope. Reaction conditions: 110 °C, 5.0 MPa H₂, 1 mmol substrate, 20 h, 1 mol% catalyst (0.7 mg Ni, 0.01 mmol, 30 mg); * 3 mol%; § 2 mol%; yields were determined by GC using *n*-dodecane as an internal standard; selectivities are given in parentheses.

Delighted and inspired by the high selectivity of our Ni@PS₆₀SiCN catalyst, we tried to extend these results and focused on the development of a selective nickel catalyst for the reductive amination of carbonyl compounds. As mentioned in chapter 2.2.2, the reductive amination is another attractive way

to synthesize primary amines. In 1921, *Mignonac* was able to aminate carbonyl compounds in the presence of nickel powder and dry ammonia. Despite this old work, developing catalysts that allow the selective reaction to primary amine is still of industrial and academic interest. The control of the imine formed *in situ*, which is reactive and able to undergo various side reactions, is challenging. In addition, the primary amine can act as an amination agent due to its increased nucleophilicity. There is frequently a parallel formation of primary, secondary and tertiary amines.

A catalyst used for this reaction must, therefore, activate the carbonyl compound to ensure the formation of imine and enable the reduction of imine to primary amine. Hence, all possible side reactions must be suppressed to obtain the primary amine selectively.

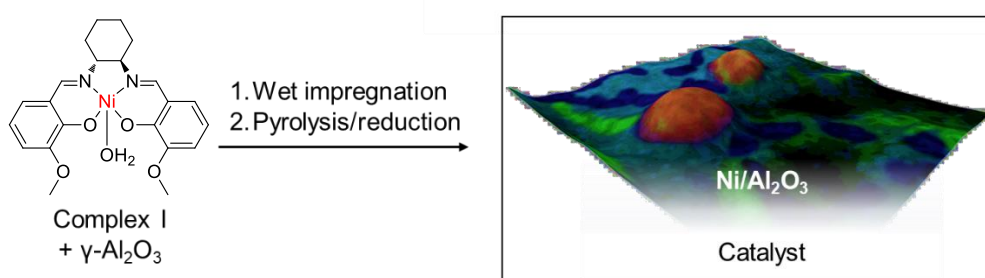


Figure 3. 4: Synthesis of the Ni/ Al_2O_3 catalyst.

In this thesis (for details see chapter 5), various commercial supports, such as activated carbon, cerium oxide or aluminium oxide, in combination with nickel as the active metal were tested. The synthesis of the different catalysts was carried out in a simple two step procedure. The support was impregnated with a solution of the nickel salen complex **I**. After the solvent had been removed, pyrolysis under N_2 and the subsequent reduction under forming gas generated nickel nanoparticles on the supports (shown in Figure 3. 4 schematically for Al_2O_3). Different pyrolysis temperatures (Table 3. 1, entry 1–3), various supports (Table 3. 1, entry 4–7) or nickel sources (Table 3. 1, entry 8 and 9) were investigated in a catalytic screening. The Ni/ Al_2O_3 , derived from complex **I** and pyrolyzed at 700 °C gave the best results in the reductive amination of benzaldehyde to benzylamine.

Table 3. 1: Catalyst screening

Entry	Metal source	Support	Pyrolysis T [°C]	Yield [%]
1	Complex I	γ -Al ₂ O ₃	600	34
2	Complex I	γ-Al₂O₃	700	78
3	Complex I	γ -Al ₂ O ₃	800	48
4	Complex I	CeO ₂	700	36
5	Complex I	Activated C	700	0
6	Complex I	SiO ₂	700	0
7	Complex I	TiO ₂	700	0
8	Ni(OAc) ₂	γ -Al ₂ O ₃	700	0
9 ^[a]	Raney Ni	-	-	38
10	-	γ -Al ₂ O ₃	-	0
11	-	CeO ₂	-	0

Reaction conditions: 1.2 mol% catalyst (10 mg catalyst, 3.5 wt% Ni, 0.006 mmol Ni, 0.35 mg Ni) or 10 mg support, 0.5 mmol benzaldehyde, 0.5 mL aq. NH₃ 25% (6.7 mmol), 2.0 mL H₂O, 80 °C, 1.0 MPa H₂, 20 h. Yields were determined by gas chromatography (GC) using *n*-dodecane as an internal standard; [a] 5 mol% (0.025 mmol Ni, 1.5 mg Ni).

A detailed characterization of the Ni/Al₂O₃ catalyst showed that the nanoparticles are embedded in an N-doped carbon layer on the support. HAADF-STEM measurements were performed in combination with EDX and EELS element maps (see Figure 3. 5). These indicate that nickel nanoparticles are present on the Al₂O₃, with an average size of 8 nm. Furthermore, it could be shown that the carbon component (C: blue) is connected to the Ni nanoparticles (Ni: red) and a weak signal of nitrogen (N: green) is present in the vicinity of the Ni nanoparticles and in the matrix as well (see figure).

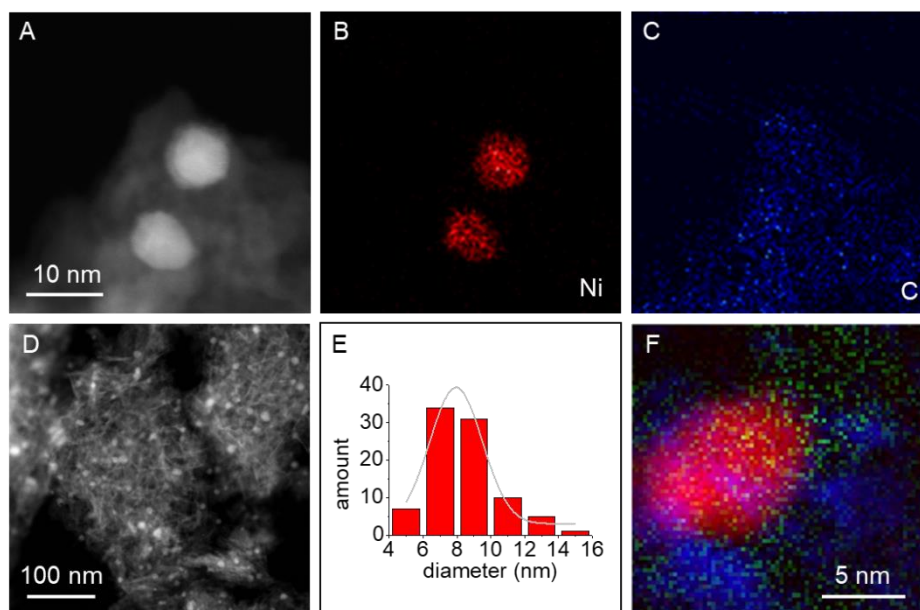


Figure 3. 5: Characterization of the Ni/Al₂O₃ catalyst. A–C) HAADF-STEM with representative EDX element maps (Ni: red; C: blue; D) HAADF-STEM overview; E) particle size distribution; F) overlapped EELS element maps (Ni: red; C: blue; N: green).

Additionally, X-ray photoelectron spectroscopy (XPS) measurements were performed to get an insight into the surface composition of the catalyst. The detail spectrum in the Ni 2p_{3/2} range indicates the presence of both metallic Ni⁰ and oxidic Ni²⁺ species on the catalyst surface (see Figure 3. 6 A). The ratio of Ni⁰:Ni²⁺ is approximately 1:1.5. The N atoms are located at the surface of the catalyst due to the ligand containing nitrogen, which decomposes during pyrolysis. Therefore, two different N species were detected (see Figure 3. 6 B). Carbon-linked N species with a binding energy of ~ 402 eV coexist with N species linked to a metal (binding energy ~ 399 eV). See chapter 5 for further characterizations (N₂-Physiosorption, TEM, high resolution TEM (HR-TEM), powder X-ray diffraction (PXRD), temperature programmed desorption (TPD), temperature programmed reduction (TPR), inductively coupled plasma optical emission spectrometry (ICP-OES)).

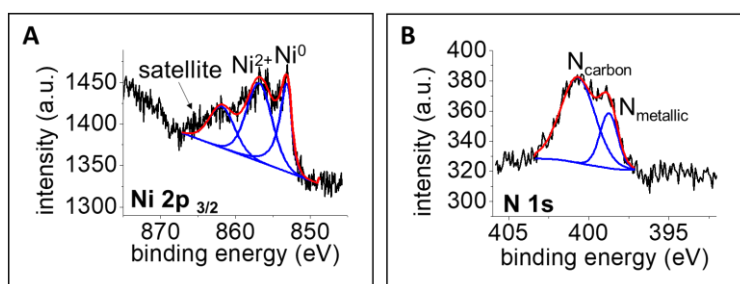


Figure 3. 6: XPS spectra of the 2p_{3/2} electrons (A) and of the N 1s electrons (B).

The influence of the solvent, the content of ammonia, the pyrolysis temperature and the metal content were optimized during the screening reactions. In summary, the reaction can be carried out smoothly and selectively with a 4 wt% Ni catalyst pyrolyzed at 700 °C, 0.5 mL of 25% aqueous ammonia

(6.7 mmol) and 2.0 mL of additional water at 80 °C and 1.0 MPa pressure of H₂. With the optimized reaction conditions in hand, we were interested in the substrate scope of our novel catalyst system. We investigated the reductive amination of aromatic and aliphatic aldehydes and ketones bearing various functional, hydrogen-sensitive groups. More than 50 examples were smoothly converted and even iodides or C-C double bonds were tolerated. Some representative examples are shown in Figure 3. 7.

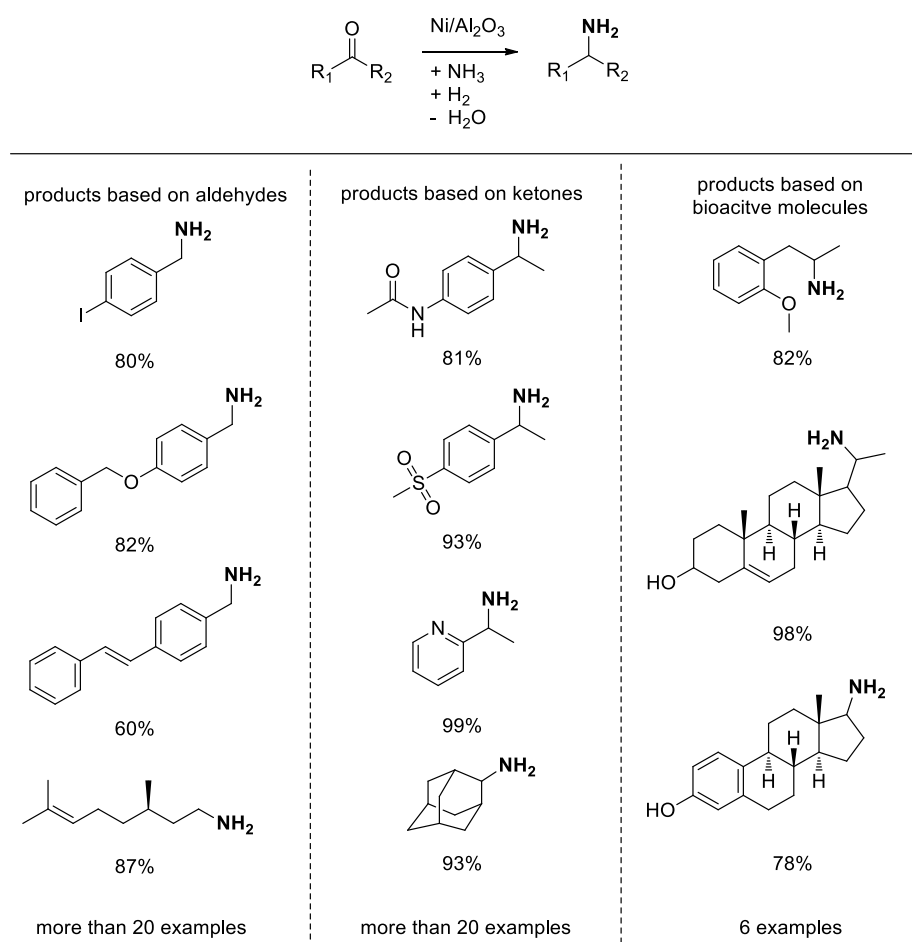


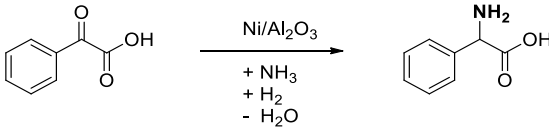
Figure 3. 7: Substrate scope; isolated yields are given for the corresponding hydrochloride salts.

Upscaling studies were carried out in order to demonstrate the enormous potential of the catalyst for industrial applications. It was possible to increase the reaction rates 20-fold without any further optimization, and the yields were similar to the 0.5 mmol approaches. Recycling studies clearly demonstrate the stability and robustness of the catalyst. No decrease in activity was recorded in the first five consecutive runs.

Several theories on the origin of life under early earth conditions are discussed. We can make a small contribution to this highly discussed topic by synthesizing amino acids under very mild conditions applying a nickel catalyst. Analogous to the biosynthesis in the human body, amino acids can be generated by reductive amination of keto acids. This motivated us to extend the applicability of our catalyst to the

synthesis of amino acids under very mild conditions. Firstly, the reaction conditions, such as ammonia content and solvent, were optimized for H₂ pressures of 0.5 and 0.1 MPa, respectively.

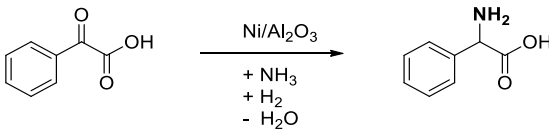
Table 3. 2: Screening of the NH₃ amount.

	
NH ₃ -25% aq. [ml]	Yield [%]
0.5	56
1.0	57
2.0	8
3.0	5

Reaction conditions: 0.5 mmol phenylglyoxylic acid, 3 mL reaction volume (solvent H₂O), 2.9 mol% Ni (24 mg Ni/Al₂O₃, 3.5 wt% Ni, 0.014 mmol Ni, 0.84 mg Ni), 1.0 MPa H₂, 80 °C, 20 h.

The amount of ammonia plays a decisive role in the amine yield, as has already been shown in preliminary experiments concerning the general reductive amination of carbonyl compounds. The synthesis of α -phenylglycine from phenylglyoxylic acid was used as a screening reaction. About 60% product could be obtained with a catalyst loading of 2.9 mol% and 1 mL 25%-aq. NH₃ (see Table 3. 2). Another important factor in catalysis is the solvent applied. Here, the behavior exhibited in preliminary tests was also confirmed.

Table 3. 3: Screening of the solvent at different H₂ pressures.

		
Solvent	H ₂ pressure [MPa]	Yield [%]
H ₂ O	1.0	57
H ₂ O	0.5	33
H ₂ O	0.1	10 ^[a]
H ₂ O	0.1	19 ^[b]
EtOH	1.0	5
EtOH	0.5	3

Reaction conditions: 0.5 mmol phenylglyoxylic acid, 1.0 mL (13.36 mmol) 25%-aq. NH₃, 2.0 mL solvent, 2.9 mol% Ni (24 mg Ni/Al₂O₃, 3.5 wt% Ni, 0.014 mmol Ni, 0.84 mg Ni), 80 °C, 20 h; [a] 10 mol% Ni (84 mg Ni/Al₂O₃, 3.5 wt% Ni, 0.05 mmol Ni, 2.94 mg Ni); [b] 10 mol% Ni (84 mg Ni/Al₂O₃, 3.5 wt% Ni, 0.05 mmol Ni, 2.94 mg Ni), 48 h.

The use of polar solvents, such as ethanol and water, has a positive influence on the activity of the catalyst. About 20% of the α -amino acid can be obtained at only 0.1 MPa H₂ with water as the solvent.

Variation of the H₂ pressure from 1.0 to 0.5 or 0.1 MPa affects the yield but not the selectivity (see Table 3. 3). With the optimized reaction conditions in hand, different amino acids were synthesized.

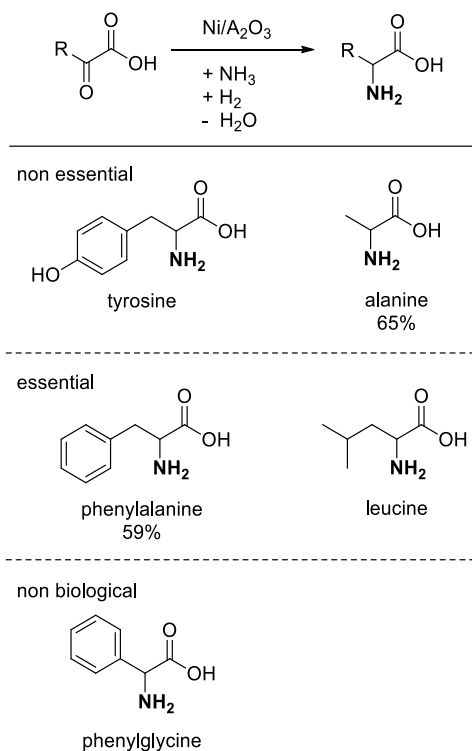


Figure 3. 8: Substrate scope; reaction conditions: 10 mol% Ni (84 mg Ni/Al₂O₃, 3.5 wt% Ni, 0.05 mmol Ni, 2.94 mg Ni), 0.5 mmol keto acid, 1.0 mL (13.36 mmol) 25%-aq. NH₃, 2.0 mL solvent, 80 °C; 48 h; isolated yields are given for the corresponding ethyl esters.

In addition to nonessential amino acids, such as tyrosine and alanine, essential ones, such as phenylalanine and leucine, and the nonbiological amino acid α -phenylglycine were obtained in good yields.

3.2 Individual contributions to joint publications

The results presented in this thesis were achieved in collaboration with others and are published or to be submitted as indicated below. The contributions of all co-authors to the respective publications are specified. The corresponding author is annotated by an asterisk (*).

Chapter 5

This work is published in *ChemCatChem* **2016**, 8, 2461 with the title

“A Reusable Mesoporous Nickel Nanocomposite Catalyst for the Selective Hydrogenation of Nitroarenes in the Presence of Sensitive Functional Groups”

Gabriela Hahn, Julia-Katharina Ewert, Christine Denner, Dominic Tilgner and Rhett Kempe*

I synthesized and characterized the catalyst, carried out the catalytic reactions and the related analytics. Rhett Kempe and I designed the experiments and co-wrote the manuscript. Julia-Katharina Ewert did preliminary work regarding the structuring of pure SiCN ceramics. Christine Denner performed the SEM measurements and was involved in the scientific discussions. Dominic Tilger performed the TEM measurements. Rhett Kempe supervised this work and was involved in the scientific discussions and the correction of the manuscript.

Chapter 6

This work is published in *Nature Catalysis* **2019**, 2, 71 with the title

“General synthesis of primary amines via reductive amination employing a reusable nickel catalyst”

Gabriela Hahn, Peter Kunnas, Niels de Jonge and Rhett Kempe*

I synthesized and characterized the catalyst, carried out the catalytic reactions and the related analytics. Rhett Kempe and I designed the experiments and co-wrote the manuscript. Peter Kunnas and Niels de Jonge performed the HAADF-STEM images coupled with EDX and EELS analysis and were involved in the scientific discussion. Rhett Kempe supervised this work and was involved in the scientific discussions and the correction of the manuscript.

Chapter 7

This work is to be submitted with the title

“A Nanostructured Earth-Abundant Metal Catalyst Can Mediate the Efficient Synthesis of Amino Acids from Ammonia Dissolved in Water under Very Mild Conditions”

Gabriela Hahn, Elena Herzog and Rhett Kempe*

I synthesized and characterized the catalyst, carried out the catalytic reactions and the related analytics and I wrote the manuscript. Rhett Kempe and I designed the experiments. Elena Herzog performed some of the screening reactions during her bachelor thesis. Rhett Kempe supervised this work and was involved in scientific discussions and the correction of the manuscript.

4 A Reusable Mesoporous Nickel Nanocomposite Catalyst for the Selective Hydrogenation of Nitroarenes in the Presence of Sensitive Functional Groups

Gabriela Hahn^[a], Julia-Katharina Ewert^[a], Christine Denner^[a], Dominic Tilgner^[a] and Rhett Kempe^{*[a]}

[a] Inorganic Chemistry II – Catalyst Design, University of Bayreuth, Universitätsstr. 30, 95440 Bayreuth (Germany).

Published in *ChemCatChem* **2016**, 8, 2461.

Keywords: heterogeneous catalysis, hydrogenation, mesoporous materials, nanocomposites, nickel

Abstract: The synthesis of aromatic amines from nitroarenes through hydrogenation is an industrially and academically important reaction. In addition, the employment of base metal catalysts in reactions that are preferentially mediated by rare noble metals is a desirable aim in catalysis and an attractive element-conservation strategy. Especially appealing is the observation of novel selectivity patterns with such inexpensive metal catalysts. Herein, we report a novel mesostructured Ni nanocomposite catalyst. It is the first example of a reusable Ni catalyst that is able to hydrogenate nitroarenes selectively to anilines in the presence of highly sensitive functional groups such as C-C bonds and nitrile, aldehyde, and iodo substituents.

4.1 Introduction

The synthesis of aromatic amines through the hydrogenation of the corresponding nitroarenes is a basic chemical reaction. Such reductions are also frequently applied in industry, as aromatic amines are important bulk chemicals, for instance, aniline, and intermediates for the production of fine chemicals, pharmaceuticals, polymers, herbicides, and more.^[1] A challenge is the selective hydrogenation of the nitro groups in the presence of functional groups highly sensitive to hydrogenation such as C-C bonds and nitrile and aldehyde substituents.^[1] Pioneering work involving the use of modified commercially available noble-metal hydrogenation catalysts was reported by Blaser and colleagues.^[1, 2] Recently, Pd-based noble-metal catalysts were developed that can also function at atmospheric hydrogen pressure and at room temperature.^[3] With regard to nonclassic hydrogenation catalysts, Corma and Serna reported a breakthrough in 2006.^[4] They used Au nanoparticles supported on TiO₂ and observed a selectivity over 95% for the reduction of the nitro group in 3-nitrostyrene, 4-nitrobenzaldehyde, 4-nitrobenzotrile, and 4-nitrobenzamide. The conservation of the elemental resources of our planet is a global challenge, and the replacement of noble metals by abundantly available transition metals (base metals) is an appealing

noble-metal conservation strategy.^[5] In this context, Beller and co-workers introduced a cobalt catalyst^[6] and a related iron catalyst^[7] with impressive selectivity and scope for the hydrogenation of nitroarenes.^[8,9] Nickel is also an inexpensive base metal and is thus another attractive alternative to existing noble-metal catalysts. To the best of our knowledge, recycling^[10] and the tolerance towards sensitive functional groups have not yet been demonstrated for heterogeneous nickel catalysts able to hydrogenate nitroarenes efficiently.^[11,12] The selectivity of our nickel catalyst is comparable to those of some state-of-the-art catalysts, such as the aforementioned cobalt and iron catalysts developed by Beller and co-workers.^[6,7] We recently developed a novel class of heterogeneous M@SiCN nanocomposite catalysts.^[13,14] The silicon carbonitride (SiCN) support is thermally very robust, chemically inert, and attractive for generating rather small metal nanoparticles in such supports.^[15] In addition, we introduced strategies to mesostructure SiCN^[16–18] and became interested in combining both approaches to synthesize highly active and selective base-metal catalysts.^[19] Herein, we report novel mesostructured Ni@SiCN nanocomposite materials easy to synthesize and scale up. The mesostructure is generated by an inexpensive polystyrene template, spheres 60 nm in diameter, and well dispersed in organic solvent, which is compatible with the generation of well-defined Ni nanoparticles. The material was characterized by powder X-ray diffraction (XRD), transmission electron microscopy (TEM), scanning electron microscopy (SEM), IR spectroscopy, and nitrogen physisorption. The nickel nanoparticles are catalytically active in the hydrogenation of nitroarenes. For the first time, we show that a reusable Ni catalyst is able to effect the selective hydrogenation of nitroarenes in the presence of hydrogenation-sensitive functional groups such as C-C bonds and nitrile, keto, aldehyde, and amide substituents.

4.2 Results and Discussion

Recently, Ewert et al.^[17,18] showed that polystyrene could be used as a soft template to generate a defined mesostructure in SiCN materials. This strategy of structuring should be compatible with the generation of metal–SiCN nanocomposites by transmetalation, crosslinking, and pyrolysis, as recently reported for a variety of metals.^[13–15] To combine both synthesis procedures, first, polystyrene spheres with a diameter of 60 nm (PS₆₀) were dispersed in toluene (Figure 4. 1). Next, we searched for a suitable Ni complex for the introduction of the metal into the mesostructured nanocomposite. The recently used nickel precursors were not stable enough under the conditions successfully applied for mesostructuring. A fine balance between stability of the metal precursor to avoid reduction and metal aggregation prior to pyrolysis should be ensured. On the other hand, the nickel complex has to be reactive enough to accomplish transmetalation—metal transfer from the metal precursor to the polysilazane. [(nacnac)₂Ni]^[20] {nacnac=deprotonated (*E*)-N-[(*Z*)-4-(phenylamino)pent-3-en-2-ylidene]aniline} was identified as a suitable nickel precursor (Figure 4. 1). After mixing a solution of [(nacnac)₂Ni] in toluene with the toluene dispersion of PS₆₀, the crosslinker and the polysilazane were added, and the mixture was stirred for 1 h to fulfill the transmetalation (Figure 4. 1). Further crosslinking at 110 °C without stirring and

slowly removing the solvent under vacuum enabled the defined arrangement of the template and nickel in the crosslinked polysilazane. During pyrolysis with the tailored program at 900 °C, the template was removed to obtain the mesoporous structure and Ni^{II} was reduced to elemental nickel nanoparticles under a reductive atmosphere (H₂ liberation) (Figure 4. 1).

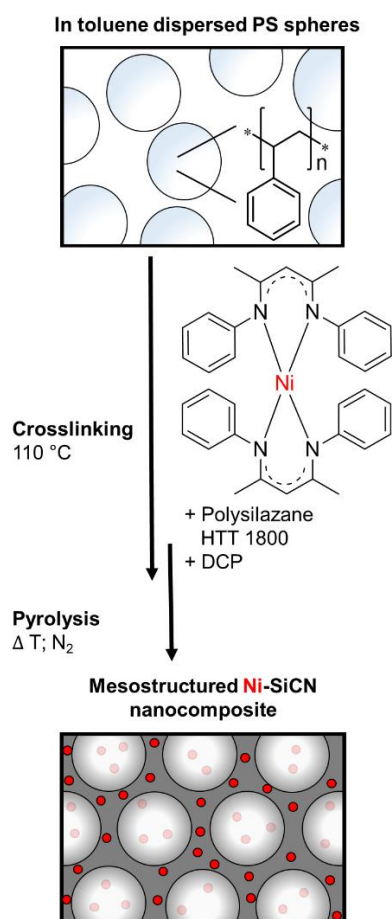


Figure 4. 1: Synthesis of the mesostructured Ni@PS₆₀SiCN nanocomposite. First, dispersion of the template polystyrene spheres with a diameter of 60 nm (PS₆₀) in toluene. Second, addition of commercially available polysilazane HTT 1800, the nacnac–nickel complex, and DCP (dicumyl peroxide, as crosslinker). Third, removal of the solvent and crosslinking at 110 °C. Fourth, pyrolysis with a tailored program at 900 °C under a N₂ atmosphere to form the mesostructured Ni-SiCN nanocomposite.

A theoretical Ni/Si ratio of 1:20 was chosen for the synthesis of Ni@PS₆₀SiCN corresponding to 2.3 wt% of Ni. Inductively coupled plasma optical emission spectrometry (ICP-OES) measurements revealed 2.34 wt% nickel in the Ni@PS₆₀SiCN nanocomposite, which is a very good agreement between the calculated and observed Ni contents. Ni@PS₆₀SiCN was further analyzed by TEM. TEM analysis indicated a homogenous distribution of the nickel nanoparticles (Ni-NPs) in the mesostructured support of Ni@PS₆₀SiCN (Figure 4. 2, top). In addition, a narrow Ni-NP distribution with the maxima at approximately 5.5 nm was observed (Figure 4. 2, bottom left). Magnetic measurements also provided evidence for the presence of small Ni-NPs, as superparamagnetism was observed (Figure 4. 2, bottom right).

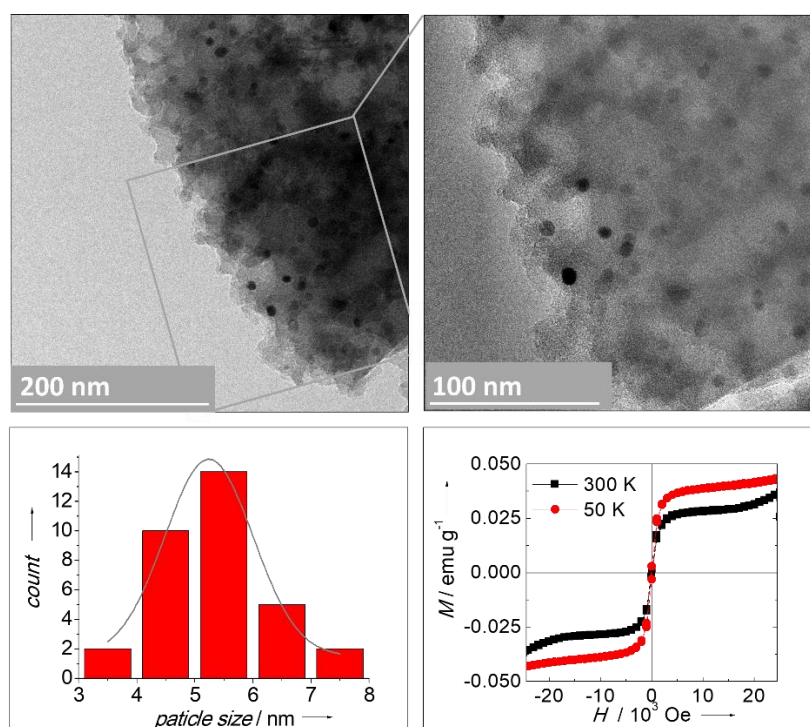


Figure 4. 2: Characterization of the mesostructured Ni@PS₆₀SiCN nanocomposite. Top) TEM images of Ni@PS₆₀SiCN. Bottom left) Ni particle-size distributions calculated from the TEM images. Bottom right) Magnetic measurements of Ni@PS₆₀SiCN at 300 and 50 K indicating superparamagnetism of the nanoparticles.

PXRD was performed to confirm the presence of an amorphous SiCN matrix and metallic Ni-NPs (Figure S1, bottom; see the Supporting Information). The reflexes at Bragg's angles of $2\theta = 44.5$ and 51.88° can be assigned to the (111) and (200) reflexes of a cubic Ni metal phase. Peak broadening is in agreement with the particle size observed by TEM. Also, TPR (temperature-programmed reduction) was performed by using unsupported NiO as a reference and the Ni@PS₆₀SiCN nanocomposite (Figure S5). An amount equal to 6% of the total nickel amount is oxidized, and 94% is metallic Ni. IR spectroscopy measurements confirmed a SiCN matrix (Figure S2). The appearance of only one broad band at $\tilde{\nu} = 600\text{--}1300\text{ cm}^{-1}$ verified the presence of Si–C and Si–N bonds. Scanning electron microscopy (SEM) (Figure 4. 3, top) established a homogeneous distribution of mesopores in Ni@PS₆₀SiCN. Nitrogen sorption measurements (Figure 3, bottom left) of Ni@PS₆₀SiCN revealed a typical type IV isotherm indicative of the presence of mesopores. The specific surface area calculated by the Brunauer–Emmett–Teller (BET) method was found to be $90\text{ m}^2\text{g}^{-1}$. In Figure 4. 3 (bottom right), the calculated pore-size distribution [N_2 at $-196.15\text{ }^\circ\text{C}$ on carbon (slit pore, NLDFT equilibrium model)] is shown. Ni@PS₆₀SiCN exhibits $> 95\%$ mesopores with a total pore volume of 0.283 mLg^{-1} and an average pore width of 8.2 nm .

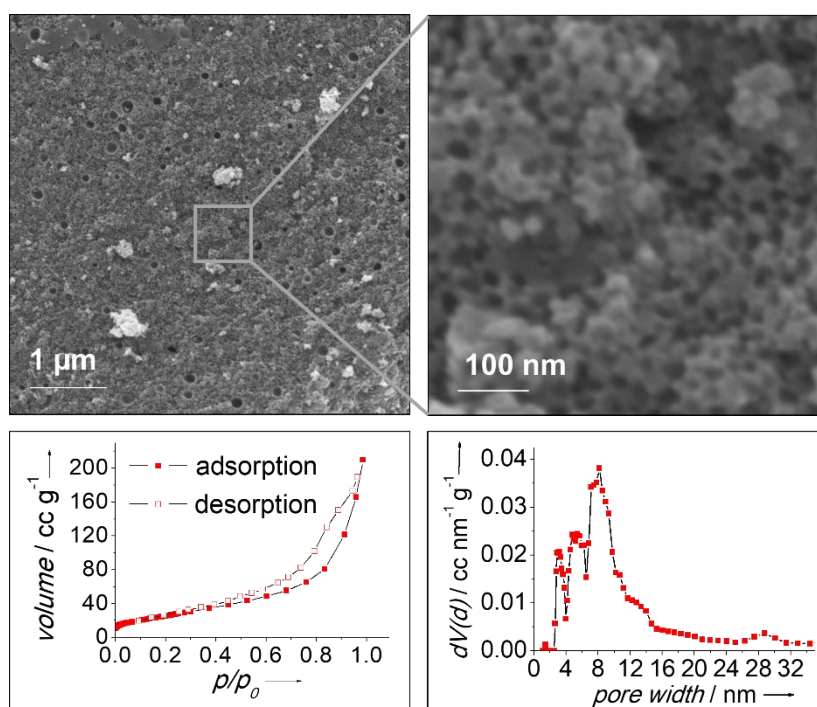


Figure 4. 3: Pore characterization of the mesoporous Ni@PS60SiCN nanocomposite. Top) SEM images showing the mesostructuring of the nanocomposite. Bottom left) Nitrogen sorption measurements. Bottom right) Calculated pore-size distribution [calculation model: N₂ at -196.15 °C on carbon (slit pore, NLDFT equilibrium model)].

The selective hydrogenation of nitroarenes to the corresponding anilines was evaluated in a 4:1 ethanol/water mixture under 5.0 MPa hydrogen. Water was added to increase the activity of the catalyst.^[21] We compared the activity of the Ni@PS₆₀SiCN nickel nanocomposite introduced here to that of a Ni@SiCN catalyst synthesized by using a slightly different procedure recently disclosed by us.^[14] Ni@SiCN was pyrolyzed at 700 °C. At this temperature, the support is more a highly crosslinked polysilazane than a stable SiCN material. Owing to low-temperature pyrolysis, remaining microporosity is observed for such a material. Even at this lower pyrolysis temperature of 700 °C, Ni^{II} is reduced to metallic Ni under the reductive atmosphere during pyrolysis. These Ni-NPs were characterized by TEM (average particle size of 1.59 nm; Figure S3) and PXRD (Figure S1). The pore characterization of the microporous Ni@SiCN nanocomposite indicated 42% micropores, only very small mesopores, a total pore volume of 0.062 mLg⁻¹, and an average pore width of 1.2 nm (Figure S4).

Both Ni catalysts showed catalytic activity and high selectivity in the hydrogenation of the nitro group at 110 °C. In comparison to the microporous Ni@SiCN catalyst, the novel mesoporous Ni@PS₆₀SiCN catalyst was found to be more active in the hydrogenation of 1-bromo-3-nitrobenzene to 3-bromoaniline. It was possible to reduce the catalyst loading from 6 to 1 mol% under the same conditions (Figure 4. 4, bottom left).

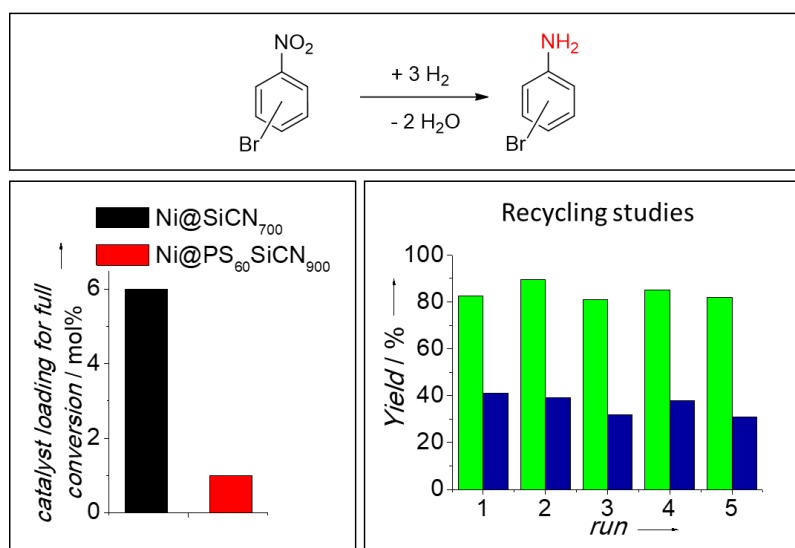
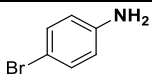
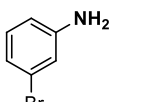
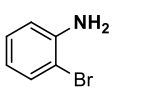
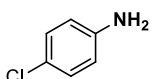


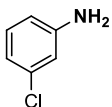
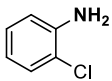
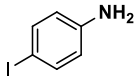
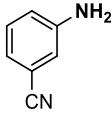
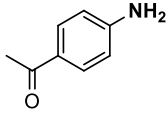
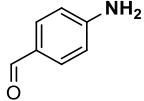
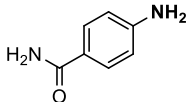
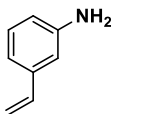
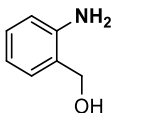
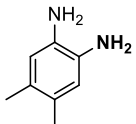
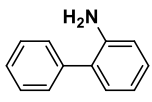
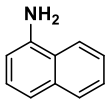
Figure 4. 4: Catalyst comparison. Top) Benchmark reaction; bottom left) comparison of catalyst loadings of both Ni catalysts for full conversion and > 99% selectivity [conditions: 110 °C, 5.0 MPa H₂, 1 mmol 1-bromo-3-nitrobenzene in 5 mL ethanol/water (4:1), 20 h]; bottom right) recycling of the Ni@PS₆₀SiCN catalyst over five consecutive runs [conditions for 80% yield (green): 110 °C, 5.0 MPa H₂, 0.5 mmol 1-bromo-4-nitrobenzene in 5 mL ethanol/water (4:1), 3 h, 6 mol% catalyst (1.76 mg Ni, 0.03 mmol, 75 mg nanocomposite); conditions for 40% yield (blue): 110 °C, 5.0 MPa H₂, 1.0 mmol 1-bromo-3-nitrobenzene in 5 mL ethanol/water (4:1), 3 h, 4 mol% catalyst (2.3 mg Ni, 0.04 mmol, 100 mg nanocomposite)], GC yield with *n*-dodecane as internal standard. A conversion of 80% was chosen to clearly see catalyst decomposition

To evidence the robustness and recyclability of the mesostructured catalyst, it was used in up to five runs (Figure 4. 4, bottom right). A conversion of 80% was chosen to clearly see any catalyst decomposition. Between the runs, the catalyst was washed with acetone to remove the substrate and then dried and reused. Even after the fifth run, no decrease in the selectivity or activity was observed. A leaching experiment demonstrated that only 0.1% of the total amount of nickel leached out of the nanocomposite during catalysis. Besides its unique recyclability, the catalyst is distinguished by its high tolerance to different functional groups. Various substituents on the phenyl ring of the nitrobenzene were tolerated under the optimized conditions (Table 4. 1).

Table 4. 1: Hydrogenation of nitroarenes to the corresponding anilines with the mesostructured Ni@PS₆₀SiCN catalyst.^[a]

Entry	Product	Conversion [%]	Selectivity [%]
1		> 99; isolated: 99	> 99
2		> 99	> 99
3 ^[b]		> 99	> 99
4		> 99	> 99

A Reusable Mesoporous Nickel Nanocomposite Catalyst for the Selective Hydrogenation of Nitroarenes in the Presence of Sensitive Functional Groups

5		> 99	> 99
6 ^[b]		> 99	>99
7		84	> 99
8		> 99	>99
9		> 99; isolated: 98	> 99
10		> 99	> 99
11 ^[b]		> 99	> 99
12		90	86
13 ^[b]		> 99	87
14 ^[c]		> 99; isolated: 93	> 99
15		isolated: 81	> 99
16		> 99	> 99
17 ^[b]		82	> 99

[a] Conditions: 110 °C, 5.0 MPa H₂, 1 mmol substrate, 20 h, 1 mol% catalyst (0.7 mg Ni, 0.01 mmol, 30 mg). [b] Catalyst: 3 mol%. [c] Catalyst: 2 mol%.

Different halogenides, including bromides, chlorides, and iodides, were tolerated (Table 4. 1, entries 1–7). No dehalogenation, not even in the presence of iodide, was observed. Only for the hydrogenation of

the sterically demanding ortho-substituted nitroarenes, the catalyst loading was increased to ensure full conversion. In addition, reducible functional groups were also successfully tolerated. For example, nitrile, keto, aldehyde, amide, and even vinyl groups were not hydrogenated by the catalyst (Table 4. 1, entries 8–12). The only byproduct formed in the reaction of 3-nitrostyrene was 3-ethylaniline (Table 4. 1, entry 12). Selective hydrogenation was observed for heterocyclic nitroquinoline (Table 4. 1, entry 16) with conservation of the aromatic system. In addition, a sterically demanding aliphatic nitro compound was hydrogenated to the corresponding amine (Table 4. 1, entry 17). All of the abovementioned nitro substrates were hydrogenated by the Ni@PS₆₀SiCN catalyst with high selectivity (82–99%).

4.3 Conclusion

In summary, we developed a novel mesoporous Ni-SiCN nanocomposite catalyst. The mesostructuring with an inexpensive polystyrene template was compatible with the generation of metallic Ni nanoparticles with diameters of 5.5 nm. The nickel nanoparticles, as the active sites of the catalyst, showed high activity in the hydrogenation of nitroarenes to the corresponding anilines. Additionally, the catalyst offered excellent tolerance to reducible groups such as C-C bonds, heteroaromatics, and nitrile, keto, aldehyde, and amide groups. Another specific advantage was the robustness of the catalyst, as it was recycled and reused over multiple runs without a decrease in activity or selectivity.

Acknowledgements

We thank the Deutsche Forschungsgemeinschaft, SFB 840, project B1, for financial support and Katja Dankhoff and Prof. Dr. Birgit Weber for magnetic measurements.

4.4 References

- [1] a) H.-U. Blaser, H. Steiner, M. Studer, *ChemCatChem* **2009**, *1*, 210–221; b) H. K. Kadam, S. G. Tilve, *RSC Adv.* **2015**, *5*, 83391–83407; c) H.-U. Blaser, *Science* **2006**, *313*, 312–313.
- [2] a) U. Siegrist, P. Baumeister, H.-U. Blaser in *Catalysis of Organic Reactions* (Ed.: F. Herkes) Chemical Industries Series 75, Marcel Dekker Inc., New York, **1998**, pp. 207; b) R. Raja, V. B. Golovko, J. M. Thomas, A. Berenguer-Murcia, W. Zhou, S. Xie, B. F. G. Johnson, *Chem. Commun.* **2005**, 2026–2028; c) H.-U. Blaser, U. Siegrist, H. Steiner, M. Studer in *Aromatic Nitro Compounds: Fine Chemicals through Heterogeneous Catalysis* (Eds.: R. A. Sheldon, H. van Bekkum), Wiley-VCH, Weinheim, **2001**, pp. 389–406.
- [3] a) Z. Li, J. Li, J. Liu, Z. Zhao, C. Xia, F. Li, *ChemCatChem* **2014**, *6*, 1333–1339; b) O. Verho, K. P. J. Gustafson, A. Nagendiran, C.-W. Tai, J.-E. Bäckvall, *ChemCatChem* **2014**, *6*, 3153–3159; c) O. Verho, A. Nagendiran, C.-W. Tai, E. V. Johnston, J.-E. Bäckvall, *ChemCatChem* **2014**, *6*, 205–211.
- [4] A. Corma, P. Serna, *Science* **2006**, *313*, 332–334.
- [5] R. M. Bullock, *Science* **2013**, *342*, 1054–1055.
- [6] F. A. Westerhaus, R. V. Jagadeesh, G. Wienhöfer, M.-M. Pohl, J. Radnik, A.-E. Surkus, J. Rabeah, K. Junge, H. Junge, M. Nielsen, A. Brückner, M. Beller, *Nat. Chem.* **2013**, *5*, 537–543.
- [7] R. V. Jagadeesh, A.-E. Surkus, H. Junge, M.-M. Pohl, J. Radnik, J. Rabeah, H. Huan, V. Schünemann, A. Brückner, M. Beller, *Science* **2013**, *342*, 1073–1076.
- [8] For further examples of Co catalyst describing the hydrogenation of nitroarenes please see: a) Z. Zhao, H. Yang, Y. Li, X. Guo, *Green Chem.* **2014**, *16*, 1274–1281; b) Z. Wei, J. Wang, S. Mao, D. Su, H. Jin, Y. Wang, F. Xu, H. Li, Y. Wang, *ACS Catal.* **2015**, *5*, 4783–4789; c) T. Stemmler, F. A. Westerhaus, A.-E. Surkus, M.-M. Pohl, K. Junge, M. Beller, *Green Chem.* **2014**, *16*, 4535–4540.
- [9] For further examples of Fe catalyst describing the hydrogenation of nitroarenes please see: a) O. Beswick, I. Yuranov, D. T. Alexander, L. Kiwi-Minsker, *Catal. Today* **2015**, *249*, 45–51; b) R. Dey, N. Mukherjee, S. Ahammed, B. C. Ranu, *Chem. Commun.* **2012**, *48*, 7982–7984; c) R. V. Jagadeesh, K. Natte, H. Junge, M. Beller, *ACS Catal.* **2015**, *5*, 1526–1529.
- [10] a) P. Baumeister, H. U. Blaser, W. Scherrer in *Studies in Surface Science and Catalysis*, Elsevier, **1991**; b) A. Corma, P. Serna, P. Concepción, J. J. Calvino, *J. Am. Chem. Soc.* **2008**, *130*, 8748–8753; c) S. Pisiewicz, D. Formenti, A.-E. Surkus, M.-M. Pohl, J. Radnik, K. Junge, C. Topf, S. Bachmann, M. Scalone, M. Beller, *ChemCatChem* **2016**, *8*, 129–134; d) P. Serna, A. Corma, *ACS Catal.* **2015**, *5*, 7114–7121; e) W. Gerhar et al., U.S. Patent 6, 395, 934, **2002**.
- [11] a) F. Cao, R. Liu, L. Zhou, S. Song, Y. Lei, W. Shi, F. Zhao, H. Zhang, *J. Mater. Chem.* **2010**, *20*, 1078–1085; b) T. Fu, M. Wang, W. Cai, Y. Cui, F. Gao, L. Peng, W. Chen, W. Ding, *ACS Catal.* **2014**, *4*, 2536–2543; c) P. Zhang, C. Yu, X. Fan, X. Wang, Z. Ling, Z. Wang, J. Qiu,

- Phys. Chem. Chem. Phys.* **2015**, *17*, 145–150; d) T. Wang, Z. Dong, T. Fu, Y. Zhao, T. Wang, Y. Wang, Y. Chen, B. Han, W. Ding, *Chem. Commun.* **2015**, *51*, 17712–17715; e) J. Xiong, J. Chen, J. Zhang, *Catal. Commun.* **2007**, *8*, 345–350; f) N. Mahata, A. F. Cunha, J. Órfão, J. L. Figueiredo, *Catal. Commun.* **2009**, *10*, 1203–1206; g) J. Wang, Z. Yuan, R. Nie, Z. Hou, X. Zheng, *Ind. Eng. Chem. Res.* **2010**, *49*, 4664–4669; h) Y. Zheng, K. Ma, H. Wang, X. Sun, J. Jiang, C. Wang, R. Li, J. Ma, *Catal. Lett.* **2008**, *124*, 268–276; i) X. Liu, X. Ma, S. Liu, Y. Liu, C. Xia, *RSC Adv.* **2015**, *5*, 36423–36427.
- [12] A heterobimetallic Rh/Ni nanocatalyst was previously shown to be capable of hydrogenating nitroarenes with reducible functional groups at room temperature by using 0.1 MPa of H₂ : S. Cai, H. Duan, H. Rong, D. Wang, L. Li, W. He, Y. Li, *ACS Catal.* **2013**, *3*, 608–612.
- [13] a) G. Glatz, T. Schmalz, T. Kraus, F. Haarmann, G. Motz, R. Kempe, *Chem. Eur. J.* **2010**, *16*, 4231–4238; b) M. Zaheer, G. Motz, R. Kempe, *J. Mater. Chem.* **2011**, *21*, 18825–18831; c) D. Forberg, J. Obenauf, M. Friedrich, S.-M. Hühne, W. Mader, G. Motz, R. Kempe, *Catal. Sci. Technol.* **2014**, *4*, 4188–4192.
- [14] M. Zaheer, C. D. Keenan, J. Hermannsdörfer, E. Roessler, G. Motz, J. Senker, R. Kempe, *Chem. Mater.* **2012**, *24*, 3952–3963.
- [15] M. Zaheer, T. Schmalz, G. Motz, R. Kempe, *Chem. Soc. Rev.* **2012**, *41*, 5102–5116.
- [16] a) S. K. T. Pillai, W. P. Kretschmer, M. Trebbin, S. Förster, R. Kempe, *Chem. Eur. J.* **2012**, *18*, 13974–13978; b) S. K. T. Pillai, W. P. Kretschmer, C. Denner, G. Motz, M. Hund, A. Fery, M. Trebbin, S. Förster, R. Kempe, *Small* **2013**, *9*, 984–989.
- [17] J. K. Ewert, C. Denner, M. Friedrich, G. Motz, R. Kempe, *Nanomaterials* **2015**, *5*, 425–435.
- [18] J. K. Ewert, D. Weingarth, C. Denner, M. Friedrich, M. Zeiger, A. Schreiber, N. Jäckel, V. Presser, R. Kempe, *J. Mater. Chem. A* **2015**, *3*, 18906–18912.
- [19] For a related SiC catalyst please see: M. Zaheer, J. Hermannsdörfer, W. P. Kretschmer, G. Motz, R. Kempe, *ChemCatChem* **2014**, *6*, 91–95.
- [20] P. C. Healy, M. R. Bendall, D. M. Doddrell, B. W. Skelton, A. H. White, *Aust. J. Chem.* **1979**, *32*, 727–735.
- [21] M. Pietrowski, M. Zieliński, M. Wojciechowska, *Catal. Lett.* **2009**, *128*, 31–35.

4.5 Supporting Information

4.5.1 Methods

4.5.1.1 General considerations

All reactions were carried out under dry argon or nitrogen using standard Schlenk and glove box techniques. Solvents were dried and distilled from sodium benzophenone ketyl before use. Deuterated solvents obtained from Cambridge Isotope Laboratories were degassed, dried using molecular sieves and distilled prior to use. All chemicals were purchased from commercial sources with purity over 95% and used without further purification. Polysilazane KiON HTT 1800 was purchased from Clariant Advanced Materials GmbH, Frankfurt (Germany) and used without further purification. Styrene (> 99% purity, Sigma Aldrich, Steinheim, Germany) and divinylbenzene (technical grade, 55%, Aldrich Chemistry, Steinheim, Germany) were destabilized over alumina B column (ICN Biomedicals GmbH, Eschwege, Germany). Ceramization was carried out under nitrogen atmosphere in a high temperature furnace (Gero, Berlin, Germany). X-ray powder diffractograms were received by a X'Pert MPD Pro (PANalytical, Almelo, NL, $\text{CuK}\alpha$ -Strahlung, 1.54178 Å) in Bragg-Brentano-geometry and with a X'Celerator detector. Transmission electron microscopy (TEM) was carried out by using a Varian LEO 9220 (200 kV) instrument. The sample was suspended in chloroform and sonicated for 5 min. Subsequently a drop of the suspended sample was placed on a grid (Plano S 166-3) and allowed to dry. SEM was performed using a Zeiss Field-Emission-Scanning-Electron-Microscope (FESEM) LEO 1530 GEMINI. The acceleration voltage was 1-5 kV. The samples were sputter-coated with a 1.3 nm layer of platinum. FT-IR measurements were received using a Perkin.Elmer FTIR-spectrum 100. N_2 sorption was performed using a Nova2000e (Quantachrome) instrument. The specific surface areas were calculated using p/p_0 -values from 0.05-0.31 (BET). The pore width and average pore volume were calculated by DFT calculations [calculation model: N_2 at -196,15 °C on carbon (slit pore, NLDFT equilibrium model)]. Magnetic measurements on the compounds were carried out using a SQUID MPMS-XL5 from Quantum Design with the field range of -3 to 3 T in hysteresis mode. The sample was prepared in a gelatin capsule held in a plastic straw under protective atmosphere. The raw data were corrected for the diamagnetic part of the sample holder. ICP-OES measurements were performed using a Vista-pro radical model from Varian. GC analysis were carried out on an Agilent 6890N Network GC system equipped with a HP-5 column (30 m x 0.32 mm x 0.25 µm) and a flame ionization detector. *N*-dodecane was used as internal standard. GC-MS analyses were carried out by using an Agilent Technologies 7890A/MSD 5985C system equipped with a HP-5 column (30 m x 0.32 mm x 0.25 µm). NMR spectra were measured with an INOVA 300 MHz spectrometer at 298 K. Chemical shifts are reported in ppm relative to the deuterated solvents.

The polystyrene spheres with a diameter of 60 nm (PS₆₀)^[S1] and the nacnac ligand^[S2] were synthesized by reported methods. According to the reported procedures for β -diiminato titanium complexes.^[S3] The nacnac-nickel (II) complex was synthesized in 90% yield.

4.5.1.2 Catalyst synthesis

Ni@PS₆₀SiCN mesoporous material was generated by the reaction of PS₆₀ spheres, the nickel complex and KiON HTT1800 in toluene. In a vial placed in a Schlenk tube, 0.5 g PS₆₀ were degassed and dispersed in 15 mL toluene under vigorous stirring. Subsequently, 0.25 g of KiON HTT 1800 (3.88 mmol), 0.025 g dicumylperoxid (10 wt% of the polysilazane) and a solution of the nacnac-nickel complex (0.102 g, 0.194 mmol, Ni/Si=1:20) in 1 mL toluene were added. Transmetalation took place by stirring the suspension for 30 min. Afterwards, the suspension was annealed at 130 °C for 20 hours without stirring, during which the solvent came out of the vial into the Schlenk tube. Removing of the solvent under vacuum and annealing the structured preceramic polymer for 20 hours at 130 °C, yielded the greenbody as a dark green solid. It was pyrolyzed under N₂ flow (pyrolysis program see Scheme S1). The ceramic yield was approximately 30%. After ball milling for 15 minutes, the catalyst was pretreated by applying it for 1 day at 100 °C and 3.0 MPa H₂ pressure.

4.5.1.3 Catalysis

The catalytic selective hydrogenation of nitroarenes to the corresponding anilines was done in a Parr autoclave under hydrogen pressure (5.0 MPa). The catalyst was placed in a glass tube and was dispersed in 4 mL ethanol and 1 mL distilled water. After adding the nitroarene and a magnetic bar, the tube was placed in the reactor and it was heated to 110 °C for 20 hours. After cooling, *n*-dodecane was added and the mixture was extracted with diethyl ether, dried over Na₂SO₄ and analyzed by GC and GC/MS. In case of the aliphatic nitro compound (entry 17), the autoclave was placed in a liquid nitrogen bath after the catalysis. After cooling, *n*-dodecane was added and the mixture was extracted with ethyl acetate, dried over Na₂SO₄ and analyzed by GC and GC/MS.

4.5.1.4 Ceramization

RT $\xrightarrow{1\text{K/min}}$ 300 °C (3 h) $\xrightarrow{1\text{K/min}}$ 400 °C (3 h) $\xrightarrow{0.5\text{K/min}}$ 500 °C (3 h) $\xrightarrow{1\text{K/min}}$ 600 °C (4 h)
 $\xrightarrow{0.5\text{ K/min}}$ 700 °C (Oh) $\xrightarrow{1\text{ K/min}}$ 900 °C (0.5 h) $\xrightarrow{4\text{ K/min}}$ RT

Scheme S1: Tailored pyrolysis program under N₂ flow for synthesis of the mesoporous Ni@PS₆₀SiCN nanocomposite.

4.5.2 Characterization

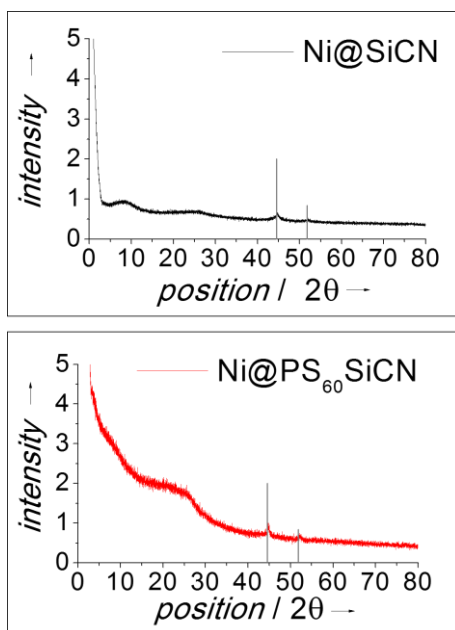


Figure S1: PXRD pattern of Ni@SiCN (top) and Ni@PS₆₀SiCN (botto) ceramic pyrolyzed at 700 °C and 900 °C, respectively. The characteristic reflections of metallic nickel (reference code: 00-004-0850) are shown at 44.5 2θ and 51.8 2θ.

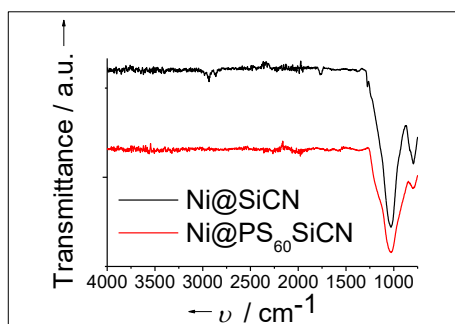


Figure S2: FT-IR measurements (red: Ni@PS₆₀SiCN; black: Ni@SiCN). The broad band at 600-1300 cm⁻¹ confirms the presence of Si-C and Si-N bonds in both nanocomposites.

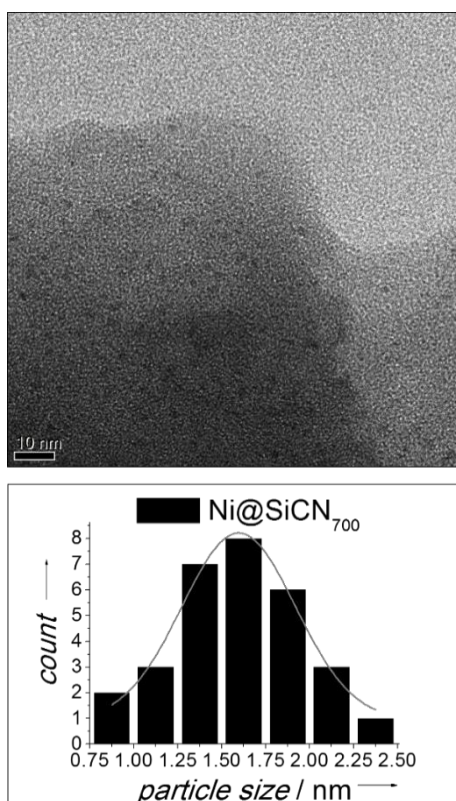


Figure S3: Characterization of the microporous Ni@SiCN nanocomposite. Top: TEM image of Ni@SiCN. Bottom: corresponding particle size distribution calculated by the TEM image. The average particle size is 1.6 nm.

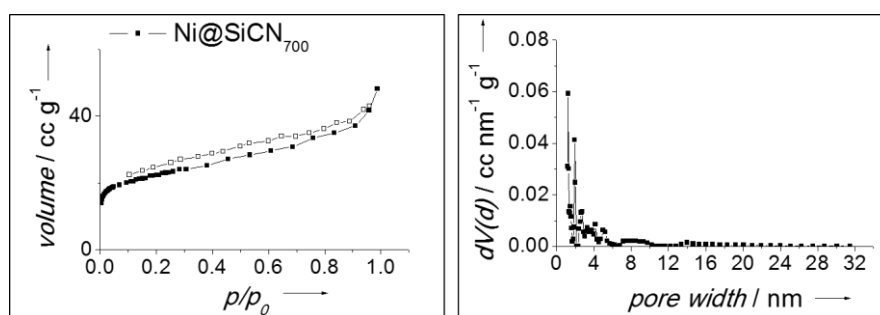


Figure S4: Pore characterization of the microporous Ni@SiCN nanocomposite indicating the 42% micropores, only very small mesopores, a total pore volume of 0.062 cc/g and an average pore width of 1.2 nm. Left: Nitrogen sorption measurements. Right: Calculated pore size distribution (calculation model: N₂ at 77 K on carbon (slit pore, NLDFT equilibrium model)).

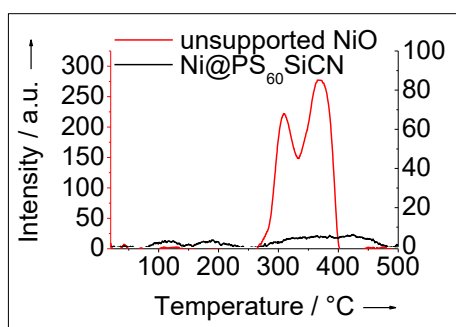


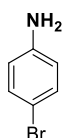
Figure S5: TPR (temperature programmed reduction) indicating 6% NiO in the Ni@PS₆₀SiCN nanocomposite.

4.5.2.1 Leaching experiment

30 mg Ni@PS₆₀SiCN catalyst and 3 mL H₂O were stirred at 110 °C and 5.0 MPa H₂ pressure for 20 hours. The water phase was separated and analyzed by ICP-OES. 0.1% of the total Nickel amount could be found.

4.5.3 Characterization of some isolated products

Table 1; Entry 1



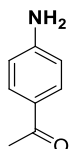
isolated yield: 170 mg (99%)

M(C₆H₆BrN): 172.02 g mol⁻¹

¹H NMR (300 MHz, CDCl₃, 298 K): δ = 7.25 (d, J = 8.2 Hz, 2H), 6.58 (d, J = 8.8 Hz, 2H), 3.66 (s_{br}, 2H) ppm.

¹³C NMR (75 MHz, CDCl₃, 298 K): δ = 145.41, 132.03, 116.72, 110.19 ppm.

Table 1, Entry 9



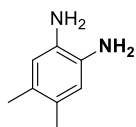
isolated yield: 132 mg (98%)

M(C₈H₉NO): 135.16 g mol⁻¹

¹H NMR (300 MHz, CDCl₃, 298 K): δ = 7.82 (d, J = 8.2 Hz, 2H), 6.66 (d, J = 8.2 Hz, 2H), 4.13 (s_{br}, 2H), 2.52 (s, 3H) ppm.

¹³C NMR (75 MHz, CDCl₃, 298 K): δ = 196.46, 151.10, 130.73, 127.71, 113.63, 26.03 ppm.

Table 1, Entry 14



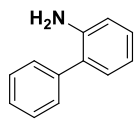
isolated yield: 126 mg (93%)

M(C₈H₁₂N₂): 136.19 g mol⁻¹

¹H NMR (300 MHz, CDCl₃, 298 K): δ = 6.53 (s, 2H), 3.20 (s_{br}, 4H), 2.14 (s, 6H) ppm.

¹³C NMR (75 MHz, CDCl₃, 298 K): δ = 132.28, 127.89, 118.49, 18.87 ppm.

Table 1, Entry 15



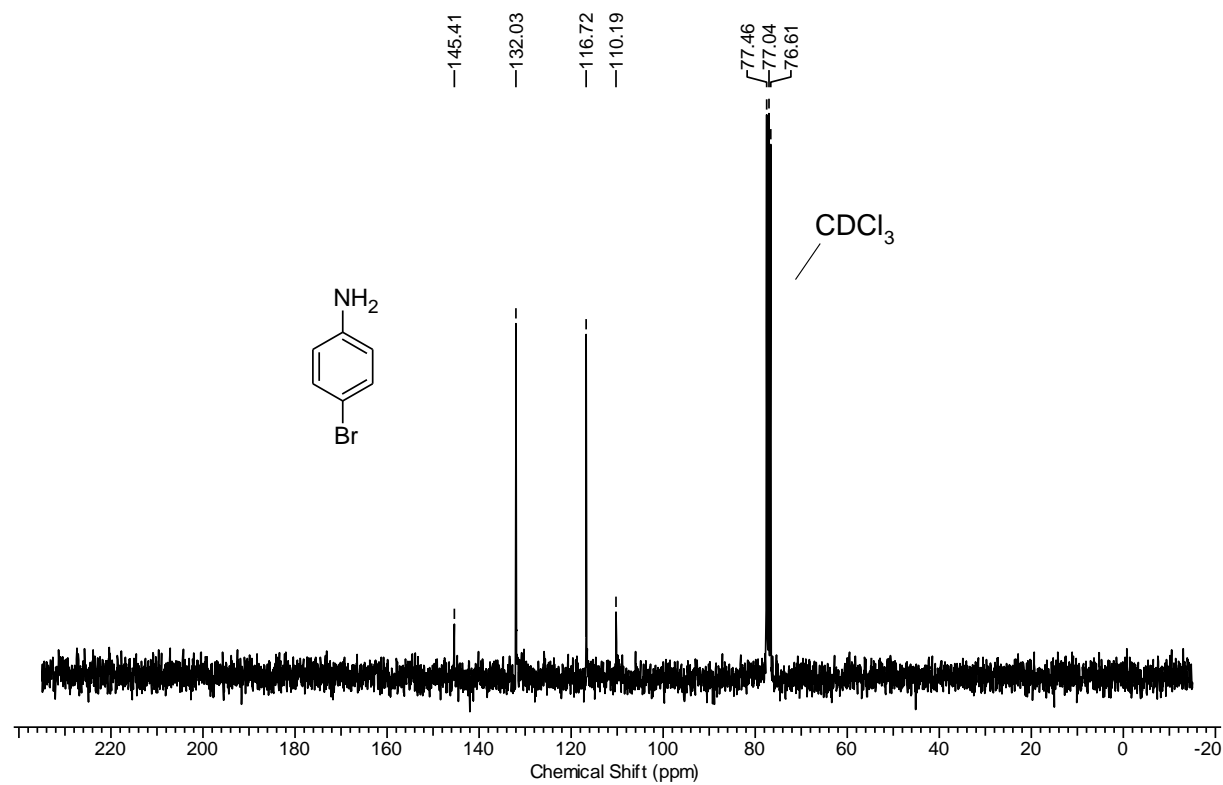
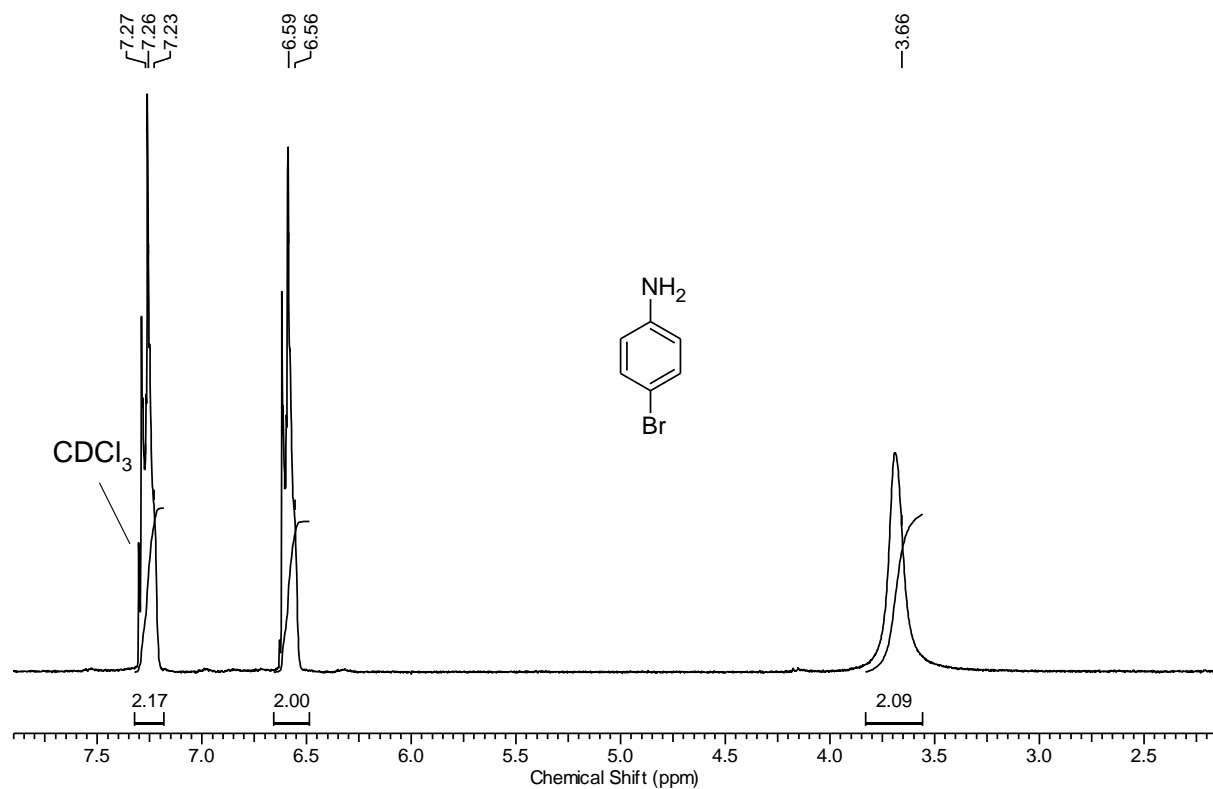
isolated yield: 137 mg (81%)

M(C₁₂H₁₁N): 169.22 g mol⁻¹

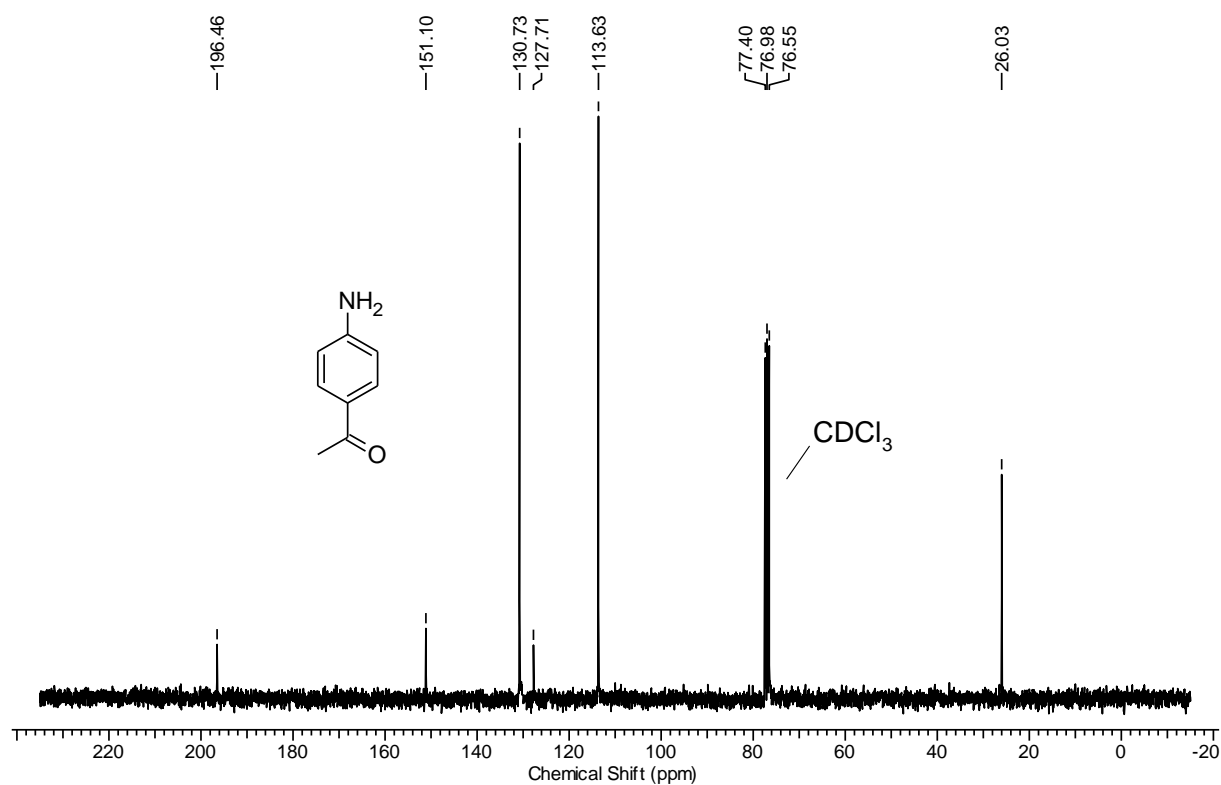
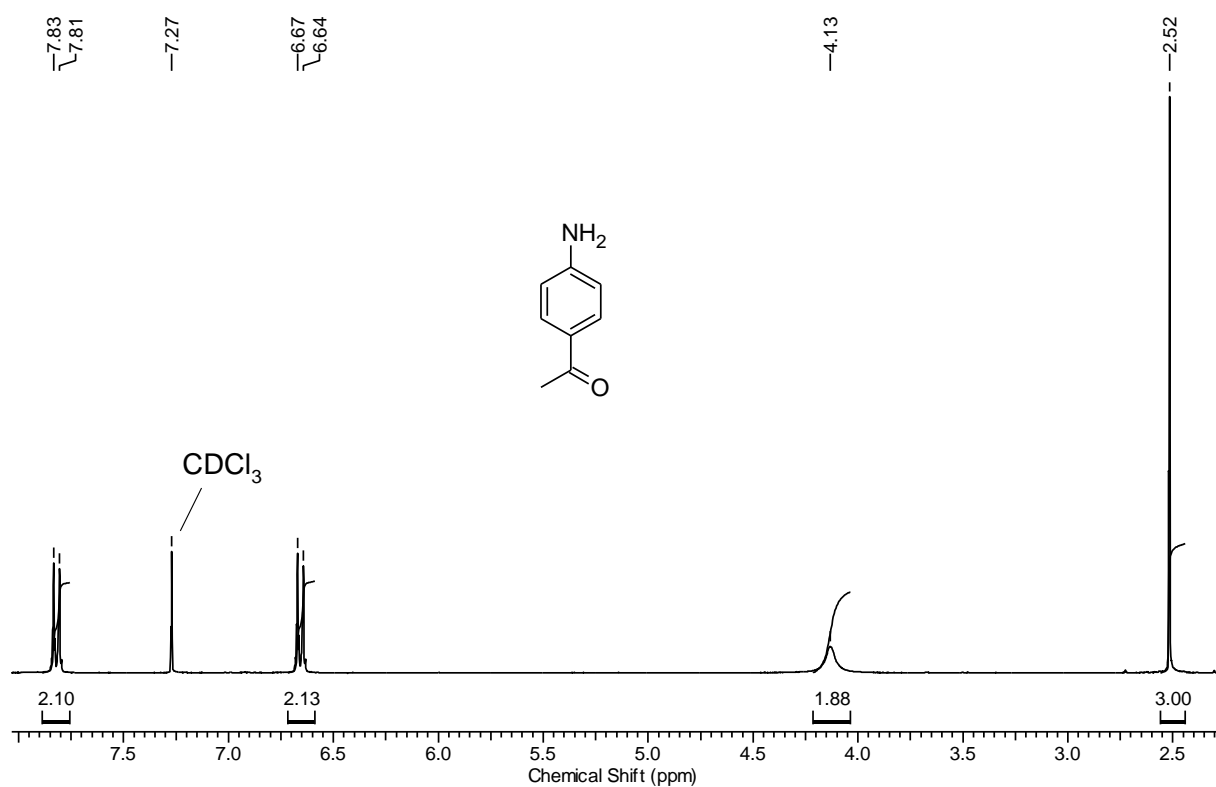
¹H NMR (300 MHz, CDCl₃, 298 K): δ = 7.48-7.43 (m, 4H), 7.39-7.34 (m, 1H), 7.21-7.14 (m, 2H), 6.88-6.79 (m, 2H), 3.67 (s_br, 2H) ppm.

¹³C NMR (75 MHz, CDCl₃, 298 K): δ = 143.49, 139.50, 132.03, 130.47, 129.10, 128.82, 128.50, 127.63, 127.18, 118.66, 116.72, 115.61 ppm.

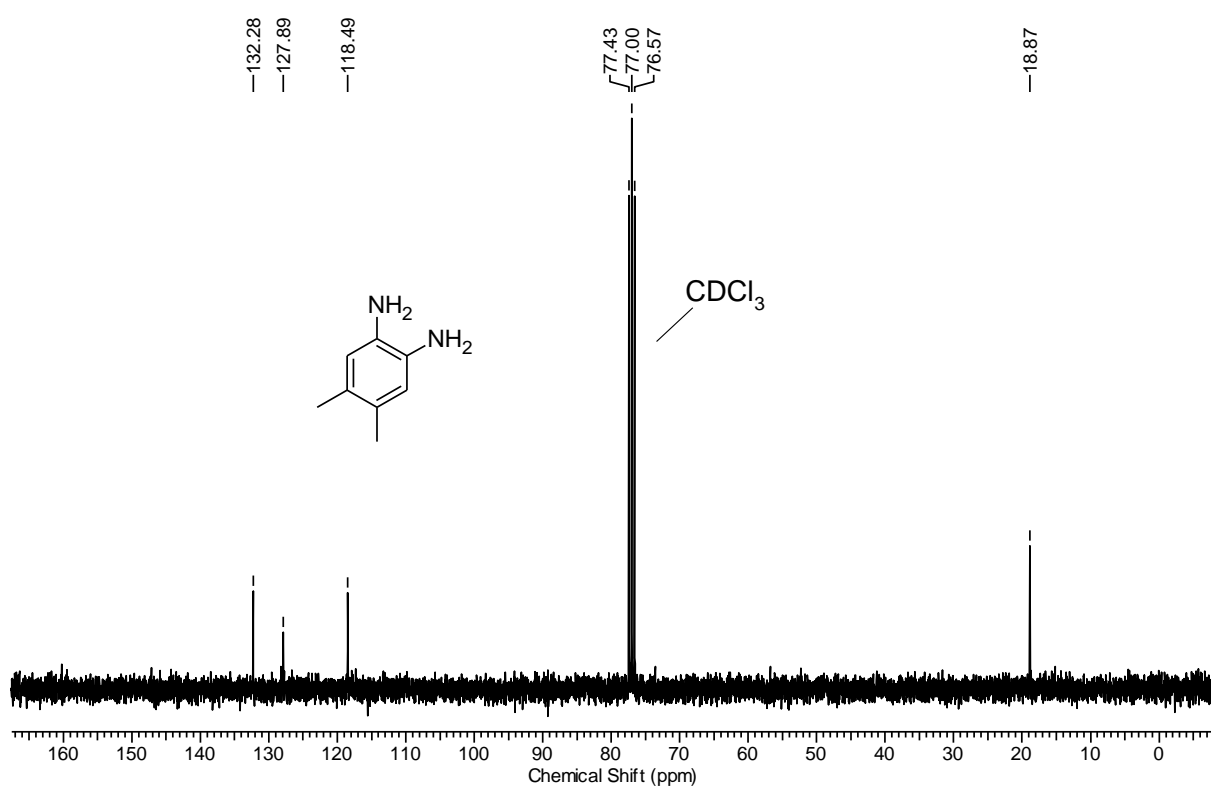
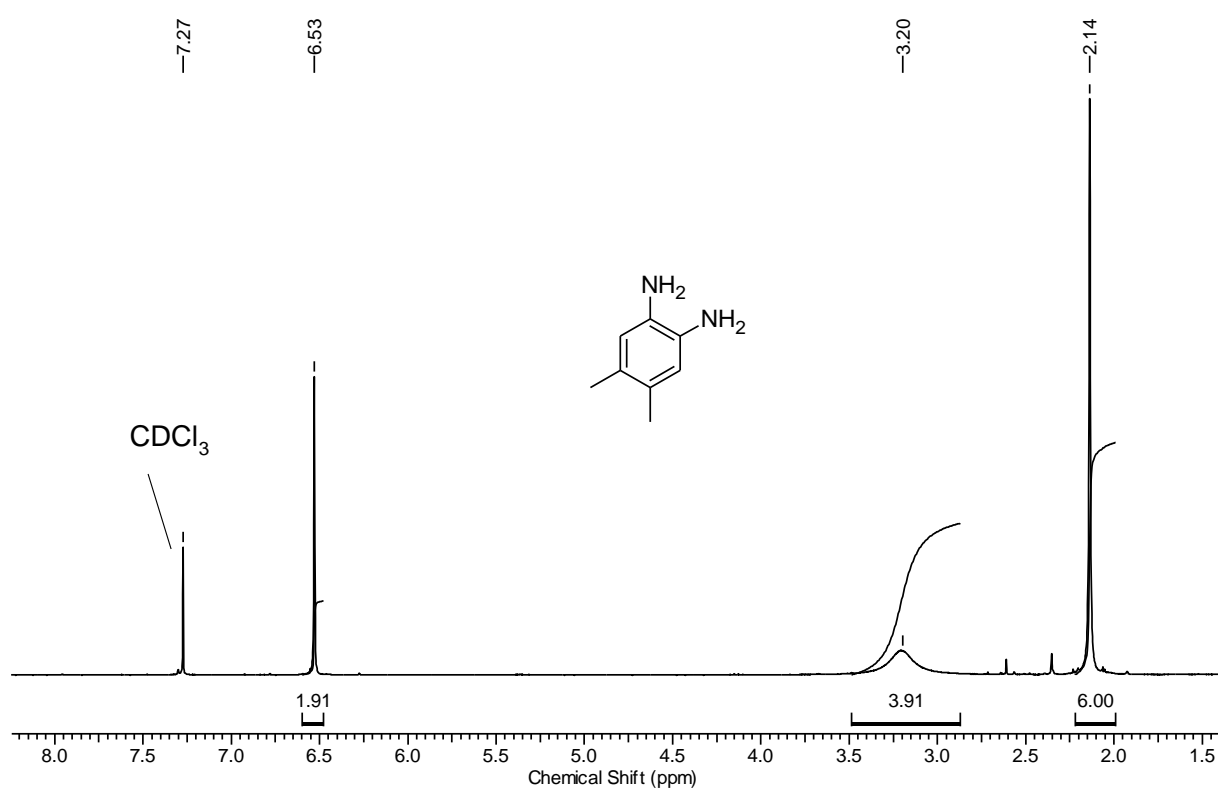
4.5.4 NMR Spectra



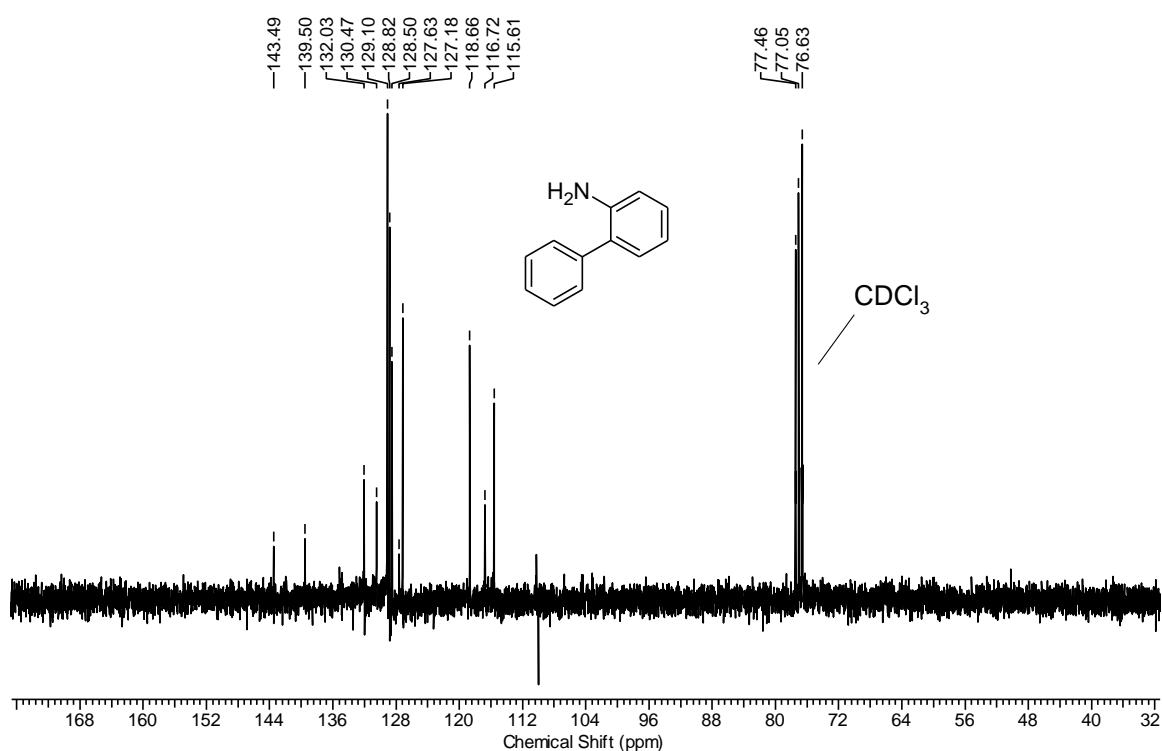
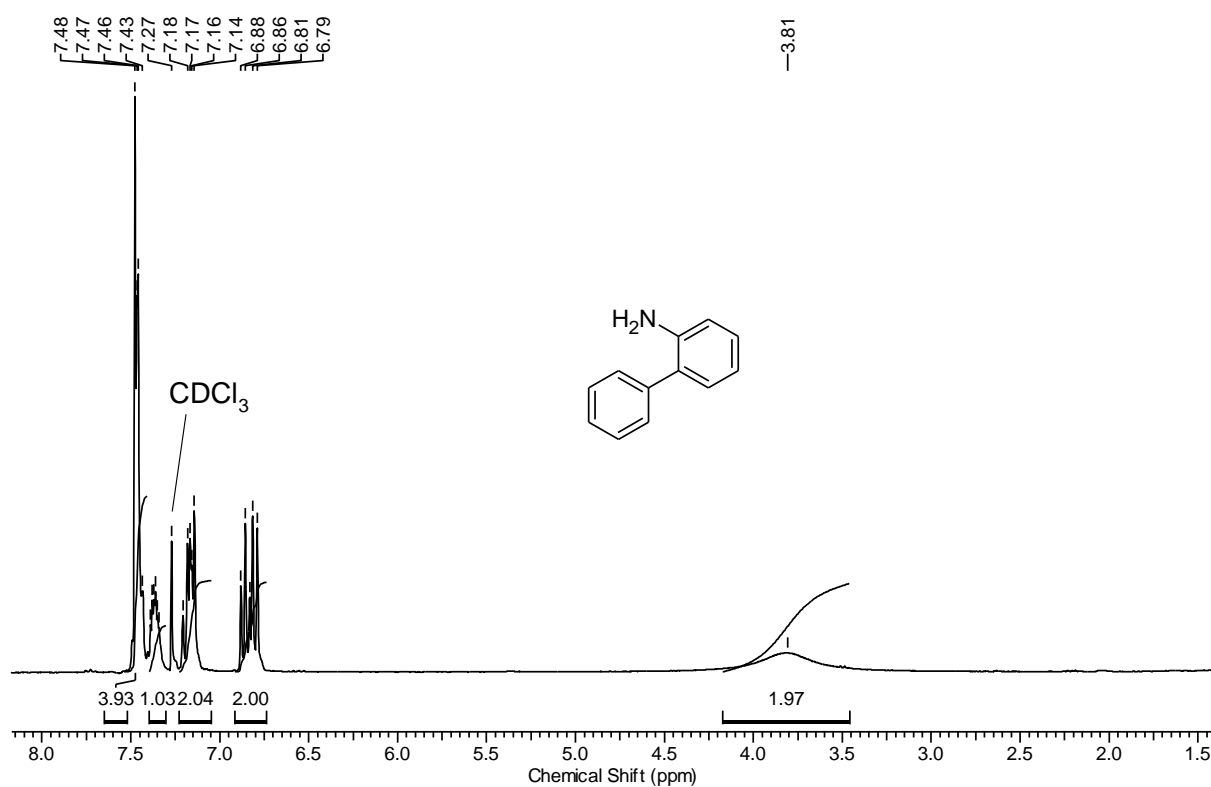
A Reusable Mesoporous Nickel Nanocomposite Catalyst for the Selective Hydrogenation of Nitroarenes in the Presence of Sensitive Functional Groups



A Reusable Mesoporous Nickel Nanocomposite Catalyst for the Selective Hydrogenation of Nitroarenes in the Presence of Sensitive Functional Groups



A Reusable Mesoporous Nickel Nanocomposite Catalyst for the Selective Hydrogenation of Nitroarenes in the Presence of Sensitive Functional Groups



4.5.5 Supplementary References

- [S1] J. K. Ewert, C. Denner, M. Friedrich, G. Motz, R. Kempe *Nanomaterials* **2015**, *5*, 425–435.
- [S2] L.-M. Tang, Y.-Q. Duan, X.-F. Li, Y.-S. Li, *J. Organomet. Chem.* **2006**, *691*, 2023–2030.
- [S3] M. Zaheer, J. Hermannsdörfer, W. P. Kretschmer, G. Motz, R. Kempe *ChemCatChem* **2014**, *6*, 91–95.

5 General synthesis of primary amines via reductive amination employing a reusable nickel catalyst

Gabriela Hahn^[a], Peter Kunnas^[b], Niels de Jonge^[b,c], Rhett Kempe^{*[a]}

[a] Inorganic Chemistry II – Catalyst Design, University of Bayreuth, Universitätsstr. 30, 95440 Bayreuth (Germany).

[b] INM – Leibniz Institute for New Materials, Campus D2 2, 66123 Saarbrücken (Germany).

[c] Department of Physics, Saarland University, Campus A5 1, 66123 Saarbrücken (Germany).

Published in *Nature Catalysis* **2019**, 2, 71.

The final publication is available at Springer via <https://doi.org/10.1038/s41929-018-0202-6>

Keywords: green chemistry, heterogeneous catalysis, inorganic chemistry, synthetic chemistry methodology

Abstract: Reusable catalysts based on earth-abundant metals with a broad applicability in organic synthesis are a key to a more sustainable production of fine chemicals, pharmaceuticals and agrochemicals. Herein, we report on a nanostructured nickel catalyst for the general and selective synthesis of primary amines via reductive amination, employing ammonia dissolved in water. Our catalyst, which operates at low temperature and pressure, is highly active, reusable and easy to handle. The synthesis from a specific nickel complex and γ -Al₂O₃ is straightforward, with the ligand-metal combination of this complex being crucial. Aldehydes (including purely aliphatic ones), aryl-alkyl, dialkyl, and diaryl ketones can all be converted smoothly into primary amines. In addition, the amination of pharmaceuticals, bioactive compounds and natural products is demonstrated. Many functional groups — including hydrogenation-sensitive examples — are tolerated. We expect that our findings will inspire others to develop reusable and nanostructured earth-abundant metal catalysts for complex organic transformations.

5.1 Introduction

The use of earth-abundant metals in catalysis, a key technology of our century, is a potential strategy for the conservation of noble metals. A further advantage is that these base metal catalysts show totally different selectivity patterns compared to known systems based on precious metals. Reactions that are

not possible with precious metal catalysts are now conceivable and the scope of reactions can be extended. Significant progress has been made regarding the development of homogeneous earth-abundant 3d metal catalysts in recent years.^[1–10] The use of reusable nanostructured earth-abundant 3d metal catalysts for a broad applicability in complex organic synthesis is highly desirable and has been disclosed only rarely.^[11–13] Amines are a very important class of chemical compounds and present in many fine chemicals^[14], drugs^[15] and materials^[16]. One of the most attractive methods for the synthesis of primary amines is the catalytic reductive amination of aldehydes and ketones by ammonia and hydrogen.^[17–21] Most of the catalysts, homogeneous^[22–24] and heterogeneous^[25–31], described for this reaction are based on noble metals. Inspired by very early work^[32,33] involving Raney nickel catalysts^[34–36] that operate under drastic conditions with low selectivity and scope, we became interested in developing a highly efficient and selective Ni catalyst. Raney nickel is pyrophoric, difficult to handle and limited with regard to its reusability. Beller's group very recently disclosed a Co catalyst for the synthesis of various amines including primary amines via reductive amination employing ammonia gas though high pressures of H₂ and ammonia were required.^[13]

Beside reductive amination, aqueous ammonia, an attractive since easy to handle source of ammonia, has been employed successfully in catalytic reactions for the synthesis of primary amines such as hydroaminomethylation^[37], telomerization of ammonia and butadiene^[38], allylic substitutions^[39,40], cross couplings^[41], benzene oxyamination^[42] and amine alkylation^[43]. We have recently introduced a variety of homogeneous earth-abundant catalysts^[44–50] and reusable nanostructured catalysts for hydrogen storage^[51] and novel organic reactions^[52], including earth-abundant metal catalysts^[53].

Herein, we report on a Ni catalyst which is easy to synthesize from a Ni complex and commercially available γ -Al₂O₃. The combination of the specific coordination compound and this oxide support is crucial. Our catalyst is simple to handle, reusable and highly selective for the synthesis of primary amines via reductive amination. We use ammonia dissolved in water and can work under very mild conditions (80 °C and 1 MPa H₂ pressure). A broad substrate scope (more than 50 examples) and a very good tolerance of functional groups have been observed. Aldehydes, including purely aliphatic ones, in addition to aryl-alkyl, dialkyl and diaryl ketones can be converted smoothly into primary amines. Furthermore, the amination of pharmaceuticals, bioactive compounds and natural products has been demonstrated. Many functional groups, including those sensitive towards hydrogenation such as C–C double bonds or an iodo-aryl substituent, can be tolerated.

5.2 Results

Catalyst synthesis and characterization

Our Ni catalyst was synthesized in a simple two-step procedure (Figure 5. 1). In the first step, commercial γ -Al₂O₃ was impregnated with a solution of the Ni complex **I** in acetonitrile. After evaporation of the solvent at 110 °C, the sample was pyrolyzed under a constant nitrogen flow at 700 °C followed by

treatment under a reductive atmosphere (N_2/H_2 95/5) at 550 °C. Inductively coupled plasma optical emission spectrometry (ICP-OES) measurement verifies an amount of 3.5 wt% nickel in the catalyst material synthesized (Supplementary Note 1). Temperature programmed reduction (TPR) measurement of the latter shows a hydrogen consumption at 300 °C, confirming the presence of accessible Ni oxide species (Supplementary Fig. 1). The nitrogen physisorption measurements (Supplementary Fig. 2) of the commercially available γ - Al_2O_3 and the catalyst material synthesized indicate a slight decrease of the specific surface area (Brunauer–Emmett–Teller method) from 220 to 210 m^2g^{-1} and a nearly identical pore size distribution (> 95% mesopores with a total pore volume of 0.560 mLg^{-1} and an average pore width of 5.8 nm). Magnetic measurements of the Ni catalyst material (Supplementary Fig. 3) indicate the presence of superparamagnetic Ni nanoparticles (Ni-NPs). Powder X-ray diffraction (PXRD) was performed (Supplementary Fig. 4) to confirm the presence of metallic Ni-NPs (cubic Ni metal phase) and, as expected, γ - Al_2O_3 .

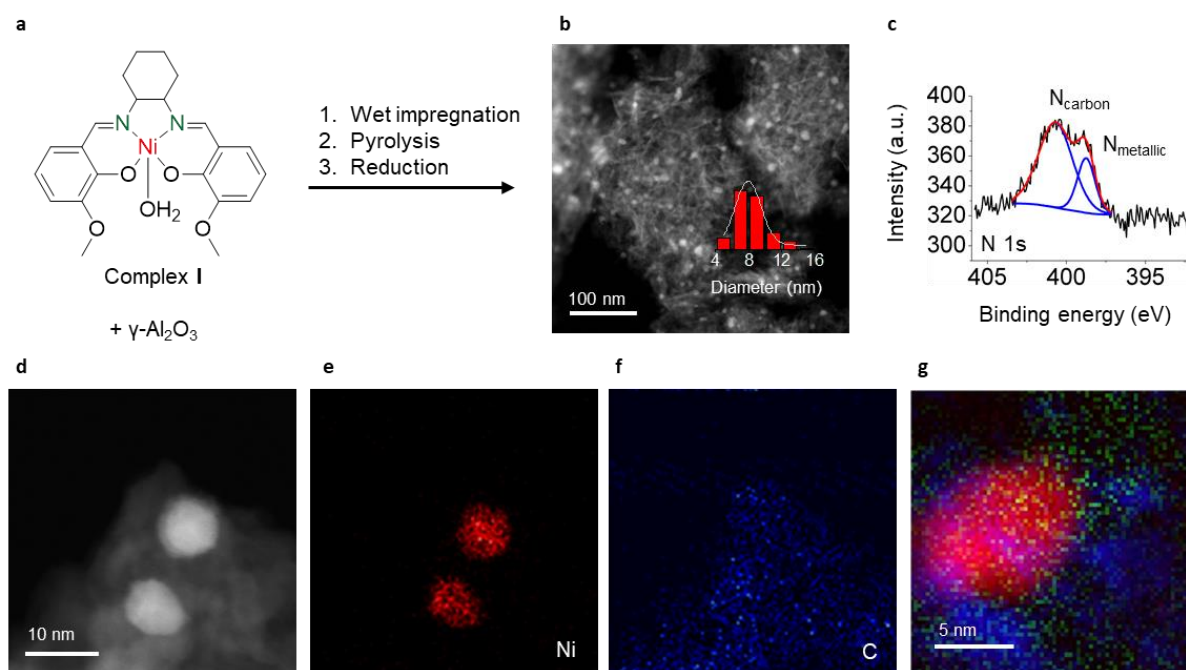


Figure 5. 1: Synthesis and characterization of the Ni catalyst. **a**, Preparation of the nickel Ni catalyst. (1) Wet impregnation of commercially available γ - Al_2O_3 with a solution of complex **I** in acetonitrile. (2) Pyrolysis of the impregnated γ - Al_2O_3 under nitrogen atmosphere up to 700 °C (2 °C/min to 300 °C [dwelling time: 30 min]; 5 °C/min to 700 °C [dwelling time: 30 min]) and reduction of the pyrolyzed sample under reductive atmosphere (5 °C/min to 550 °C [dwelling time: 180 min]). **b**, HAADF image of the Ni/ Al_2O_3 catalyst. Al_2O_3 is covered with homogeneously dispersed Ni-nanoparticles. **c**, XPS of the N 1s electrons. The different N species are labelled as N_{carbon} for the nitrogen bond to carbon and $N_{metallic}$ for the nitrogen bond to the metal. Due to the ligand containing nitrogen, which decomposes during pyrolysis, N atoms are located at the surface of the catalyst. **d–g**, HAADF-STEM analysis of Ni/ Al_2O_3 , representative EDX element maps of nickel (**e**, red) and carbon (**f**, blue) and the overlapped EELS element maps (**g**) of Ni (red), C (blue) and N (green).

Transmission electron microscopy (TEM) analysis provides evidence for the presence of small Ni-NPs with an average diameter of 8 nm and a homogeneous distribution (Supplementary Fig. 5, 6). Additionally, the Ni catalyst material was investigated by high-angle annular dark-field scanning transmission electron microscopy (HAADF-STEM) measurements and the corresponding energy-dispersed X-ray (EDX) element maps (for nickel (red) and carbon (blue) see Figure 5. 1 d-f; for aluminum and oxygen

see Supplementary Fig. 7). To get an insight of the direct environment of the nanoparticle, electron energy loss spectroscopy (EELS) was performed. A high magnification ($4 \cdot 10^6$ fold) areal density map shows the interface of the matrix and the Ni NP (Figure 5. 1 g and Supplementary Fig. 8). Here, the carbon component (C: blue) is connected to the Ni NP (Ni: red) and a weak signal of nitrogen (N: green) is present in the vicinity of the Ni NP and in the matrix as well. X-ray photoelectron spectroscopy (XPS) measurements (Figure 5. 1 c and Supplementary Fig. 9) identifies two different N species. Carbon-linked N species with a binding energy of ~ 402 eV coexist with N species linked to a metal (binding energy ~ 399 eV). Furthermore, XPS indicates the presence of both metallic Ni^0 and Ni^{2+} species on the catalyst surface (see Supplementary Fig. 9). The ratio of $\text{Ni}^0:\text{Ni}^{2+}$ is approximately 1:1.5. We conclude from the HAADF-STEM and the XPS investigations that the surface of the alumina partially covered by homogeneously distributed Ni-NPs embedded in an N-doped carbon layer, caused by the decomposition of the Ni complex **I**. Finally, NH_3 -temperature programmed desorption (TPD) was carried out to identify available acidic sites and to confirm that the carbon layer is not covering the $\gamma\text{-Al}_2\text{O}_3$ completely (Supplementary Fig. 10). It is conceivable that these acidic sites promote the activation of the carbonyl groups, especially for the challenging transformation of ketones.

Screening of the optimal reaction conditions

The synthesis of benzylamine from benzaldehyde and aqueous ammonia was investigated to find broadly applicable reaction conditions for the Ni-catalyzed reductive amination. Solvent screening (Supplementary Table 1) revealed that the formation of primary amines takes place preferentially in protic solvents and, most importantly, water can suppress the formation of the undesired by-product N-benzylidene-1-phenylmethanamine efficiently. A significantly lower amine formation is observed if solutions of ammonia in ethanol or dioxane are used instead of ammonia in water (see Supplementary Table 2). Other significant influences on the yield of primary amine are the amount of ammonia, the pyrolysis temperature of the catalyst and the metal loading of the catalyst (Supplementary Table 3, 4). In summary, the reaction can be carried out smoothly and selectively with a 4 wt% Ni catalyst pyrolyzed at 700 °C, 0.5 mL of 25% aqueous ammonia (6.7 mmol) and 2.0 mL of addition water at 80 °C and 1 MPa pressure of H_2 . Attempts to conduct reactions at 0.1 MPa H_2 pressure (orsat blowball or autoclave) failed. Low primary amine formation (acetophenone) or nearly quantitative byproduct formation (benzaldehyde) were observed despite an increase of catalyst loading (8.6 mol%) and a prolongation of the reaction time (48 h) (see Supplementary Table 5). We were interested in comparing different commercial supports and various Ni sources to demonstrate the superior activity of our catalyst, which we believed is based on the combination of complex **I** and $\gamma\text{-Al}_2\text{O}_3$ (Table 5. 1). It is remarkable that only the use of CeO_2 and our Ni complex **I** showed some activity in the reductive amination of benzaldehyde, while catalysts based on other supports, such as activated carbon, SiO_2 or TiO_2 , are not suitable for this reaction. NH_3 -TPD studies of our catalyst indicate the presence of acidic sites suitable for ammonia binding. In addition, the meso-pores (95 %) of the $\gamma\text{-Al}_2\text{O}_3$ support permit a good dispersion of complex **I** during catalyst

synthesis. Furthermore, the Ni complex **I** was replaced by the common salt namely Ni(II) acetate ($\text{Ni}(\text{OAc})_2 \cdot 4\text{H}_2\text{O}$). However, no yield of benzylamine could be detected. The use of Raney Ni or Ni powder gave no yield of the product desired with the same catalyst loading. Applying a four times higher catalyst loading resulted in some product formation for Raney Ni (Table 5. 1).

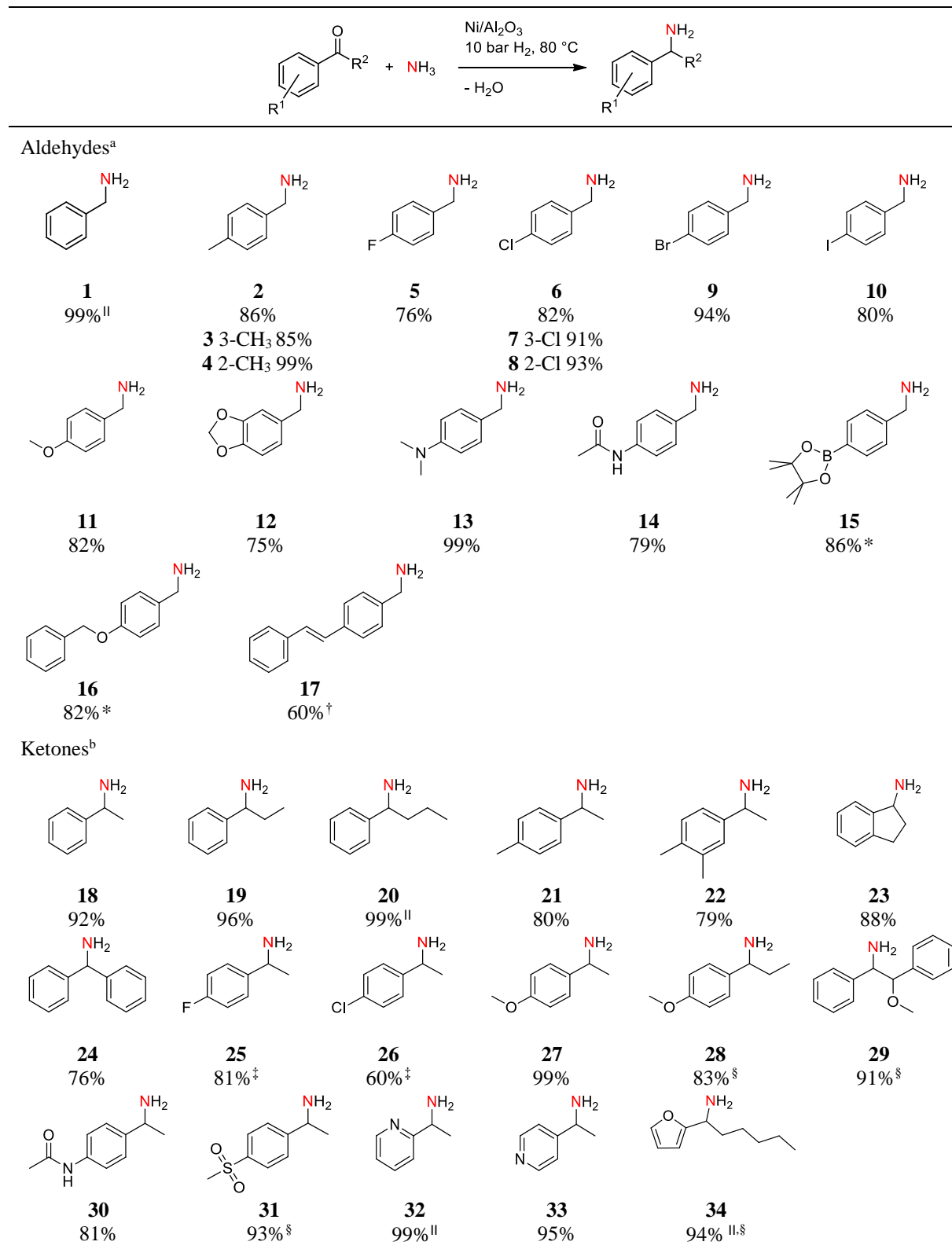
Table 5. 1: Catalyst screening

Entry	Metal source	Support	Pyrolysis temperature [°C]	Yield [%]
1	Complex I	$\gamma\text{-Al}_2\text{O}_3$	600	34
2	Complex I	$\gamma\text{-Al}_2\text{O}_3$	700	78
3 ^a	Complex I	$\gamma\text{-Al}_2\text{O}_3$	700	99
4	Complex I	$\gamma\text{-Al}_2\text{O}_3$	800	48
5	Complex I	CeO_2	700	36
6	Complex I	Activated C	700	0
7	Complex I	SiO_2	700	0
8	Complex I	TiO_2	700	0
9	$\text{Ni}(\text{OAc})_2$	$\gamma\text{-Al}_2\text{O}_3$	700	0
10 ^b	Raney Ni	-	-	38
11 ^b	Ni powder	-	-	5
12	-	$\gamma\text{-Al}_2\text{O}_3$	-	0
13	-	CeO_2	-	0

Reaction conditions: 1.2 mol% catalyst (10 mg catalyst, 3.5 wt% Ni, 0.006 mmol Ni, 0.35 mg Ni) or 10 mg support, 0.5 mmol benzaldehyde, 0.5 mL aq. NH_3 25 % (6.7 mmol), 2.0 mL H_2O , 80 °C, 1 MPa H_2 , 20 h. Yields were determined by gas chromatography (GC) using *n*-dodecane as an internal standard; ^a1.4 mol% catalyst (12 mg catalyst, 3.5 wt% Ni, 0.007 mmol Ni, 0.42 mg Ni); ^b5 mol% (0.025 mmol Ni, 1.5 mg Ni).

Substrate Scope

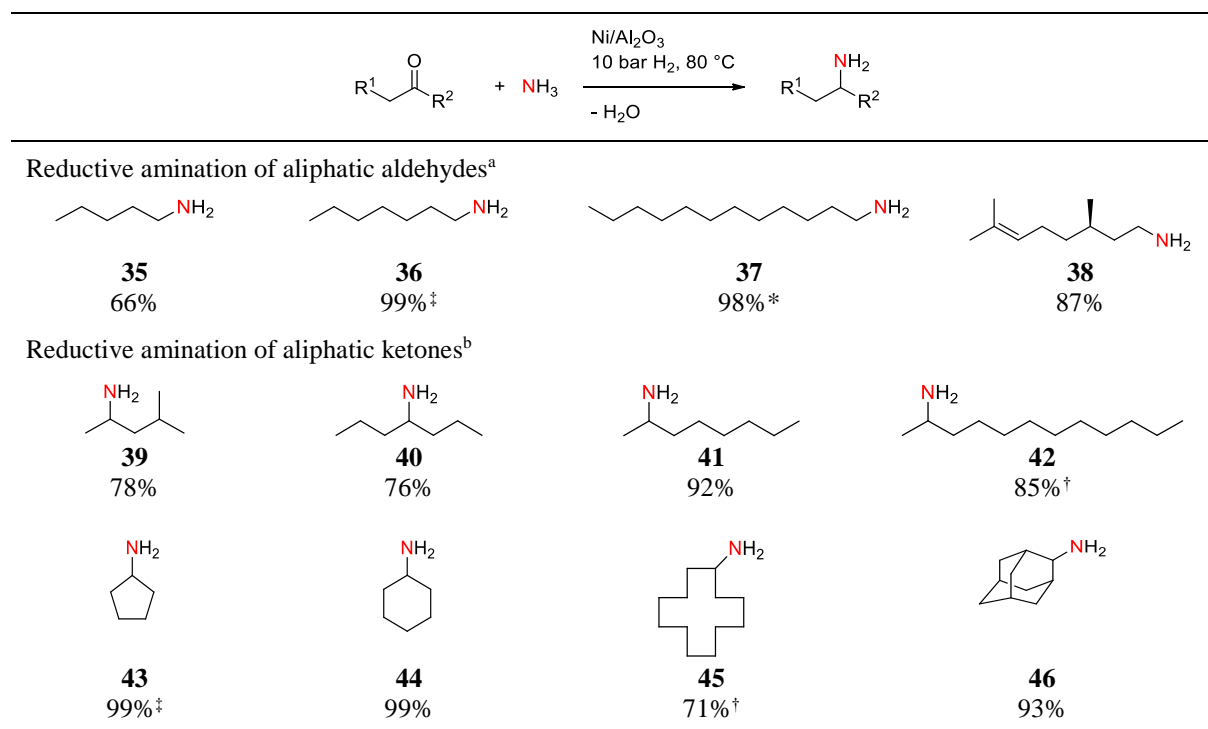
With the optimized reaction conditions in hand, we were interested in the substrate scope of our novel catalyst system. Firstly, we investigated benzylic aldehydes (Table 5. 2, top). The position of the substituent, investigated for 2-, 3- or 4-methylbenzaldehyde and 2-, 3- or 4-chlorobenzaldehyde has only a minor influence on the yield of the corresponding amines (Table 5. 2, compounds **2–4** and **6–8**). Halogenated aldehydes, such as fluorides, chlorides, bromides and even iodides, were smoothly converted into the corresponding products (Table 5. 2, compounds **5–10**).

Table 5. 2: Scope of the reductive amination using carbonyl compounds containing an aromatic moiety.


Reaction conditions: ^a12 mg Ni/Al₂O₃ (3.5 wt% Ni, 1.4 mol%), 0.5 mmol aldehyde, 0.5 mL aq. NH₃ 25% (6.7 mmol), 2 mL H₂O, 20 h, 1 MPa H₂, 80 °C; ^{*}24 mg Ni/Al₂O₃ (3.5 wt% Ni, 2.8 mol%); [†]48 mg Ni/Al₂O₃ (3.5 wt% Ni, 5.6 mol%), 1.0 mL aq. NH₃ 25% (13.4 mmol), 1.5 mL EtOH, 0.5 MPa H₂; ^b24 mg Ni/Al₂O₃ (3.5 wt% Ni, 2.8 mol%), 0.5 mmol ketone, 1.0 mL aq. NH₃ 25% (13.4 mmol), 1.5 mL H₂O, 20 h, 1 MPa H₂, 80 °C; [‡]1.5 mL EtOH as solvent; [§]48 mg Ni/Al₂O₃ (3.5 wt% Ni, 5.6 mol%), 2.5 mL aq. NH₃ 25% (33.4 mmol). ^{||}GC yields using *n*-dodecane as internal standard. Isolated yields are given for the corresponding hydrochloride salts.

Other functional groups, such as methoxy, amine, amide, ether and 4,4,5,5-tetramethyl-1,3,2-dioxaborolanyl (Table 5. 2, compounds **11–15**), are also tolerated. The tolerance of a benzyloxy substituent (Table 5. 2, compound **16**) is interesting in the light of many known Ni catalysts that can cleave aryl-benzyl ethers via hydrogenolysis^[54]. The disubstituted olefin (E)-4-styrylbenzaldehyde (Table 5. 2, compound **17**) could be converted to the corresponding unsaturated primary amine in 60 % isolated yield. Attempts to aminate 3-vinylbenzaldehyde failed due to its polymerization under standard conditions. The transformation of ketones is more challenging^[17–21] and we increased the catalyst loading and the ammonia amount slightly to guarantee high conversions. Aryl-alkyl and diaryl ketones can be converted smoothly into their primary amines with yields of products > 90% for 9 out of 17 examples (Table 2, bottom). Fluorides and chlorides are well tolerated (Table 5. 2, compounds **25** and **26**). The conversion of electron-rich methoxy substituted aryl-alkyl ketones runs efficiently (Table 5. 2, compounds **27–29**). Substrates containing amido- and sulfonyl-functionalities and a variety of different heterocycles were introduced, and the corresponding primary amines were obtained in good to excellent yields (Table 5. 2, compounds **30–34**).

Table 5. 3: Scope of reductive amination using purely aliphatic carbonyl compounds.

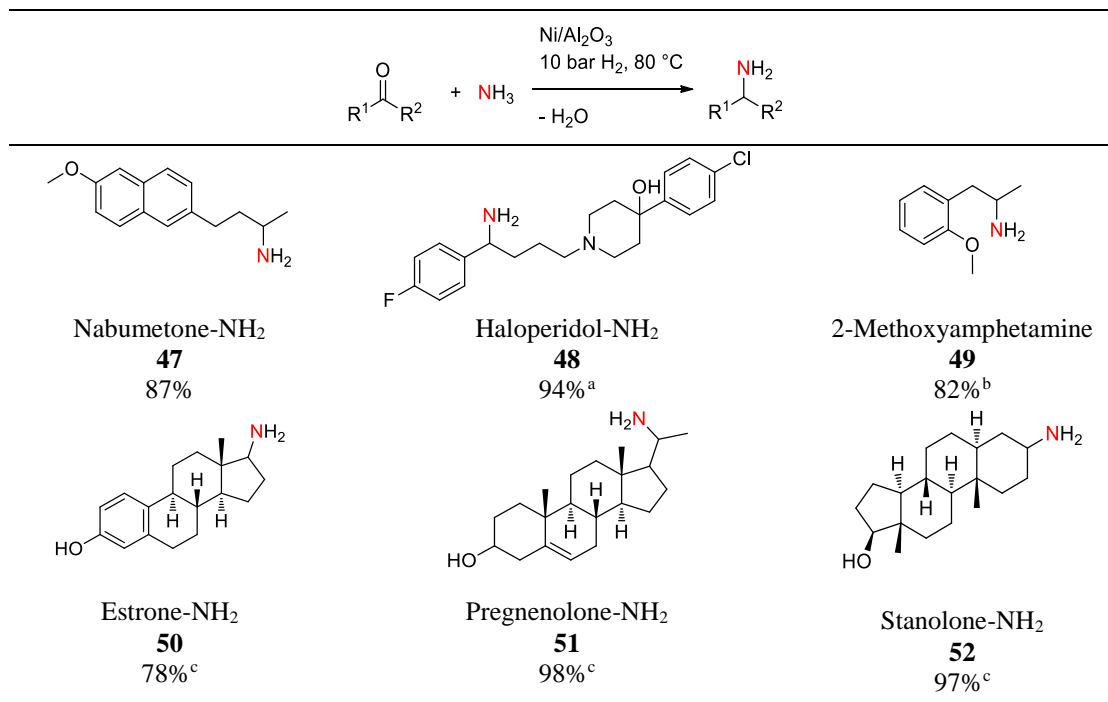


Reaction conditions: ^a12 mg Ni/Al₂O₃ (3.5 wt% Ni, 1.4 mol%), 0.5 mmol aldehyde, 0.5 mL aq. NH₃ 25% (6.7 mmol), 2 mL H₂O, 20 h, 1 MPa H₂, 80 °C; ^{*}24 mg Ni/Al₂O₃ (3.5 wt% Ni, 2.8 mol%), 2 mL EtOH as solvent; ^b24 mg Ni/Al₂O₃ (3.5 wt% Ni, 2.8 mol%), 0.5 mmol ketone, 1.0 mL aq. NH₃ 25% (13.4 mmol), 1.5 mL H₂O, 20 h, 1 MPa H₂, 80 °C; [†]48 mg Ni/Al₂O₃ (3.5 wt% Ni, 5.6 mol%), 2.5 mL aq. NH₃ 25% (33.4 mmol). [‡]GC yields using *n*-dodecane as internal standard. Isolated yields are given for the corresponding hydrochloride salts.

We next looked at purely aliphatic carbonyl compounds. Aldehydes or ketones gave good to excellent yields (Table 5. 3, compounds **35–42**) and even citronellal (Table 5. 3, compound **38**) bearing a C-C

double bond was very selectively converted into the corresponding unsaturated primary amine. Cycloalkylketones with various ring sizes were also aminated successfully (Table 5. 3, compounds **43–46**). Finally, we became interested in the reductive amination of pharmaceuticals and natural products or biologically active and highly functionalized molecules, such as nabumetone, haloperidol or steroids (Table 5. 4, compounds **47–52**). To our delight, all carbonyl compounds were smoothly and selectively converted into their corresponding primary amines applying our catalyst system.

Table 5. 4: Reductive amination of biologically active molecules.



Reaction conditions: 24 mg Ni/Al₂O₃ (3.5 wt% Ni, 2.8 mol%), 0.5 mmol substrate, 0.5 mL aq. NH₃ 25% (6.7 mmol), 2 mL EtOH, 20 h, 1 MPa H₂, 80 °C; ^a0.25 mmol substrate; ^b48 mg Ni/Al₂O₃ (3.5 wt% Ni, 5.6 mol%), 2.5 mL aq. NH₃ 25% (33.4 mmol); ^c48 mg Ni/Al₂O₃ (3.5 wt% Ni, 5.6 mol%), 0.5 mL aq. NH₃ 25% (6.7 mmol). Isolated yields are given for the corresponding hydrochloride salts.

Reusability and upscaling of the reaction

The reductive amination of benzaldehyde at about 60 % was chosen as the test reaction for reusability studies. The catalyst has been used five times consecutively without a loss of activity as concluded from initial rate measurements. The catalyst was separated by filtration and washed prior to its reuse (Supplementary Fig. 11, Supplementary Note 2). Separation of the solution (standard conditions) from the catalyst via hot filtration stops the formation of benzylamine indicating that irreversibly leached nickel species play a minor role in formation of the primary amines (Supplementary Note 3). Reactions with a 20 times higher amount of the substrate (10 mmol) were performed to demonstrate the applicability of our novel catalyst system for multi-gram scale syntheses (Supplementary Table 6, Supplementary Note 4). Both 4-chlorobenzaldehyde (86% yield), exemplary for a halogenated aldehyde, and acetophenone (84% yield), exemplary for a ketone, were converted into the corresponding primary amines. The yields are in agreement with the 0.5 mmol reactions.

5.3 Discussion

A catalyst system based completely on earth-abundant elements for the reductive amination of carbonyl compounds by ammonia has been reported. The products of the catalytic synthesis — primary amines — are highly important and figure prominently in natural products, pharmaceuticals and organic materials. We can use ammonia dissolved in water (rather than pressurized ammonia gas) and work under very mild conditions. Our catalyst is easy to synthesize in a two-step procedure. Impregnation of commercially available γ -Al₂O₃ with a specific Ni complex and a tailored decomposition leads to a highly active catalyst. It consists of Ni-NPs, with a mean size of 8 nm, embedded in an N-doped carbon layer, which partially covers the alumina support. Our methodology has a very broad scope and tolerates many functional groups. We can aminate aldehydes, including purely aliphatic examples, and aryl-alkyl, diaryl or dialkyl ketones. In addition, the amination of pharmaceuticals, bioactive compounds and natural products has been demonstrated. The functional groups we can tolerate, such as a C–C double bond and an iodo substituent, are easily hydrogenated or aren't resistant towards hydrogenolysis (benzyl ether). The catalyst has been used five times consecutively without a loss of activity and upscaling is smoothly accomplished with yields similar to the small-scale experiments. The combination Ni-NPs stabilized by an N-doped carbon layer and an acidic support might be the key to the observed activity/selectivity, the long-term stability, and the very convenient handling of the catalyst.

5.4 Methods

Catalyst preparation

A solution of 162 mg of complex **I** (0.355 mmol; 20.8 mg of Ni) in 6 mL acetonitrile was added to 500 mg γ -Al₂O₃ and the suspension was stirred vigorously for 5 min. After evaporation of the solvent at 110 °C, the impregnated sample was pyrolyzed under N₂ and finally reduced by a N₂/H₂ mixture with the following program:

RT $\xrightarrow[\text{N}_2]{2\text{ }^\circ\text{C}/\text{min}}$ 300 °C (dwelling time: 0.5 h) $\xrightarrow[\text{N}_2]{10\text{ }^\circ\text{C}/\text{min}}$ 700 °C (dwelling time: 0.5 h) $\xrightarrow[\text{N}_2]{20\text{ }^\circ\text{C}/\text{min}}$
 100 °C $\xrightarrow[\text{N}_2/\text{H}_2]{5\text{ }^\circ\text{C}/\text{min}}$ 550 °C (dwelling time: 3.0 h) $\xrightarrow[\text{N}_2/\text{H}_2]{20\text{ }^\circ\text{C}/\text{min}}$ RT

Reductive amination of carbonyl compounds – general procedure

A 5-mL reaction vial was charged with a magnetic stirring bar, 0.5 mmol carbonyl compound, 0.5 mL 25% aqueous NH₃ (6.7 mmol), 2 mL H₂O and 12 mg Ni/Al₂O₃ catalyst (3.5 wt% Ni, 0.42 mg Ni, 0.007 mmol Ni, 1.4 mol% Ni). The vial was placed in a 250 mL high-pressure autoclave (Parr Instruments) which was flushed three times with 2 MPa hydrogen. After pressurizing the autoclave with the desired pressure of typically 1 MPa, the reaction was stirred for 20 h at 80 °C. The autoclave was cooled

to room temperature and the hydrogen was released. The catalyst was removed by centrifugation and the aqueous layer was extracted several times using ethyl acetate. The organic phases were combined, dried over Na_2SO_4 , filtered and the solvent was removed under reduced pressure. The crude product was purified by column chromatography, using silica gel and a mixture of ethyl acetate and methanol as eluent, to yield the primary amine. This was converted to the corresponding hydrochloride salt by adding 0.7 mmol of HCl in ether and was further analyzed by ^1H and ^{13}C NMR spectroscopy (Supplementary Fig. 12–57). High-resolution mass spectroscopy was carried out for products with incomplete spectroscopic literature data (Supplementary Fig. 58–60)

Acknowledgements

We thank the Deutsche Forschungsgemeinschaft for financial support (B1, SFB 840) and E. Arzt for his support through INM. In addition, we thank F. Puchtler and M. Ries for PXRD, U. Lacher for HRMS, J. Thiessen for NH_3 -TPD and J. Seidel, TU Bergakademie Freiberg, Institut für Physikalische Chemie, for XPS. We thank J. Schmauch for the assistance with the EELS measurements.

Author contributions

G.H. carried out the synthesis of the catalyst, the catalyst characterization and the catalytic reactions. P.K. and N.J. performed the HAADF-STEM images coupled with EDX and EELS analysis. G.H. and R.K. designed the experiments and co-wrote the manuscript.

5.5 References

- [1] Boddien, A. et al. Efficient dehydrogenation of formic acid using an iron catalyst. *Science* **333**, 1733–1736 (2011).
- [2] Tondreau, A. M. et al. Iron catalysts for selective anti-Markovnikov alkene hydrosilylation using tertiary silanes. *Science* **335**, 567–570 (2012).
- [3] Zuo, W., Lough, A. J., Li, Y. F. & Morris, R. H. Amine(imine)diphosphine iron catalysts for asymmetric transfer hydrogenation of ketones and imines. *Science* **342**, 1080–1083 (2013).
- [4] Friedfeld, M. R. et al. Cobalt precursors for high-throughput discovery of base metal asymmetric alkene hydrogenation catalysts. *Science* **342**, 1076–1080 (2013).
- [5] Hoyt, J. M., Schmidt, V. A., Tondreau, A. M. & Chirik, P. J. Iron-catalyzed intermolecular [2+2] cycloadditions of unactivated alkenes. *Science* **349**, 960–963 (2015).
- [6] Korstanje, T. J., van der Vlugt, Jarl Ivar, Elsevier, C. J. & Bruin, B. de. Hydrogenation of carboxylic acids with homogeneous cobalt catalyst. *Science* **350**, 298–302 (2015).
- [7] Yu, R. P., Hesk, D., Rivera, N., Pelczer, I. & Chirik, P. J. Iron-catalysed tritiation of pharmaceuticals. *Nature* **529**, 195–199 (2016).
- [8] Friedfeld, M. R., Zhong, H., Ruck, R. T., Shevlin, M. & Chirik, P. J. Cobalt-catalyzed hydrogenation of enamides enabled by single-electron reduction. *Science* **360**, 888–893 (2018).
- [9] Filonenko, G. A., van Putten, R., Hensen, E. J. M. & Pidko, E. A. Catalytic (de)hydrogenation promoted by non-precious metals – Co, Fe and Mn: recent advances in an emerging field. *Chem. Soc. Rev.* **47**, 1459–1483 (2018).
- [10] Kallmeier, F. & Kempe, R. Manganese complexes for (de)hydrogenation catalysis: a comparison to cobalt and iron catalysts. *Angew. Chem. Int. Ed.* **57**, 46–60 (2018).
- [11] Jagadeesh, R. V. et al. Nanoscale Fe₂O₃-based catalysts for selective hydrogenation of nitroarenes to anilines. *Science* **342**, 1073–1076 (2013).
- [12] Westerhaus, F. A. et al. Heterogenized cobalt oxide catalysts for nitroarene reduction by pyrolysis of molecularly defined complexes. *Nat. Chem.* **5**, 537–543 (2013).
- [13] Jagadeesh, R. V. et al. MOF-derived cobalt nanoparticles catalyze a general synthesis of amines. *Science* **358**, 326–332 (2017).
- [14] Weissermel, K. & Arpe, H.-J. *Industrial Organic Chemistry* (Wiley-VCH, Weinheim, 2008).
- [15] Vardanyan, R. S. & Hruby, V. J. *Synthesis of Best-Seller Drugs* (Academic Press, Amsterdam, 2016).
- [16] Lawrence, S. A. *Amines. Synthesis, Properties and Applications* (Cambridge University Press, Cambridge, UK, New York, 2004).
- [17] Gomez, S., Peters, J. A. & Maschmeyer, T. The reductive amination of aldehydes and ketones and the hydrogenation of nitriles: mechanistic aspects and selectivity control. *Adv. Synth. Catal.* **344**, 1037–1057 (2002).

- [18] Klinkenberg, J. L. & Hartwig, J. F. Catalytic organometallic reactions of ammonia. *Angew. Chem. Int. Ed.* **50**, 86–95 (2011).
- [19] Kim, J., Kim, H. J. & Chang, S. Synthetic uses of ammonia in transition-metal catalysis. *Eur. J. Org. Chem.* **2013**, 3201–3213 (2013).
- [20] Alinezhad, H., Yavari, H. & Salehian, F. Recent advances in reductive amination catalysis and its applications. *Curr. Org. Chem.* **19**, 1021–1049 (2015).
- [21] Legnani, L., Bhawal, B. & Morandi, B. Recent developments in the direct synthesis of unprotected primary- amines. *Synthesis* **49**, 776–789 (2017).
- [22] Gross, T., Seayad, A. M., Ahmad, M. & Beller, M. Synthesis of primary amines. First homogeneously catalyzed reductive amination with ammonia. *Org. Lett.* **4**, 2055–2058 (2002).
- [23] Ogo, S., Uehara, K., Abura, T. & Fukuzumi, S. pH-Dependent chemoselective synthesis of alpha-amino acids. Reductive amination of alpha-keto acids with ammonia catalyzed by acid-stable iridium hydride complexes in water. *J. Am. Chem. Soc.* **126**, 3020–3021 (2004).
- [24] Gallardo-Donaire, J., Ernst, M., Trapp, O. & Schaub, T. Direct synthesis of primary amines via ruthenium-catalysed amination of ketones with ammonia and hydrogen. *Adv. Synth. Catal.* **358**, 358–363 (2016).
- [25] Bódis, J., Lefferts, L., Müller, T. E., Pestman, R. & Lercher, J. A. Activity and selectivity control in reductive amination of butyraldehyde over noble metal catalysts. *Catal. Lett.* **104**, 23–28 (2005).
- [26] Dong, B. *et al.* Heterogeneous Ru-based catalysts for one-pot synthesis of primary amines from aldehydes and Ammonia. *Catalysts* **5**, 2258–2270 (2015).
- [27] Nakamura, Y., Kon, K., Touchy, A. S., Shimizu, K.-I. & Ueda, W. Selective synthesis of primary amines by reductive amination of ketones with ammonia over supported Pt catalysts. *ChemCatChem* **7**, 921–924 (2015).
- [28] Chatterjee, M., Ishizaka, T. & Kawanami, H. Reductive amination of furfural to furfurylamine using aqueous ammonia solution and molecular hydrogen. An environmentally friendly approach. *Green Chem.* **18**, 487–496 (2016).
- [29] Nishimura, S., Mizuhori, K. & Ebitani, K. Reductive amination of furfural toward furfurylamine with aqueous ammonia under hydrogen over Ru-supported catalyst. *Res. Chem. Intermed.* **42**, 19–30 (2016).
- [30] Liang, G. *et al.* Production of primary amines by reductive amination of biomass-derived aldehydes/ketones. *Angew. Chem. Int. Ed.* **56**, 3050–3054 (2017).
- [31] Komanoya, T., Kinemura, T., Kita, Y., Kamata, K. & Hara, M. Electronic effect of ruthenium nanoparticles on efficient reductive amination of carbonyl compounds. *J. Am. Chem. Soc.* **139**, 11493–11499 (2017).
- [32] Alexander, E. R. & Misegades, A. L. A low pressure reductive alkylation method for the conversion of ketones to primary amines. *J. Am. Chem. Soc.* **70**, 1315–1316 (1948).

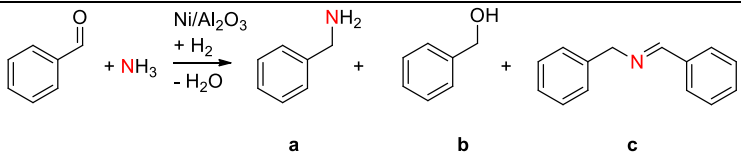
- [33] Klyuev, M. V. & Khidekel', M. L. Catalytic amination of alcohols, aldehydes, and ketones. *Russ. Chem. Rev.* **49**, 14–27 (1980).
- [34] Winans, C. F. Hydrogenation of aldehydes in the presence of ammonia. *J. Am. Chem. Soc.* **61**, 3566–3567 (1939).
- [35] Chan, A. S., Chen, C.-C. & Lin, Y.-C. Catalytic reductive amination of α -ketocarboxylic acids as a useful route to amino acids. *Appl. Catal. A Ge.* **119**, L1-L5 (1994).
- [36] Dolezal, P. et al. Reductive amination of cyclopentanone. *Appl. Catal. A Gen.* **286**, 202–210 (2005).
- [37] Zimmermann, B., Herwig, J. & Beller, M. The first efficient hydroaminomethylation with ammonia: With dual metal catalysts and two-phase catalysis to primary amines. *Angew. Chem. Int. Ed.* **38**, 2372-2375 (1999).
- [38] Prinz, T. & Driessen-Hölscher B., Biphasic Catalyzed Telomerization of Butadiene and Ammonia: Kinetics and New Ligands for Regioselective Reactions. *Chem. Eur. J.* **5**, 2069-2076 (1999).
- [39] Nagano, T. & Kobayashi, S. Palladium-Catalyzed Allylic Amination Using Aqueous Ammonia for the Synthesis of Primary Amines. *J. Am. Chem. Soc.* **131**, 4200-4201 (2009).
- [40] Das, K., Shibuya, R., Nakahara, Y., Germain, N., Ohshima, T. & Mashima, K. Platinum-Catalyzed Direct Amination of Allylic Alcohols with Aqueous Ammonia: Selective Synthesis of Primary Allylamines. *Angew. Chem. Int. Ed.* **51**, 150-154 (2012).
- [41] Schranck, J. & Tlili, A. Transition-Metal-Catalyzed Monoarylation of Ammonia. *ACS Catal.* **8**, 405-418 (2018).
- [42] Guo, B., Zhang, Q., Li, G., Yao, J. & Hu, C. Aromatic C–N bond formation via simultaneous activation of C–H and N–H bonds: direct oxyamination of benzene to aniline. *Green Chem.* **14**, 1880-1883 (2012).
- [43] Fujita, K.-I., Furukawa, S., Morishima, N., Shimizu, M. & Yamaguchi, R. N-Alkylation of Aqueous Ammonia with Alcohols Leading to Primary Amines Catalyzed by Water-Soluble N-Heterocyclic Carbene Complexes of Iridium. *ChemCatChem* **10**, 1993-1997 (2018).
- [44] Rösler, S., Obenauf, J. & Kempe, R. A Highly active and easily accessible cobalt catalyst for selective hydrogenation of C=O bonds. *J. Am. Chem. Soc.* **137**, 7998–8001 (2015).
- [45] Rösler, S., Ertl, M., Irrgang, T. & Kempe, R. Cobalt-catalyzed alkylation of aromatic amines by alcohols. *Angew. Chem. Int. Ed.* **54**, 15046–15050 (2015).
- [46] Deibl, N. & Kempe, R. General and mild cobalt-catalyzed C-alkylation of unactivated amides and esters with alcohols. *J. Am. Chem. Soc.* **138**, 10786–10789 (2016).
- [47] Kallmeier, F., Irrgang, T., Dietel, T. & Kempe, R. Highly active and selective manganese C=O bond hydrogenation catalysts: the importance of the multidentate ligand, the ancillary ligands, and the oxidation state. *Angew. Chem. Int. Ed.* **55**, 11806–11809 (2016).

- [48] Deibl, N. & Kempe, R. Manganese-catalyzed multicomponent synthesis of pyrimidines from alcohols and amidines. *Angew. Chem. Int. Ed.* **56**, 1663–1666 (2017).
- [49] Kallmeier, F., Dudzic, B., Irrgang, T. & Kempe, R. Manganese-catalyzed sustainable synthesis of pyrroles from alcohols and amino alcohols. *Angew. Chem. Int. Ed.* **56**, 7261–7265 (2017).
- [50] Zhang, G., Irrgang, T., Dietel, T., Kallmeier, F. & Kempe, R. Manganese-catalyzed dehydrogenative alkylation or α -Olefination of alkyl-substituted N-heteroarenes with alcohols. *Angew. Chem. Int. Ed.* **57**, 9131–9135 (2018).
- [51] Forberg, D. et al. Single-catalyst high-weight% hydrogen storage in an N-heterocycle synthesized from lignin hydrogenolysis products and ammonia. *Nat. Commun.* **7**, 13201 (2016).
- [52] Forberg, D., Schwob, T. & Kempe, R. Catalytic condensation for the formation of polycyclic heteroaromatic compounds. *Nat. Commun.* **9**, 1751 (2018).
- [53] Schwob, T. & Kempe, R. A reusable co catalyst for the selective hydrogenation of functionalized nitroarenes and the direct synthesis of imines and benzimidazoles from nitroarenes and aldehydes. *Angew. Chem. Int. Ed.* **55**, 15175–15179 (2016).
- [54] Zaheer, M. & Kempe, R. Catalytic hydrogenolysis of aryl ethers. A key step in lignin valorization to valuable chemicals. *ACS Catal.* **5**, 1675–1684 (2015).

5.6 Supporting Information

5.6.1 Supplementary Tables

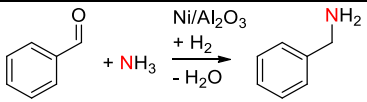
Supplementary Table 1: Solvent screening for the model substrate benzaldehyde.



Solvent [2.3 mL]	Yield [%]		
	a	b	c
H₂O	54	0	0
EtOH	47	11	39
diglyme	0	3	33
THF	0	5	25
toluene	0	0	39

Reaction conditions: 1.2 mol% Ni (10 mg Ni/Al₂O₃, 3.5 wt% Ni, 0.006 mmol Ni, 0.35 mg Ni), 0.5 mmol benzaldehyde, 80 °C, 1 MPa H₂, 0.2 mL aq. NH₃ 25 % (2.7 mmol), 20 h. Yields were determined by GC using *n*-dodecane as an internal standard.

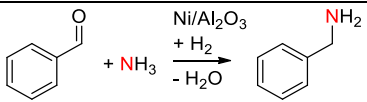
Supplementary Table 2: Screening of different ammonia solutions.



Ammonia solution	Yield [%]
NH₃ in water	26
NH ₃ in EtOH	0
NH ₃ in dioxane	0

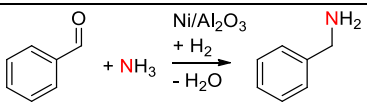
Reaction conditions: 1.2 mol% Ni (10 mg Ni/Al₂O₃, 3.5 wt% Ni, 0.006 mmol Ni, 0.35 mg Ni), 0.5 mmol benzaldehyde, 2.5 mL ammonia solution (0.5 M, 1.25 mmol); 80 °C, 1 MPa H₂, 20 h. Yields were determined by GC using *n*-dodecane as an internal standard.

Supplementary Table 3: Screening of the NH₃ amount for the model substrate benzaldehyde.

	
aq. NH ₃ 25 %	Yield [%]
0.04 mL (0.5 mmol)	19
0.10 mL (1.3 mmol)	26
0.20 mL (2.7 mmol)	54
0.50 mL (6.7 mmol)	78
1.00 mL (13.4 mmol)	68
2.50 mL (33.4 mmol)	0

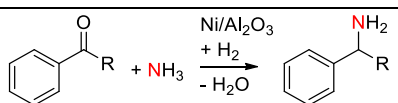
Reaction conditions: 1.2 mol% Ni (10 mg Ni/Al₂O₃, 3.5 wt% Ni, 0.006 mmol Ni, 0.35 mg Ni), 0.5 mmol benzaldehyde, 80 °C, 1 MPa H₂, 20 h. The reaction mixture was filled up with H₂O to an absolute volume of 2.5 mL. Yields were determined by GC using *n*-dodecane as an internal standard.

Supplementary Table 4: Screening of the metal loading of the catalyst.

	
Theoretical wt% of Ni	Yield [%]
1 wt%	0
4 wt% (ICP: 3.5 wt%)	78
8 wt%	64

Reaction conditions: 1.2 mol% Ni (0.006 mmol Ni, 0.35 mg Ni), 0.5 mmol benzaldehyde, 0.5 mL aq. NH₃ 25 % (6.7 mmol), 2.0 mL H₂O, 80 °C, 1 MPa H₂, 20 h. Yields were determined by GC using *n*-dodecane as an internal standard.

Supplementary Table 5: Screening of the hydrogen pressure.

				
R	Catalyst loading [mol%]	H ₂ pressure [MPa]	Reaction time [h]	Yield [%]
CH ₃ ^[a]	2.8	1.0	20	92
CH ₃ ^[b]	8.6	0.1	48	18
H ^[a]	1.4	1.0	20	99
H ^[b]	8.6	0.1	48	6

Reaction conditions: 0.5 mmol substrate, 80 °C; [a] 1.0 mL aq. NH₃ 25 % (13.4 mmol), 1.5 mL H₂O, 20 h for acetophenone; 0.5 mL aq. NH₃ 25 % (6.7 mmol), 2 mL H₂O, 20 h for benzaldehyde; [b] 1.0 mL aq. NH₃ 25 % (13.4 mmol), 1.5 mL H₂O, 48 h, for acetophenone; 0.5 mL aq. NH₃ 25 % (6.7 mmol), 2 mL H₂O, 48 h for benzaldehyde.

Supplementary Table 6: Up-scaling of the reaction.

Entry	Product	Isolated Yield [g]	Yield [%]
1		1.538	86
2		1.317	84

Reaction conditions: **entry 1**, 240 mg Ni/Al₂O₃ (3.5 wt%, 1.4 mol%), 10 mmol aldehyde, 10 mL aq. NH₃ 25 % (0.13 mol), 40 mL H₂O, 20 h, 1 MPa H₂, 80 °C; **entry 2**, 480 mg Ni/Al₂O₃ (3.5 wt%, 2.8 mol%), 10 mmol ketone, 20 mL aq. NH₃ 25 % (0.27 mol), 30 mL H₂O, 20 h, 1.0 MPa H₂, 80 °C. Yields are of isolated products.

5.6.2 Supplementary Notes

Supplementary Note 1: ICP-OES

Theoretical Ni content: 4.0 wt%

Measured Ni content: 3.5 wt%

Supplementary Note 2: Reusability

The reductive hydrogenation of benzaldehyde with aqueous ammonia was chosen to investigate the recyclability of the novel nickel nanocomposite catalyst. For this study, the optimized reaction conditions were used. The yield of benzylamine was determined by GC using *n*-dodecane as an internal standard. After each run, the catalyst was centrifuged, washed several times with ethyl acetate, dried and was used directly in the subsequently run. This procedure was done for 5 runs without any decrease of activity (see Supplementary Fig. 11).

Supplementary Note 3: Leaching experiment

To demonstrate, that our catalyst does not form homogeneous species during the catalysis, a hot filtration test was performed. A 5-mL reaction vial was charged with a magnetic stirring bar, 0.5 mmol benzaldehyde, 0.5 mL 25 % aqueous NH₃ (6.7 mmol), 2 mL H₂O and 10 mg Ni/Al₂O₃ (1.2 mol% Ni, 3.5 wt% Ni, 0.006 mmol Ni, 0.35 mg Ni). The vial was placed in a 250 mL high-pressure autoclave (Parr Instruments) which was flushed three times with 2 MPa hydrogen. After pressurizing the autoclave with 1 MPa, the reaction was stirred at 80 °C. When 56 % yield of benzylamine were generated, the hot catalytic mixture was filtered to remove the catalyst. Afterwards, 0.5 mmol benzaldehyde were added to the filtrate and

the mixture was stirred at the catalytic conditions mentioned above. The filtrate did not show any activity and the desired product benzylamine was not generated, only the coupling product N-benzylidenebenzylamine could be detected.

Supplementary Note 4: Up-Scaling of the reaction

For the up-scaling reactions 4-chlorobenzaldehyde and acetophenone were used as representative substrates for carbonyl compounds. The optimized reaction conditions were scaled up for 10 mmol substrate. For the aldehyde, 240 mg Ni/Al₂O₃ (3.5 wt%, 1.4 mol%), 10 mL aq. NH₃ 25 % (0.13 mol), 40 mL H₂O, 20 h, 1 MPa H₂, 80 °C and for the ketone, 480 mg Ni/Al₂O₃ (3.5 wt%, 2.8 mol%), 20 mL aq. NH₃ 25 % (0.27 mol), 30 mL H₂O, 20 h, 1 MPa H₂, 80 °C were used. The reaction was performed in a 50 mL glass vial equipped with a magnetic stirring bar. This vial was placed in a 250 mL high-pressure autoclave (Parr Instruments) and the autoclave was flushed three times with 2.0 MPa hydrogen. After pressurizing the autoclave with the desired pressure of typically 1 MPa, the reaction was stirred for 20 h at 80 °C. The autoclave was cooled to room temperature and the hydrogen was released. The workup was identical to the 0.5 mmol reactions (see Supplementary Table 6).

5.6.3 Supplementary Methods

5.6.3.1 General considerations

Air- and moisture sensitive reactions were carried out under dry argon or nitrogen using standard Schlenk or glove box techniques. Solvents were dried and distilled from sodium benzophenone, stored over molecular sieves (3 Å) before use or were obtained from Acros. All chemicals were purchased from commercial sources with purity over 95 % and used without further purification. γ -Al₂O₃ was purchased from Alfa Aesar and used without further purification.

NMR-Spectra were collected on Varian INOVA 300 (300 MHz for ¹H, 75 MHz for ¹³C) or Bruker Avance III HD 500 (500 MHz for ¹H, 125.7 MHz for ¹³C) instruments at 298 K. Chemical shifts are reported in ppm relative to the residual solvent signal (CDCl₃: 7.26 ppm (¹H), 77.16 ppm (¹³C); DMSO-D₆: 2.50 ppm (¹H), 39.51 ppm (¹³C)). Coupling constants (*J*) are reported in Hz (coupling patterns: d = doublet, t = triplet, q = quartet, sxt = sextet, spt = septet, m = multiplet).

GC analyses were carried out on an Agilent 6850 GC system equipped with an Optima 17 column (30 m x 0.32 mm x 0.25 μm). *N*-dodecane was used as internal standard.

GC-MS analyses were carried out on an Agilent 7890A GC system equipped with a HP-5MS column (30 m x 0.32 mm x 0.25 μm) and a 5975C inert MSD detector (EI, 70 eV).

High resolution mass spectra (HRMS) were obtained from a Thermo Scientific Q-Exactive (Orbitrap) instrument in ESI+ mode.

Transmission electron microscopy (TEM) was carried out by using a LEO 922o (200 kV) instrument and a JEOL JEM 2200FS (200 kV). The sample was suspended in chloroform and sonicated for 5 min.

Subsequently 2 μL of the suspended sample was placed on a CF200-Cu-grid or a LC200-Cu-grid (Electron Microscopy Sciences) and allowed to dry.

A TEM/STEM (ARM200F, JEOL, Japan) equipped with EDX detector (JEOL) and an energy filter (GATAN) was used for the High-angle annular dark-field scanning transmission electron (HAADF-STEM) imaging and elemental mapping of the specimen. Data acquisition was done with following parameters: HAADF-STEM collection angle 68-280 mrad, image size 1024x1024 pixels, pixel size 0.47 nm, dwell time 20 μs , probe current 140 pA. EDX-mapping image size 128x128 pixels, pixel size 3.8 nm, pixel dwell time 1 ms, 10 sweeps integrated, probe current 1000 pA. EELS spectrum image collection angle 111 mrad, electron probe convergence semi-angle 20-30 mrad, image size 76x71 pixels, pixel size 0.23 nm, pixel dwell time 50 ms. The energy dispersion of the spectrometer was set to 0.25 eV/channel and the elemental maps were collected in three different energy regions to cover all elements of interest. In addition, a spectrum image at the zero-loss regime was collected for the calculation of the inelastic mean free path length of the sampled area, resulting in a value of the relative thickness 0.41 IMFP (SD=0.07).

Data processing and analysis of EDX mapping was conducted with JEOL Analysis Station v.3,8,0,34. Elemental peaks were identified and their areas integrated in an automatic manner to produce the elemental maps presented here.

For EELS-mapping, Gatan Digital Micrograph v2.1.1- software equipped with EELS Analysis-plugin v2.1.1 was used for the background subtraction and the production of elemental maps. The appropriate pre-edge area was manually chosen so that the real-time fit of the Power-law background model was fitting well the pre-edge background based on the visual inspection. After the automatic calculation of the elemental maps for each of the elements, they were manually aligned using the Stack Averager-plugin v2.0 for Digital Micrograph created by D.R.G. Mitchel.

X-ray powder diffractograms were received by a X'Pert MPD Pro (PANalytical, Almelo, NL, $\text{CuK}\alpha$ -radiation, 1.54178 Å) in Bragg-Brentano-geometry and with a X'Celerator detector.

Inductively coupled plasma optical emission spectrometry (ICP-OES) measurements were carried out by using a Vista-pro radical model from Varian.

For XPS (X-ray photoelectron spectroscopy) measurements the samples were prepared on a carbon tape. The measurement were carried out by using a Specs Phoibos 150 R6 with HAS 3500 and MCD-9 detector. The excitation was managed by a Specs focus 500 monochromator equipped with a XR50M X-ray tube (Al-anode, 13 KV, 200 W). For the detail spectra a pass energy of 15 eV (10 scans, 0.075 eV increment, 0.5 s dwelling time) was used. The spectra were calibrated on C_{1s} with a binding energy of 284.8 eV. Charge compensation was carried out by a flood gun.

N_2 physisorption measurements were determined at -196°C using a Nova2000e (Quantachrome) apparatus. The specific surface areas were calculated using p/p_0 values from 0.05-0.31 (BET). The pore width and average pore volume were calculated by DFT calculations [N_2 at -196.15°C on carbon (cylindrical pore, NLDFT equilibrium model)].

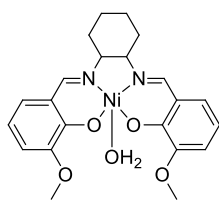
Pyrolysis and Reduction were carried out under nitrogen atmosphere and forming gas (90/10) in a high temperature furnace (EHA 12/450B200, Carbolite) or alternative using ChemBET.

Hydrogen chemisorption measurements were carried out by using a ChemBET Pulsar TPR/TPD instrument from Quantachrome.

Magnetic measurements of the compounds were carried out using a SQUID MPMS-XL5 from Quantum Design with the field range of -3 to 3 T in hysteresis mode. The sample was prepared in a gelatine capsule held in a plastic straw under protective atmosphere. The raw data were corrected for the diamagnetic part of the sample holder.

Macherey Nagel silica gel 60 (40–63 μm particle size) was used for column chromatography. All compounds were characterized by ^1H and ^{13}C NMR analyses. The conversion of achiral and chiral ketones gave the corresponding enantiomeric and diastereomeric mixtures of the primary amines, respectively. Compounds with incomplete spectroscopic literature data were further analyzed via HRMS.

5.6.3.2 Synthesis of the Ni salen complex I



Ni salen complex I

The Ni salen complex **I** was synthesized according to literature in a two step procedure.^[1]

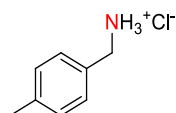
First, the ligand was synthesized. 3.04 g (20 mmol, 2 eq) *o*-vanillin were dissolved in 50 mL ethanol and 1.32 mL (11 mmol, 1.1 eq) (\pm)-trans-1,2-diaminocyclohexane were added. The solution was heated under reflux (oil bath 110 $^{\circ}\text{C}$) for 1 h.

After removal of the solvent under reduced pressure, the residue was recrystallized in methanol to yield the product as a yellow crystalline powder (3.57 g, 85 %).

For the synthesis of the Ni salen complex **I**, the ligand (2.32 g, 6.0 mmol, 1 eq) was dissolved in 40 mL methanol and a methanolic solution of 1.49 g $\text{Ni}(\text{OAc})_2 \cdot 4\text{H}_2\text{O}$ (6.0 mmol, 1 eq) in 40 mL MeOH was added. An orange-brown precipitate was formed during stirring for 2 h at room temperature, which was separated by filtration.

5.6.3.3 Characterization of isolated products

p-tolylmethanaminium chloride (**2'**)^[2]



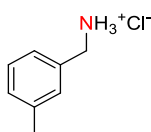
FW ($\text{C}_8\text{H}_{12}\text{ClN}$) = 157.64 g mol^{-1}

^1H NMR (300 MHz, $\text{DMSO-}d_6$): δ = 8.52 (s, 3 H), 7.39 (d, J = 8.20 Hz, 2 H), 7.21 (d, J = 8.20 Hz, 2 H), 3.94 (q, J = 5.86 Hz, 2 H), 2.30 (s, 3 H) ppm

^{13}C NMR (75 MHz, $\text{DMSO-}d_6$): δ = 137.68, 131.08, 129.03, 128.92, 41.83, 20.74 ppm.

Yield: 86 % (0.43 mmol, 68 mg) as an off white solid.

***m*-tolylmethanaminium chloride (3')^[3]**



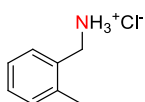
FW (C₈H₁₂ClN) = 157.64 g mol⁻¹

¹H NMR (300 MHz, DMSO-D₆): δ = 8.47 (s, 3 H), 7.28-7.30 (m, 3 H), 7.18-7.20 (m, 1 H), 3.94-3.96 (m, 2 H), 2.31 (s, 3 H) ppm.

¹³C NMR (75 MHz, DMSO-D₆): δ = 137.7, 133.99, 129.47, 128.95, 128.48, 125.93, 142.07, 20.94 ppm.

Yield: 85 % (0.43 mmol, 67 mg) as a white solid.

***o*-tolylmethanaminium chloride (4')^[2]**



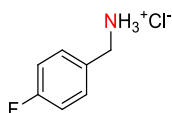
FW (C₈H₁₂ClN) = 157.64 g mol⁻¹

¹H NMR (300 MHz, DMSO-D₆): δ = 8.41 (s, 3 H), 7.39-7.42 (m, 1 H), 7.21-7.28 (m, 3 H), 3.99 (q, *J* = 5.27 Hz, 2 H), 2.35 (s, 3 H) ppm.

¹³C NMR (75 MHz, DMSO-D₆): δ = 136.64, 132.30, 130.31, 129.09, 128.47, 126.04, 18.79 ppm.

Yield: 99% (0.50 mmol, 79 mg) as a white solid.

(4-fluorophenyl)methanaminium chloride (5')^[2]



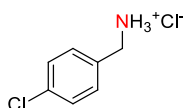
FW (C₇H₉ClFN) = 161.60 g mol⁻¹

¹H NMR (300 MHz, DMSO-D₆): δ = 8.51 (s, 3H), 7.54-7.59 (m, 2 H), 7.23-7.28 (m, 2 H), 4.0 (q, *J* = 5.27 Hz, 2 H) ppm.

¹³C NMR (75 MHz, DMSO-D₆): δ = 131.43, 131.30, 115.50, 115.22, 41.37 ppm.

Yield: 76 % (0.38 mmol, 62 mg) as a white solid.

(4-chlorophenyl)methanaminium chloride (6')^[2]



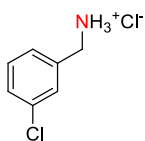
FW (C₇H₉Cl₂N) = 178.06 g mol⁻¹

¹H NMR (300 MHz, DMSO-D₆): δ = 8.65 (s, 3 H), 7.56 (d, *J* = 8.20 Hz, 2 H), 7.47 (d, *J* = 8.20 Hz, 2 H), 3.95-4.05 (m, 2 H) ppm.

¹³C NMR (75 MHz, DMSO-D₆): δ = 133.17, 133.07, 131.01, 128.45, 41.34 ppm.

Yield: 82 % (0.41 mmol, 73 mg) as a white solid.

(3-chlorophenyl)methanaminium chloride (7')^[4]



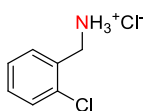
FW (C₇H₉Cl₂N) = 178.06 g mol⁻¹

¹H NMR (300 MHz, DMSO-D₆): δ = 8.67 (s, 3 H), 7.65 (s, 1 H), 7.42-7.49 (m, 3 H), 4.03 (s, 2 H) ppm.

¹³C NMR (75 MHz, DMSO-D₆): δ = 136.54, 133.01, 130.37, 128.89, 128.27, 127.73, 41.42 ppm.

Yield: 91 % (0.45 mmol, 81 mg) as a white solid.

(2-chlorophenyl)methanaminium chloride (8')^[5]



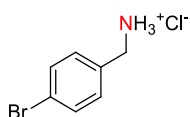
FW (C₇H₉Cl₂N) = 178.06 g mol⁻¹

¹H NMR (300 MHz, DMSO-D₆): δ = 8.74 (s, 3 H), 7.66-7.69 (m, 1 H), 7.51-7.55 (m, 1H), 7.40-7.43 (m, 2 H), 4.11 (s, 2 H) ppm.

¹³C NMR (75 MHz, DMSO-D₆): δ = 132.85, 131.65, 130.66, 130.30, 129.43, 127.46, 39.37 ppm.

Yield: 93 % (0.47 mmol, 83 mg) as a white solid.

(4-bromophenyl)methanaminium chloride (9')^[2]



FW (C₇H₉BrClN) = 222.51 g mol⁻¹

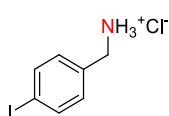
¹H NMR (300 MHz, DMSO-D₆): δ = 8.73 (s, 3 H), 7.59 (d, *J* = 8.21 Hz, 2 H), 7.50 (d, *J* = 8.21 Hz, 2 H), 3.98 (s, 2 H) ppm.

¹³C NMR (75 MHz, DMSO-D₆): δ = 133.55, 131.36, 121.68, 41.42 ppm.

Yield: 94 % (0.47 mmol, 105 mg) as a white solid.

The spectroscopic data correspond to those reported in the literature.^[11]

(4-iodophenyl)methanaminium chloride (10')^[2]



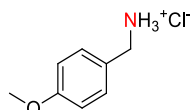
FW (C₇H₉ClIN) = 269.51 g mol⁻¹

¹H NMR (300 MHz, DMSO-D₆): δ = 8.65 (s, 3 H), 7.77 (d, *J* = 7.62 Hz, 2 H), 7.33 (d, *J* = 8.20 Hz, 2 H), 3.95 (s, 2 H) ppm.

¹³C NMR (75 MHz, DMSO-D₆): δ = 137.21, 133.85, 131.30, 94.79, 41.54 ppm.

Yield: 80 % (0.40 mmol, 105 mg) as a white solid.

(4-methoxyphenyl)methanaminium chloride (11')^[2]



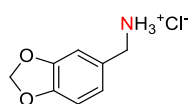
FW (C₈H₁₂ClNO) = 173.64 g mol⁻¹

¹H NMR (300 MHz, DMSO-D₆): δ = 8.60 (s, 3 H), 7.45 (d, *J* = 8.20 Hz, 2 H), 6.93 (d, *J* = 8.20 Hz, 2 H), 3.90 (s, 2 H), 3.73 (s, 3H) ppm.

¹³C NMR (75 MHz, DMSO-D₆): δ = 159.23, 130.57, 125.95, 113.80, 55.18, 41.54 ppm.

Yield: 82 % (0.41 mmol, 71 mg) as a white solid.

benzo[d][1,3]dioxol-5-ylmethanaminium chloride (12')^[6]



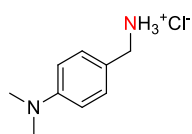
FW (C₈H₁₀ClNO₂) = 187.62 g mol⁻¹

¹H NMR (300 MHz, DMSO-D₆): δ = 8.59 (s, 3 H), 7.16 (s, 1 H), 6.89-6.99 (m, 2 H), 6.02 (s, 2 H), 3.90-3.88 (m, 2 H) ppm.

¹³C NMR (75 MHz, DMSO-D₆): δ = 147.19, 127.67, 122.88, 109.53, 108.16, 101.17, 41.89 ppm.

Yield: 75 % (0.37 mmol, 70 mg) as a white solid.

(4-(dimethylamino)phenyl)methanaminium chloride (13')^[6]



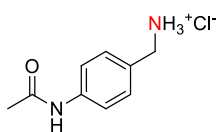
FW (C₉H₁₅N₂Cl) = 186.68 g mol⁻¹

¹H NMR (300 MHz, DMSO-D₆): δ = 8.73 (s, 3H), 7.65-7.71 (m, 4 H), 4.03-4.01 (m, 2H), 3.07 (s, 6 H) ppm.

¹³C NMR (75 MHz, DMSO-D₆): δ = 131.81, 130.59, 119.84, 44.71, 41.43 ppm.

Yield: 99 % (0.49 mmol, 92 mg) as a white solid.

(4-acetamidophenyl)methanaminium chloride (14')^[7]



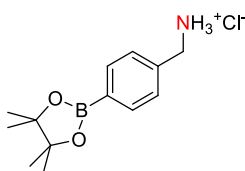
FW (C₉H₁₃ClN₂O) = 200.67 g mol⁻¹

¹H NMR (300 MHz, DMSO-D₆): δ = 10.29 (s, 1 H), 8.49 (s, 3 H), 7.63 (d, *J* = 8.20 Hz, 2 H), 7.41 (d, *J* = 8.20 Hz, 2 H), 3.92 (q, *J* = 5.85 Hz, 2 H), 2.05 (s, 3 H) ppm.

¹³C NMR (75 MHz, DMSO-D₆): δ = 168.50, 139.56, 129.50, 128.31, 118.84, 41.78, 24.01 ppm.

Yield: 79 % (0.39 mmol, 79 mg) as a yellow/white solid.

(4-(4,4,5,5-tetramethyl-1,3,2-dioxaborolan-2-yl)phenyl)methanaminium chloride (15')^[6]



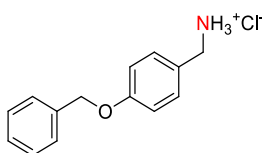
FW (C₁₃H₂₁BClNO₂) = 269.58 g mol⁻¹

¹H NMR (300 MHz, DMSO-D₆): δ = 8.62 (s, 3 H), 7.69 (d, *J* = 7.61 Hz, 2 H), 7.51 (d, *J* = 8.20 Hz, 2 H), 4.02 (s, 2 H), 1.29 (s, 12 H) ppm.

¹³C NMR (75 MHz, DMSO-D₆): δ = 137.32, 134.51, 128.28, 83.74, 42.01, 24.65 ppm.

Yield: 86 % (0.43 mmol, 116 mg) as an off white solid.

(4-(benzyloxy)phenyl)methanaminium chloride (16')^[6]



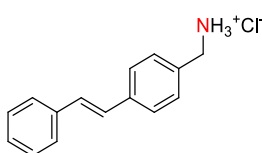
FW (C₁₄H₁₆ClNO) = 249.74 g mol⁻¹

¹H NMR (300 MHz, DMSO-D₆): δ = 8.44 (s, 3 H), 7.32-7.45 (m, 7 H), 7.04 (d, *J* = 8.20 Hz, 2 H), 5.13 (s, 2 H), 3.92-3.91 (m, 2 H) ppm.

¹³C NMR (75 MHz, DMSO-D₆): δ = 158.31, 136.93, 130.53, 128.42, 127.81, 127.60, 126.21, 114.81, 69.14, 41.60 ppm.

Yield: 82 % (0.41 mmol, 103 mg) as an off white solid.

(*E*)-(4-styrylphenyl)methanaminium chloride (17')^[6]



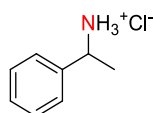
FW (C₁₅H₁₆ClN) = 245.75 g mol⁻¹

¹H NMR (500 MHz, DMSO- D_6): δ = 8.56 (s, 3 H), 7.65-7.60 (m, 4 H), 7.51 (d, J = 8.24 Hz, 2 H), 7.38 (m, 3 H), 7.29 (d, J = 6.41 Hz, 2 H), 4.00 (q, J = 5.80 Hz, 2 H) ppm.

¹³C NMR (125.7 MHz, DMSO- D_6): δ = 137.16, 136.88, 133.36, 129.39, 129.01, 128.84, 128.76, 127.82, 127.77, 126.55, 41.87 ppm.

Yield: 60 % (0.30 mmol, 74 mg) as a yellow solid.

1-phenylethanaminium chloride (18')^[6]



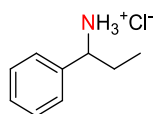
FW ($C_8H_{12}ClN$) = 157.64 g mol⁻¹

¹H NMR (300 MHz, DMSO- D_6): δ = 8.67 (s, 3 H), 7.50-7.57 (m, 2 H), 7.31-7.45 (m, 3 H), 4.30-4.40 (m, 1 H), 1.52 (d, J = 6.44 Hz, 3 H) ppm.

¹³C NMR (75 MHz, DMSO- D_6): δ = 139.48, 128.65, 128.30, 126.83, 49.98, 20.83 ppm.

Yield: 92 % (0.46 mmol, 72 mg) as a white solid.

1-phenylpropan-1-aminium chloride (19')^[8]



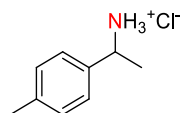
FW ($C_9H_{14}ClN$) = 171.68 g mol⁻¹

¹H NMR (300 MHz, DMSO- D_6): δ = 8.73 (s, 3 H), 7.51-7.54 (m, 2 H), 7.37-7.43 (m, 3 H), 4.05-4.15 (m, 1 H), 2.01-2.05 (m, 1 H), 1.79-1.85 (m, 1 H), 0.70-0.75 (t, J = 7.62 Hz, 3 H) ppm.

¹³C NMR (75 MHz, DMSO- D_6): δ = 137.80, 128.59, 128.37, 127.52, 55.82, 27.47, 10.00 ppm.

Yield: 96 % (0.48 mmol, 83 mg) as a white solid.

1-(*p*-tolyl)ethanaminium chloride (21')^[9]



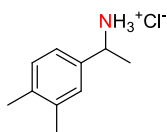
FW ($C_9H_{14}ClN$) = 171.68 g mol⁻¹

¹H NMR (300 MHz, DMSO- D_6): δ = 8.72 (s, 3 H), 7.43 (d, J = 7.62 Hz, 2 H), 7.20 (d, J = 8.20 Hz, 2 H), 4.26-4.34 (m, 1 H), 2.28 (s, 3 H), 1.50 (d, J = 7.03 Hz, 3 H) ppm.

¹³C NMR (75 MHz, DMSO- D_6): δ = 137.54, 136.55, 129.11, 126.85, 49.81, 20.86, 20.73 ppm.

Yield: 80 % (0.40 mmol, 68 mg) as a white solid.

1-(3,4-dimethylphenyl)ethanaminium chloride (22')^[10]



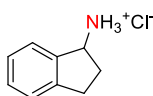
FW (C₁₀H₁₆ClN) = 185.69 g mol⁻¹

¹H NMR (300 MHz, DMSO-D₆): δ = 8.63 (s, 3 H), 7.29 (s, 1 H), 7.14-7.25 (m, 2 H), 7.15 (d, *J* = 6.0 Hz, 1 H), 4.21-4.29 (m, 1H), 2.21 (d, *J* = 3.51 Hz, 6 H), 1.49 (d, *J* = 6.45 Hz, 3 H) ppm.

¹³C NMR (75 MHz, DMSO-D₆): δ = 136.84, 136.34, 136.26, 129.61, 127.93, 124.12, 49.76, 20.82, 19.46, 19.05 ppm.

Yield: 79 % (0.39 mmol, 73 mg) as a white solid.

2,3-dihydro-1*H*-inden-1-aminium chloride (23')^[6]



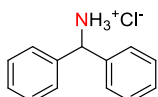
FW (C₉H₁₂ClN) = 169.65 g mol⁻¹

¹H NMR (300 MHz, DMSO-D₆): δ = 8.77 (s, 3 H), 7.70-7.72 (m, 1 H), 7.27-7.31 (m, 3 H), 4.66 (s, 1H), 3.05-3.07 (m, 1 H), 2.85-2.88 (m, 1 H), 2.43-2.48 (m, 1 H), 2.04-2.06 (m, 1 H) ppm.

¹³C NMR (75 MHz, DMSO-D₆): δ = 143.91, 139.44, 128.82, 126.51, 125.17, 124.77, 54.51, 30.28, 29.84 ppm.

Yield: 88 % (0.44 mmol, 75 mg) as an off white solid.

diphenylmethanaminium chloride (24')^[11]



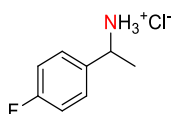
FW (C₁₃H₁₄ClN) = 219.71 g mol⁻¹

¹H NMR (300 MHz, DMSO-D₆): δ = 9.32 (s, 3 H), 7.57-7.60 (m, 4 H), 7.33-7.43 (m, 6 H), 5.60-5.62 (m, 1 H) ppm.

¹³C NMR (75 MHz, DMSO-D₆): δ = 138.46, 128.71, 128.21, 127.40, 57.10 ppm.

Yield: 76 % (0.38 mmol, 83 mg) as a white solid.

1-(4-fluorophenyl)ethanaminium chloride (25')^[9]



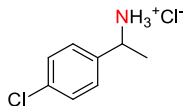
FW (C₈H₁₁ClFN) = 175.63 g mol⁻¹

¹H NMR (300 MHz, DMSO-D₆): δ = 8.75 (s, 3 H), 7.60-7.64 (m, 2 H), 7.21-7.27 (m, 2 H), 4.38-4.41 (m, 1H), 1.52 (d, *J* = 7.03, 3 H) ppm.

^{13}C NMR (75 MHz, DMSO- D_6): δ = 163.51, 160.28, 135.77, 129.20, 115.54, 115.25, 49.34, 20.77 ppm.

Yield: 81% (0.41 mmol, 71 mg) as an off white solid.

1-(4-chlorophenyl)ethanaminium chloride (26')^[9]



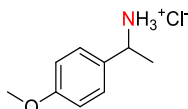
FW ($\text{C}_8\text{H}_{11}\text{Cl}_2\text{N}$) = 192.09 g mol⁻¹

^1H NMR (300 MHz, DMSO- D_6): δ = 8.75 (s, 3 H), 7.59 (d, J = 8.79, 2 H), 7.48 (d, J = 8.79, 2 H), 4.35-4.45 (m, 1H), 1.51 (d, J = 7.03, 3 H) ppm.

^{13}C NMR (75 MHz, DMSO- D_6): δ = 138.44, 132.92, 128.95, 128.57, 49.32, 20.65 ppm.

Yield: 60 % (0.30 mmol, 58 mg) as a white solid.

1-(4-methoxyphenyl)ethanaminium chloride (27')^[6]



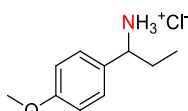
FW ($\text{C}_9\text{H}_{14}\text{ClNO}$) = 187.67 g mol⁻¹

^1H NMR (300 MHz, DMSO- D_6): δ = 8.66 (s, 3 H), 7.48 (d, J = 8.78 Hz, 2 H), 6.95 (d, J = 8.78 Hz, 2 H), 4.26-4.34 (m, 3 H), 1.50 (d, J = 7.13 Hz, 3 H) ppm.

^{13}C NMR (75 MHz, DMSO- D_6): δ = 159.18, 131.43, 128.33, 113.94, 55.23, 49.52, 20.79 ppm.

Yield: 99 % (0.49 mmol, 93 mg) as a white solid.

1-(4-methoxyphenyl)propan-1-aminium chloride (28')^[8]



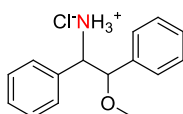
FW ($\text{C}_{10}\text{H}_{16}\text{ClNO}$) = 201.69 g mol⁻¹

^1H NMR (300 MHz, DMSO- D_6): δ = 8.61 (s, 3H), 7.45 (d, J = 8.78 Hz, 2 H), 6.97 (d, J = 8.78 Hz, 2 H), 4.00-4.02 (m, 1 H), 3.76 (s, 3 H), 1.97-2.03 (m, 1 H), 1.76-1.81 (m, 1H), 0.70-0.75 (m, 3 H) ppm.

^{13}C NMR (75 MHz, DMSO- D_6): δ = 159.23, 129.60, 128.89, 113.96, 55.36, 55.18, 27.39, 10.11 ppm.

Yield: 83 % (0.42 mmol, 84 mg) as a white solid.

2-methoxy-1,2-diphenylethanaminium chloride (29') (diastereomeric mixture)^[12]



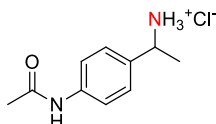
FW ($\text{C}_{15}\text{H}_{18}\text{ClNO}$) = 263.76 g mol⁻¹

¹H NMR (300 MHz, DMSO-*D*₆): δ = 8.96 (s, 3 H), 7.06-7.38 (m, 10 H), 5.05 (d, *J* = 3.51 Hz, 0.5 H), 4.72 (d, *J* = 9.96 Hz, 0.5 H), 4.38-4.42 (m, 1 H), 3.21 (d, *J* = 3.51, 3 H) ppm.

¹³C NMR (75 MHz, DMSO-*D*₆): δ = 136.58, 134.58, 129.00, 128.59, 128.27, 127.83, 127.83, 127.66, 126.82, 84.13, 82.13, 59.33, 58.89, 57.04, 56.13 ppm.

Yield: 91 % (0.45 mmol, 120 mg) as a white solid.

1-(4-acetamidophenyl)ethanaminium chloride (30')^[13]



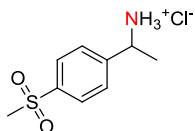
FW (C₁₀H₁₅ClN₂O) = 214.69 g mol⁻¹

¹H NMR (300 MHz, DMSO-*D*₆): δ = 10.29 (s, 1 H), 8.58 (s, 3 H), 7.63 (d, *J* = 8.20 Hz, 2 H), 7.44 (d, *J* = 8.20 Hz, 2 H), 4.28-4.31 (m, 1 H), 2.04 (s, 3 H), 1.49 (d, *J* = 6.45 Hz, 3 H) ppm.

¹³C NMR (75 MHz, DMSO-*D*₆): δ = 168.47, 139.44, 133.64, 127.29, 118.96, 49.61, 23.99, 20.60 ppm.

Yield: 81 % (0.41 mmol, 87 mg) as a white solid.

1-(4-(methylsulfonyl)phenyl)ethanaminium chloride (31')^[6]



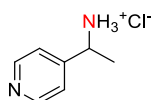
FW (C₉H₁₄ClNO₂S) = 235.73 g mol⁻¹

¹H NMR (300 MHz, DMSO-*D*₆): δ = 8.93 (s, 3 H), 7.97 (d, *J* = 8.20 Hz, 2 H), 7.85 (d, *J* = 8.20 Hz, 2 H), 4.51-4.55 (m, 1 H), 3.24 (s, 3 H), 1.55 (d, *J* = 6.45 Hz, 3 H) ppm.

¹³C NMR (75 MHz, DMSO-*D*₆): δ = 145.16, 140.64, 128.05, 127.31, 49.60, 43.43, 20.74 ppm.

Yield: 93 % (0.47 mmol, 110 mg) as an off white solid.

1-(pyridin-4-yl)ethanaminium chloride (33')^[14]



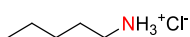
FW (C₇H₁₂ClN₂) = 158.63 g mol⁻¹

¹H NMR (300 MHz, DMSO-*D*₆): δ = 8.89 (s, 3 H), 8.59-8.63 (m, 2 H), 7.56-7.58 (m, 2 H), 4.41 (q, *J* = 6.44 Hz, 1 H), 1.52 (d, *J* = 7.03 Hz, 3 H) ppm.

¹³C NMR (75 MHz, DMSO-*D*₆): δ = 157.55, 142.78, 125.05, 49.14, 20.18 ppm.

Yield: 95 % (0.47 mmol, 75 mg) as a white solid.

pentan-1-aminium chloride (35')^[2]



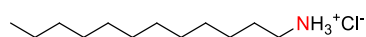
FW (C₅H₁₄ClN) = 123.62 g mol⁻¹

¹H NMR (300 MHz, DMSO-D₆): δ = 8.12 (s, 3 H), 2.67-2.77 (m, 2 H), 1.51-1.60 (m, 2 H), 1.27-1.29 (m, 4 H), 0.86 (t, *J* = 6.5 Hz, 3 H) ppm.

¹³C NMR (75 MHz, DMSO-D₆): δ = 38.61, 27.99, 26.56, 21.63, 13.74 ppm.

Yield: 66 % (0.33 mmol, 41 mg) as a white solid.

dodecan-1-aminium chloride (37')^[2]



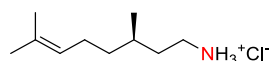
FW (C₁₂H₂₈ClN) = 221.81 g mol⁻¹

¹H NMR (300 MHz, DMSO-D₆): δ = 8.14 (s, 3 H), 2.7-2.80 (m, 2 H), 1.50-1.65 (m, 2 H), 1.20-1.35 (m, 18 H), 0.85-0.90 (m, 3 H) ppm.

¹³C NMR (75 MHz, DMSO-D₆): δ = 38.67, 31.30, 29.06, 29.03, 28.95, 28.86, 28.72, 28.57, 26.89, 25.90, 22.10, 13.92 ppm.

Yield: 98 % (0.49 mmol, 110 mg) as a white solid.

(*R*)-3,7-dimethyloct-6-en-1-aminium chloride (38')^[15]



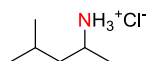
FW (C₁₀H₂₂ClN) = 191.74 g mol⁻¹

¹H NMR (300 MHz, DMSO-D₆): δ = 8.13 (s, 3 H), 5.07 (t, *J* = 7.03 Hz, 1 H), 2.68-2.79 (m, 2 H), 1.98-1.89 (m, 2 H), 1.63 (s, 3 H), 1.56 (s, 3 H), 1.51-1.07 (m, 5 H), 0.85 (d, *J* = 6.45 Hz, 3 H) ppm.

¹³C NMR (75 MHz, DMSO-D₆): δ = 130.63, 124.41, 36.89, 36.31, 33.77, 29.44, 25.50, 24.79, 19.06, 17.54 ppm.

Yield: 87 % (0.43 mmol, 83 mg) as a white solid.

4-methylpentan-2-aminium chloride (39')^[16]



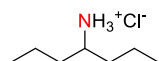
FW (C₆H₁₈ClN) = 137.65 g mol⁻¹

¹H NMR (300 MHz, DMSO-D₆): δ = 8.10 (s, 3 H), 3.14 (q, *J* = 6.44 Hz, 1 H), 1.60-1.74 (m, 1 H), 1.43-1.50 (m, 1 H), 1.23-1.35 (m, 2 H), 1.18 (d, *J* = 6.44 Hz, 3 H), 0.86 (dd, *J* = 11.72, 6.44 Hz, 6 H) ppm.

¹³C NMR (75 MHz, DMSO-D₆): δ = 44.97, 43.23, 23.78, 22.83, 21.73, 18.32 ppm.

Yield: 78 % (0.39 mmol, 54 mg) as a white solid.

heptan-4-aminium chloride (40')^[17]



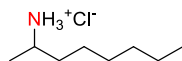
FW (C₇H₁₈ClN) = 151.68 g mol⁻¹

¹H NMR (300 MHz, DMSO-D₆): δ = 7.98 (s, 3 H), 3.00-3.06 (m, 1 H), 1.34-1.51 (m, 8 H), 0.87 (t, *J* = 7.03 Hz, 6 H) ppm.

¹³C NMR (75 MHz, DMSO-D₆): δ = 50.21, 34.12, 17.80, 13.77 ppm.

Yield: 76 % (0.38 mmol, 58 mg) as a white solid.

octan-2-aminium chloride (41')^[6]



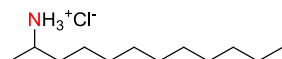
FW (C₈H₂₀ClN) = 165.70 g mol⁻¹

¹H NMR (300 MHz, DMSO-D₆): δ = 8.13 (s, 3 H), 3.00-3.15 (m, 1 H), 1.20-1.65 (m, 10 H), 1.87 (d, *J* = 6.44 Hz, 3 H), 0.80-0.90 (m, 3 H) ppm.

¹³C NMR (75 MHz, DMSO-D₆): δ = 46.70, 34.02, 31.04, 28.42, 24.71, 21.96, 18.03, 13.89 ppm.

Yield: 92 % (0.46 mmol, 76 mg) as an off white solid.

dodecan-2-aminium chloride (42')^[18]



FW (C₁₂H₂₈ClN) = 221.81 g mol⁻¹

¹H NMR (300 MHz, DMSO-D₆): δ = 8.21 (s, 3 H), 2.95-3.15 (m, 1 H), 1.18-1.70 (m, 18 H), 1.17 (d, *J* = 6.44 Hz, 3 H), 0.78-0.88 (m, 3 H) ppm.

¹³C NMR (75 MHz, DMSO-D₆): δ = 46.74, 34.00, 31.32, 29.03, 29.00, 28.91, 28.83, 28.74, 24.85, 22.12, 17.95, 13.89 ppm.

Yield: 85 % (0.42 mmol, 94 mg) as a white solid.

cyclohexanaminium chloride (44')^[6]



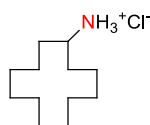
FW (C₆H₁₄ClN) = 135.64 g mol⁻¹

¹H NMR (300 MHz, DMSO-D₆): δ = 8.06 (s, 3 H), 2.89-2.92 (m, 1 H), 1.06-1.93 (m, 10 H) ppm.

¹³C NMR (75 MHz, DMSO-D₆): δ = 49.24, 30.23, 24.60, 23.73 ppm.

Yield: 99 % (0.49 mmol, 67 mg) as a white solid.

cyclododecanaminium chloride (45')^[19]



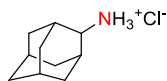
FW (C₁₂H₂₆ClN) = 219.79 g mol⁻¹

¹H NMR (300 MHz, DMSO-D₆): δ = 8.06 (s, 3 H), 3.08-3.17 (m, 1 H), 1.30-1.63 (m, 23 H) ppm.

^{13}C NMR (75 MHz, DMSO- D_6): $\delta = 47.78, 27.56, 23.50, 23.21, 22.77, 20.27$ ppm.

Yield: 71 % (0.36 mmol, 78 mg) as a white solid.

adamantan-2-aminium chloride (46')^[6]



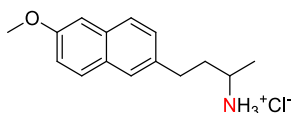
FW ($\text{C}_{10}\text{H}_{18}\text{ClN}$) = 187.71 g mol⁻¹

^1H NMR (300 MHz, DMSO- D_6): $\delta = 8.39$ (s, 3 H), 3.15-3.20 (m, 1 H), 1.48-2.09 (m, 14 H) ppm.

^{13}C NMR (75 MHz, DMSO- D_6): $\delta = 54.63, 36.84, 36.12, 29.87, 29.45, 26.39$ ppm.

Yield: 93% (0.46 mmol, 87 mg) as a white solid.

4-(6-methoxynaphthalen-2-yl)butan-2-aminium chloride (47')^[6]



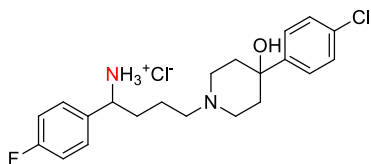
FW ($\text{C}_{10}\text{H}_{16}\text{ClNO}$) = 265.78 g mol⁻¹

^1H NMR (300 MHz, DMSO- D_6): $\delta = 8.22$ (s, 3 H), 7.76 (d, $J = 9.38$ Hz, 2 H), 7.64 (s, 1 H), 7.33-7.39 (m, 1 H), 7.28 (s, 1 H), 7.13 (dd, $J = 8.79$ Hz, 1.75 Hz, 1 H), 3.85 (s, 3 H), 3.12-3.19 (m, 1H), 2.71-2.87 (m, 2 H), 1.75-2.09 (m, 2 H), 1.27 (d, $J = 6.44$ Hz, 3 H) ppm.

^{13}C NMR (75 MHz, DMSO- D_6): $\delta = 157.31, 136.54, 133.28, 129.27, 129.04, 128.03, 127.34, 126.43, 119.09, 106.26, 55.61, 46.89, 36.27, 31.26, 18.57$ ppm.

Yield: 87 % (0.43 mmol, 115 mg) as a white solid.

4-(4-(4-chlorophenyl)-4-hydroxypiperidin-1-yl)-1-(4-fluorophenyl)butan-1-aminium chloride (48') (diastereomeric mixture)



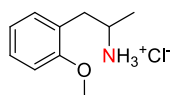
FW ($\text{C}_{21}\text{H}_{27}\text{Cl}_2\text{FN}_2\text{O}$) = 413.36 g mol⁻¹

^1H NMR (300 MHz, DMSO- D_6): $\delta = 11.18$ (s, 1H), 8.85 (s, 1 H), 7.27-8.07 (m, 8 H), 5.67 (s, 1 H), 3.16-3.40 (m, 9 H), 2.07-2.09 (m, 2 H), 1.76-1.80 (m, 4 H) ppm.

^{13}C NMR (75 MHz, DMSO- D_6): $\delta = 197.78, 147.56, 133.66, 131.89, 131.45, 131.31, 128.49, 127.12, 116.34, 116.05, 68.54, 55.80, 53.45, 48.73, 35.89, 35.26, 18.40$ ppm.

Yield: 94 % (0.23 mmol, 97 mg) as a white solid.

1-(2-methoxyphenyl)propan-2-aminium chloride (49')^[6]



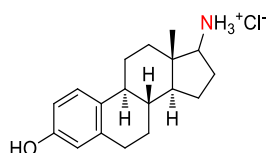
FW (C₁₀H₁₆NO) = 201.69 g mol⁻¹

¹H NMR (300 MHz, DMSO-D₆): δ = 8.34 (s, 3 H), 6.86-7.26 (m, 4 H), 3.77 (s, 3 H), 3.34-3.41 (m, 1 H), 3.00-3.60 (m, 1 H), 2.67-2.74 (m, 1 H), 1.09 (d, *J* = 6.44 Hz, 3 H) ppm.

¹³C NMR (75 MHz, DMSO-D₆): δ = 157.29, 130.91, 128.34, 124.67, 120.39, 110.92, 55.35, 46.73, 34.87, 17.63 ppm.

Yield: 82 % (0.41 mmol, 82 mg) as a red/white solid.

(8*R*,9*S*,13*S*,14*S*)-3-hydroxy-13-methyl-7,8,9,11,12,13,14,15,16,17-decahydro-6*H*-cyclopenta[*a*]phenanthren-17-aminium chloride (50') (diastereomeric mixture)^[6]



FW (C₁₈H₂₆ClNO) = 307.86 g mol⁻¹

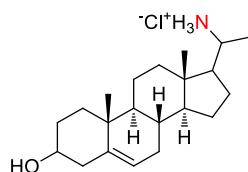
¹H NMR (500 MHz, DMSO-D₆): δ = 9.09 (s, 1H), 8.20 (s, 1H), 7.03 (d, *J* = 8.24 Hz, 1 H), 6.49 (m, 2 H), 2.43 (s, 1H), 1.22-2.41 (m, 15 H), 0.81 (s, 1.5 H), 0.75 (s, 1.5 H) ppm.

¹³C NMR (125.7 MHz, DMSO-D₆): δ = 155.07, 155.05, 137.07, 136.98, 129.93, 129.85, 126.04, 114.97, 114.95, 112.82, 112.78, 59.43, 58.73, 50.78, 49.57, 47.33, 43.45, 43.11, 42.84, 42.02, 38.19, 37.96, 36.72, 35.38, 31.36, 29.06, 27.02, 26.23, 26.14, 25.60, 25.56, 23.06, 21.14, 17.84, 13.52, 11.64 ppm.

HRMS (ESI+) *m/z* calcd. for [C₁₈H₂₆NO]⁺ 272.20089, found 272.20023.

Yield: 78 % (0.39 mmol, 119 mg) as a white solid.

1-((8*S*,9*S*,10*R*,13*S*,14*S*)-3-hydroxy-10,13-dimethyl-2,3,4,7,8,9,10,11,12,13,14,15,16,17-tetradecahydro-1*H*-cyclopenta[*a*]phenanthren-17-yl)ethanaminium chloride (51') (diastereomeric mixture)^[6]



FW (C₂₁H₃₆ClNO) = 353.97 g mol⁻¹

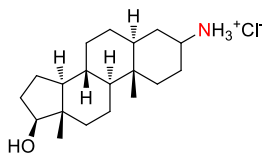
¹H NMR (500 MHz, DMSO-D₆): δ = 7.95 (s, 3 H), 5.26 (s, 1 H), 4.64 (s, 1 H), 3.20-3.30 (m, 1 H), 3.00-3.30 (m, 1 H), 1.60-2.30 (m, 27 H), 0.64-0.71 (m, 3 H) ppm.

¹³C NMR (125.7 MHz, DMSO-D₆): δ = 141.28, 120.29, 69.97, 55.83, 53.88, 53.77, 50.11, 49.46, 49.38, 48.20, 42.20, 41.68, 41.37, 38.37, 37.00, 36.92, 36.06, 36.05, 31.40, 31.31, 31.24, 26.22, 25.49, 23.75, 23.54, 20.44, 20.35, 19.18, 19.14, 18.89, 18.77, 11.62, 11.48 ppm.

HRMS (ESI+) m/z calcd. for $[C_{21}H_{36}NO]^+$ 318.27914, found 318.27840.

Yield: 98 % (0.49 mmol, 172 mg) as a white solid.

(5*S*,8*R*,9*S*,10*S*,13*S*,14*S*,17*S*)-17-hydroxy-10,13-dimethylhexadecahydro-1*H*-cyclopenta[*a*]phenanthren-3-aminium chloride (52') (diastereomeric mixture)^[6]



FW ($C_{19}H_{34}ClNO$) = 327.93 $g\ mol^{-1}$

1H NMR (500 MHz, DMSO- D_6): δ = 8.12 (s, 3H), 4.45 (s, 1H), 3.41 (s, 1H), 0.84-2.36 (m, 23 H), 0.74 (s, 3H), 0.61 (s, 3H) ppm.

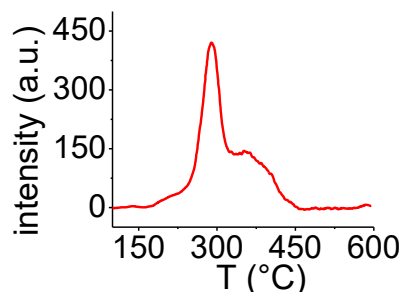
^{13}C NMR (125.7 MHz, DMSO- D_6): δ = 80.03, 56.59, 53.77, 53.63, 53.33, 53.20, 50.73, 50.57, 49.44, 46.19, 44.13, 43.87, 42.56, 37.94, 36.64, 36.03, 35.54, 36.10, 35.02, 34.92, 32.28, 31.15, 30.79, 30.51, 29.83, 27.97, 27.87, 27.75, 26.36, 25.75, 25.57, 23.82, 23.05, 20.64, 20.32, 19.93, 11.82, 11.34, 11.09 ppm.

HRMS (ESI+) m/z calcd. for $[C_{19}H_{34}NO]^+$ 292.26349, found 292.26243.

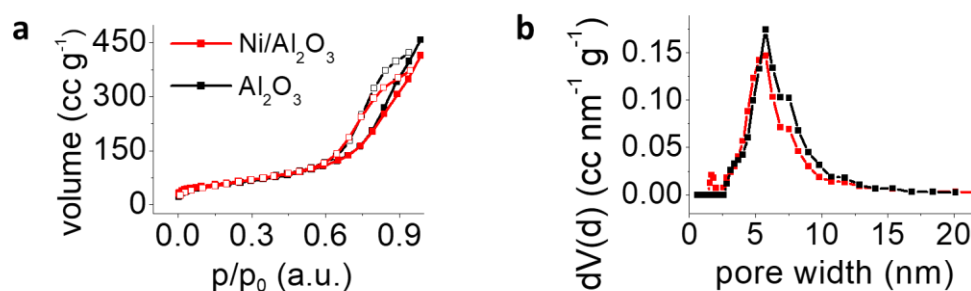
Yield: 97 % (0.48 mmol, 159 mg) as a white solid.

5.6.4 Supplementary Figures

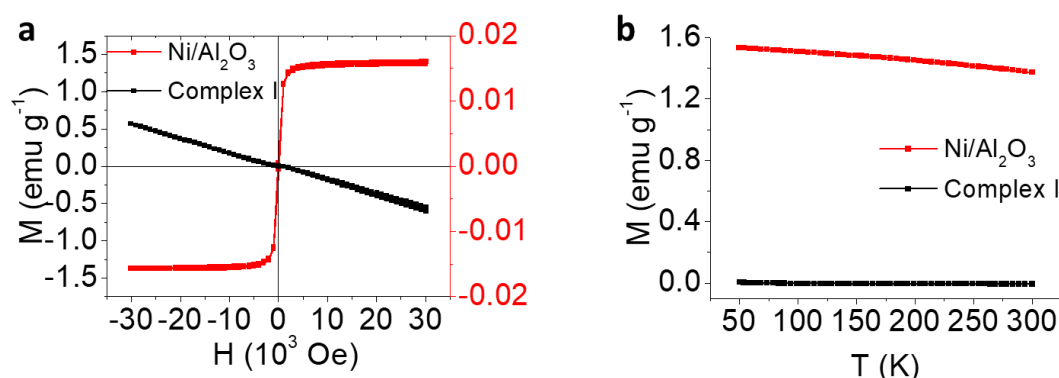
5.6.4.1 Catalyst characterization



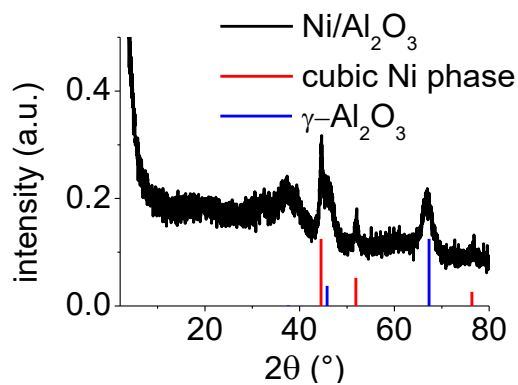
Supplementary Figure 1: Temperature programmed reduction (TPR) of the Ni/Al₂O₃ catalyst after pyrolysis. Hydrogen consumption at 300 °C verifies the presence of an oxidic nickel species.



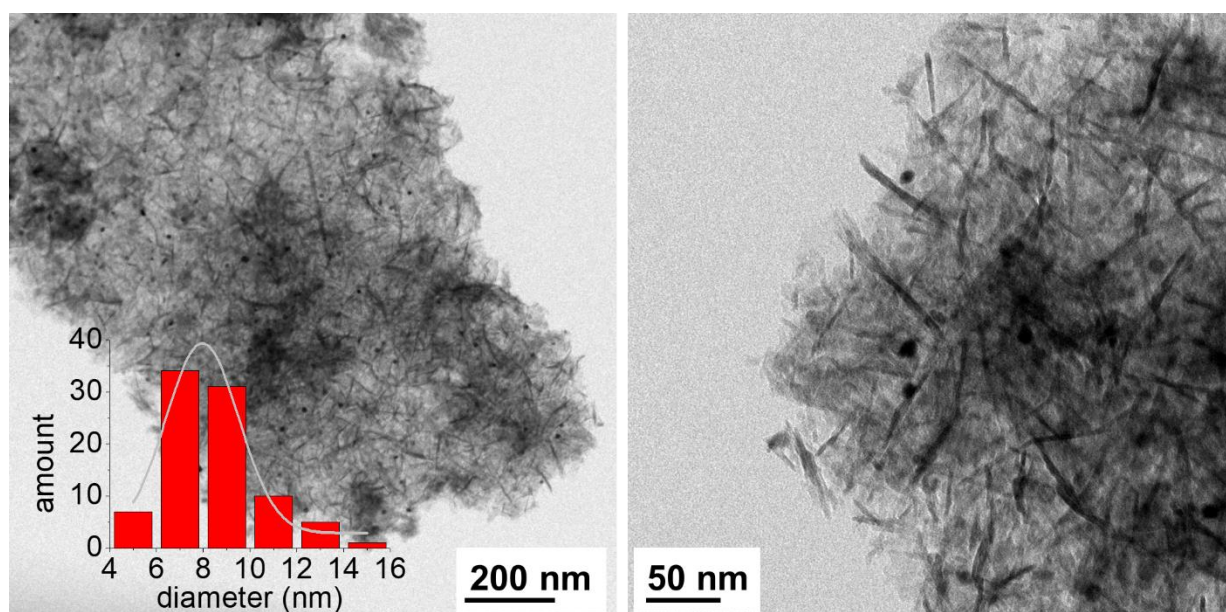
Supplementary Figure 2: Characterization of the surface area of the catalyst by nitrogen physisorption measurements. **a**, Isotherms of the Ni/Al₂O₃ catalyst (red) and the commercial γ -Al₂O₃ support (black). Both materials show the typical hysteresis of mesoporous materials. Due to the impregnation of the Al₂O₃ support with complex **I**, only a slight decrease from 220 to 210 m² g⁻¹ of the surface area can be observed. **b**, Corresponding calculated pore size distributions [N₂ at -196.15 °C on carbon (cylindrical pore, NLDFT equilibrium model), red: Ni/ Al₂O₃, black: Al₂O₃]. show no significant differences for both samples.



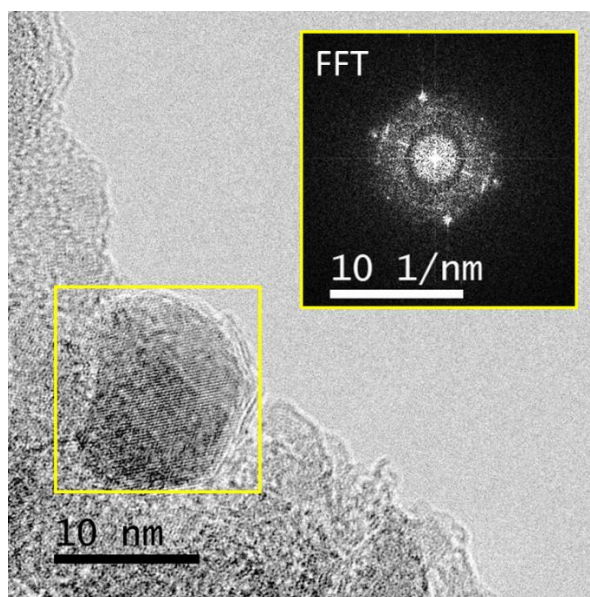
Supplementary Figure 3: Characterization of the magnetic properties of the catalyst. **a**, Magnetic measurements of the complex **I** (black) and the Ni/Al₂O₃ catalyst (red) at 27 °C. Due to the formation of small Ni nanoparticles during pyrolysis and reduction a change from diamagnetism (black) to superparamagnetism (red) was observed. **b**, Temperature-dependent magnetization of the complex **I** (black) and Ni/Al₂O₃ (red) show the typical trend for the diamagnetic complex (no magnetization all over the temperature range) and the magnetic catalyst (magnetization of 1.37 emu g⁻¹ at 27 °C and 1.53 emu g⁻¹ at -223 °C).



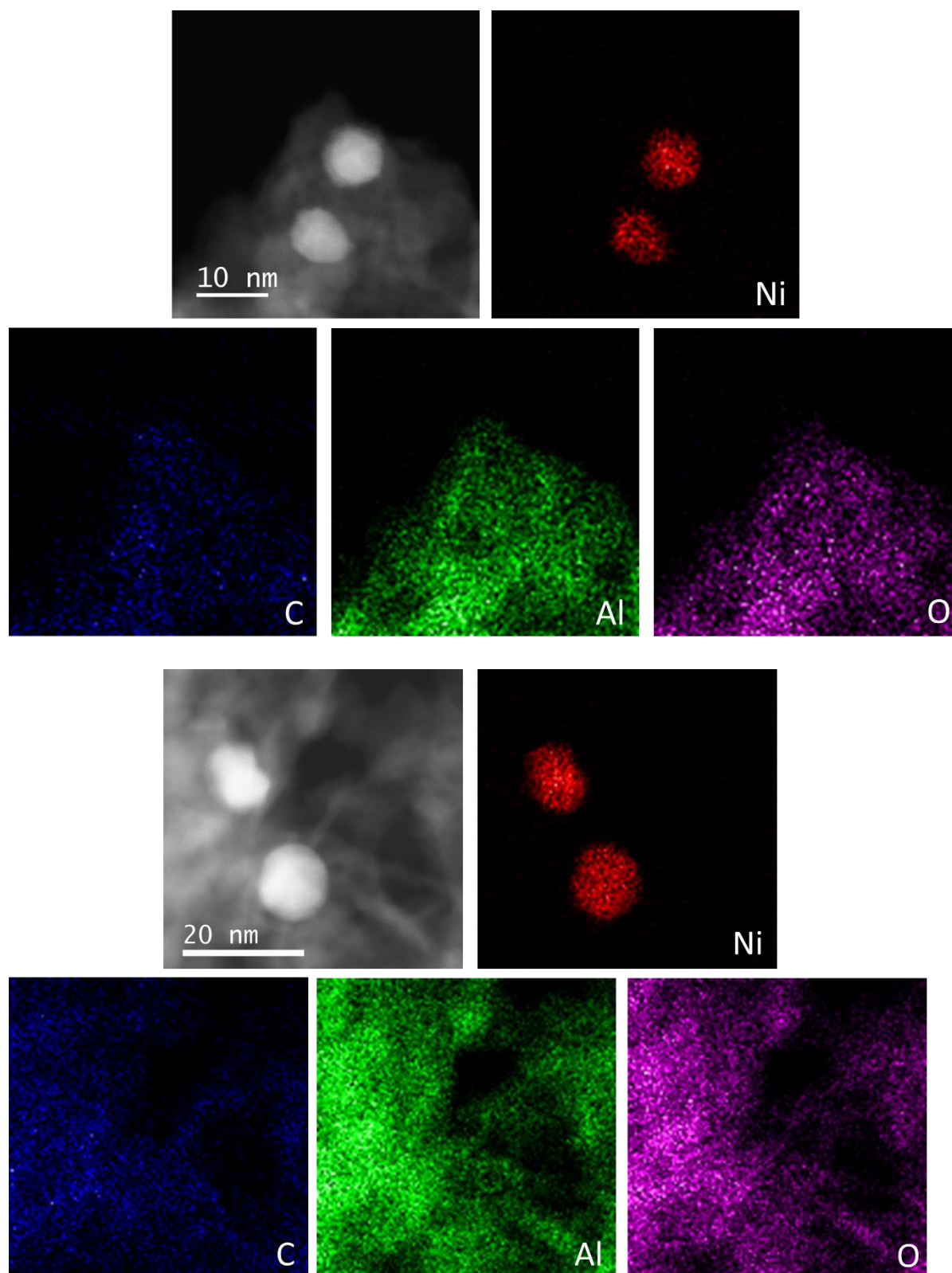
Supplementary Figure 4: Powder X-ray diffraction (PXRD). The reflexes at 2θ values of 44.5° , 51.8° and 76.4° can be assigned to the (111), (200) and (220) reflexes of cubic Ni^0 (blue). The reflexes at 2θ values of 37.6° , 45.8° and 67.3° can be assigned to the (311), (400) and (440) reflexes of $\gamma\text{-Al}_2\text{O}_3$ (blue).



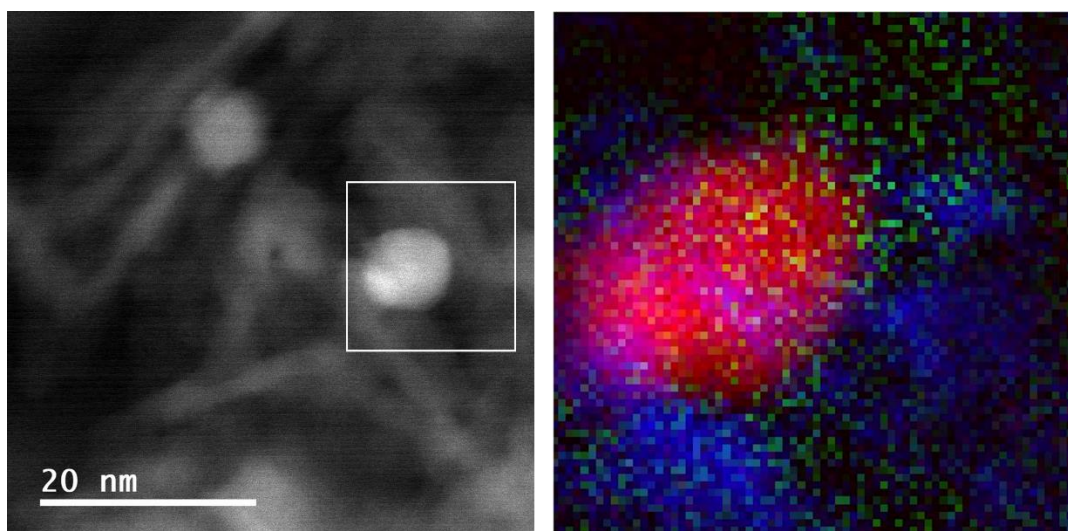
Supplementary Figure 5: Characterization of the nickel nanoparticles by transmissions electron microscopy (TEM). An average particle size of 8 nm could be observed.



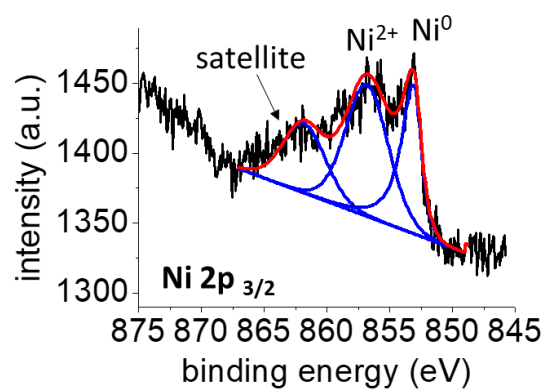
Supplementary Figure 6: Characterization of the nickel nanoparticles by TEM. The characteristic lattice planes and the corresponding fast fourier transform (FFT) indicates metallic nickel. The analysis resulted in a d-spacing of 202.4 pm, which is in accordance with the expected value of 203.4 pm for the (111) reflex of cubic crystalline Ni.



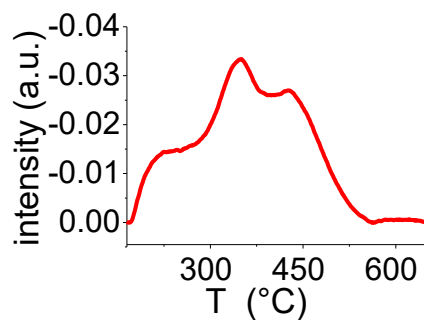
Supplementary Figure 7: Characterization of the nickel nanoparticles by high-angle annular dark-field scanning TEM (HAADF-STEM) analysis combined with energy-dispersed X-ray (EDX) element maps. Al_2O_3 (Al: green, O: magenta) is covered with homogeneously dispersed Ni nanoparticles (Ni: red). The nanoparticles are embedded in a carbon layer (C: blue).



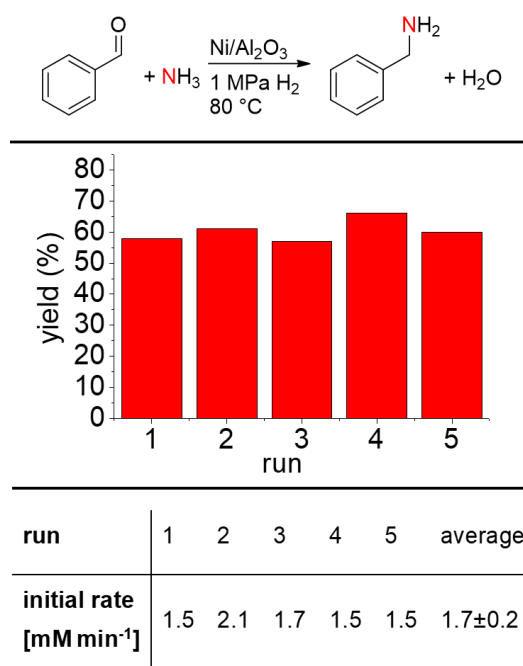
Supplementary Figure 8: Characterization of the nickel nanoparticles by high-angle annular dark-field scanning TEM (HAADF-STEM) analysis combined with electron energy loss spectroscopy (EELS) element maps. High magnification (4Mx) areal density map (EELS) shows the interface of the matrix and a Ni nanoparticle (Ni: red, N: green, C: blue).



Supplementary Figure 9: X-ray photoelectron spectra (XPS) of the Ni 2p_{3/2}. The different Ni species are labelled as Ni⁰ for metallic nickel and Ni²⁺ for an oxidic nickel species. The ratio of Ni⁰:Ni²⁺ is approximately 1:1.5.

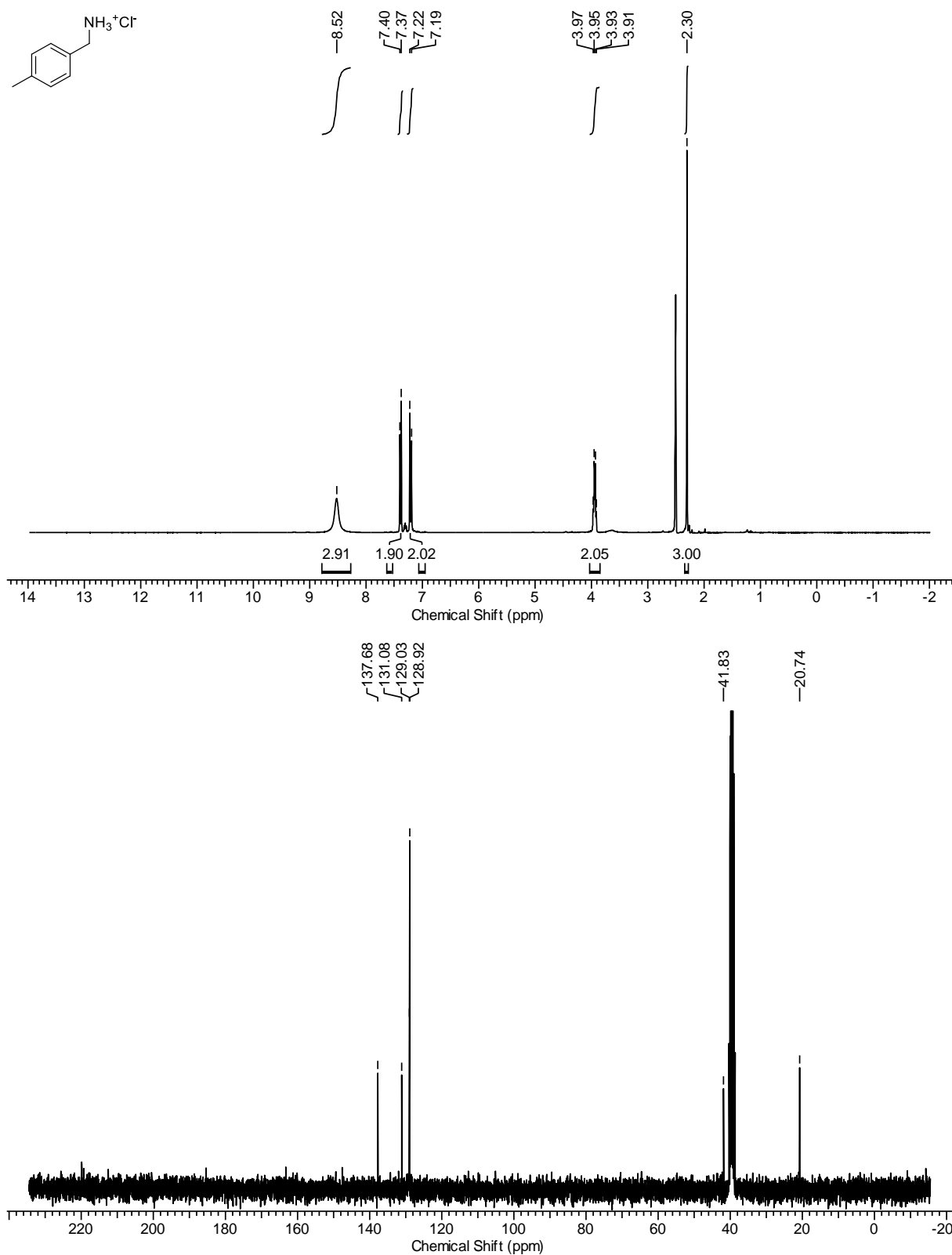


Supplementary Figure 10: NH₃ temperature programmed desorption (NH₃-TPD). The desorption of NH₃ at approx. 400 °C identifies the acidic sites of the Ni/Al₂O₃ catalyst.

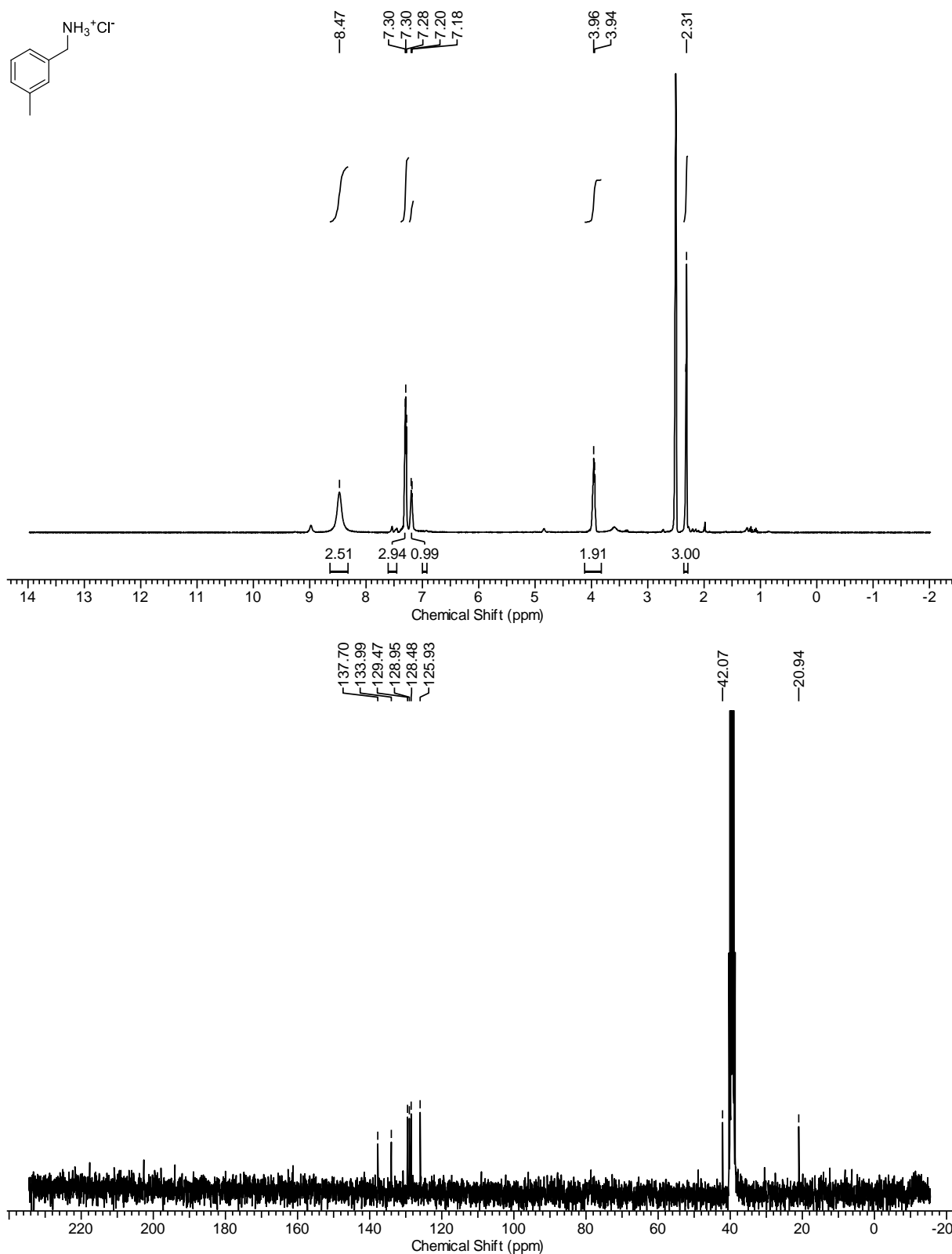


Supplementary Figure 11: Recycling study. The reusability of the Ni/Al₂O₃ catalyst was tested for the reductive amination of benzylamine in 5 consecutive runs. For the recycling study the optimized reaction conditions (1 MPa H₂, 0.5 mL aq. NH₃ 25 % (6.7 mmol), 2 mL H₂O, 80 °C) were used. Neither at 60 %, nor at 20 % yield of benzylamine any decrease of activity was observed. The initial rate for this reaction is 1.7±0.2 mM min⁻¹.

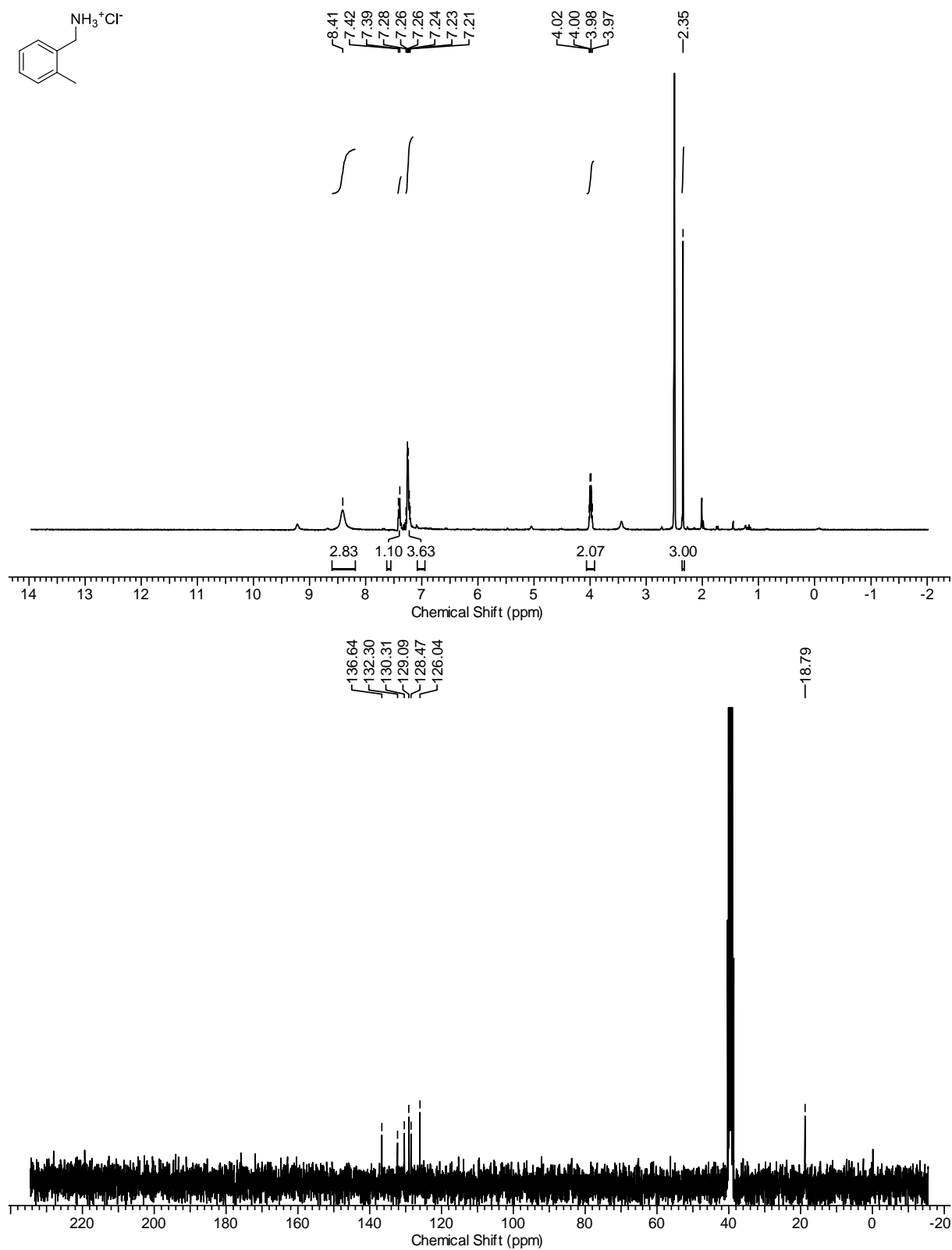
5.6.4.2 NMR Spectra



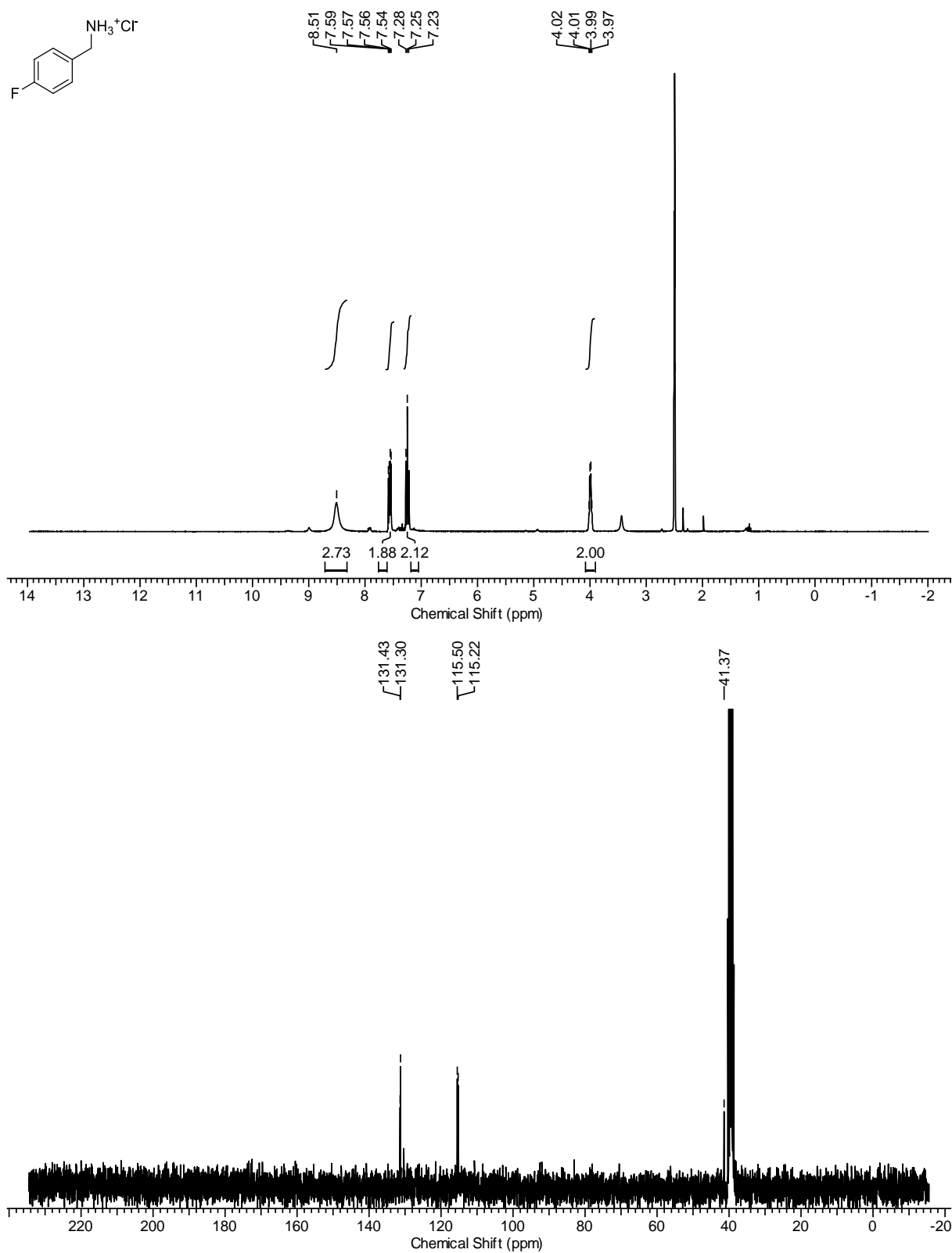
Supplementary Figure 12: NMR Spectra of compound 2'.



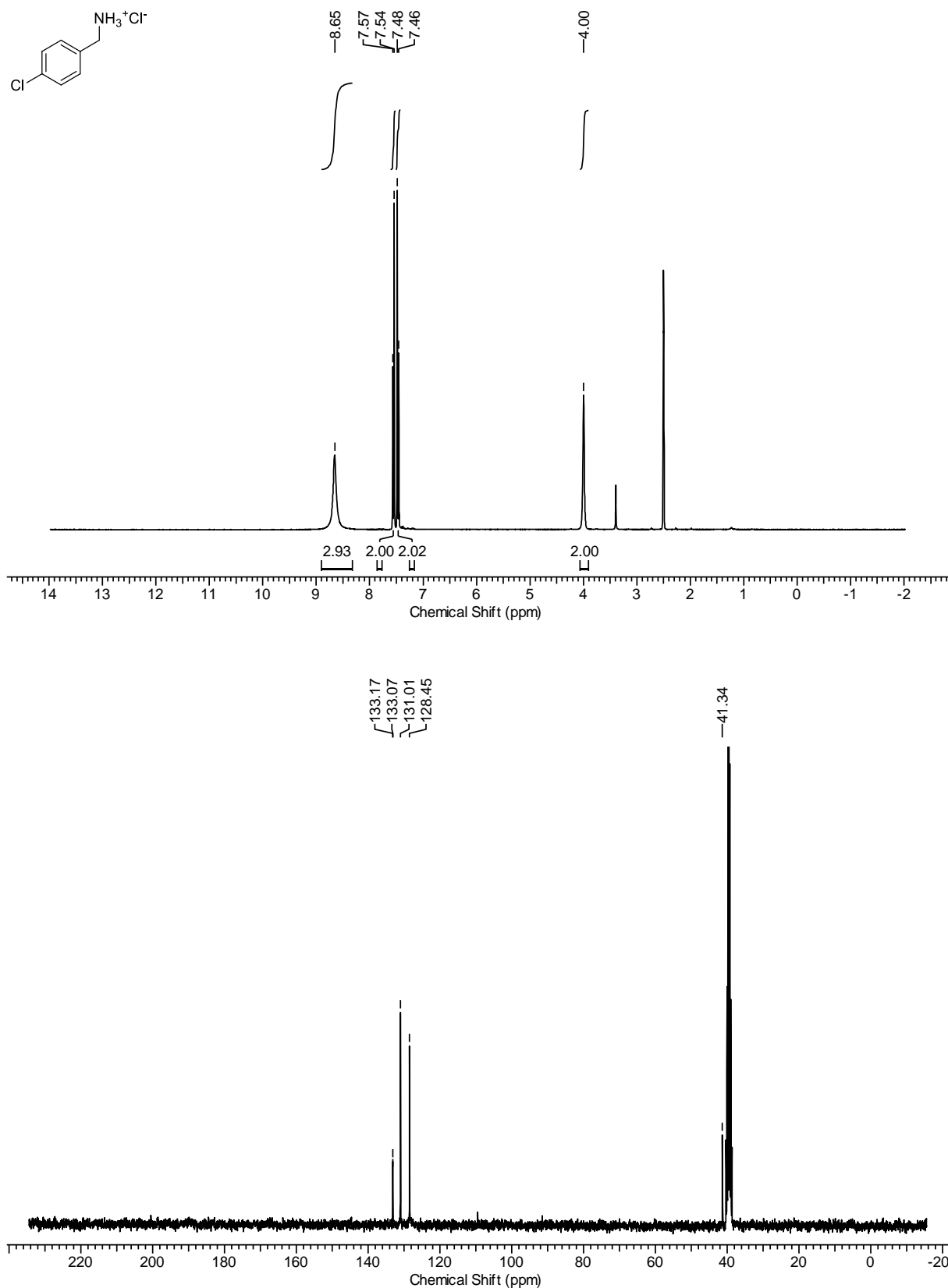
Supplementary Figure 13: NMR Spectra of compound 3'.



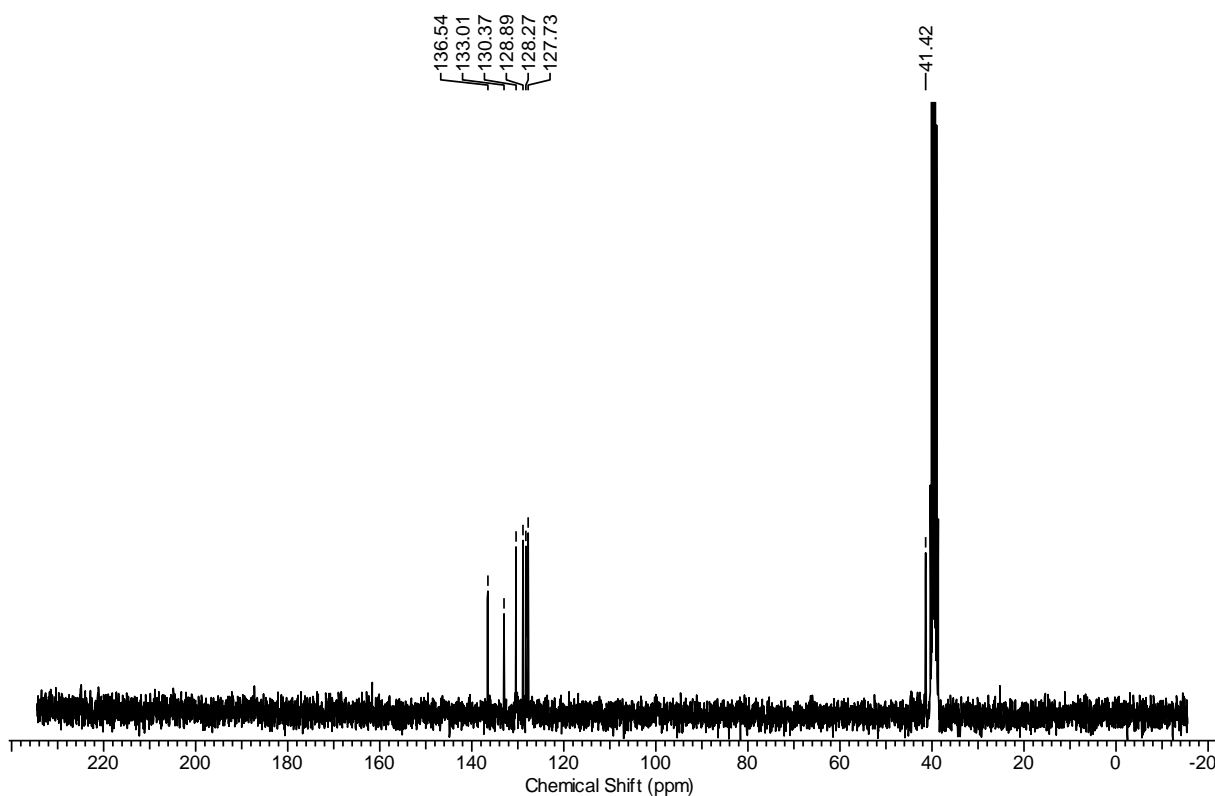
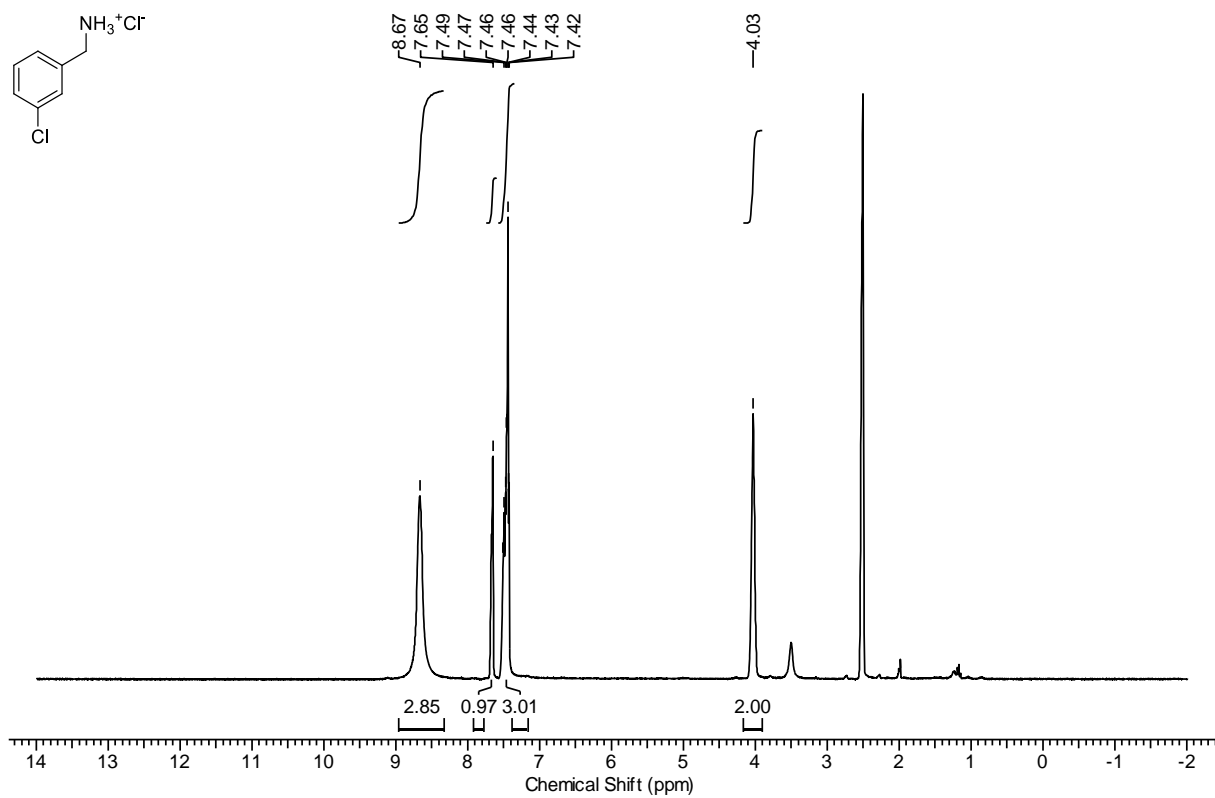
Supplementary Figure 14: NMR Spectra of compound 4'.



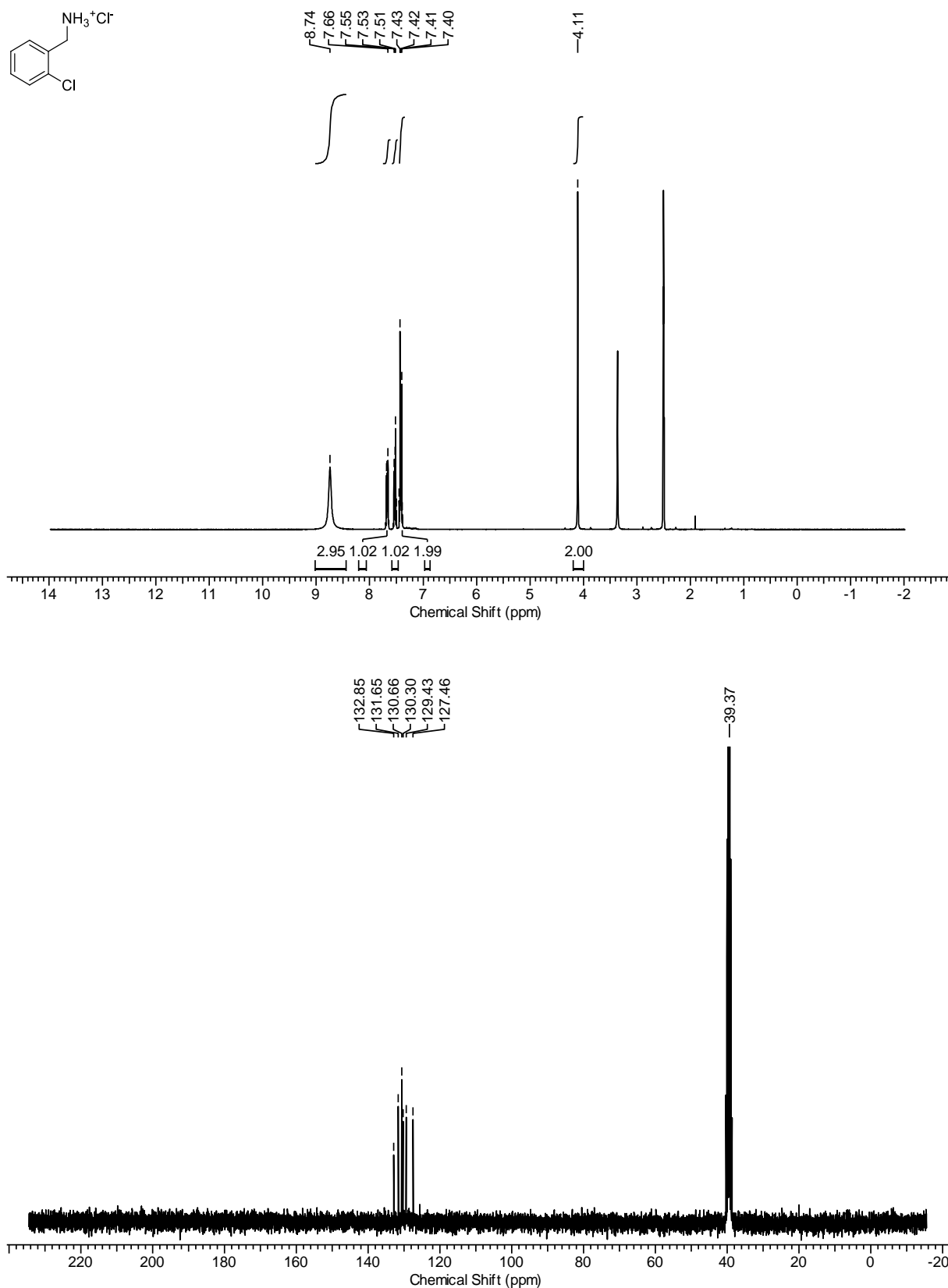
Supplementary Figure 15: NMR Spectra of compound 5'.



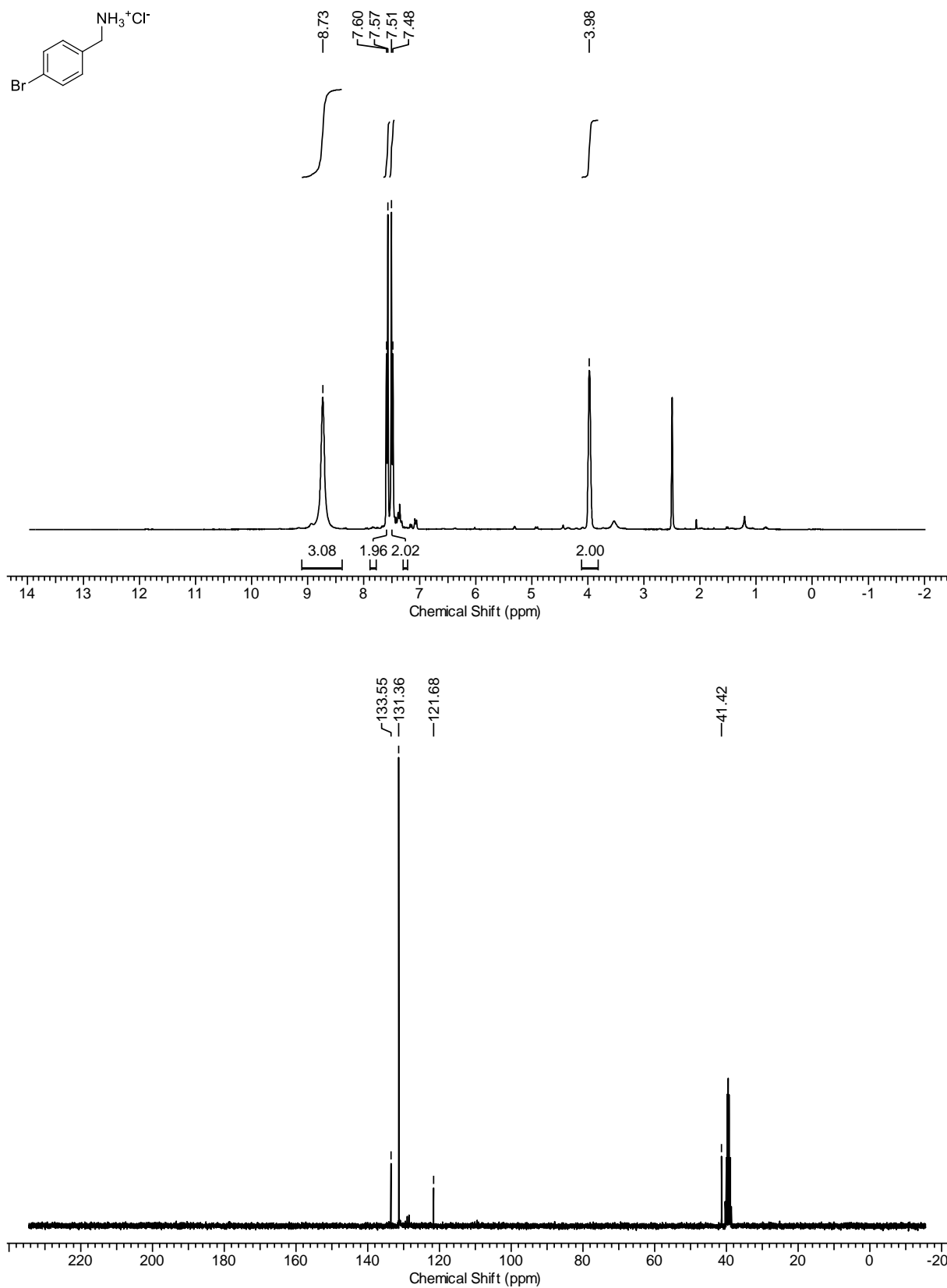
Supplementary Figure 16: NMR Spectra of compound 6'.



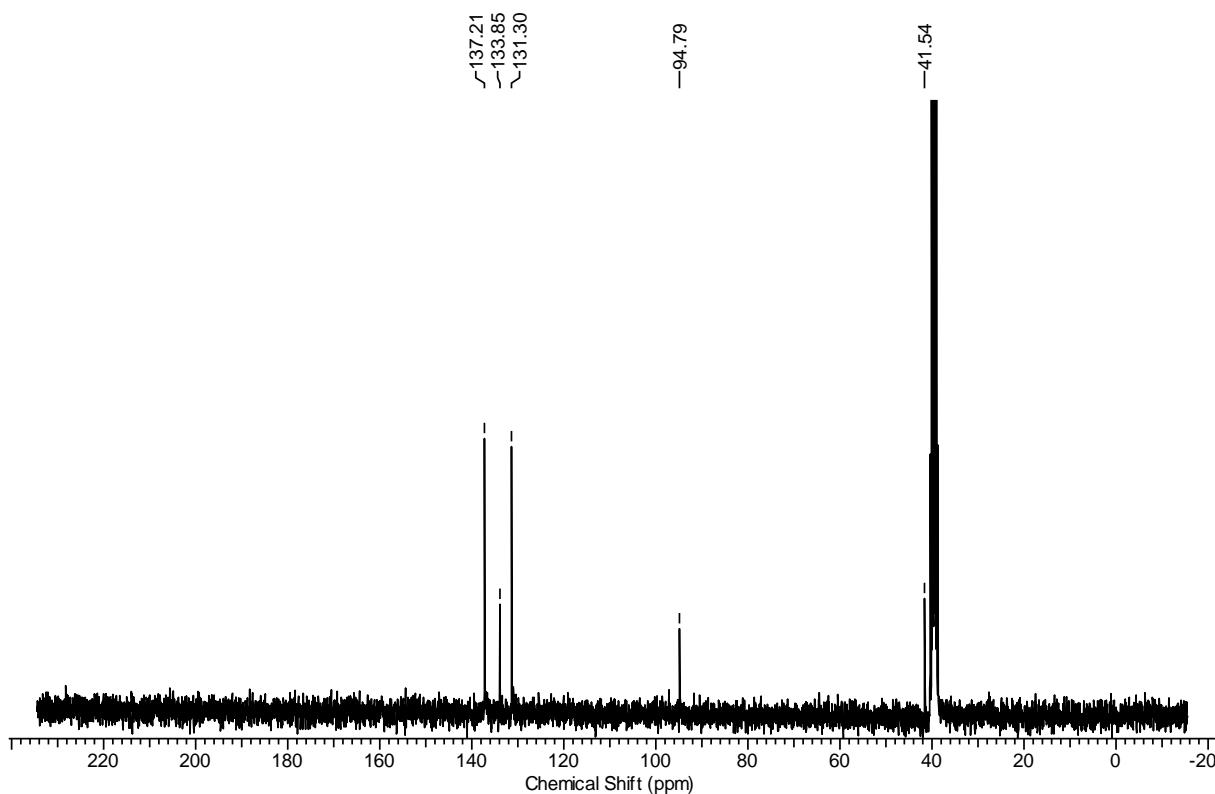
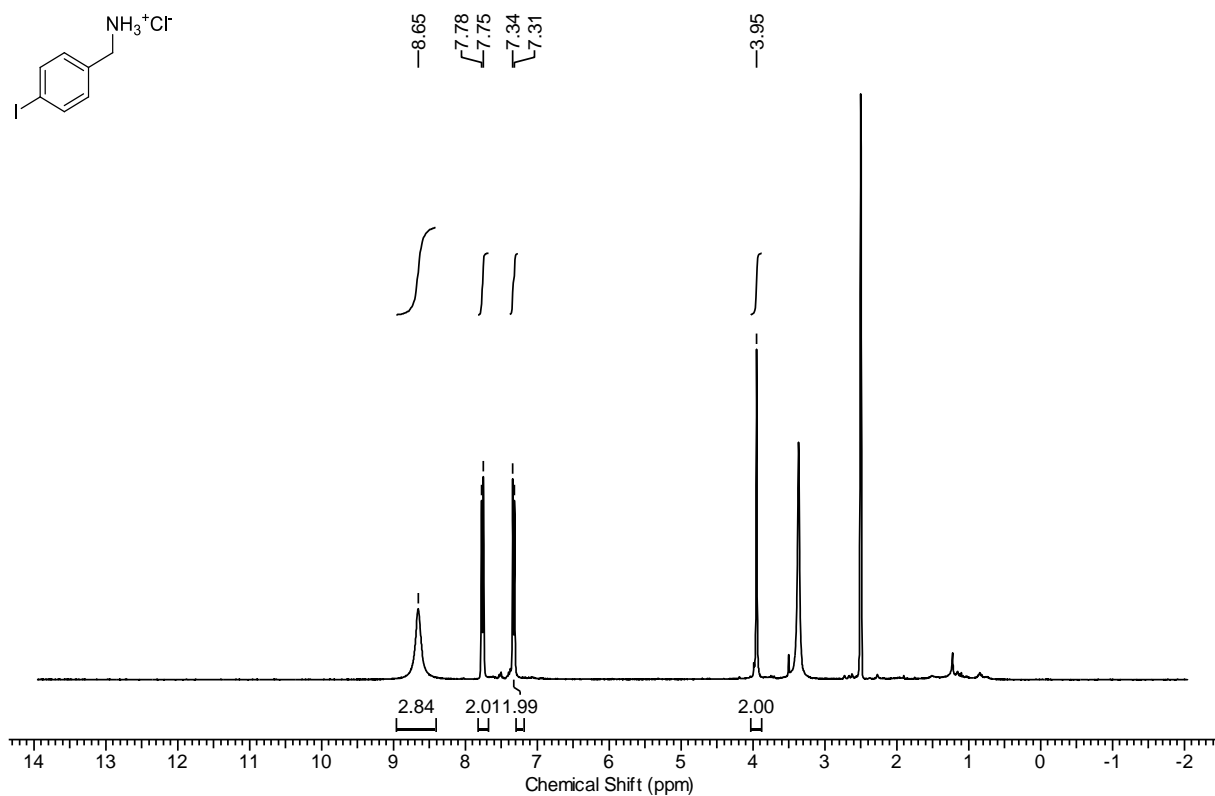
Supplementary Figure 17: NMR Spectra of compound 7'.



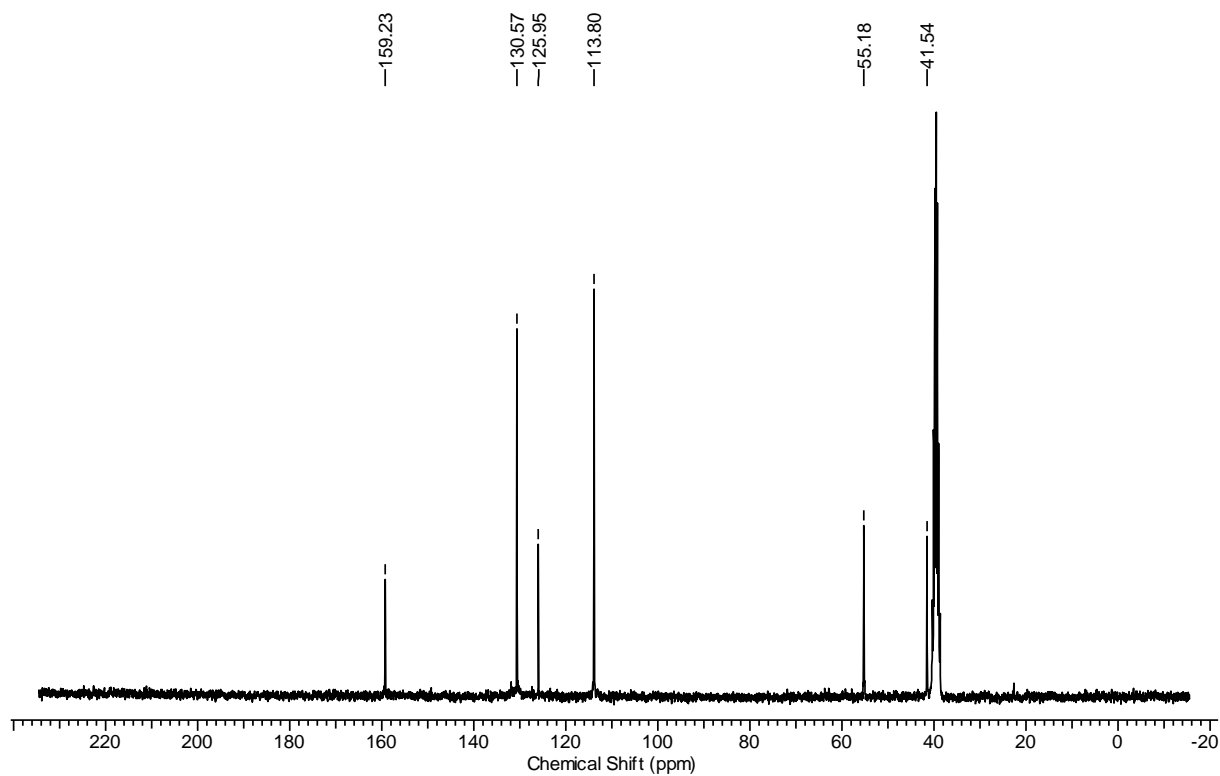
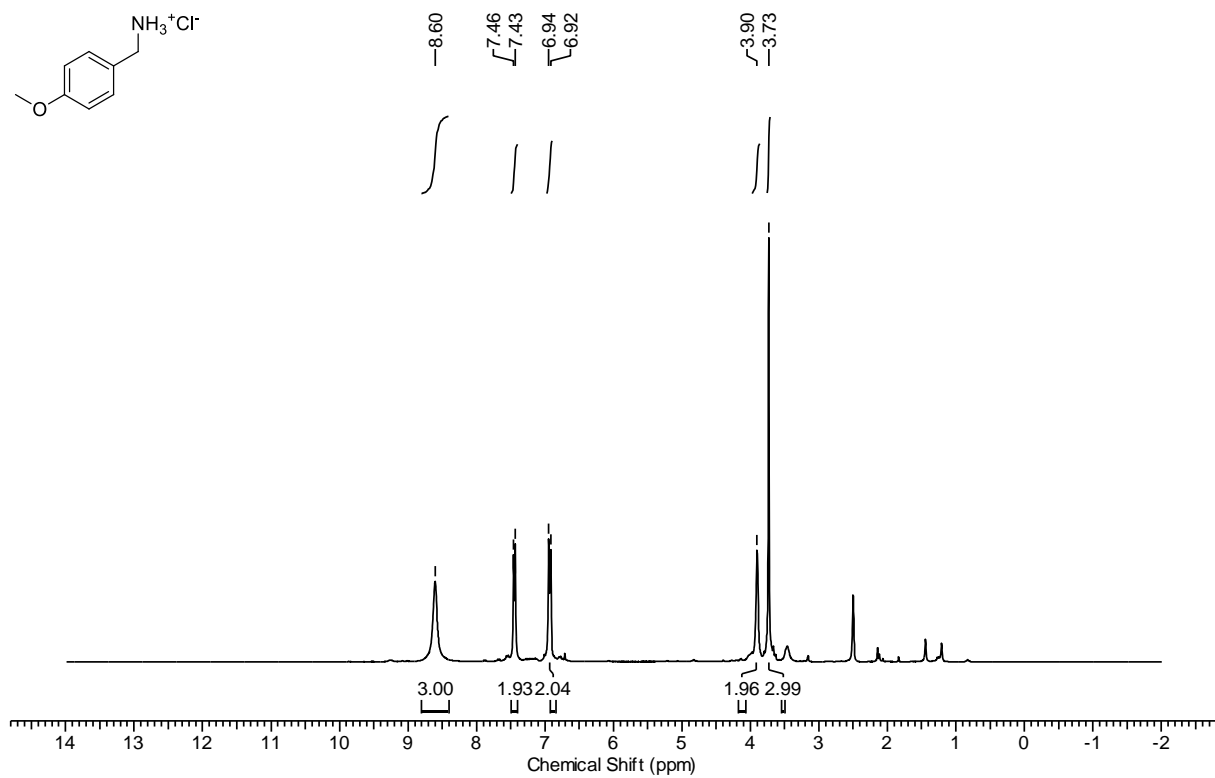
Supplementary Figure 18: NMR Spectra of compound 8'.



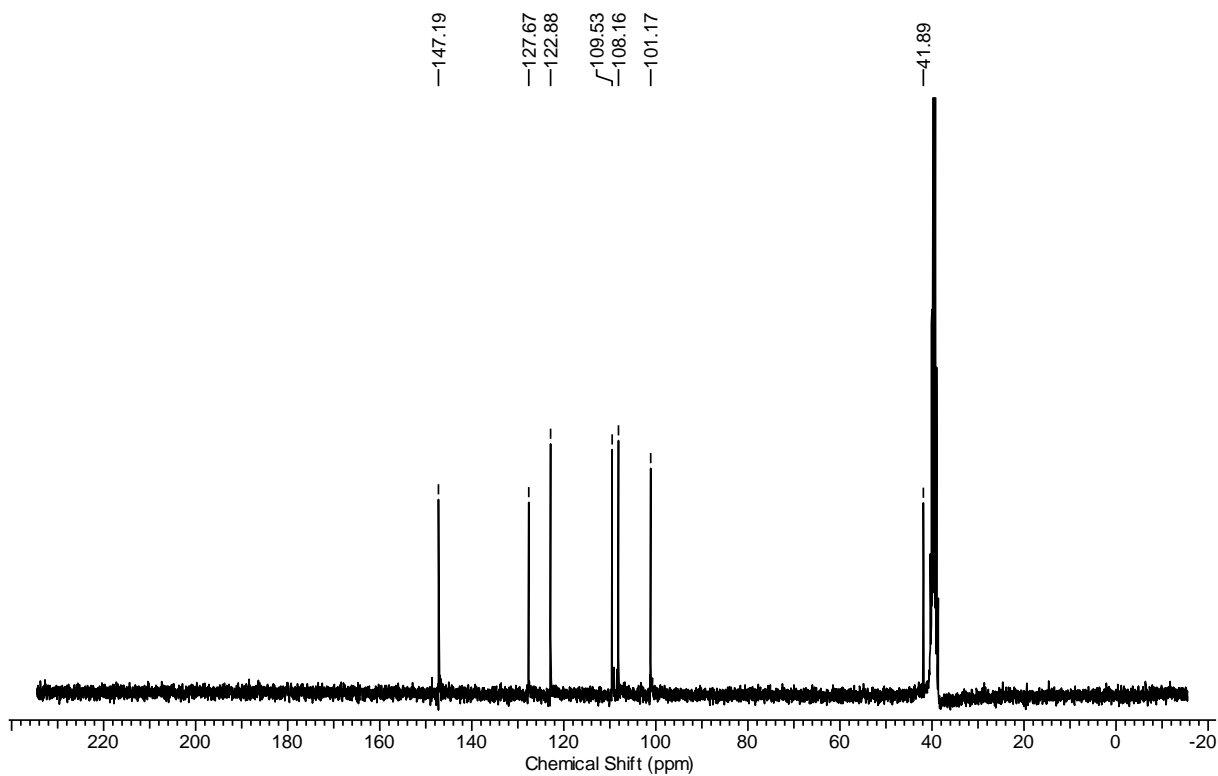
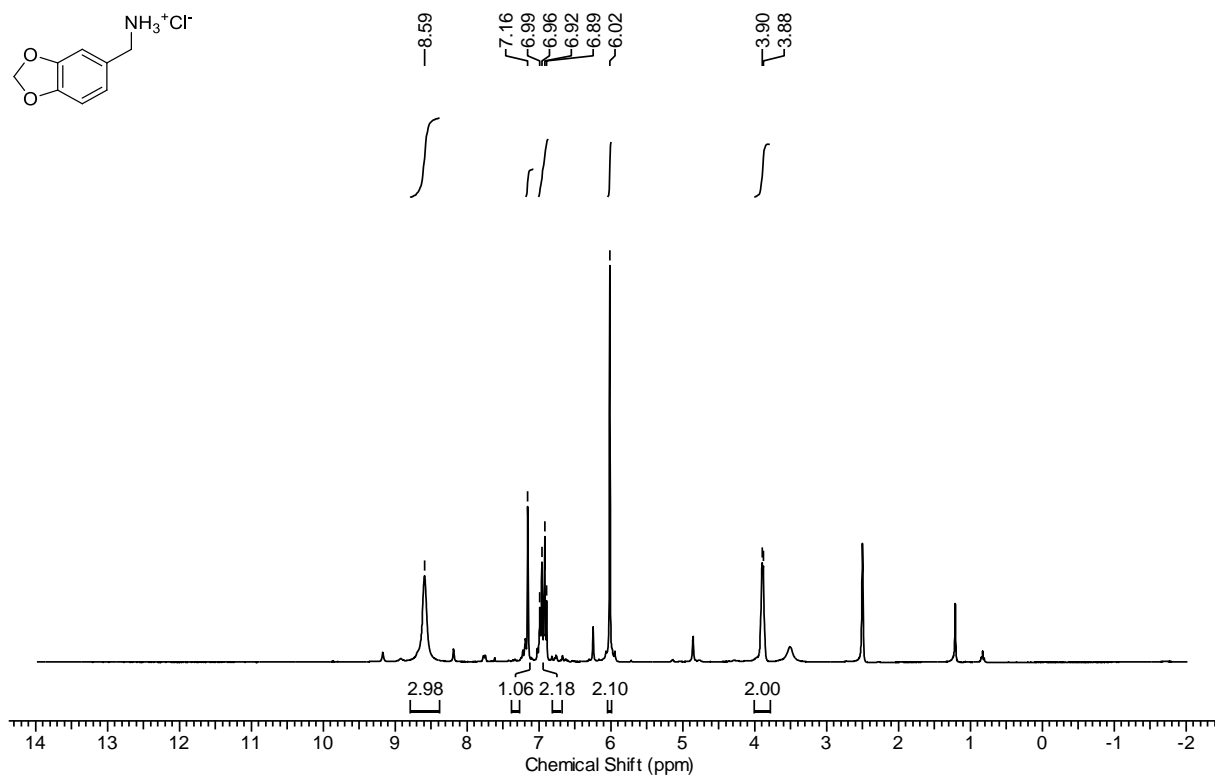
Supplementary Figure 19: NMR Spectra of compound 9'.



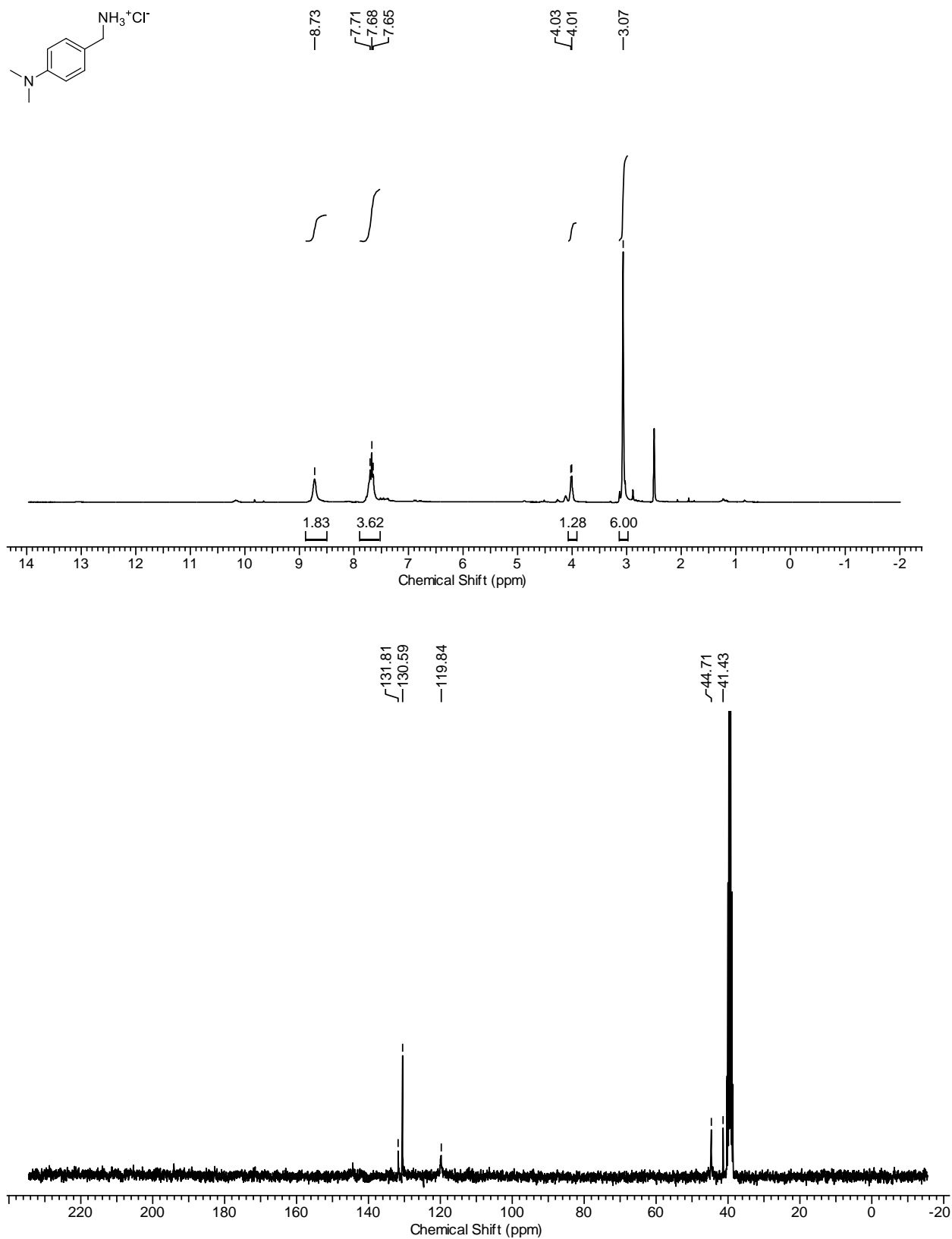
Supplementary Figure 20: NMR Spectra of compound 10'.



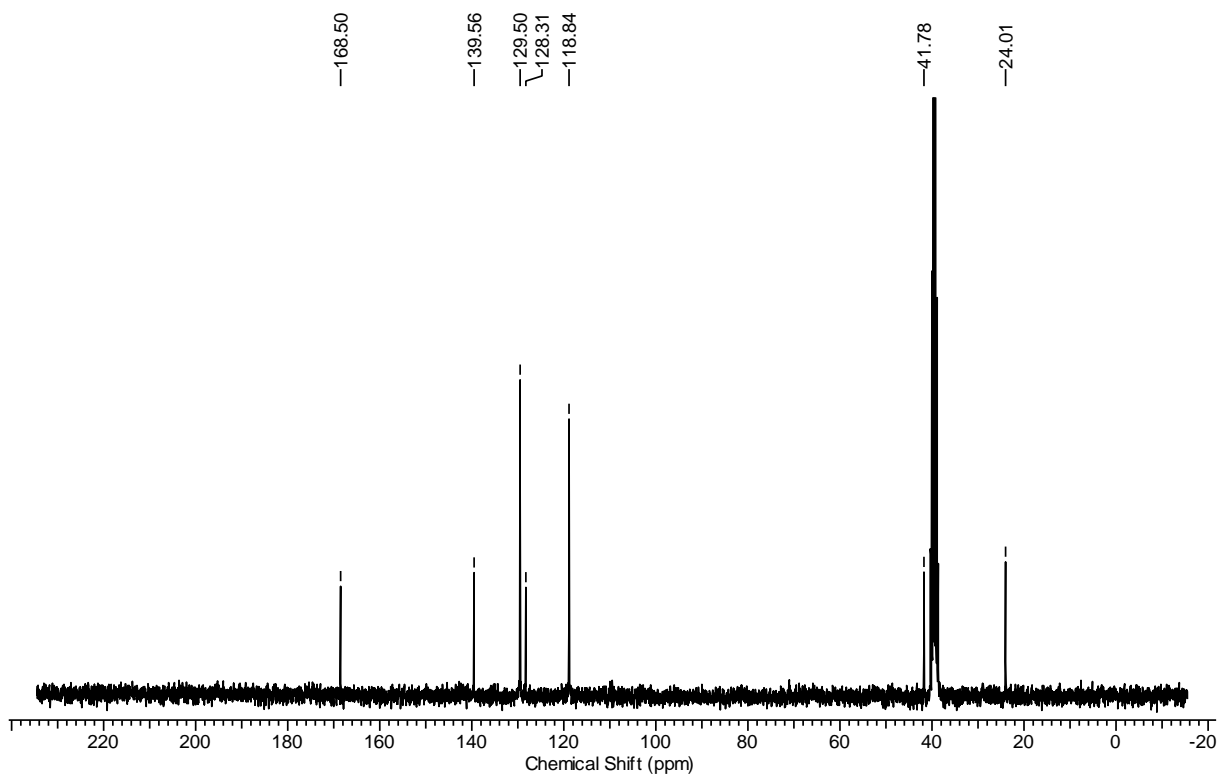
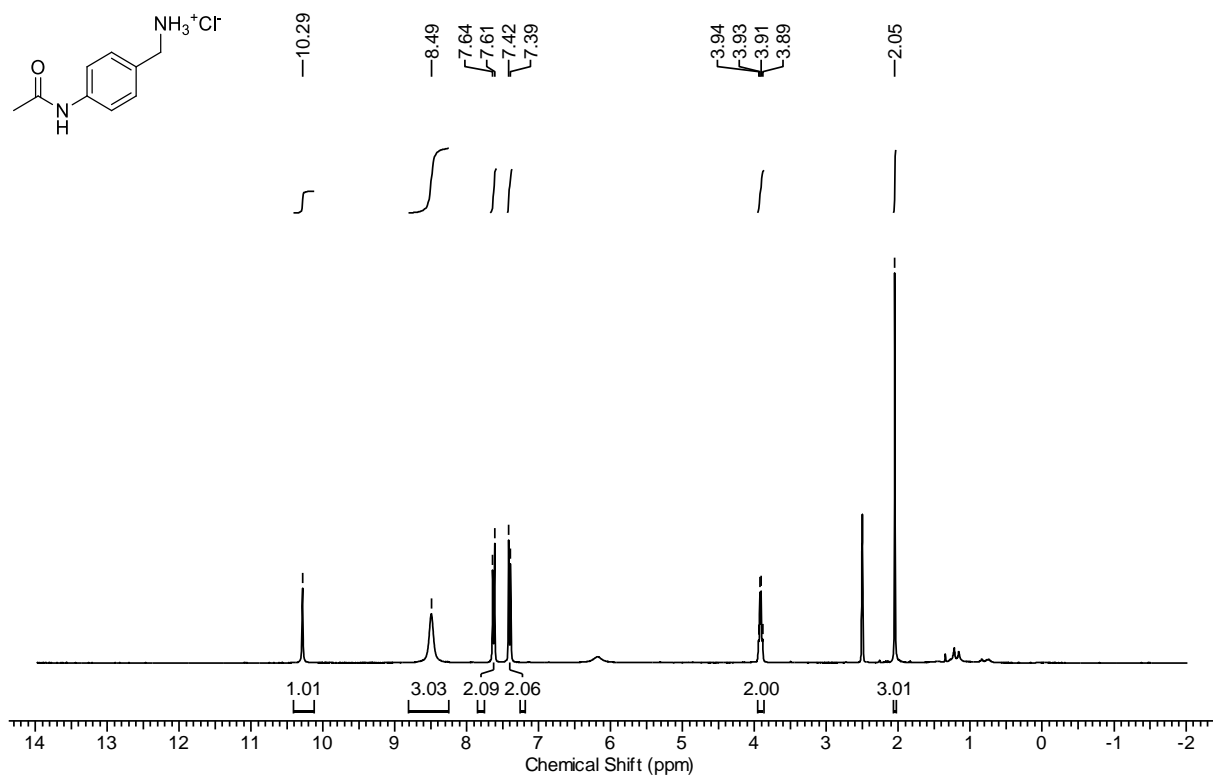
Supplementary Figure 21: NMR Spectra of compound 11'.



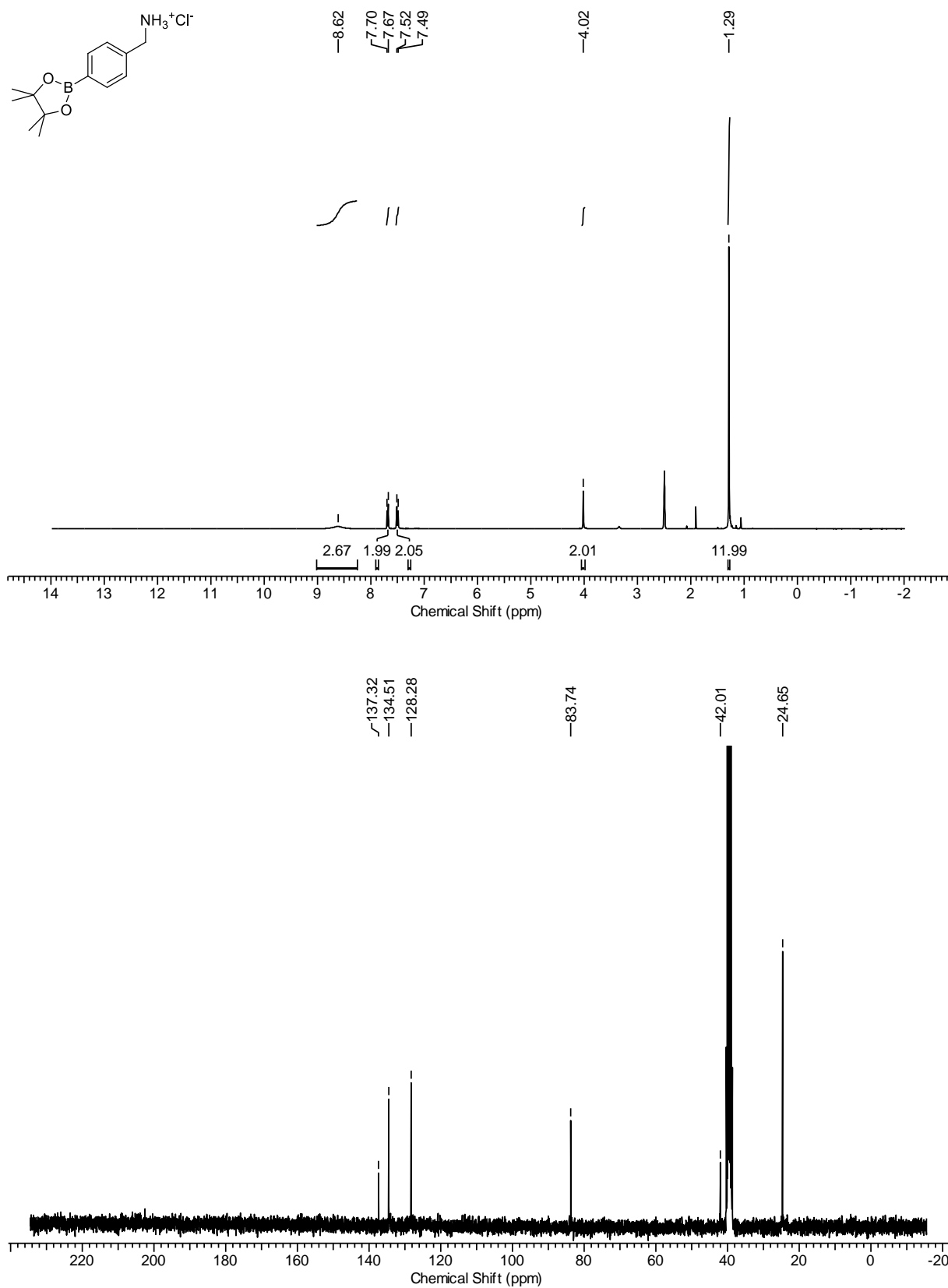
Supplementary Figure 22: NMR Spectra of compound 12'.



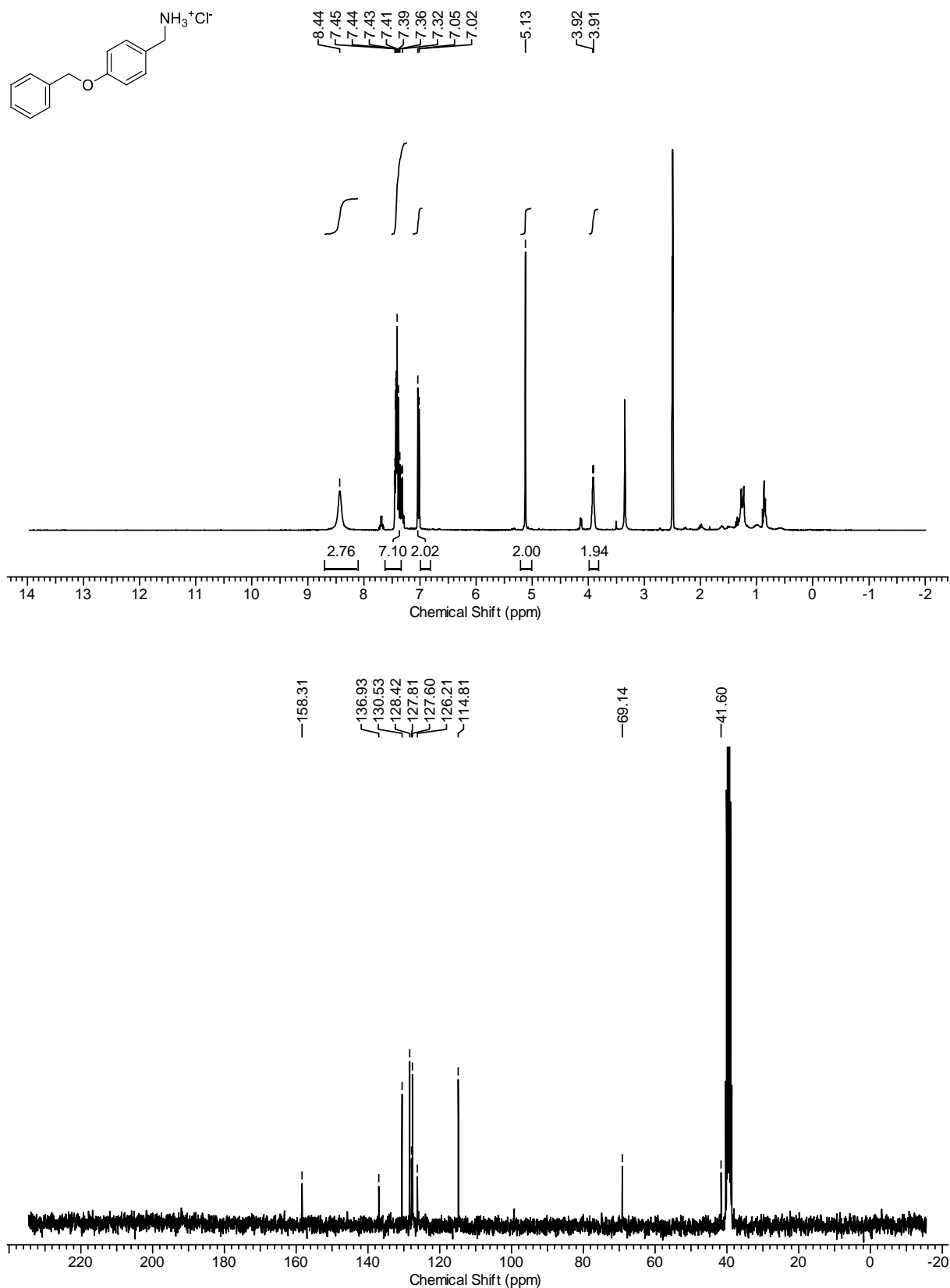
Supplementary Figure 23: NMR Spectra of compound 13'.



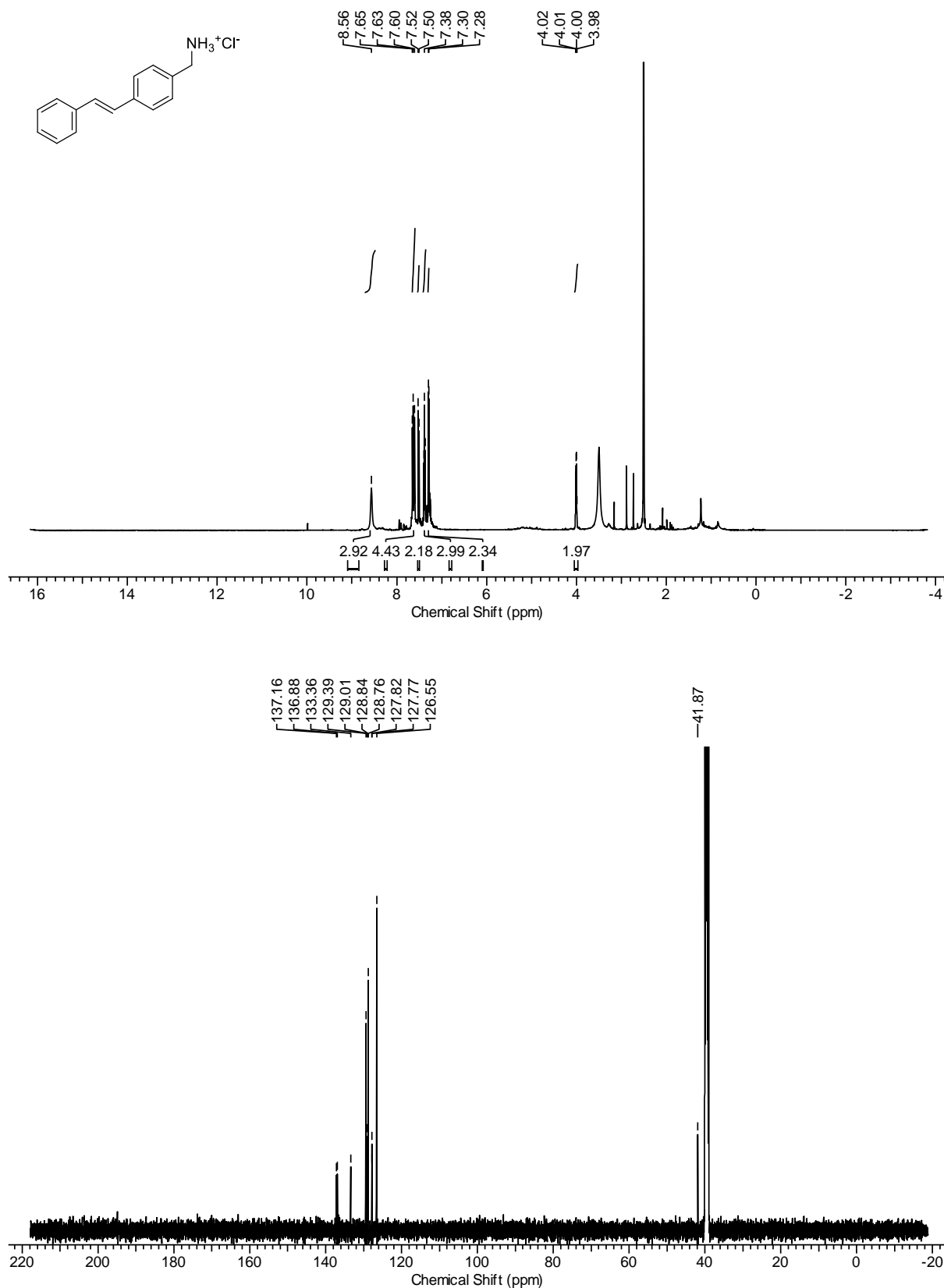
Supplementary Figure 24: NMR Spectra of compound 14'.



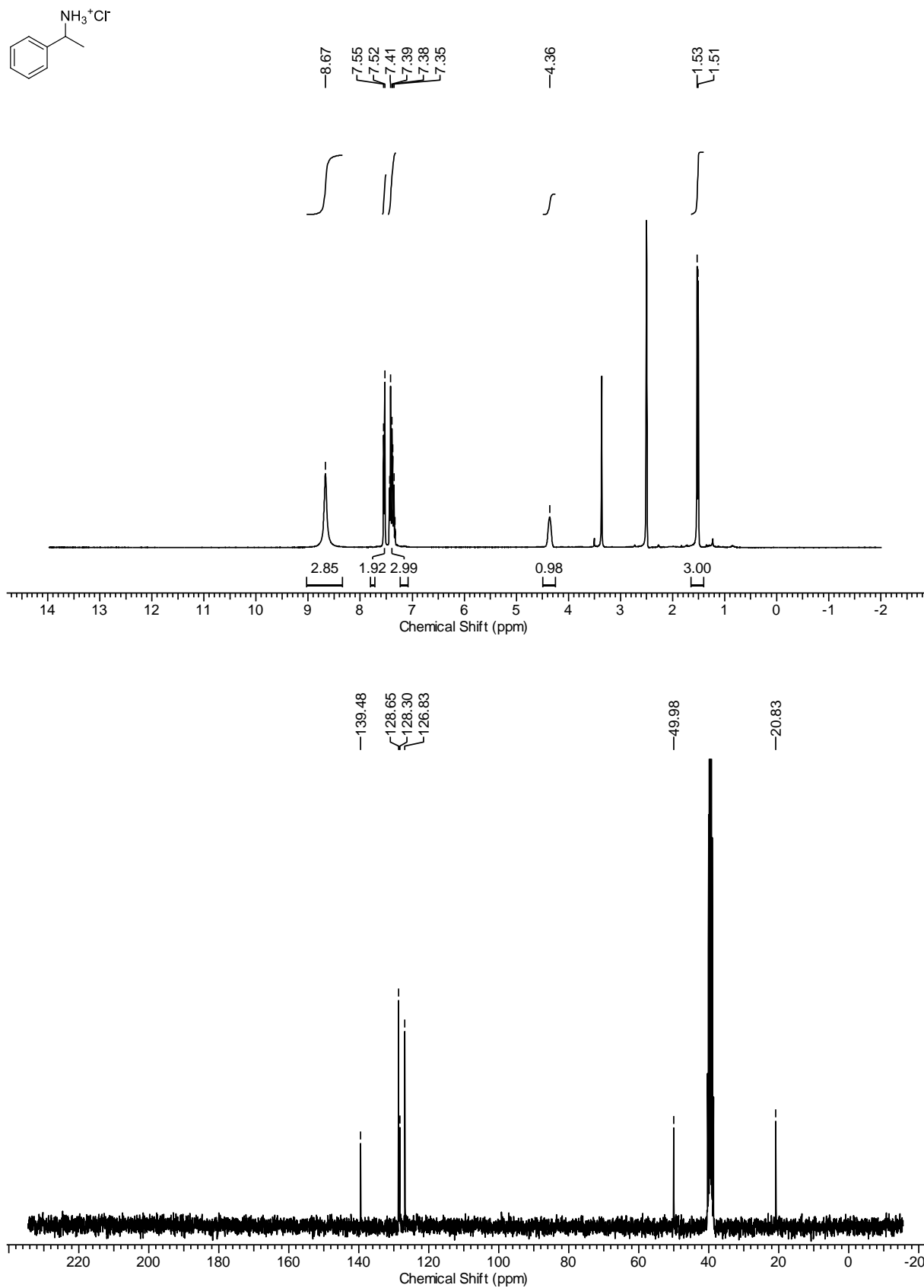
Supplementary Figure 25: NMR Spectra of compound 15'.



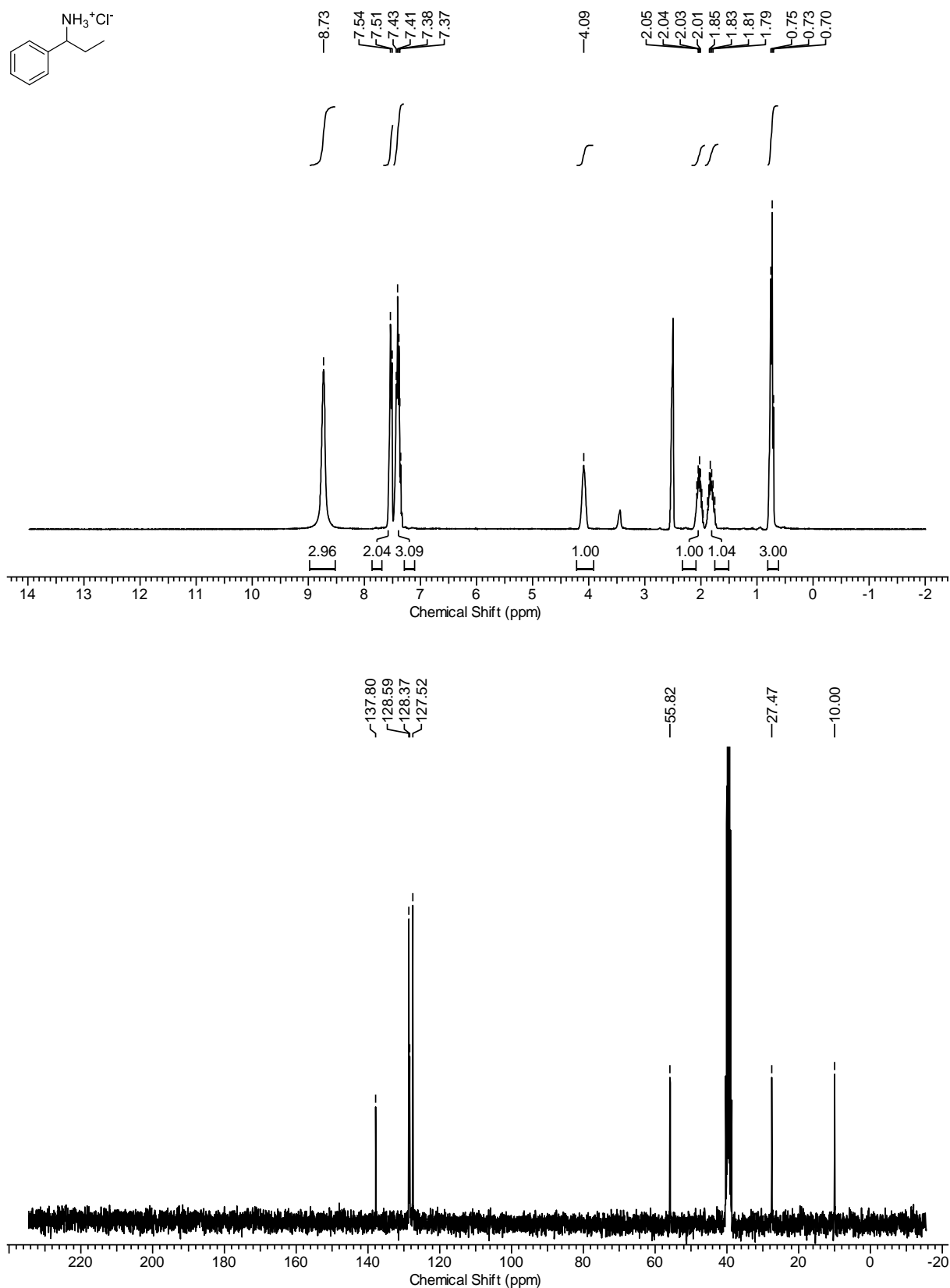
Supplementary Figure 26: NMR Spectra of compound 16'.



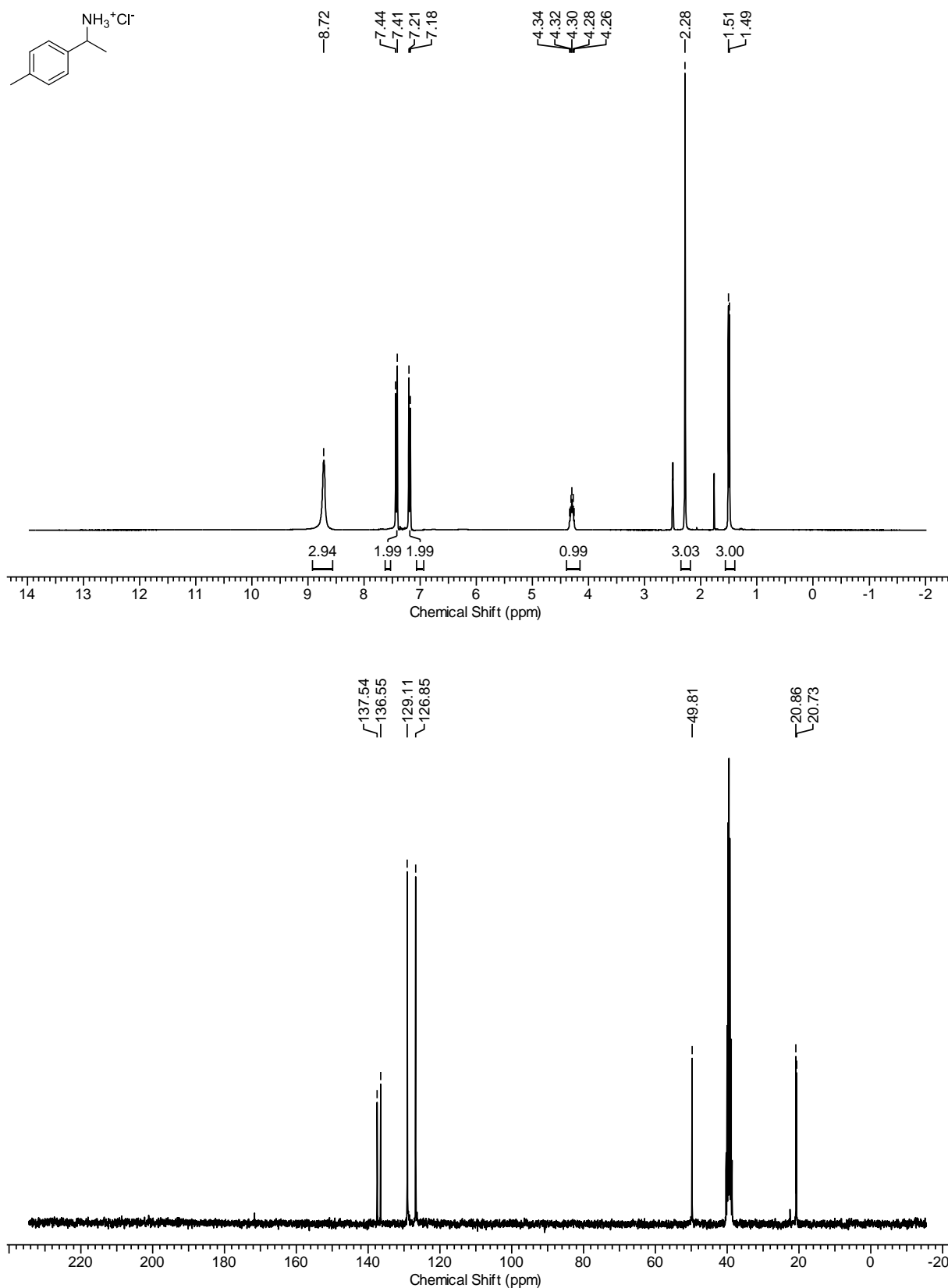
Supplementary Figure 27: NMR Spectra of compound 17'.



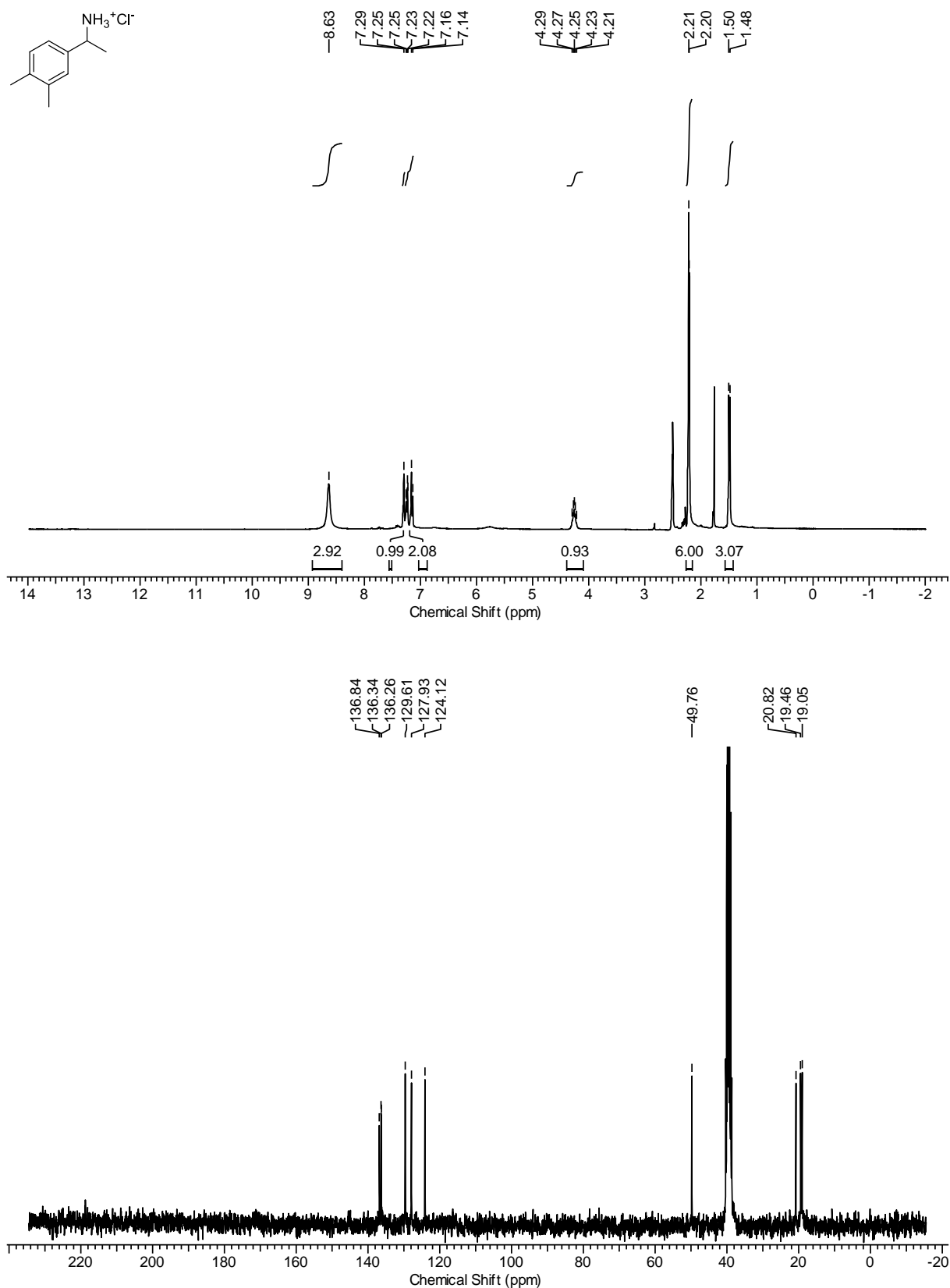
Supplementary Figure 28: NMR Spectra of compound 18'.



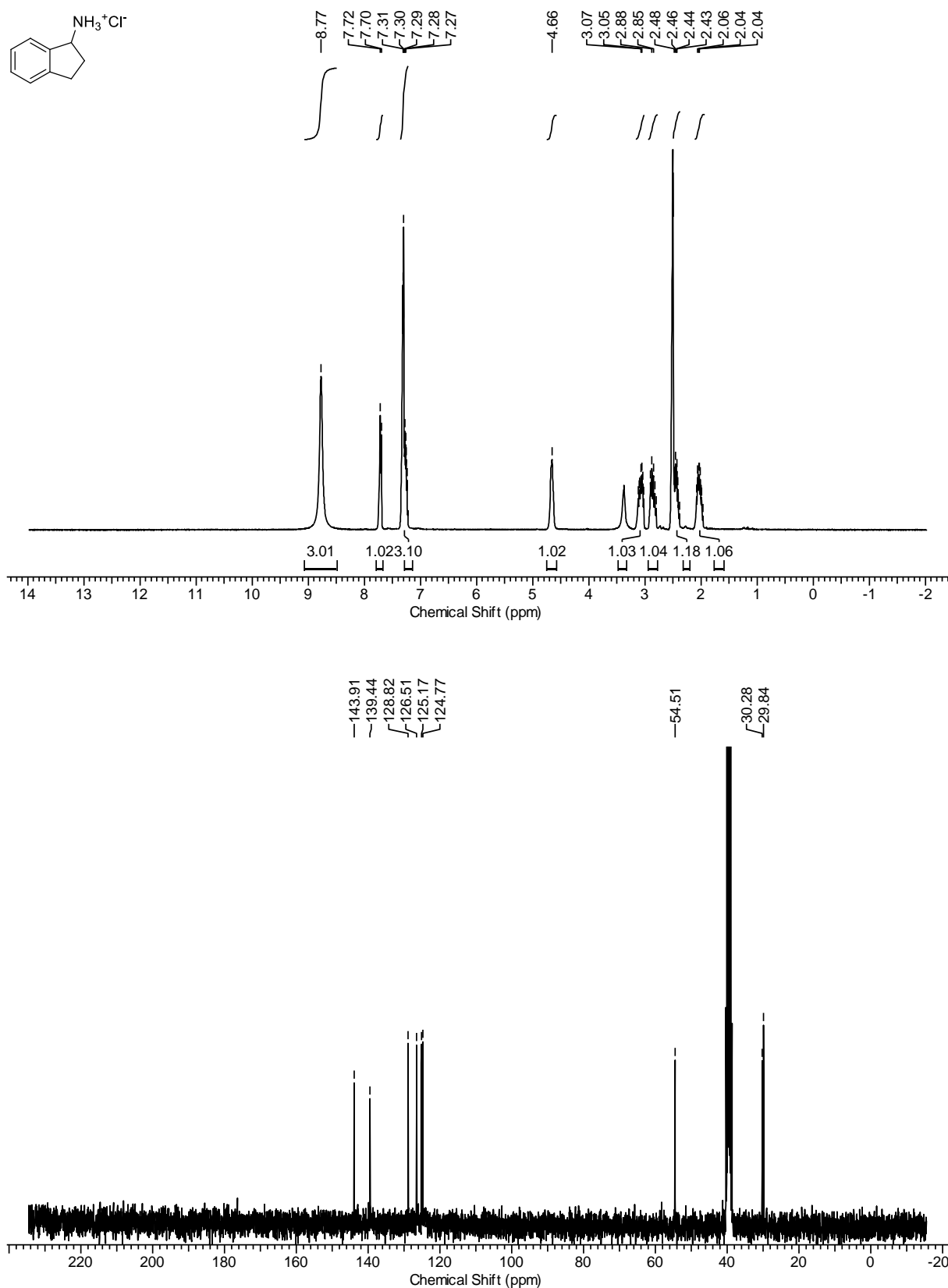
Supplementary Figure 29: NMR Spectra of compound 19'.



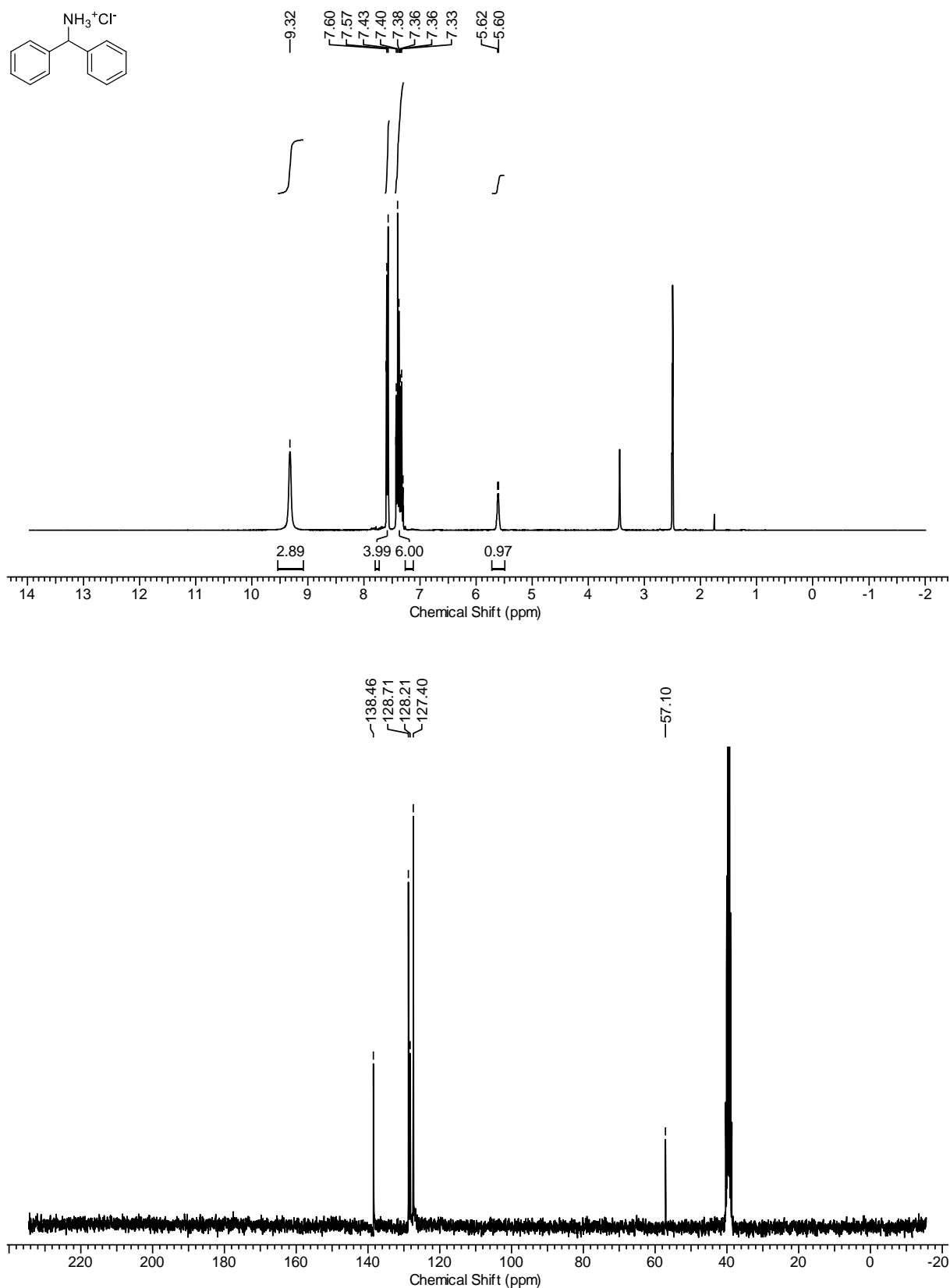
Supplementary Figure 30: NMR Spectra of compound 21'.



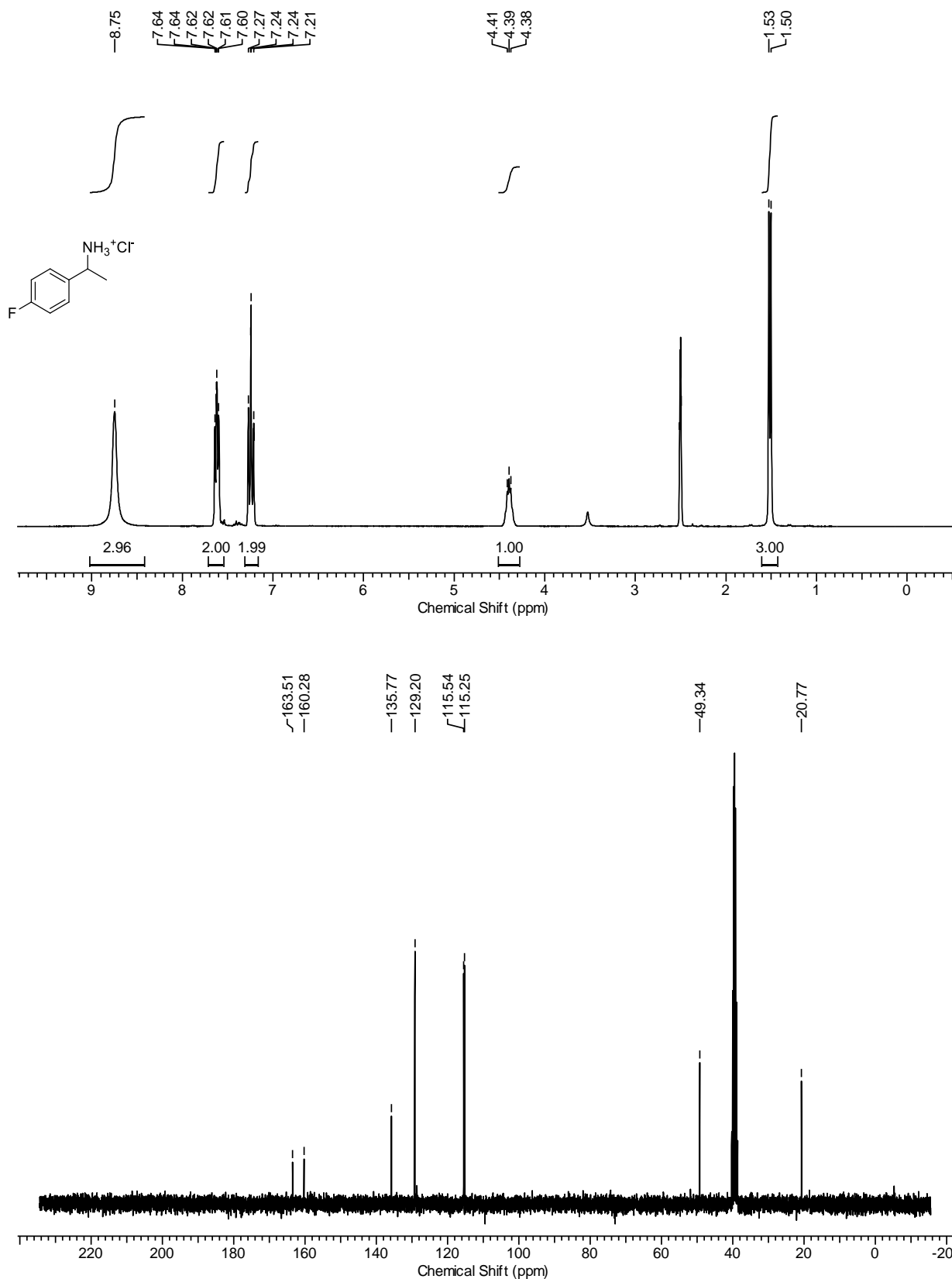
Supplementary Figure 31: NMR Spectra of compound 22'.



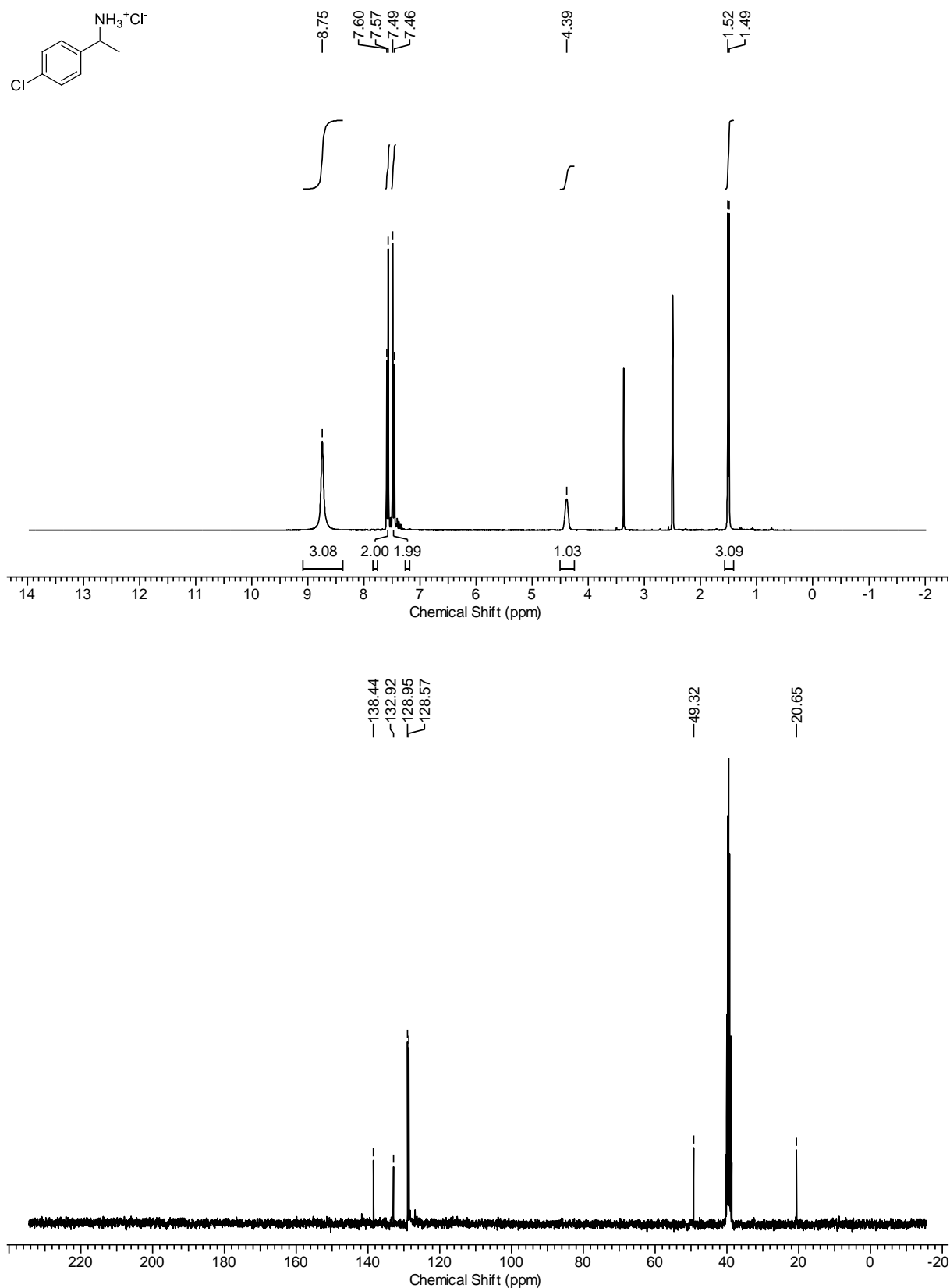
Supplementary Figure 32: NMR Spectra of compound 23'.



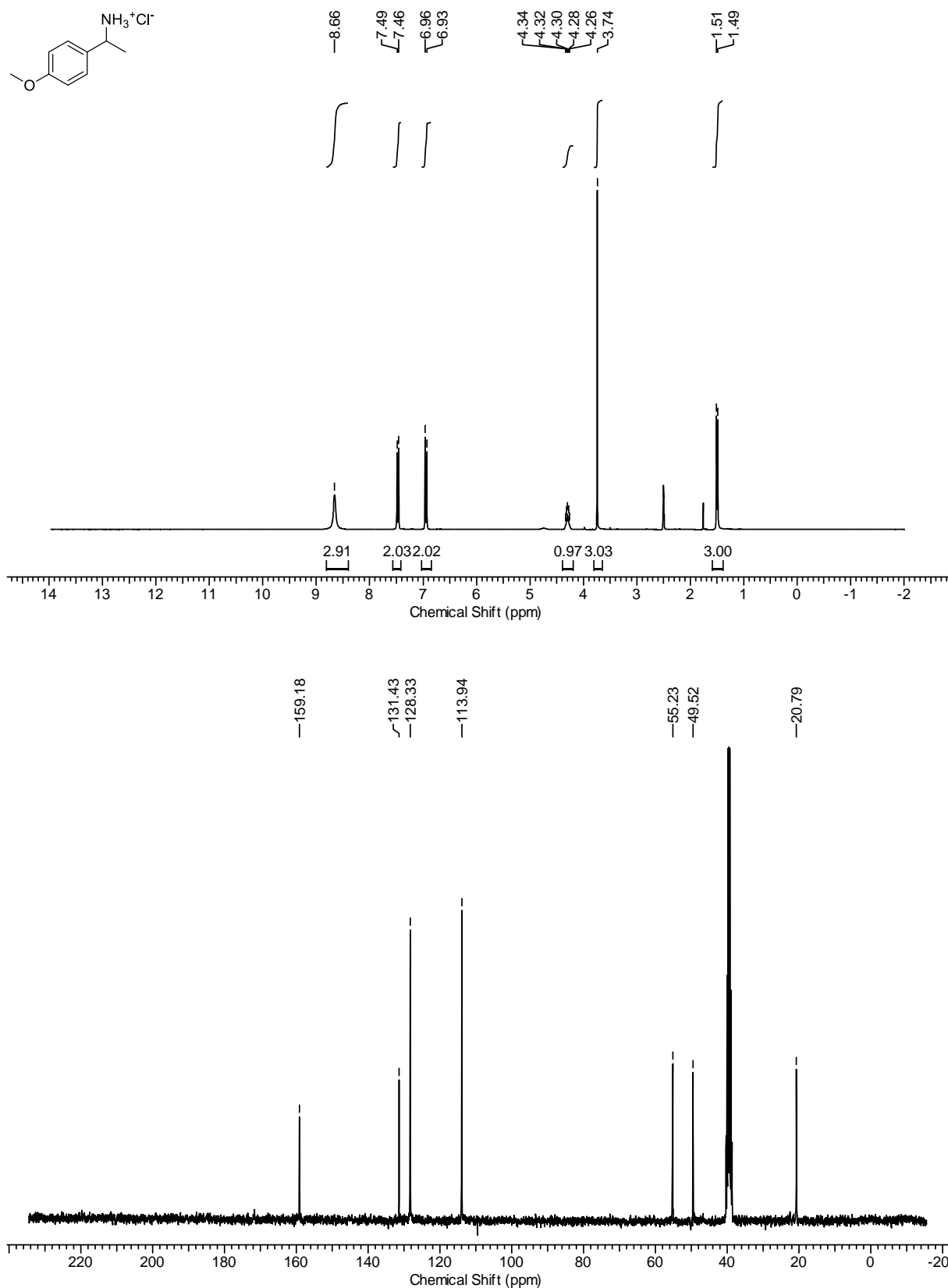
Supplementary Figure 33: NMR Spectra of compound 24'.



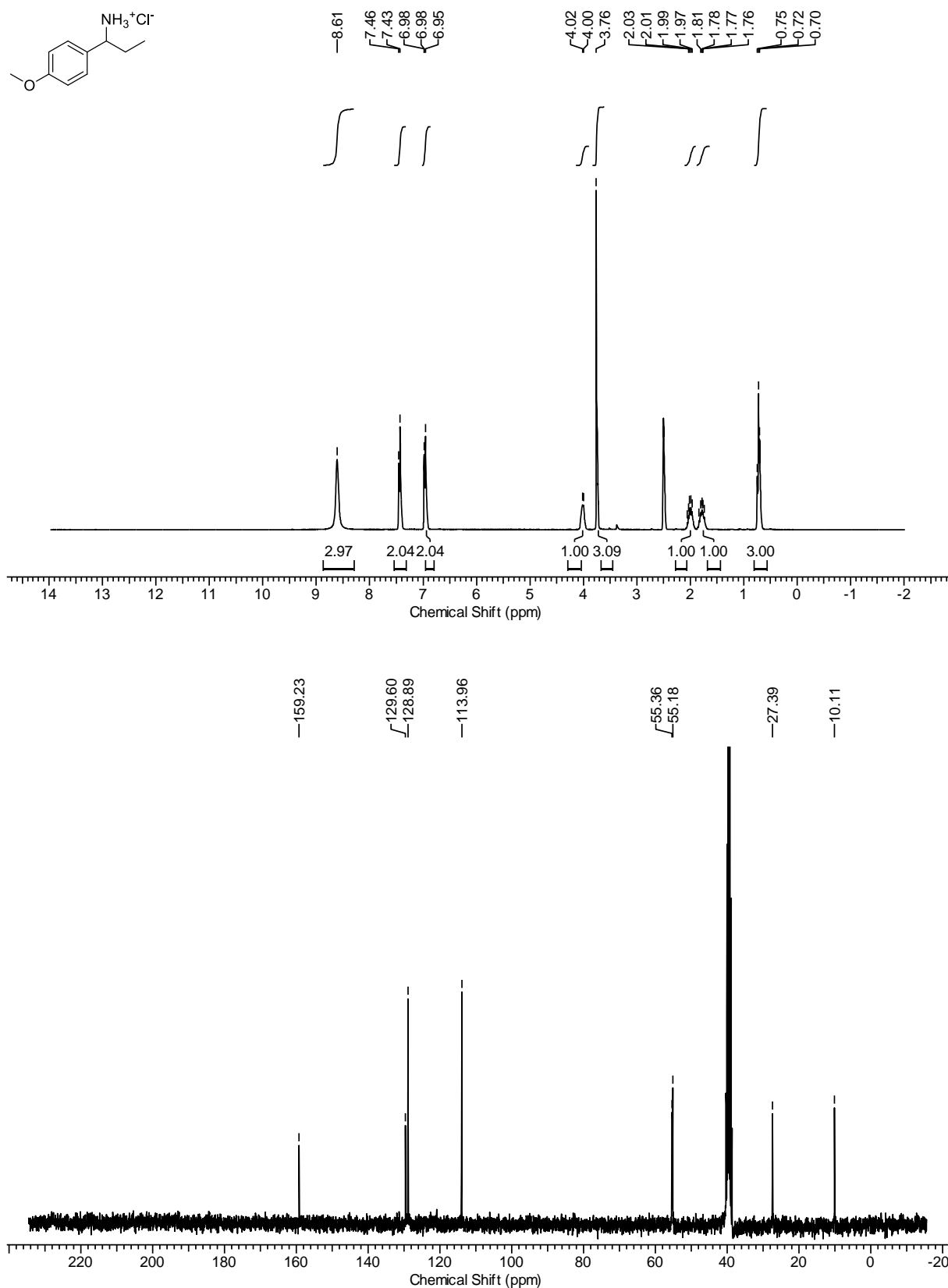
Supplementary Figure 34: NMR Spectra of compound 25'.



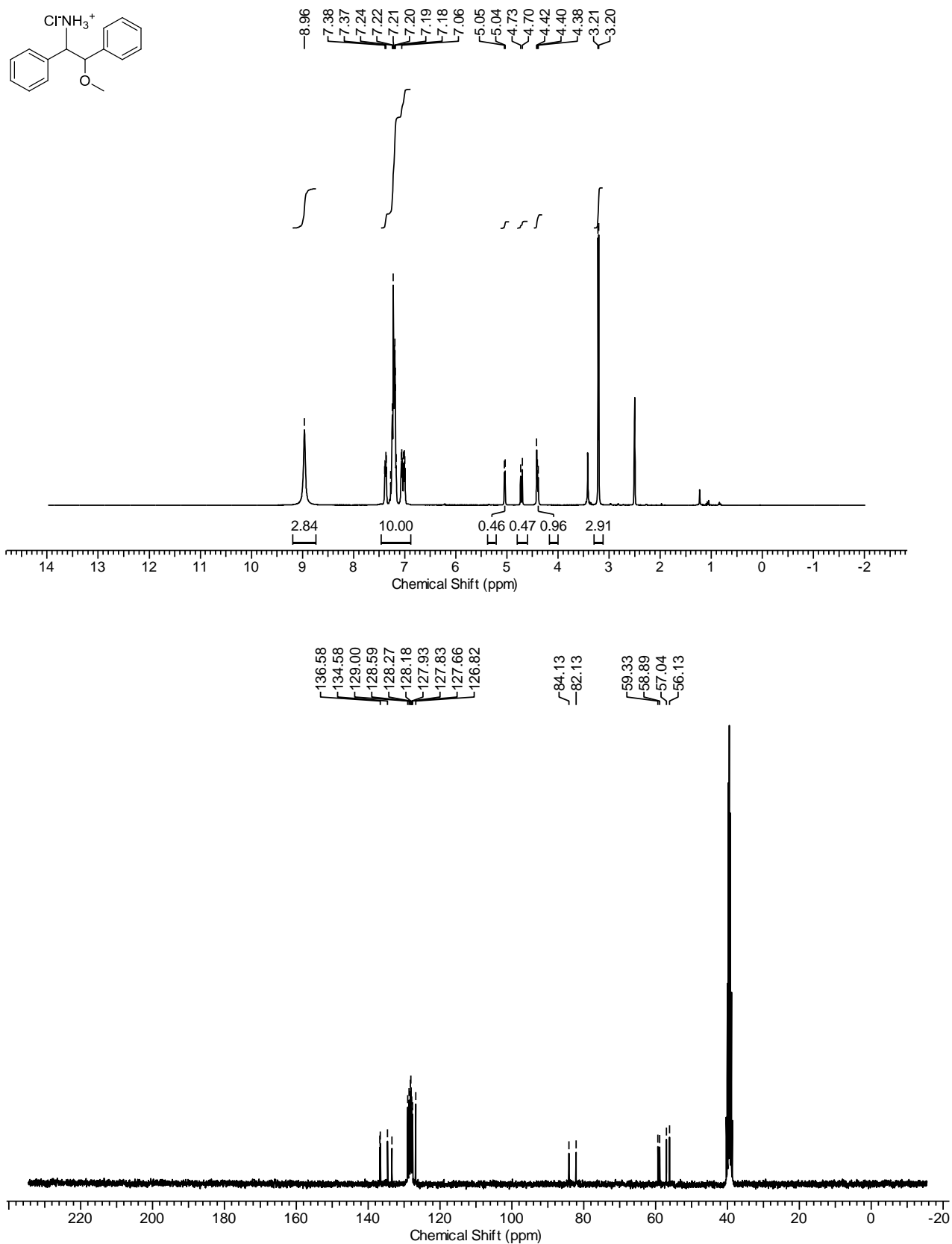
Supplementary Figure 35: NMR Spectra of compound 26'.



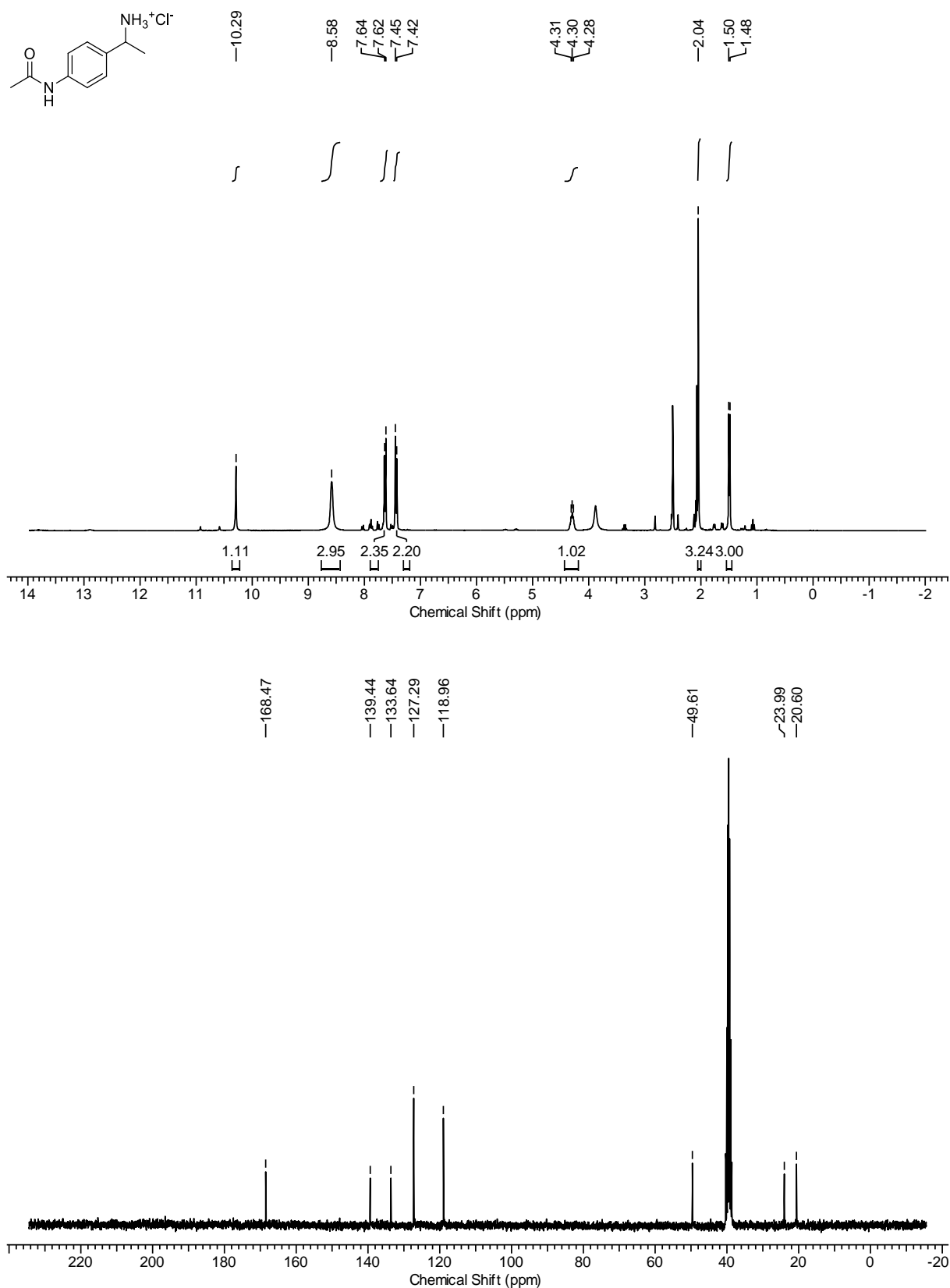
Supplementary Figure 36: NMR Spectra of compound 27'.



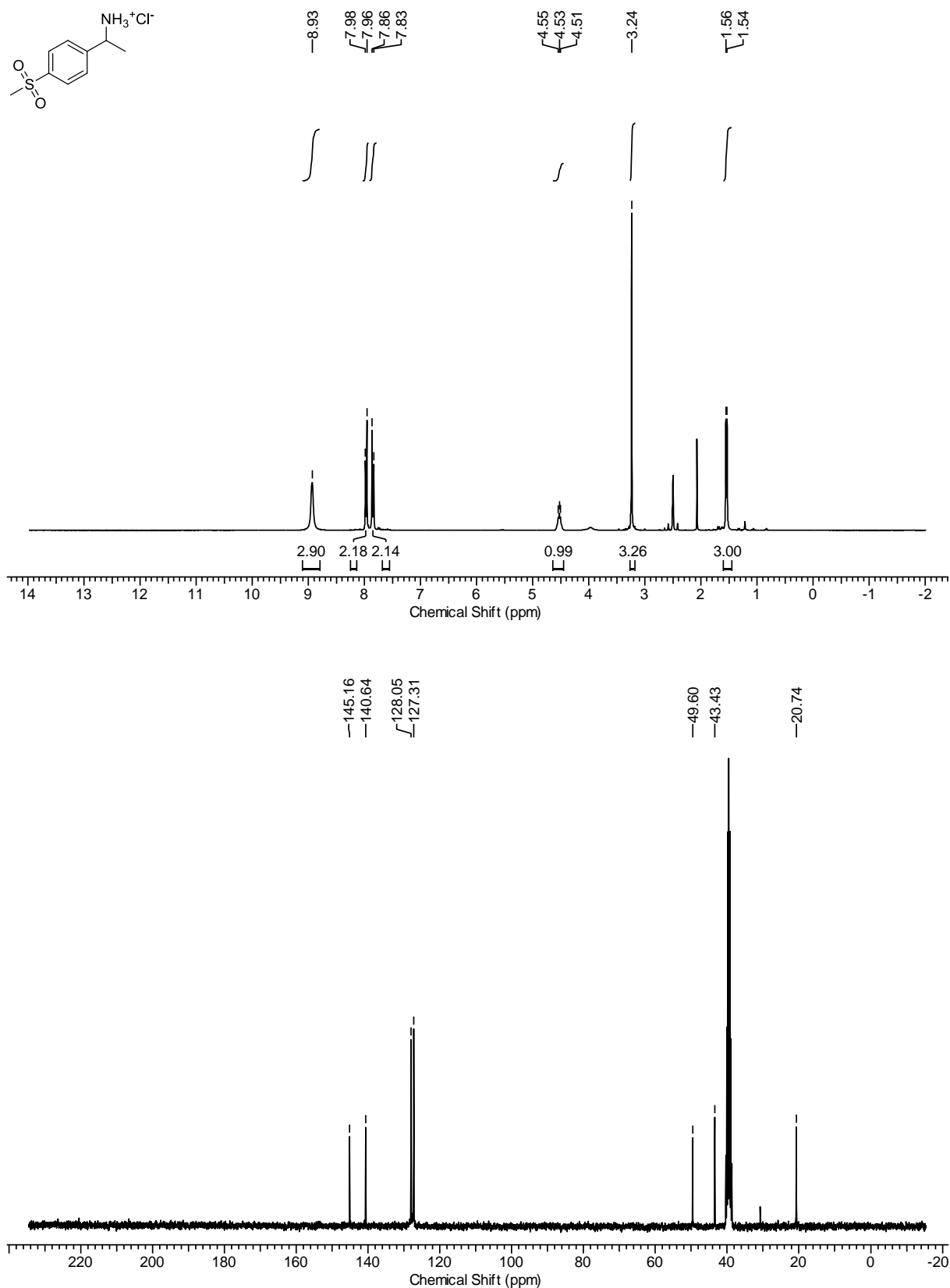
Supplementary Figure 37: NMR Spectra of compound 28'.



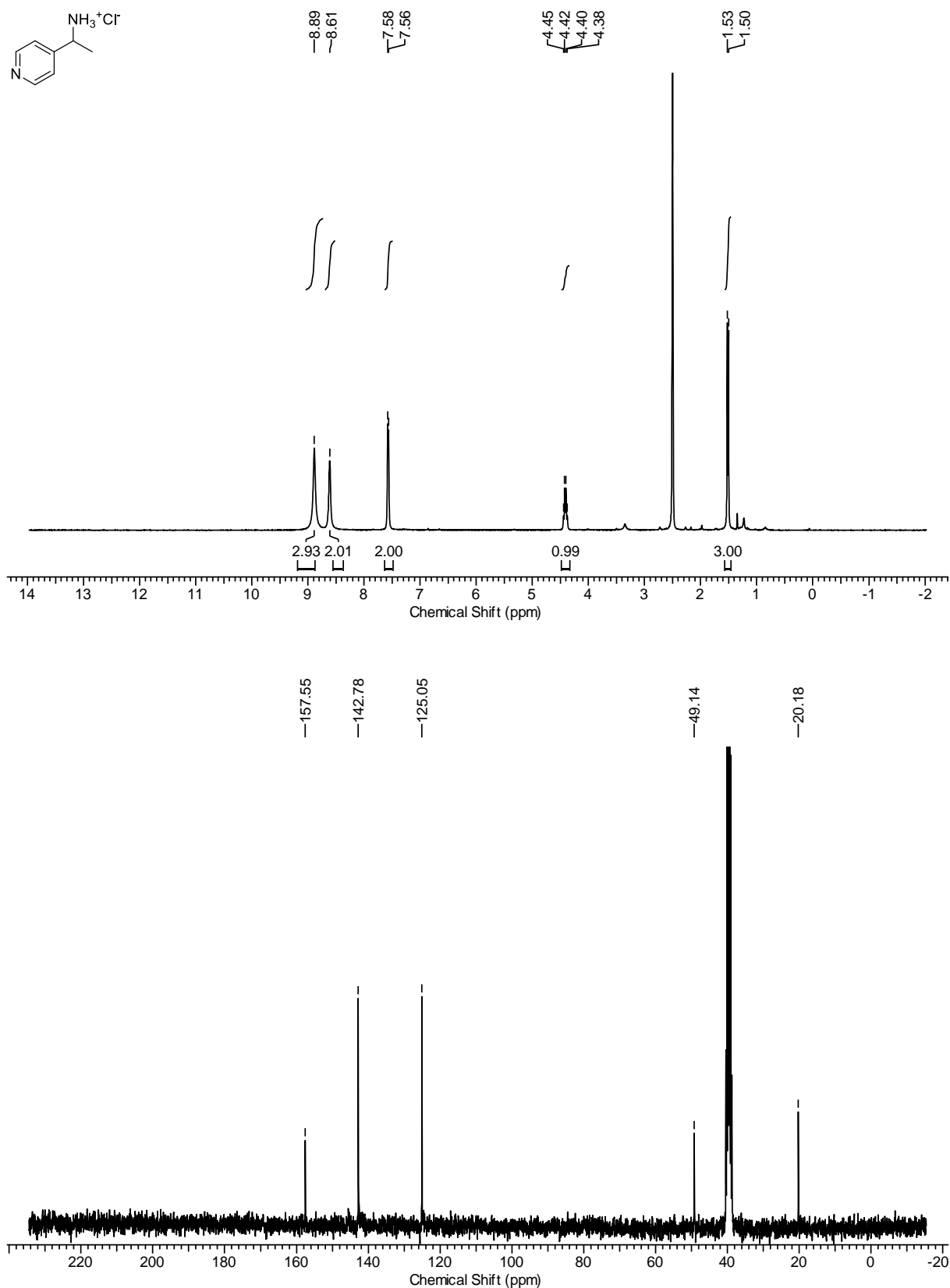
Supplementary Figure 38: NMR Spectra of compound 29'.



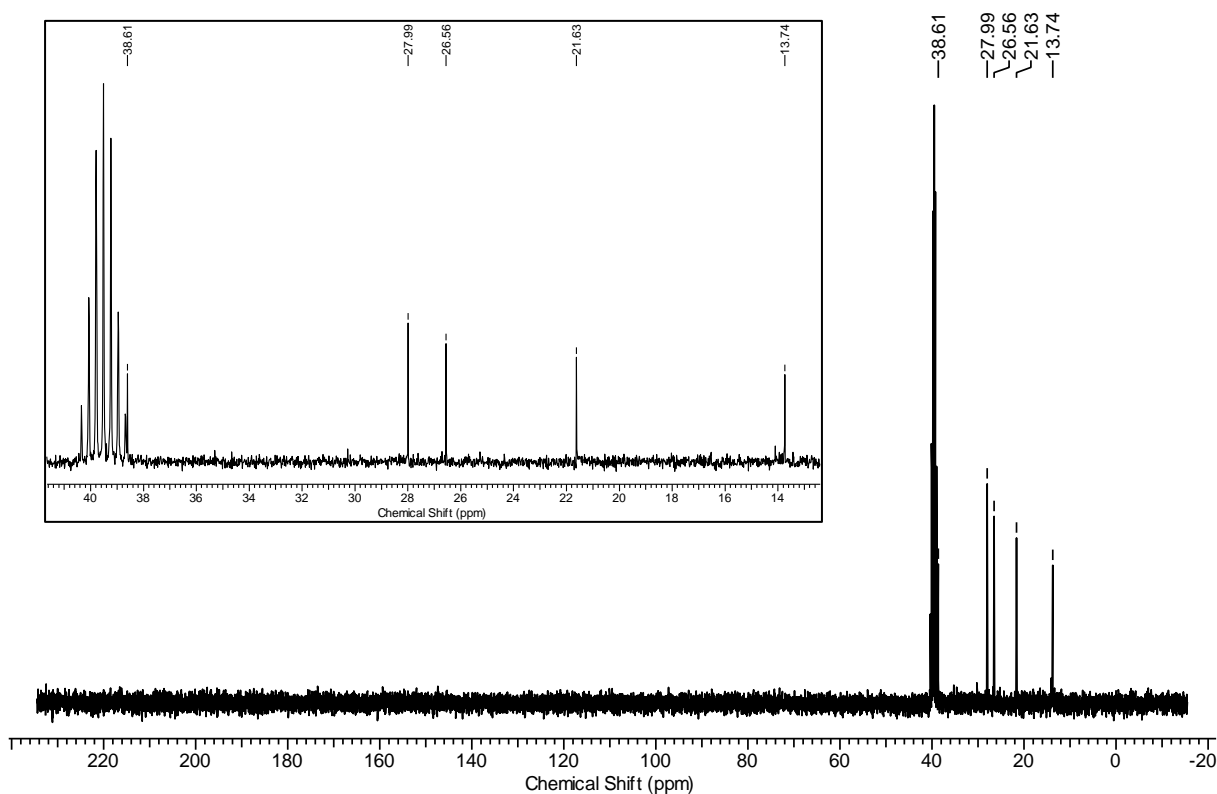
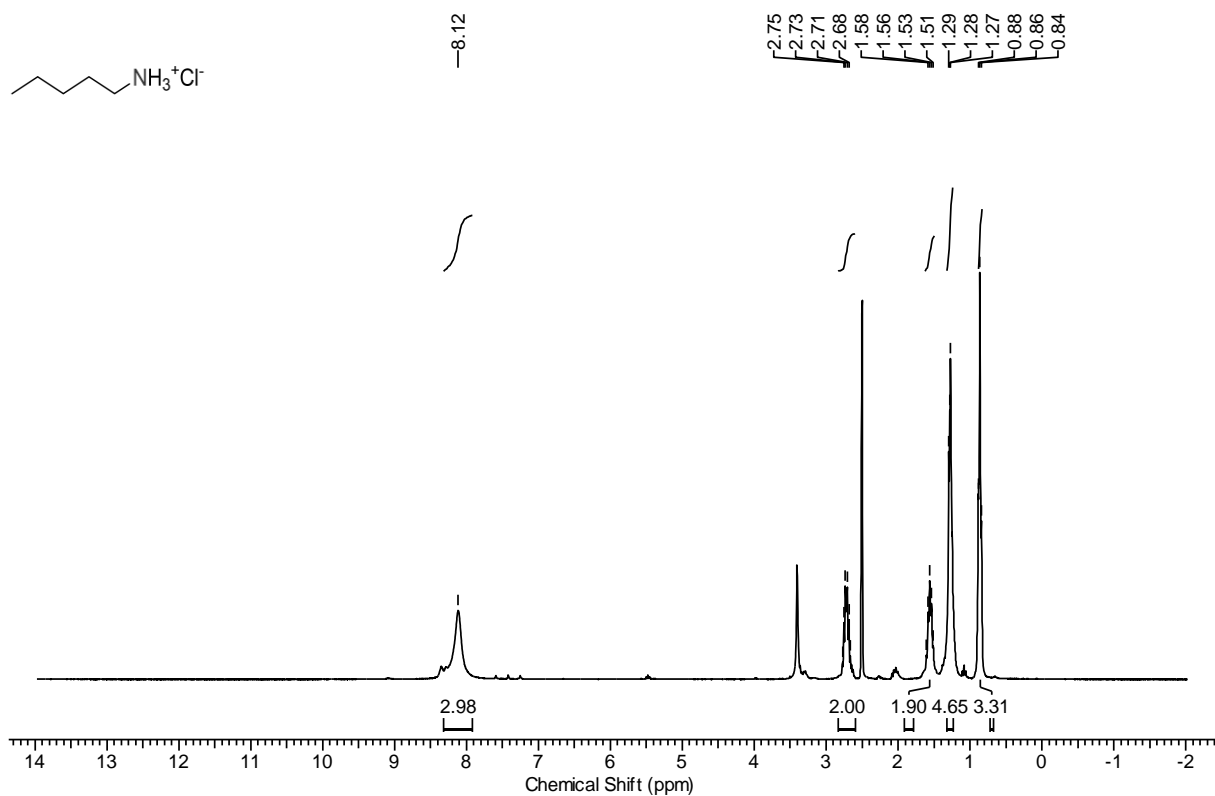
Supplementary Figure 39: NMR Spectra of compound 30'.



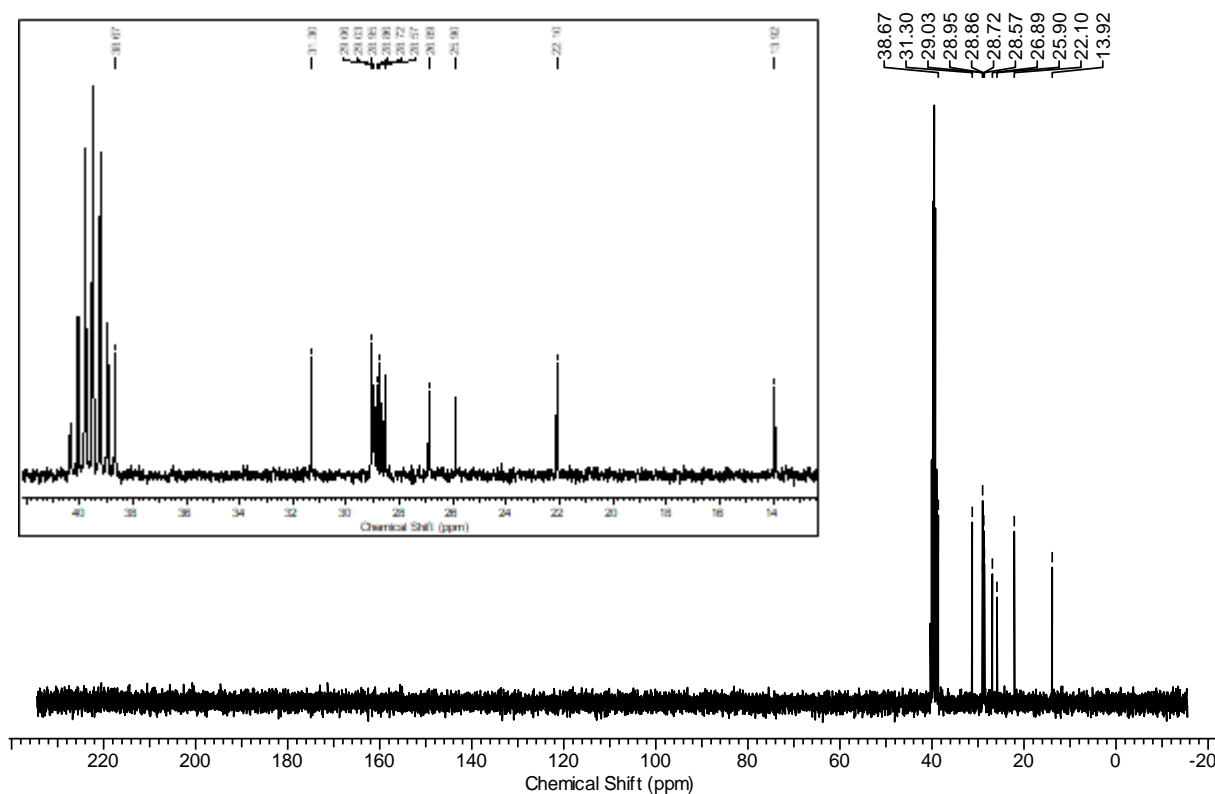
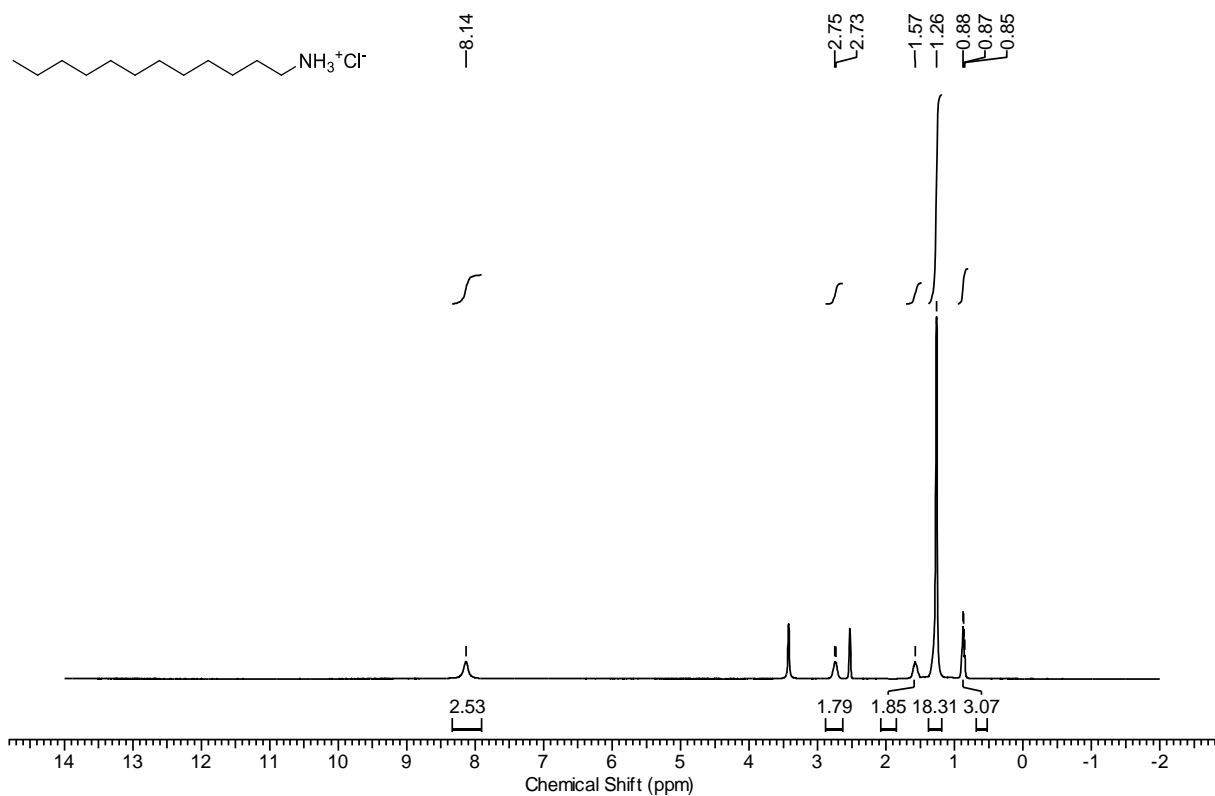
Supplementary Figure 40: NMR Spectra of compound 31'.



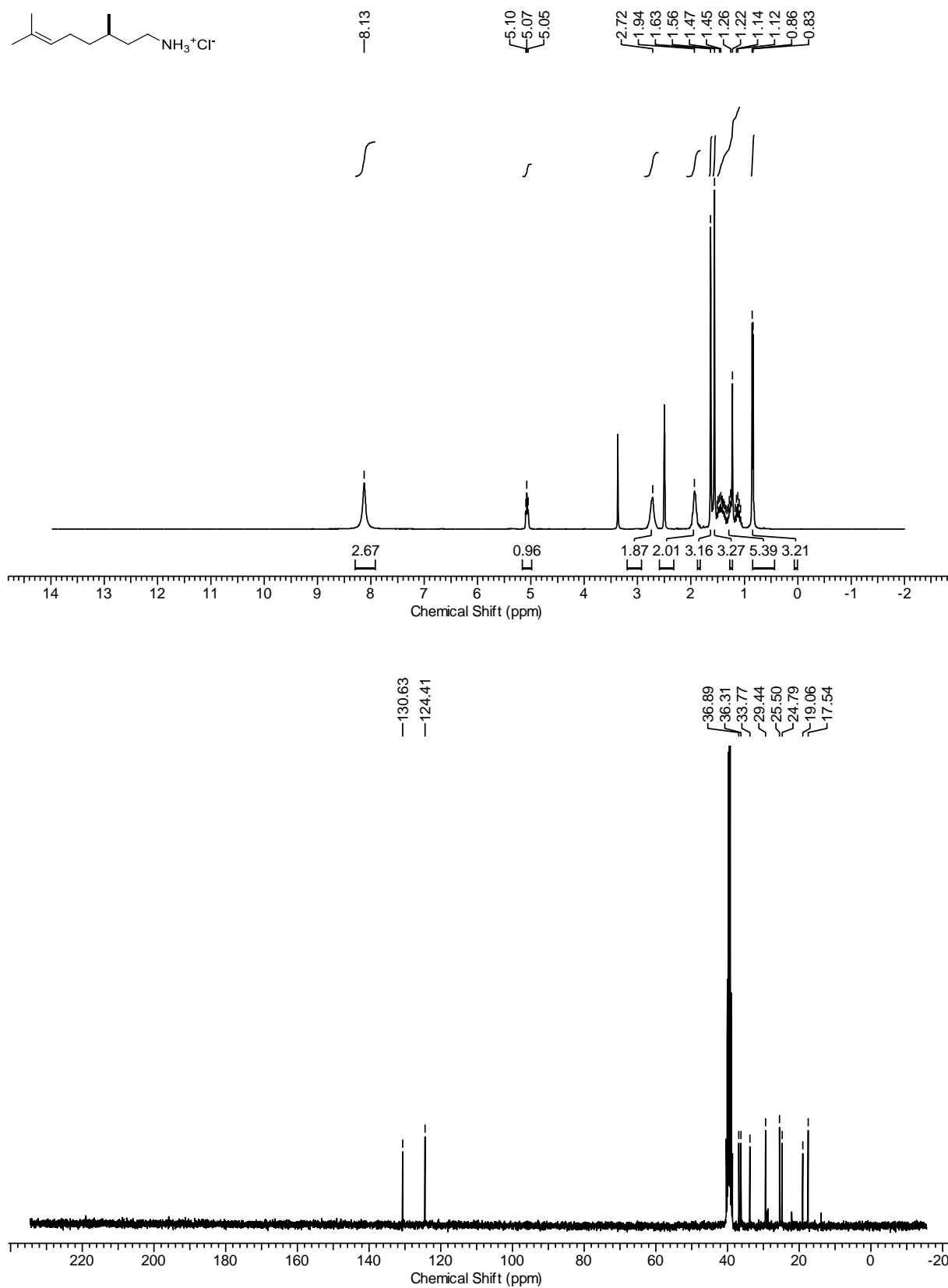
Supplementary Figure 41: NMR Spectra of compound 33'.



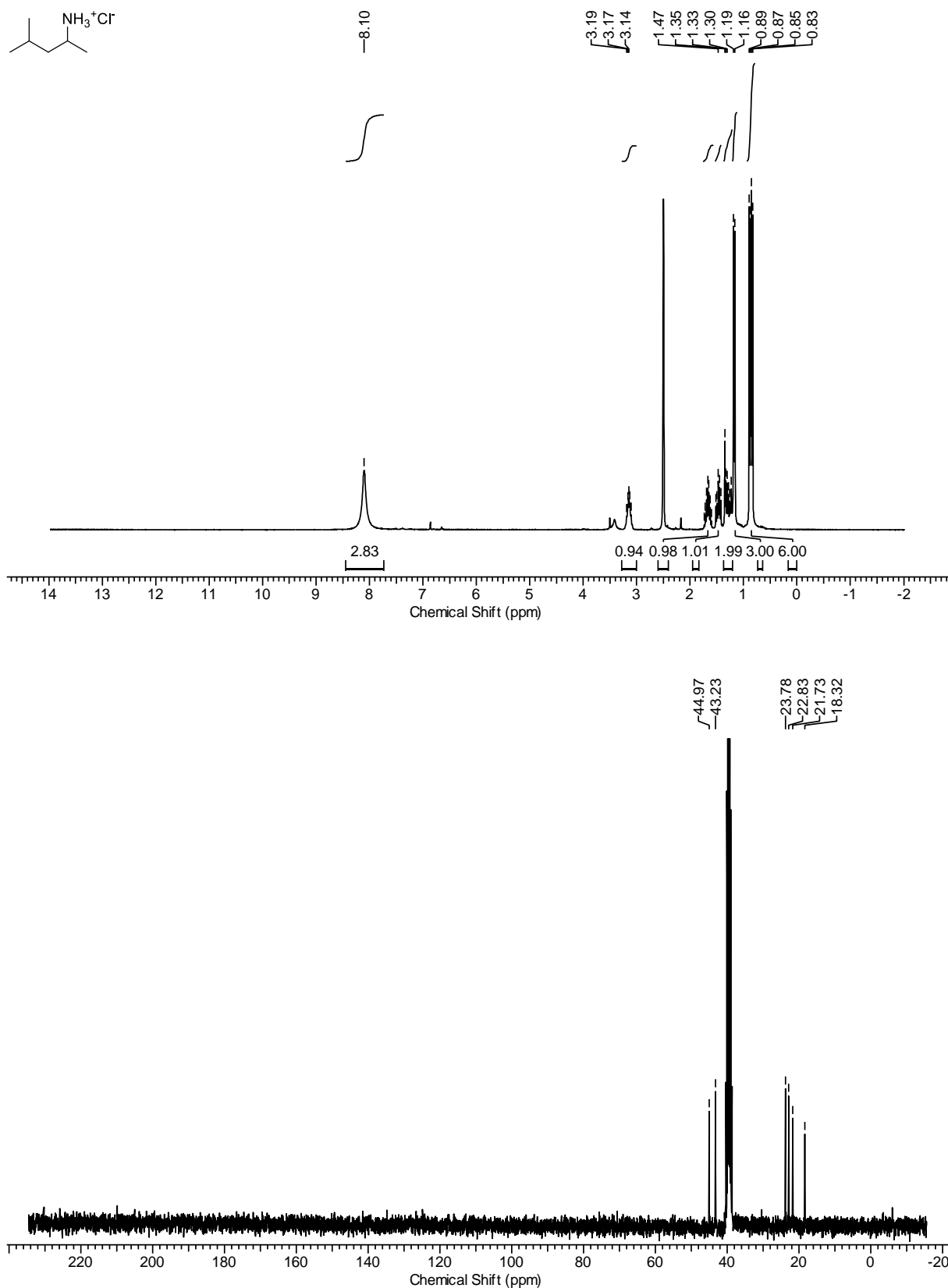
Supplementary Figure 42: NMR Spectra of compound 35'.



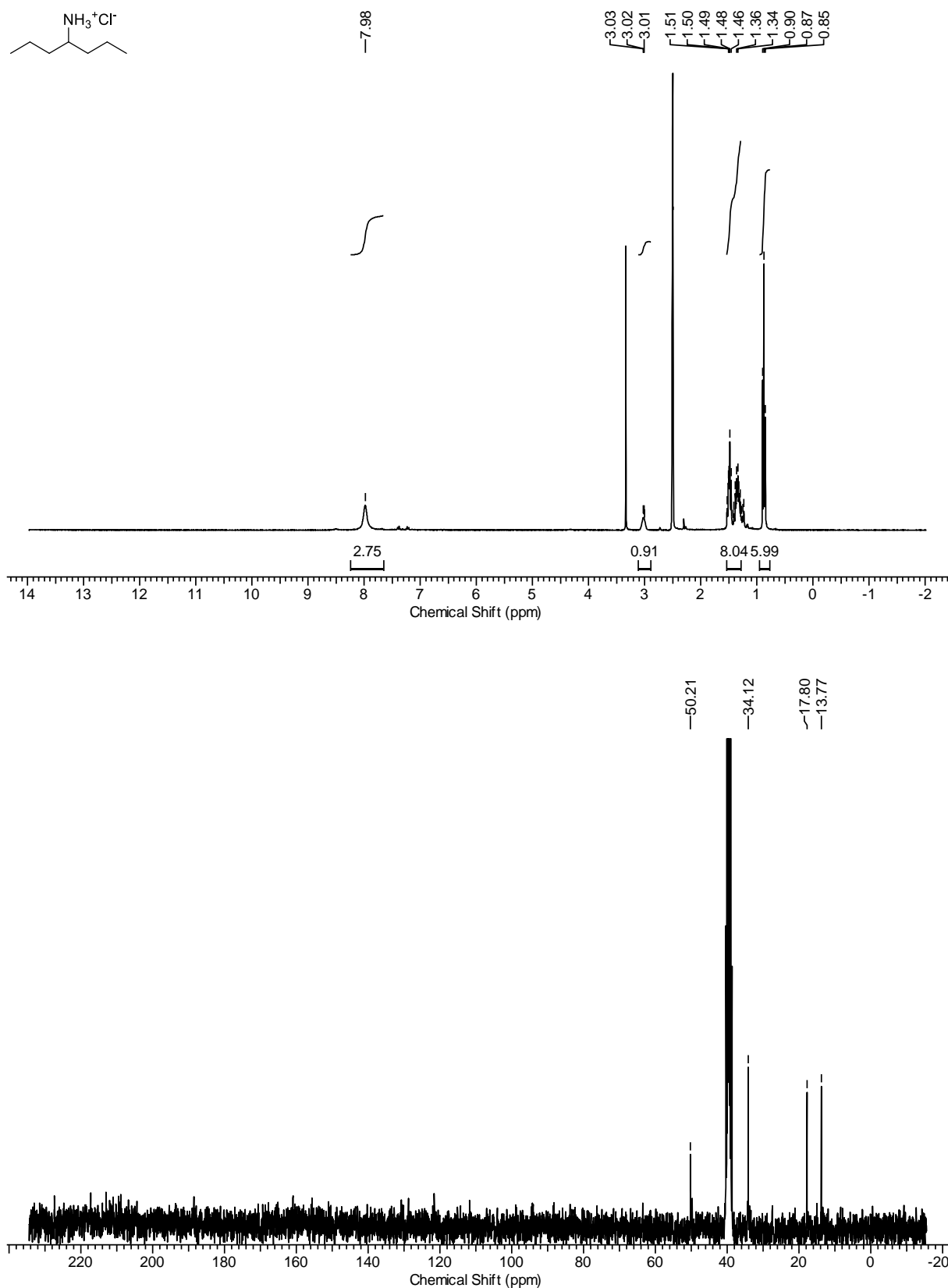
Supplementary Figure 43: NMR Spectra of compound 37'.



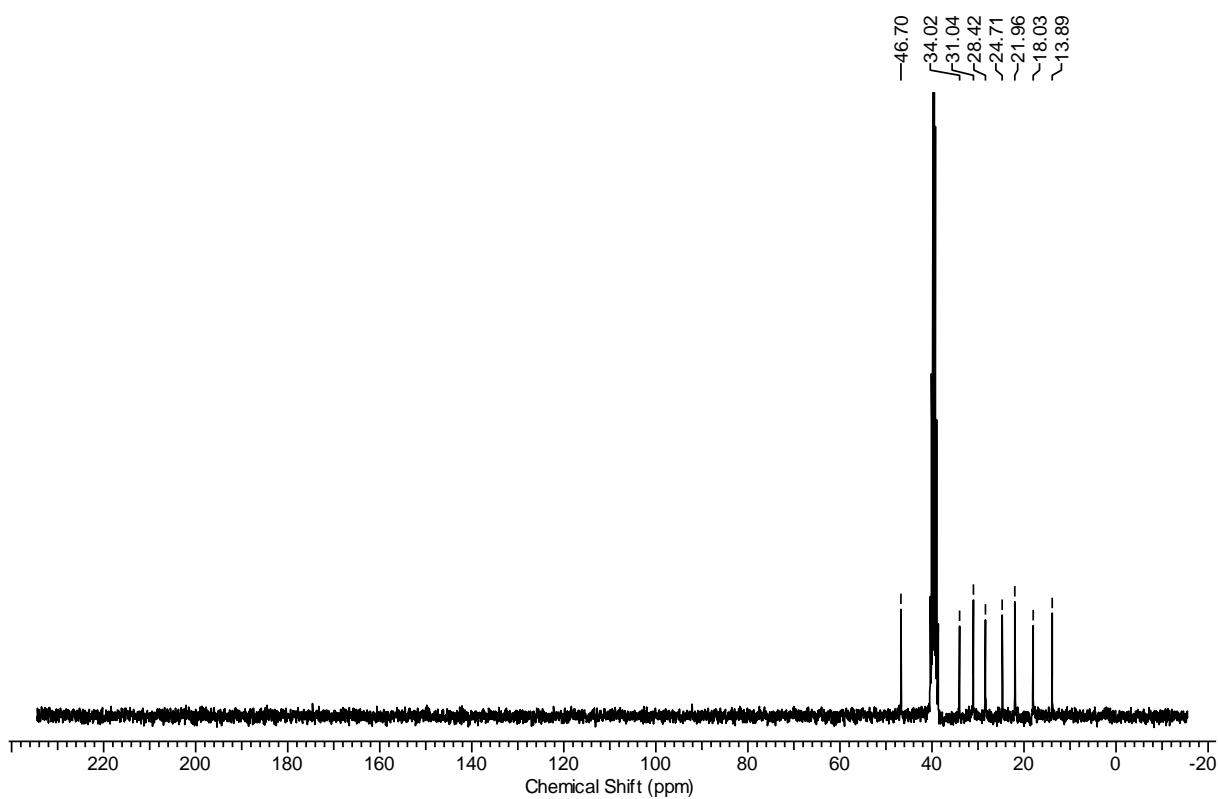
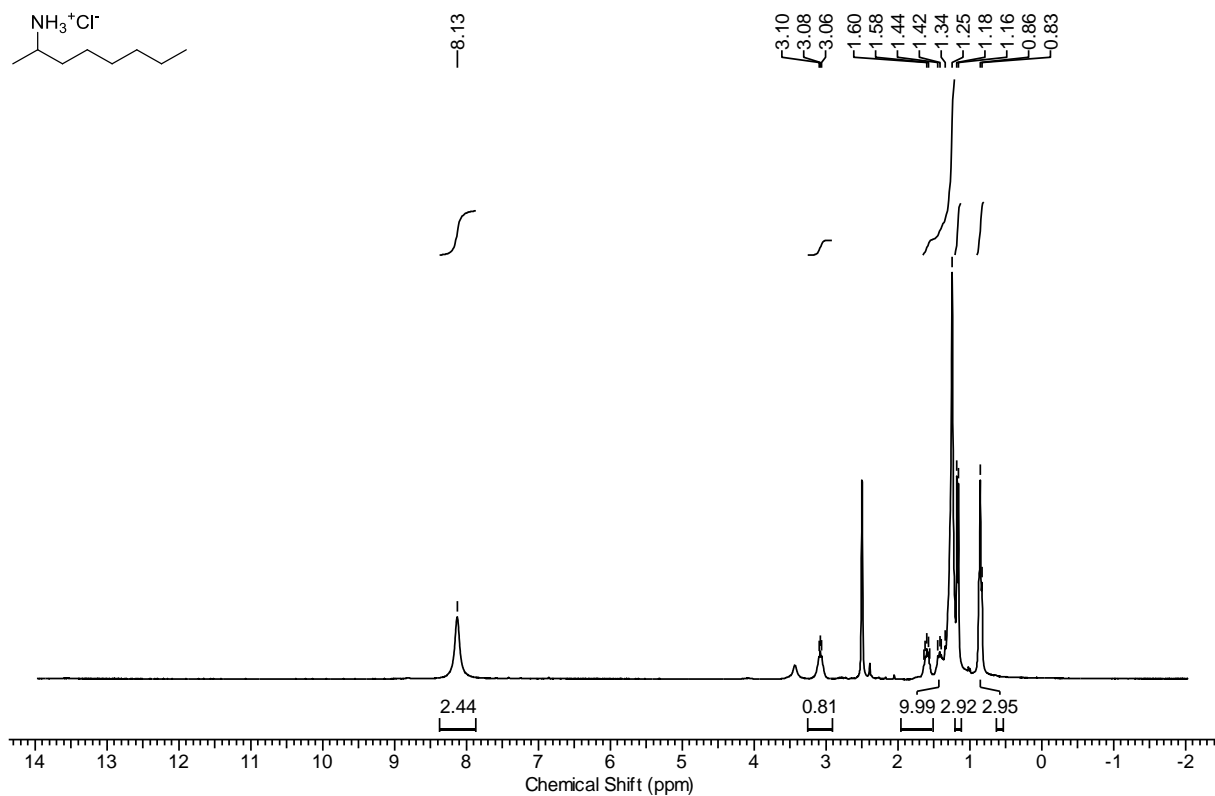
Supplementary Figure 44: NMR Spectra of compound 38'.



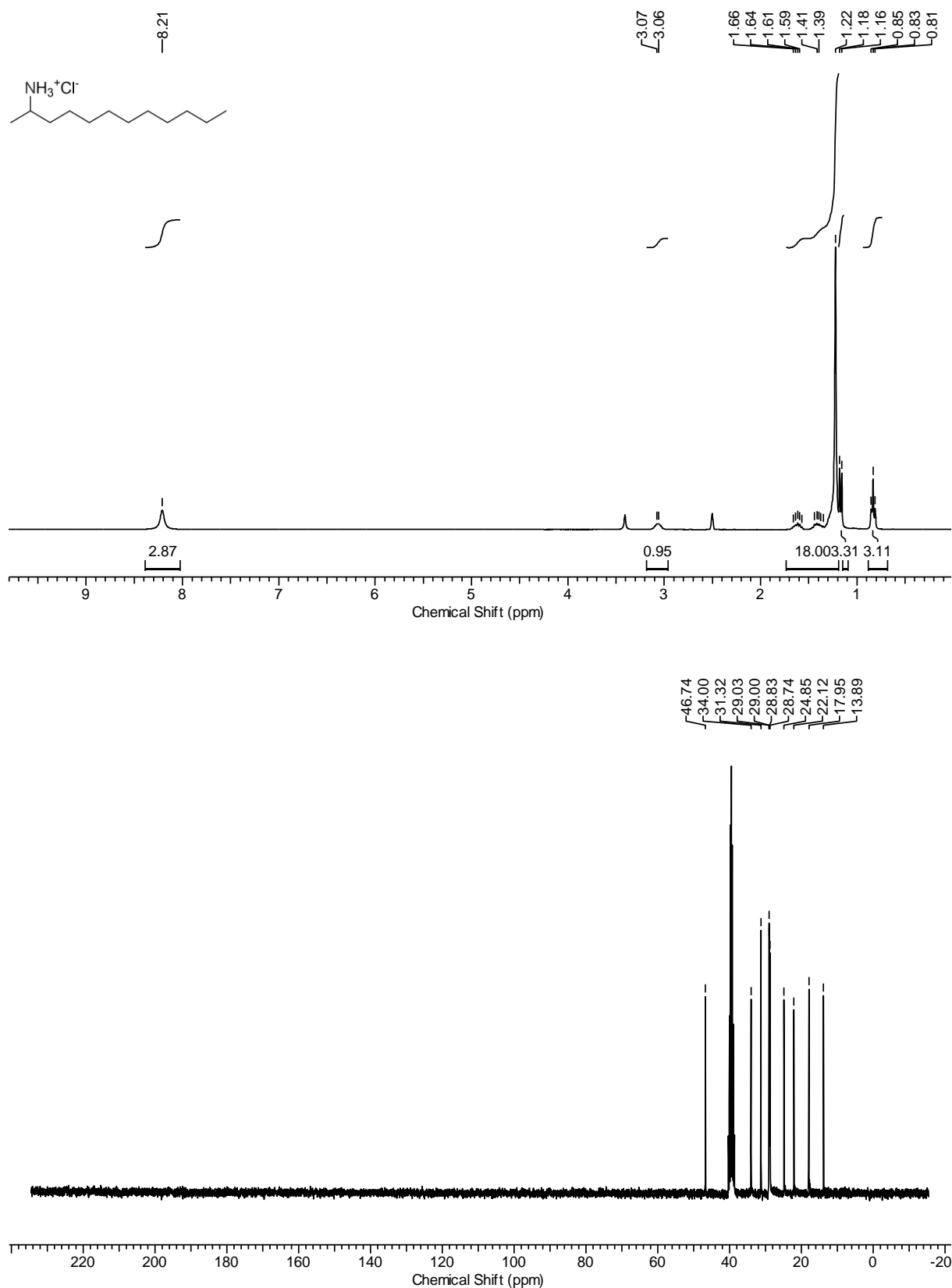
Supplementary Figure 45: NMR Spectra of compound 39'.



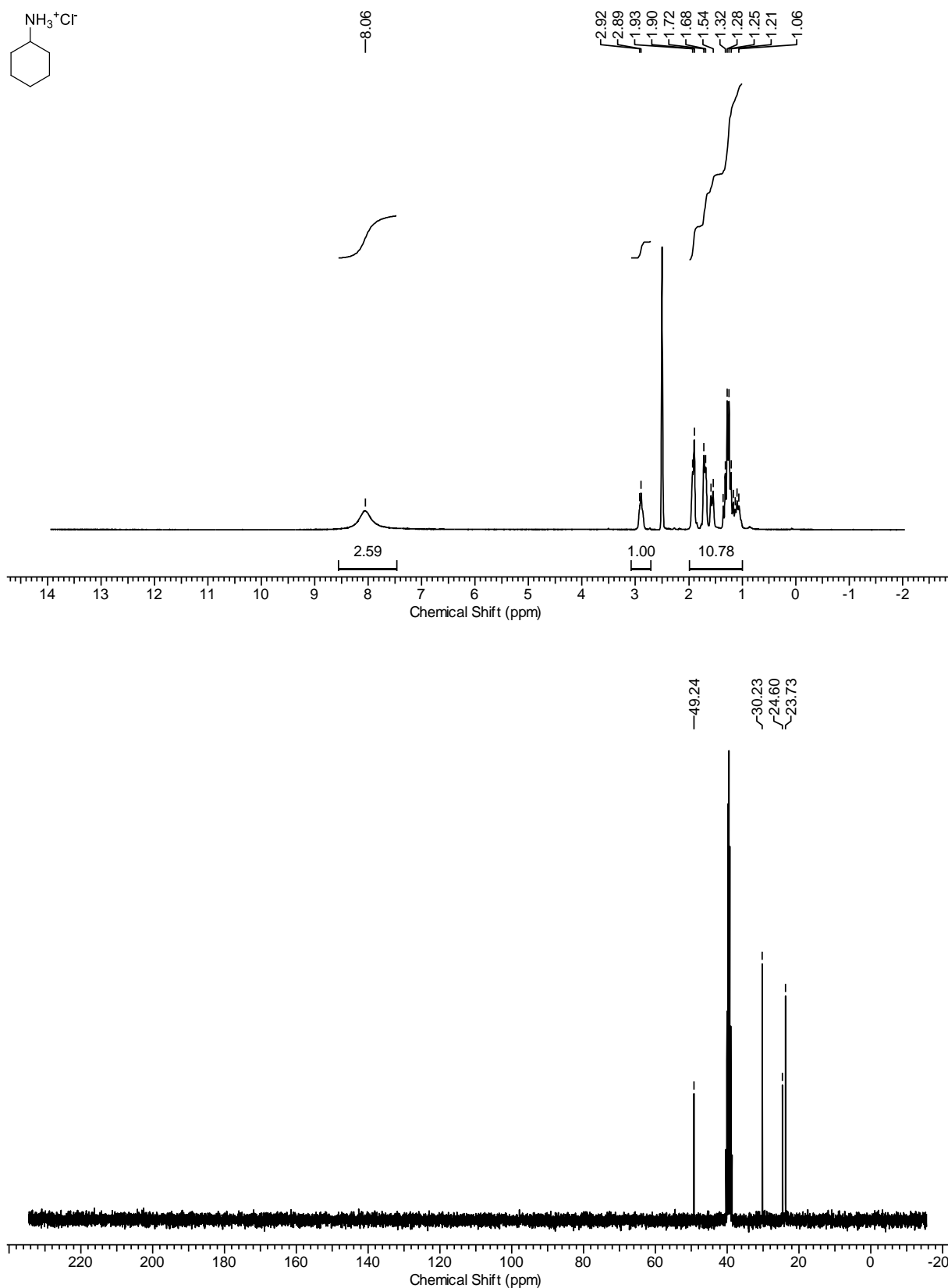
Supplementary Figure 46: NMR Spectra of compound 40'.



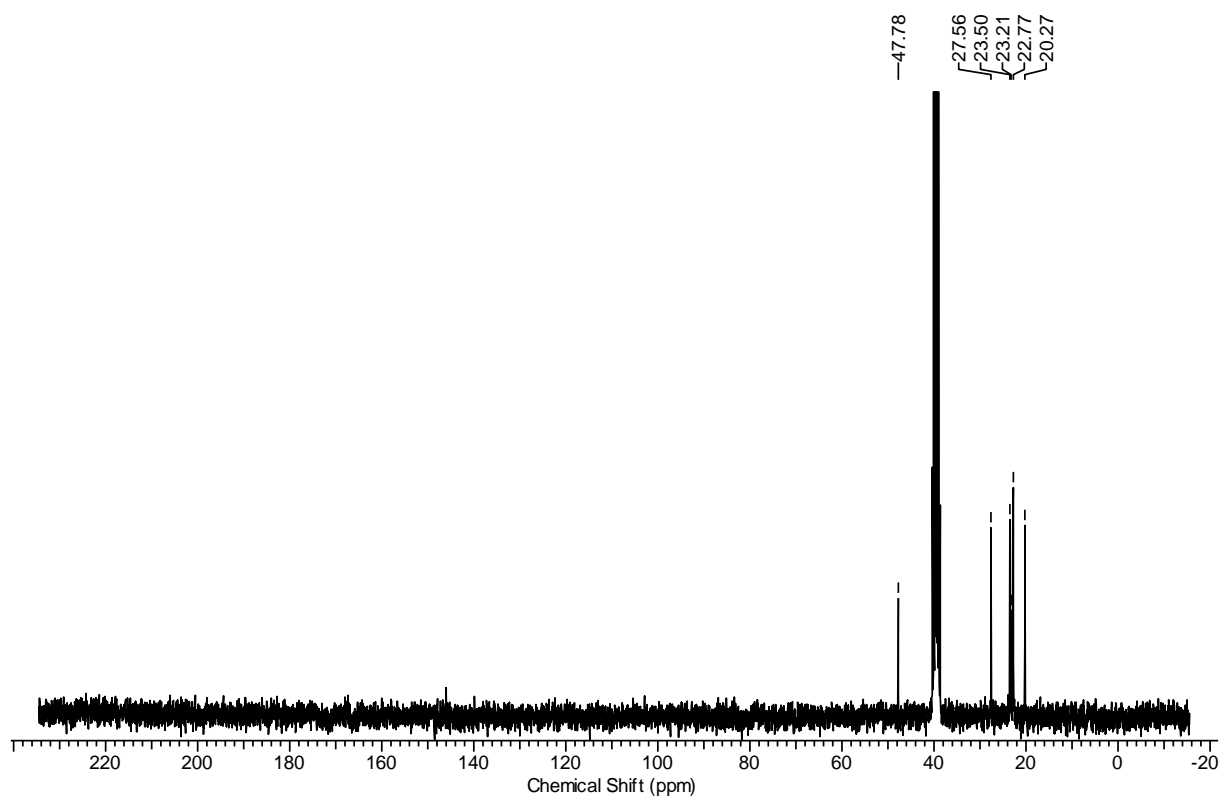
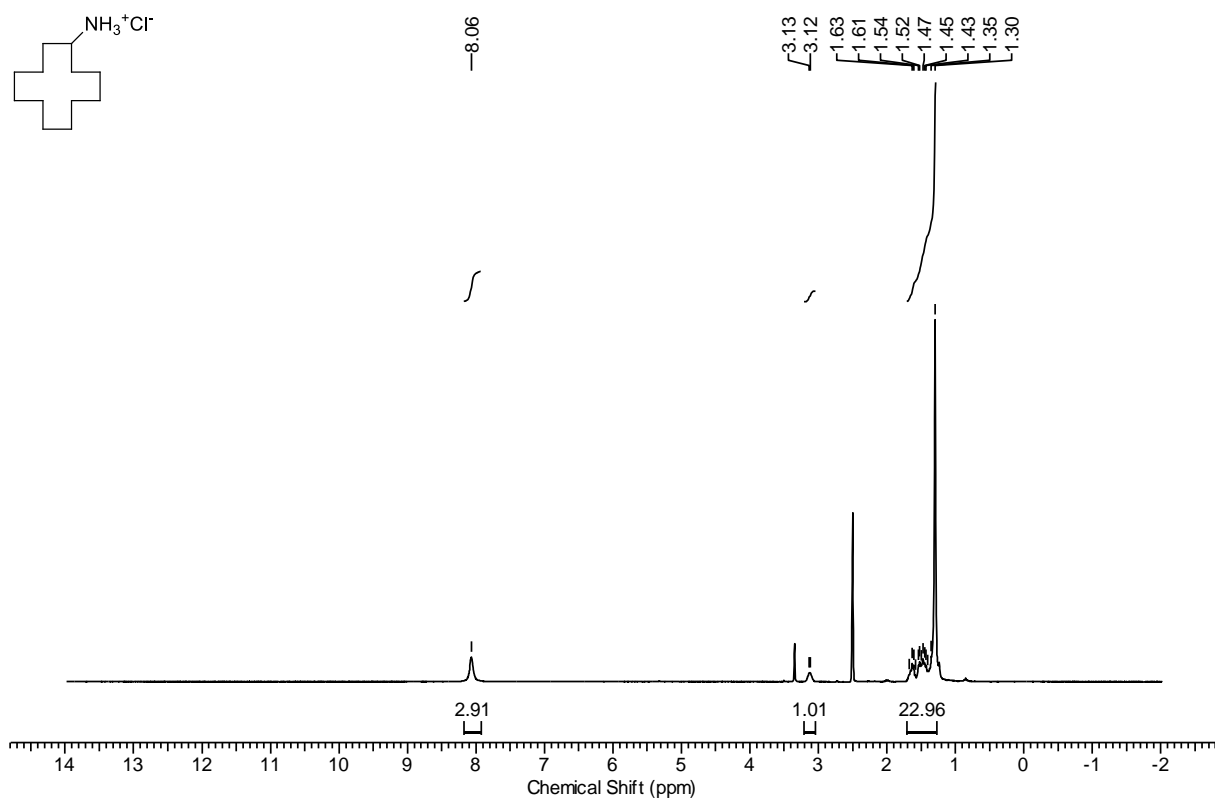
Supplementary Figure 47: NMR Spectra of compound 41'.



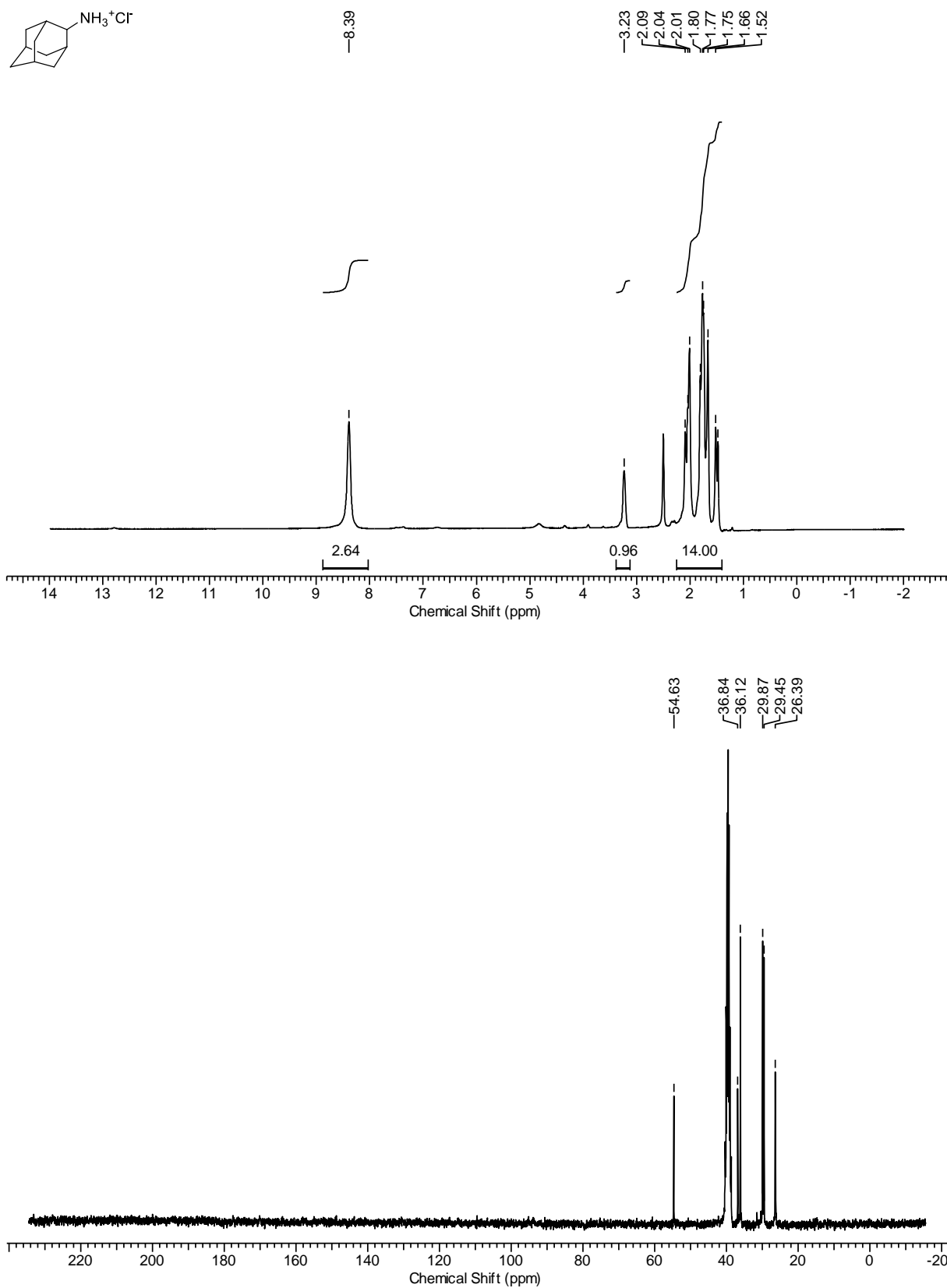
Supplementary Figure 48: NMR Spectra of compound 42'.



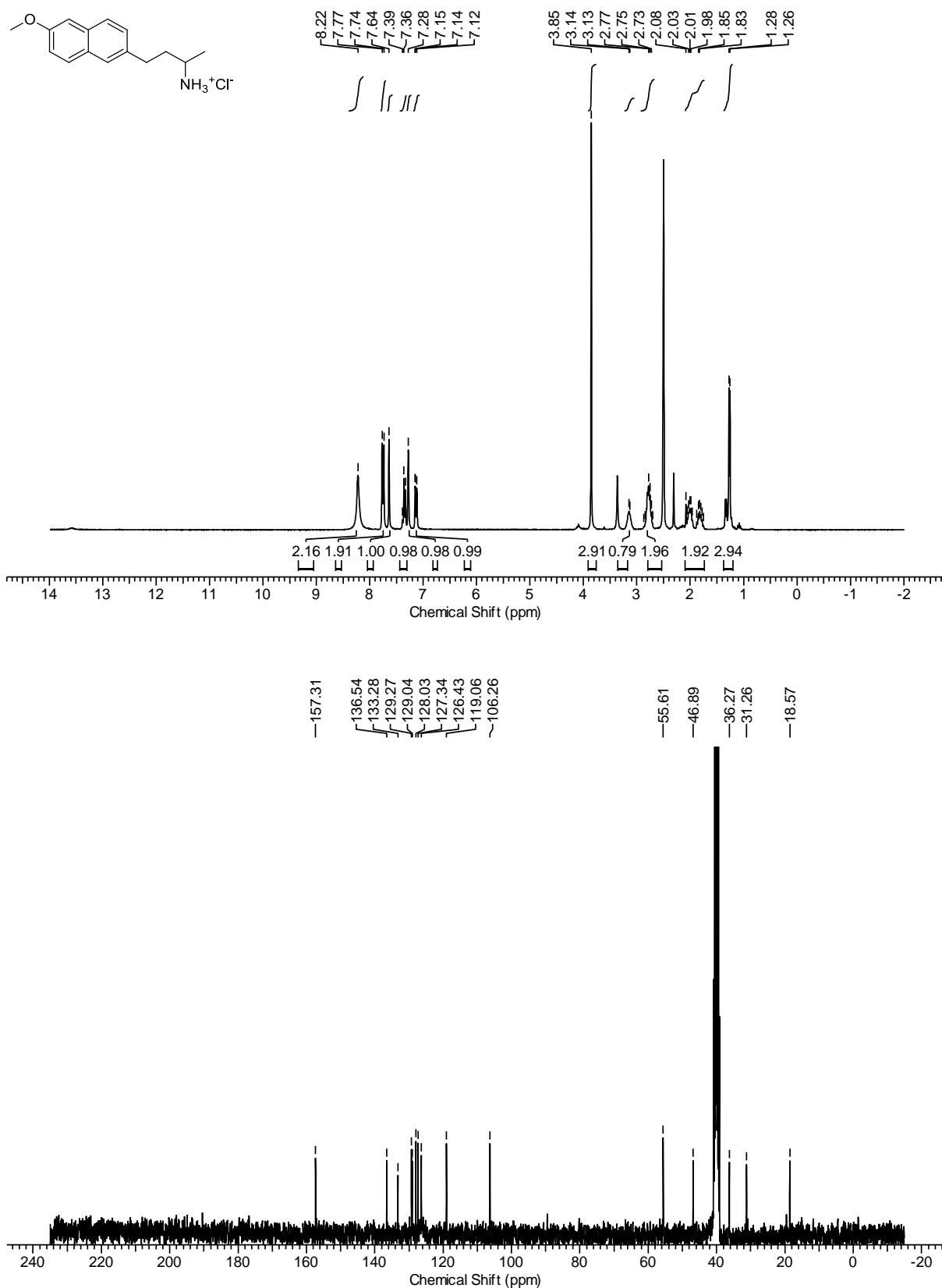
Supplementary Figure 49: NMR Spectra of compound 44'.



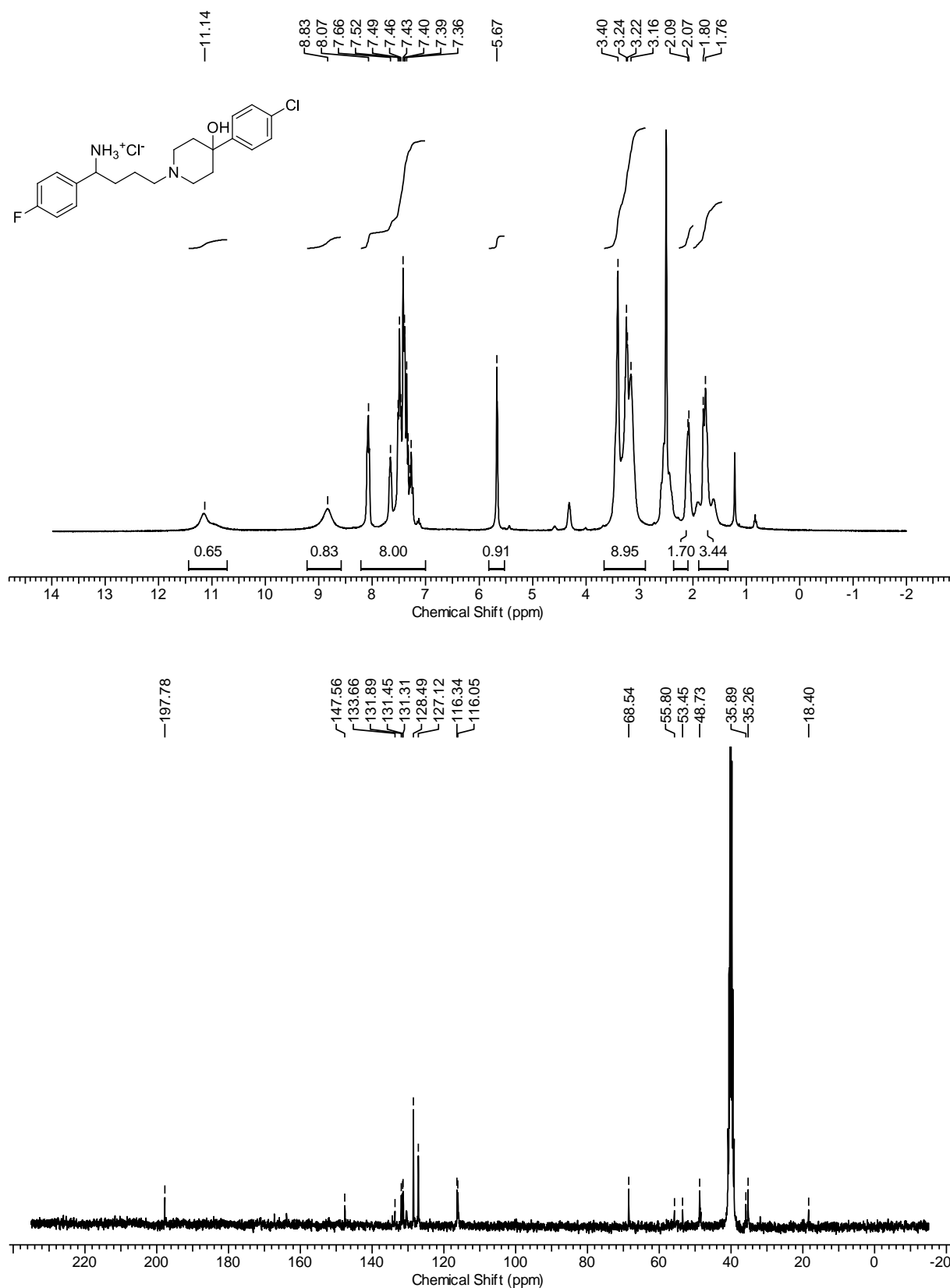
Supplementary Figure 50: NMR Spectra of compound 45'.



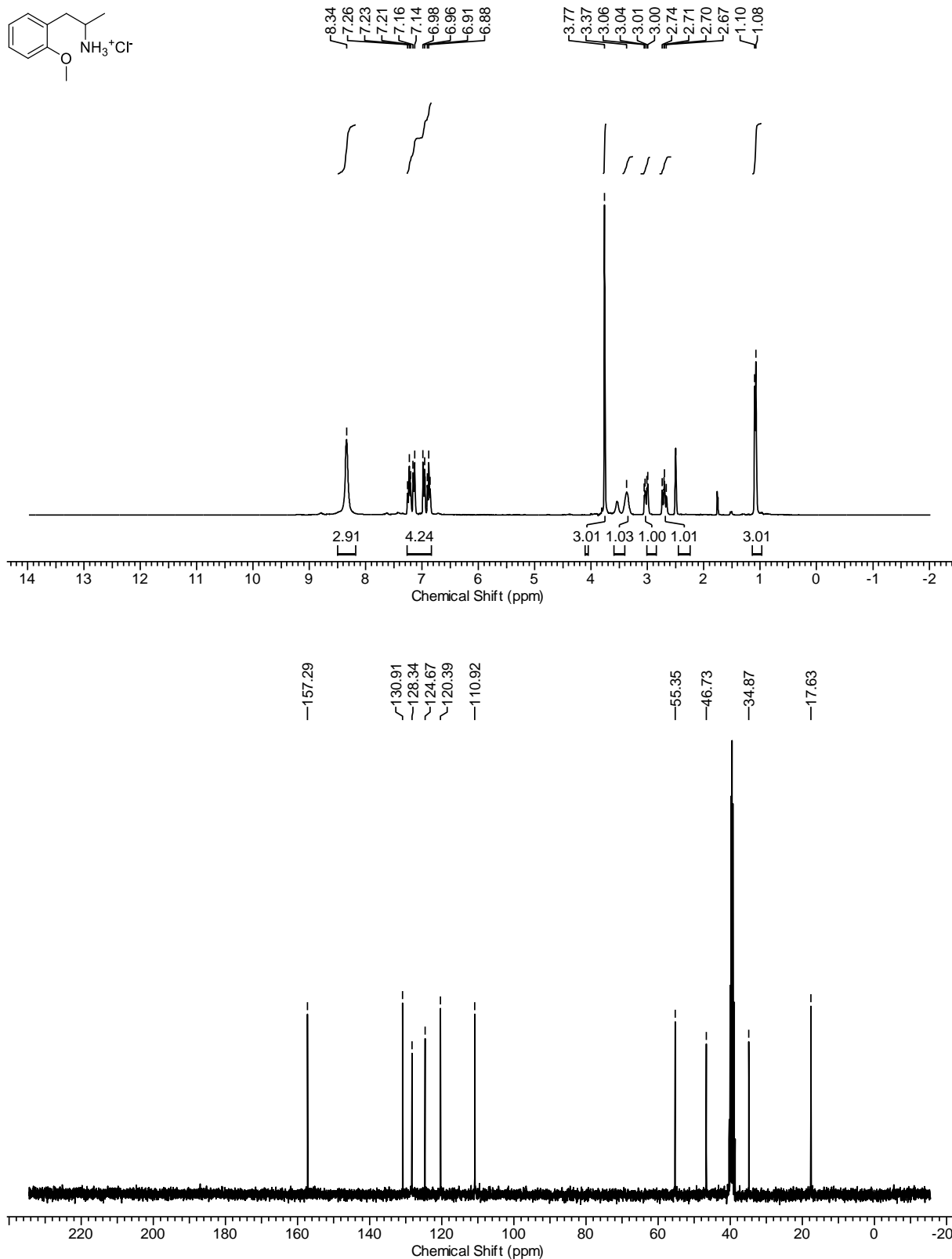
Supplementary Figure 51: NMR Spectra of compound 46'.



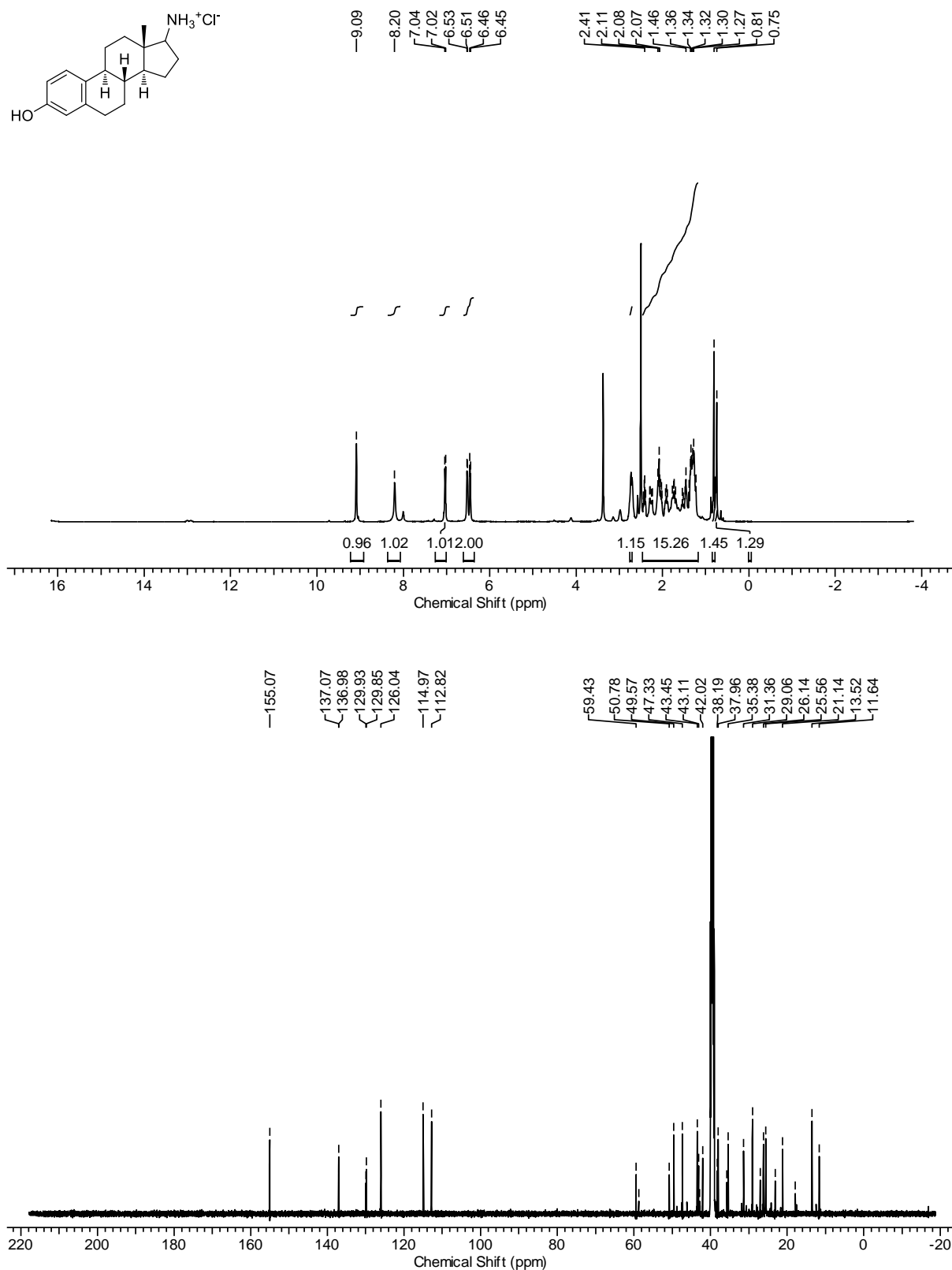
Supplementary Figure 52: NMR Spectra of compound 47'.



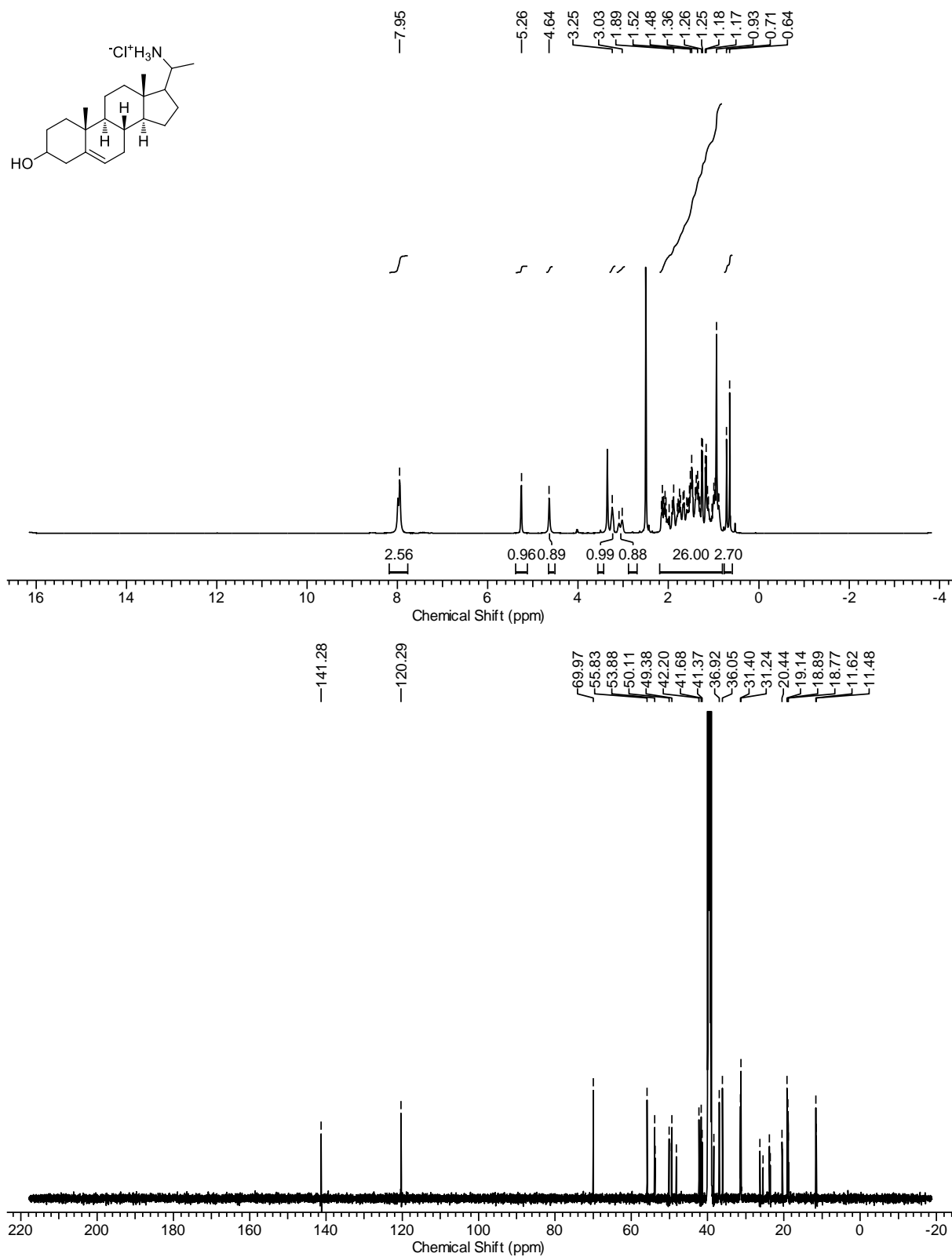
Supplementary Figure 53: NMR Spectra of compound 48'.



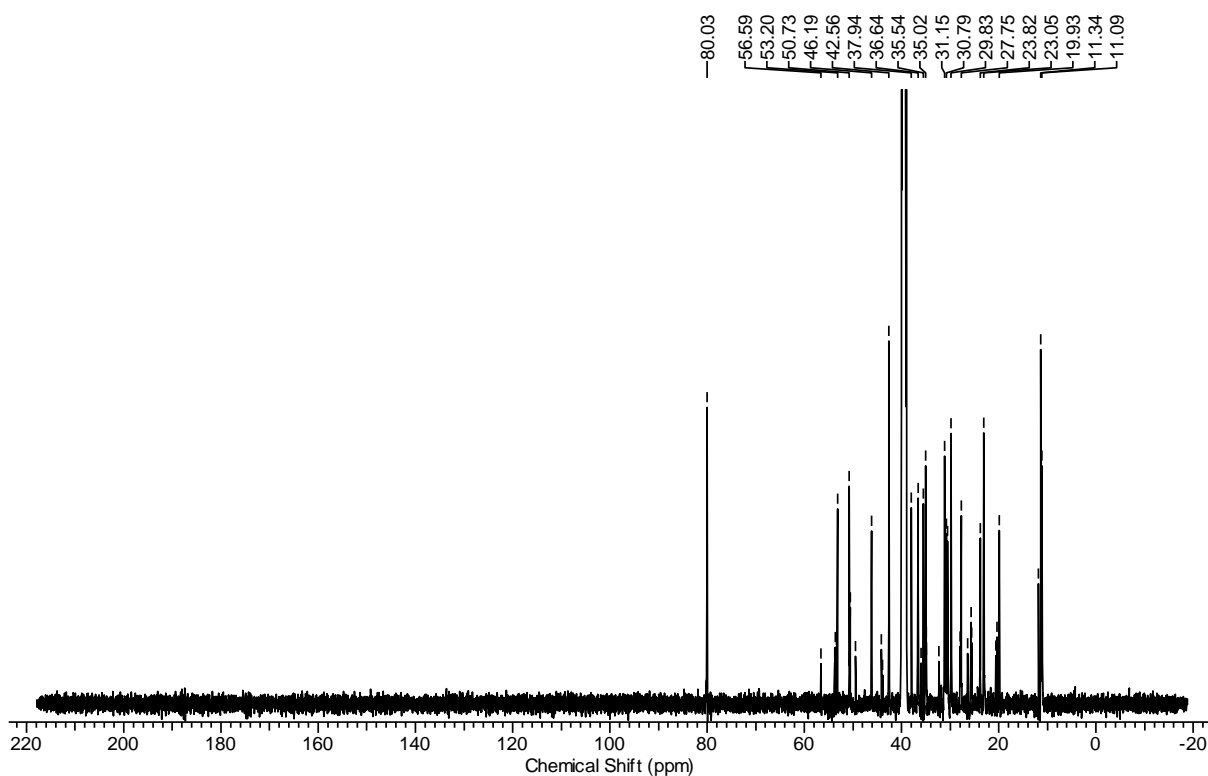
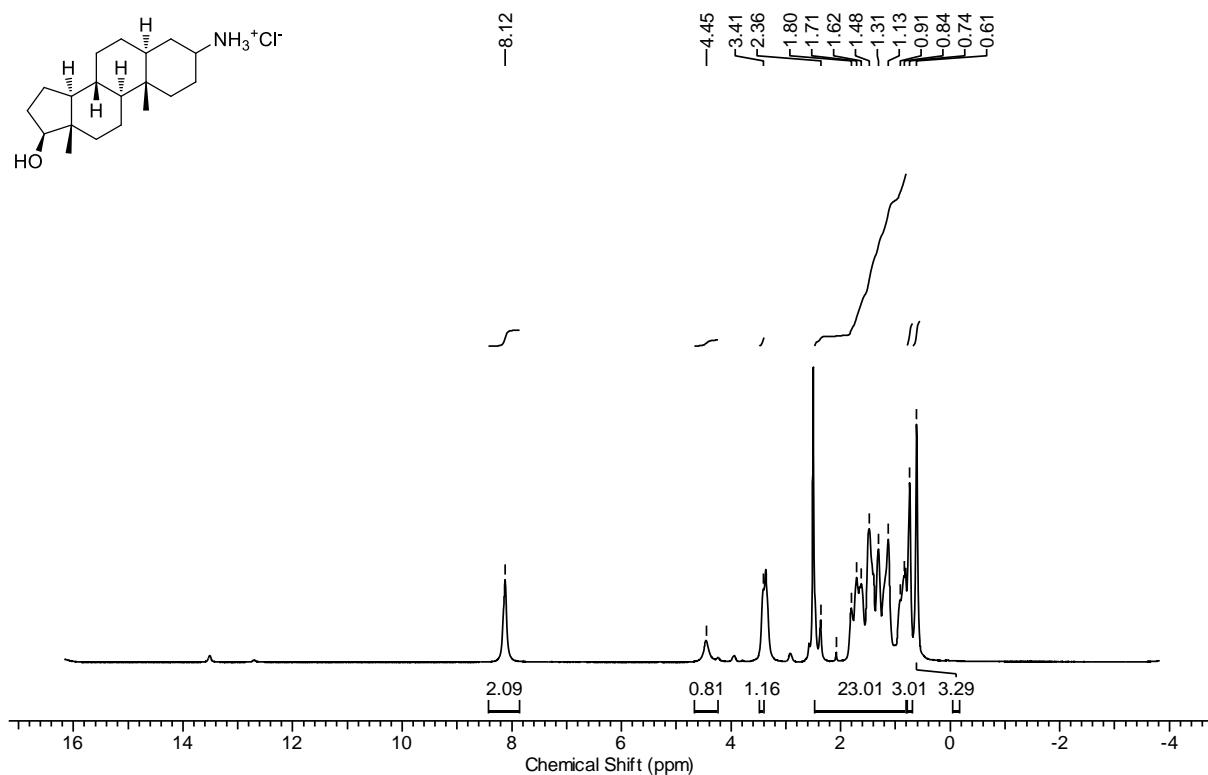
Supplementary Figure 54: NMR Spectra of compound 49'.



Supplementary Figure 55: NMR Spectra of compound 50'.

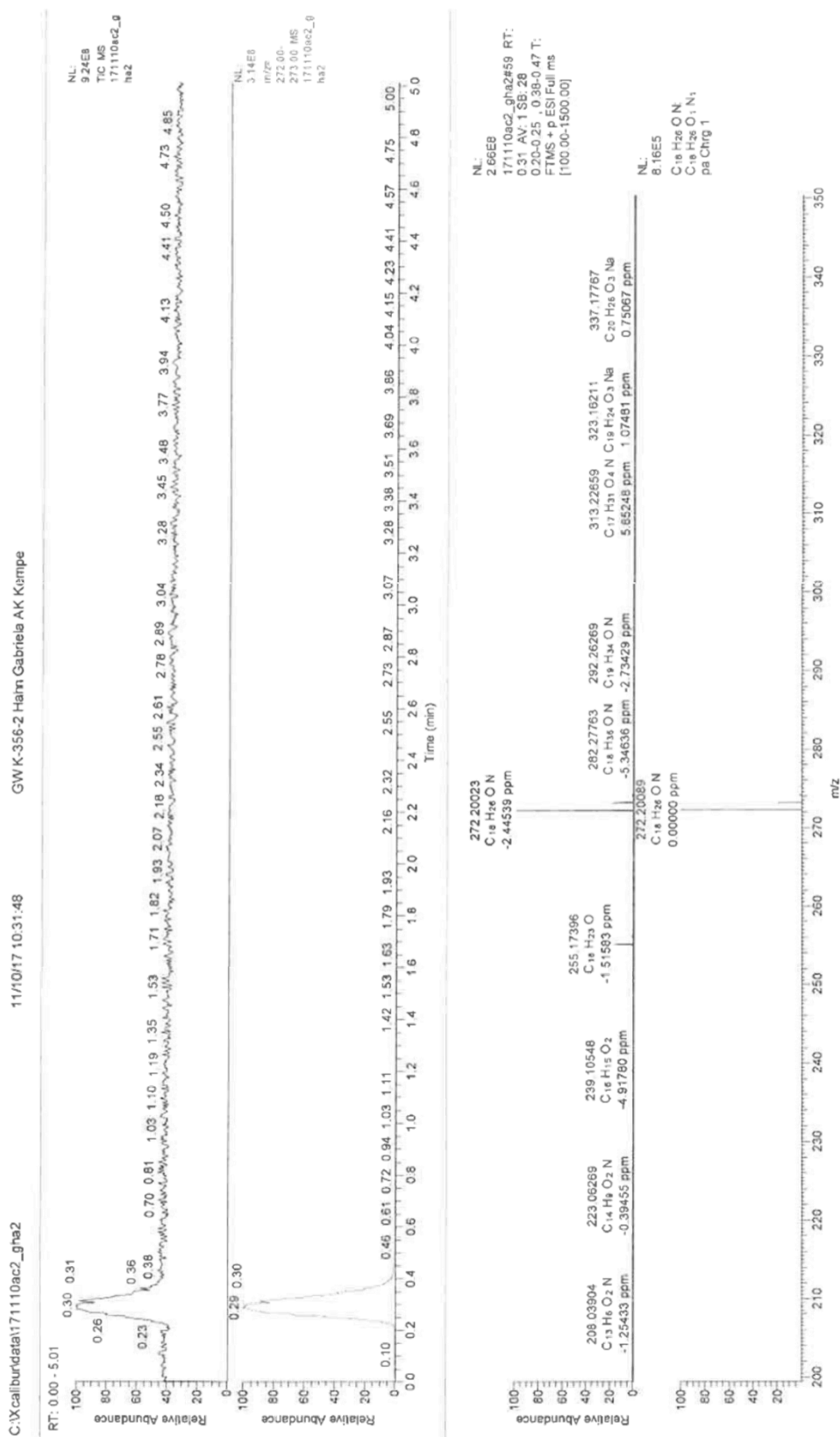


Supplementary Figure 56: NMR Spectra of compound 51'.

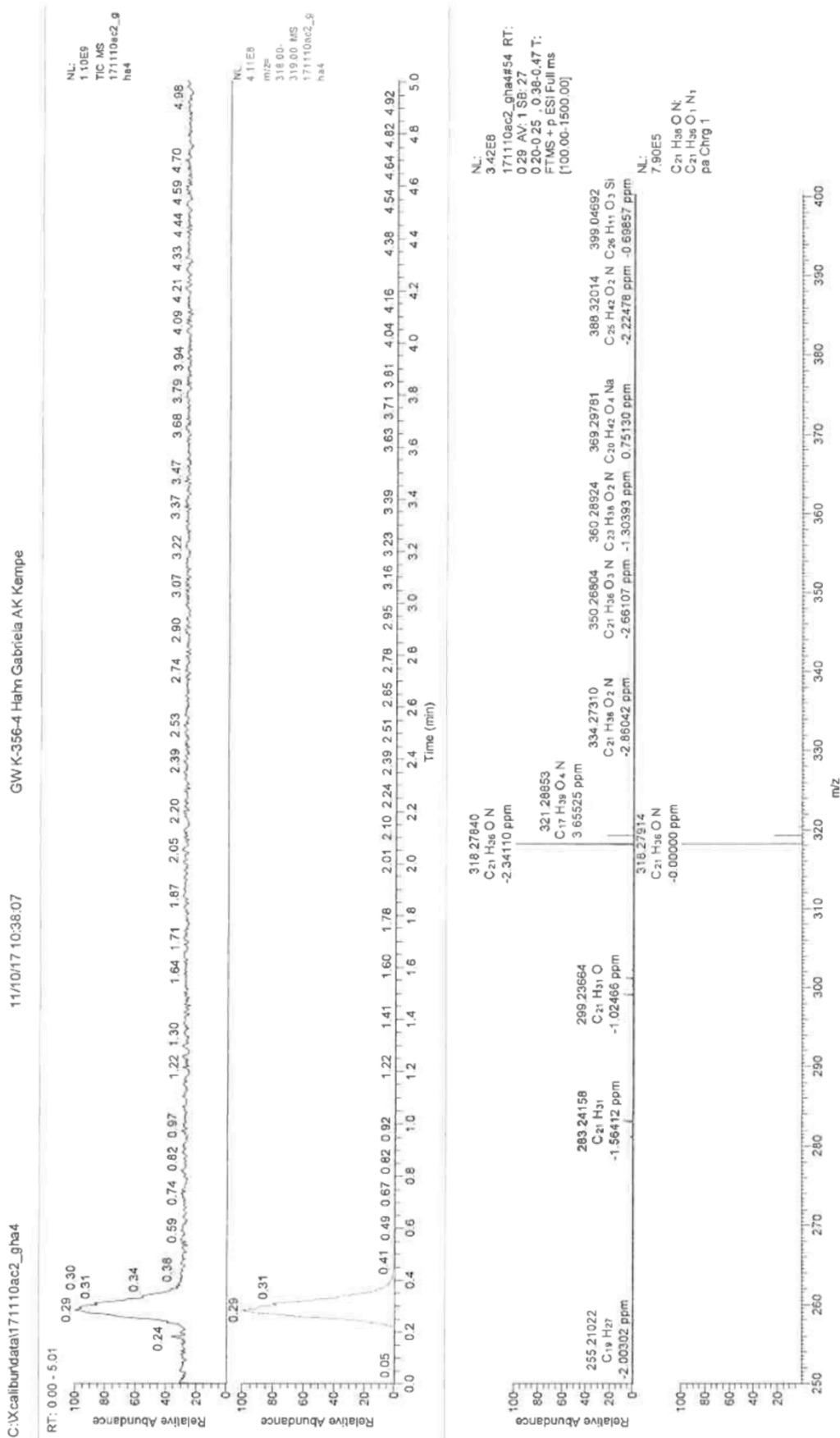


Supplementary Figure 57: NMR Spectra of compound 52'.

5.6.4.3 HRMS Spectra



Supplementary Figure 58: HRMS Spectra of compound 50[†].



Supplementary Figure S9: HRMS Spectra of compound 51'.

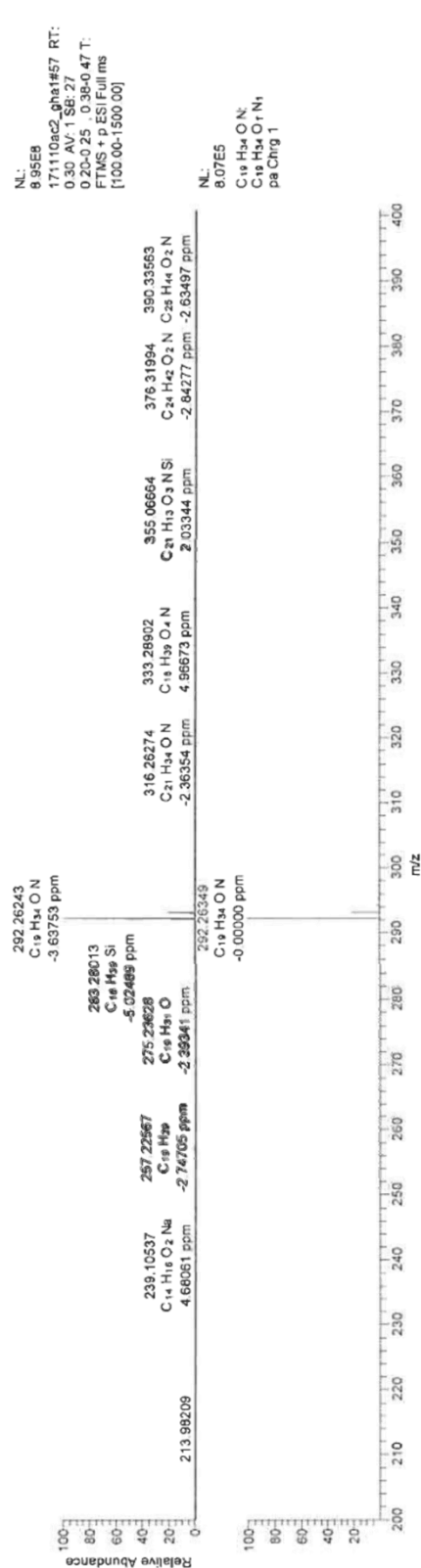
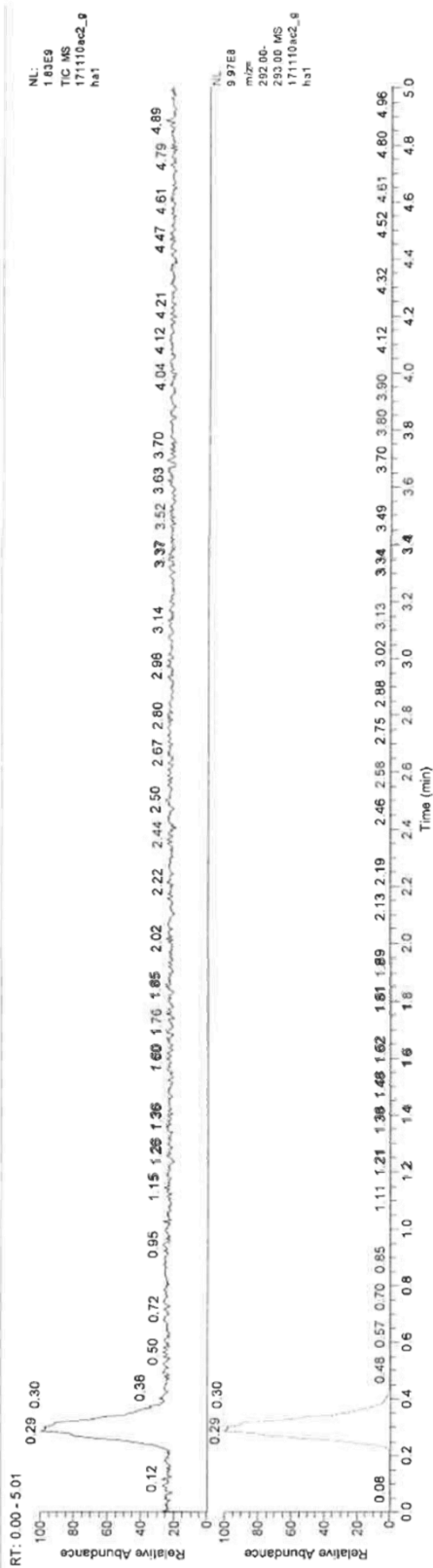
171110ac2_gha AK Kempe

ESI pos

C:\xcalibur\data\171110ac2_gha1

11/10/17 10:25:27

GWK-356-1 Hahn Gabriele AK Kempe



Supplementary Figure 60: HRMS Spectra of compound 52'.

5.6.5 Supplementary References

- [1] Wen, H.-R. *et al.* A family of nickel–lanthanide heterometallic dinuclear complexes derived from a chiral Schiff-base ligand exhibiting single-molecule magnet behaviors. *Inorg. Chim. Acta* **435**, 274–282 (2015).
- [2] Dai, H. & Guan, H. Switching the Selectivity of Cobalt-Catalyzed Hydrogenation of Nitriles. *ACS Catal.* **8**, 9125–9130 (2018).
- [3] H. R. Snyder, Clayton T. Elston & David B. Kellom. Polyphosphoric acid as a reagent in organic chemistry. IV. Conversion of aromatic acids and their derivatives to amines. *J. Am. Chem. Soc.* **75**, 2014–2015 (1953).
- [4] Guan, Q. *et al.* Direct cycle between co-product and reactant: an approach to improve the atom economy and its application in the synthesis and protection of primary amines. *Green Chem.* **18**, 5794–5799 (2016).
- [5] Chen, F. *et al.* Stable and inert cobalt catalysts for highly selective and practical hydrogenation of C≡N and C=O bonds. *J. Am. Chem. Soc.* **138**, 8781–8788 (2016).
- [6] Jagadeesh, R. V. *et al.* MOF-derived cobalt nanoparticles catalyze a general synthesis of amines. *Science* **358**, 326–332 (2017).
- [7] Lenstra, D. C., Lenting, P. E. & Mecinović, J. Sustainable organophosphorus-catalysed Staudinger reduction. *Green Chem.* **20**, 4418–4422 (2018).
- [8] Zwierzak, A. Synthesis of α -arylalkylamines by addition of grignard reagents to N-(diethoxyphosphoryl)aldimines. *Synthesis* **1999**, 930–934 (1999).
- [9] Lyle, R. E. & Troscianiec, H. J. Molecular rearrangements. VI. The rearrangement of oximes on reduction with lithium aluminium hydride. *J. Org. Chem.* **20**, 1757–1760 (1955).
- [10] Seeger, E. *Tertiary Amines. United States Patent Office* (1964).
- [11] Niwa, T., Yorimitsu, H. & Oshima, K. Palladium-catalyzed benzylic arylation of N-benzylal2nthone imine. *Organic letters* **10**, 4689–4691 (2008).
- [12] Fischer, F. & Strauss, D. Darstellung und sterische Zuordnung der Diastereomeren des 1-Methoxy-2-amino-1.2-diphenyl-äthans. *Justus Liebigs Ann. Chem.* **673**, 36–39 (1964).
- [13] Guy, A., Lemor, A., Doussot, J. & Lemaire, M. Selective conversion of benzylic C-H bonds to an amine function by oxidative nucleophilic substitution. *Synthesis* **11**, 900–902 (1988).
- [14] Howard E. Smith, L. J. Schaad, R. Bruce. Banks, Christopher J. Wiant & and Charles F. Jordan. Optically active amines. XIV. Circular dichroism of 1-(2-, 3-, and 4-pyridyl)ethylamine and some related compounds. *J. Am. Chem. Soc.* **95**, 811–818 (1973).
- [15] Gössnitzer, E., Malli, R., Schuster, S., Favre, B. & Ryder, N. S. Novel high energy intermediate analogues with triazasterol-related structures as inhibitors of ergosterol biosynthesis. Part I: synthesis and antifungal activity of N-alkyl-N'-(phenethyl- and cyclohexenylethyl)guanidines and N2-substituted 2-imidazolinamines. *Archiv der Pharmazie* **335**, 535–546 (2002).

- [16] Schwoegler, Edward J. and Adkins, Homer. Preparation of certain amines. *J. Am. Chem. Soc.* **61**, 3499–3502 (1939).
- [17] Zwierzak, A. & ślusarska, E. A novel grignard synthesis of primary amines. *Synthesis* **1979**, 691–693 (1979).
- [18] Brown L. Murr and Chas. T. Lester. The preparation of long chain alkylamine hydrochlorides. *J. Am. Chem. Soc.* **77**, 1685 (1955).
- [19] Zakharkin, L. I. & Korneva, V. V. Synthesis of some cycloundecane derivatives from 1,5,9-cyclododecatriene. *Russ Chem Bull* **11**, 1724–1726 (1962).

6 A Nanostructured Earth-abundant Metal Catalyst Can Mediate the Efficient Synthesis of Amino Acids from Ammonia Dissolved in Water under Very Mild Conditions

Gabriela Hahn^[a], Elena Herzog^[a] and Rhett Kempe ^{*[a]}

[a] Inorganic Chemistry II – Catalyst Design, University of Bayreuth, Universitätsstraße 30, 95440 Bayreuth (Germany).

To be submitted

Keywords: amino acids; ammonia; nickel catalyst; origin of life; reductive amination

Abstract: Catalysts based on earth-abundant metals could play an important role in the formation of small molecules, such as amine acids, relevant to the origin of life. Their abundancy makes them more relevant than rare noble metals classically associated with catalysis leading to those small molecules. Herein, we report on a nanostructured nickel catalyst for the general and selective synthesis of α -amino acids via reductive amination employing aqueous ammonia as a nitrogen source. Our nanostructured and reusable nickel catalyst can convert keto acids into the corresponding amino acids at very mild conditions. Essential, nonessential and nonbiological amino acids were synthesized in good isolated yields.

6.1 Introduction

A plausible time range of the abiogenesis (the origin of life from inorganic materials through chemical evolution) is 3.8–3.5 Ga before the present day.^[1] The origin of life and conditions on the early earth are highly discussed topics. Many different theories about the primitive earth, including the primordial soup theory by *A. Oparin*^[2] and *J. Haldane*^[3], were established in the last century.^[4,5] *S. Miller* demonstrated in his experiments that amino acids can be produced in an atmosphere of methane, ammonia, water and hydrogen. He circulated these gases past an electric discharge and found amino acids, such as alanine, glycine or aspartic acid, in the resulting mixture.^[6] Further experiments with cyan amide as an educt and electric discharge as an energy source followed, whereby the reaction mixture was not analyzed before 2014.^[7] However, many other energy sources are credible on the early earth. Thermal energy, introduced by *Harada and Fox*^[8] (T ~ 900–100 °C), ultraviolet radiation^[9–11], shock waves^[12] or ionizing radiation^[13] were tested experimentally by several research groups.^[14] All these experiments show that amino acids and other organic molecules can be produced easily from methane, ammonia and water under the

influence of this highly activating form of energy.^[15] Hydrogen cyanide and formaldehyde have frequently been observed as reactive intermediates in the synthesis of amino acids. Further investigations applying formaldehyde and various N sources (hydroxylamine with hydrogen cyanide^[16,17] or ammonia^[18]) in combination with moderate heat as a less destructive energy source ($T \leq 150\text{ }^{\circ}\text{C}$) were used to synthesize amino acids. This experimental work was further proven by mechanistic investigations in 1974.^[19]

Prebiotic synthesis concepts of amino acids

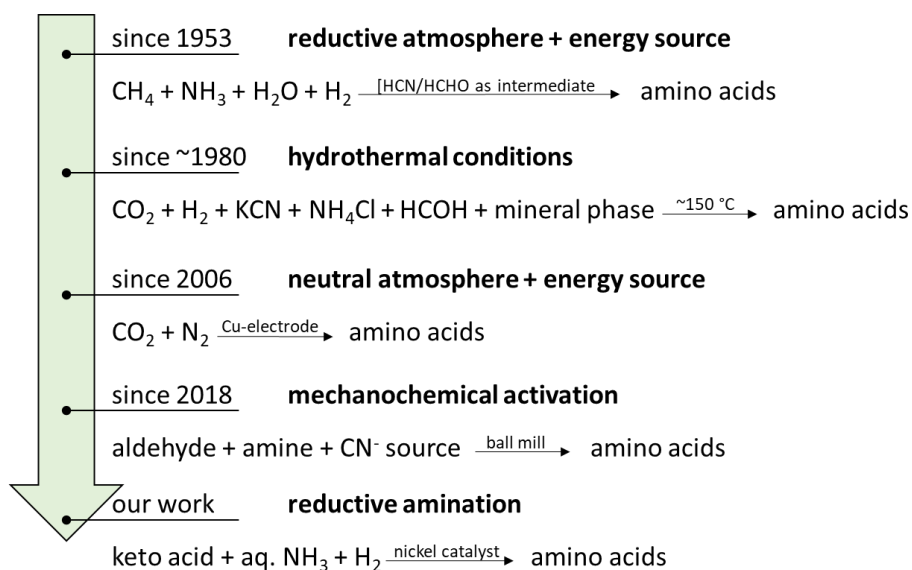


Figure 6. 1: Overview of the development of different synthetic concepts for amino acids.

All these experiments are based on the fact that the atmosphere had a reducing character during the origin of life. However, new findings of geochemical research contradict this. The atmosphere, after hydrogen and helium escaped to space due to their low weight, is determined by volcanic outgassing and impacts of asteroids and comets. Therefore, the main components of the primitive atmosphere were CO_2 and N_2 , while CH_4 and NH_3 were decomposed under ultraviolet radiation. Furthermore, NH_3 was dissolved in the ocean due to its good water solubility.^[20–23] New concepts were developed which produce amino acids under these conditions, only slightly reducing to nonreducing gas mixtures in the atmosphere. *Plankensteiner et al.* was able to generate amino acids by electric discharge in 2006 using a Cu electrode in a gas mixture of CO_2 and N_2 .^[24,25]

A conceptual alternative to the concepts discussed above is the origin of life near hydrothermal vents.^[26] The discovery of hydrothermal sources around 1980 provided a further impulse for the developments in synthesis concepts. It has been demonstrated that the abiotic synthesis of amino acids is possible at $150\text{ }^{\circ}\text{C}$, 10 atm pressure of a mixture of $\text{CO}_2\text{:H}_2$ (3:1), in the presence of KCN, NH_4Cl , formaldehyde, HCl and a mineral phase consisting, for example, of Pt powder, TiO_2 and illite.^[27] Small changes, such as the use of NH_4HCO_3 instead of NH_4Cl , also permit the generation of amino acids.^[28] *Shock* gave

evidence for the experiments by thermodynamic calculations.^[22] Mechanochemical activation of iron cyano complexes demonstrated very recently a prebiotic scenario for the synthesis of amino acids. Benzaldehyde was experimentally mechanically activated with benzylamine, SiO₂ as an additive and a cyanoferrate complex as a CN⁻ source using a ball mill. The resulting aminonitriles can be transformed by hydrolysis into the corresponding amino amides and then by ageing into the amino acids.^[29]

Catalytic research has focused on the development of novel base metal catalysts^[30–39] for the conservation of noble metals in the last few years. In addition to various homogeneous catalysts^[40–46], only a few heterogeneous catalyst systems^[47–51] have been introduced in our group. Furthermore, we have recently described the development of a reusable and highly active nickel catalyst for the reductive amination of carbonyl compounds to primary amines. Similar to a reaction in biochemistry, where the amino acids glutamate and glutamine are produced via reductive amination of α -ketoglutarate^[52], many carbonyl compounds were selectively converted to the primary amines.^[53] These results motivated us to introduce our novel catalyst system for the synthesis of amino acids in early earth conditions.

6.2 Results and Discussion

We developed a Ni/Al₂O₃ catalyst in our recent study. It is synthesized in a simple two-step procedure. Firstly, commercial γ -Al₂O₃ is impregnated with a specific Ni salen complex dissolved in acetonitrile. Further pyrolysis at 700 °C under nitrogen atmosphere and reduction at 550 °C under forming gas generated nickel nanoparticles embedded in a nitrogen-doped carbon layer on the Al₂O₃ support (for details see SI). The catalyst was fully characterized and highly active in the synthesis of primary amines via reductive amination.^[53] Investigations revealed that significantly milder conditions (lower H₂ pressures) did not influence the selectivity of the conversion of ketones. Only lower yields were observed. This motivated us to optimize our novel catalyst system for reductive amination under mild conditions (comparable to early earth conditions).

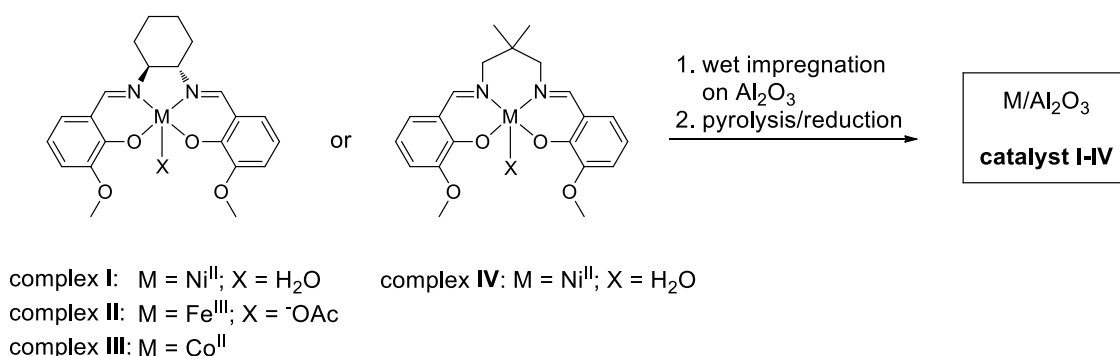


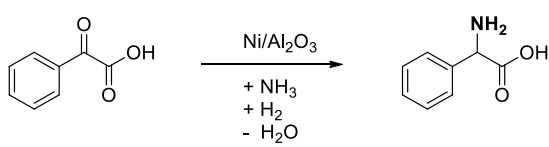
Figure 6. 2: Schematic preparation of different base metal catalysts.

Firstly, the known Ni/Al₂O₃ catalyst **I** (based on complex **I**) was compared to other base metal catalysts synthesized in a similar way. The schematic synthesis with different metal complexes (complex **I–IV**) is shown in Figure 6. 2. The salen ligand, synthesized by condensation of o-vanillin and cyclohexane-

A Nanostructured Earth-abundant Metal Catalyst Can Mediate the Efficient Synthesis of Amino Acids from Ammonia Dissolved in Water under Very Mild Conditions

1,2-diamines, was converted with different metal salts to the base metal salen complexes **I–III**. The respective $M/\text{Al}_2\text{O}_3$ catalysts were obtained after wet impregnation on commercial $\gamma\text{-Al}_2\text{O}_3$ and pyrolysis under nitrogen and reduction under forming gas. Furthermore, 2,2-dimethylpropane-1,3-diamine was used instead of cyclohexane-1,2-diamine for the generation of nickel complex **IV**. A further $\text{Ni}/\text{Al}_2\text{O}_3$ catalyst **IV** was obtained analogous to the synthesis described above.

Table 6. 1: Catalyst screening.



Entry	Metal source	Catalyst	Yield [%]
1	Complex I	$\text{Ni}/\text{Al}_2\text{O}_3$ I	60
2	Complex II	$\text{Fe}/\text{Al}_2\text{O}_3$ II	0
3	Complex III	$\text{Co}/\text{Al}_2\text{O}_3$ III	0
4	Complex IV	$\text{Ni}/\text{Al}_2\text{O}_3$ IV	23

Reaction conditions: 0.5 mmol phenylglyoxylic acid, 3.3 mol% catalyst (theoretical: 4 wt% $M/\text{Al}_2\text{O}_3$; $M = \text{Ni, Fe, Co}$), 0.5 mL aq. NH_3 25% (6.7 mmol), 2.5 mL H_2O , 1.0 MPa, 80 °C, 20 h. GC yields of the corresponding ethyl esters using *n*-dodecane as an internal standard.

The reaction of phenylglyoxylic acid with aqueous ammonia to phenylglycine was thoroughly investigated to find applicable reaction conditions. Only nickel-based catalysts showed reductive amination activities (entry 1 and 4). However, it should be noted that even small changes in the ligand (complex **I** vs. **IV**) have an influence on the activity of the catalyst. Thus, the $\text{Ni}/\text{Al}_2\text{O}_3$ catalyst **I** based on complex **I** achieved the best yields (entry 1). However, no amount of the desired product could be yielded with the corresponding $\text{Fe}/\text{Al}_2\text{O}_3$ catalyst **II** or $\text{Co}/\text{Al}_2\text{O}_3$ catalysts **III** (entry 2,3).

The amount of ammonia had a great influence on the yield of the desired product in our previous work. We altered the amount of aqueous ammonia and found that 1.0 mL (13.4 mmol) gave the best yields (about 60%) of the desired product (see Table 6. 2).

A Nanostructured Earth-abundant Metal Catalyst Can Mediate the Efficient Synthesis of Amino Acids from Ammonia Dissolved in Water under Very Mild Conditions

Table 6. 2: Screening of the amount of ammonia.

c1ccc(cc1)C(=O)C(=O)O
 $\xrightarrow[\text{+ NH}_3, \text{+ H}_2, \text{- H}_2\text{O}]{\text{Ni/Al}_2\text{O}_3 \text{ cat. I}}$
c1ccc(cc1)C(N)C(=O)O

NH ₃ - 25% aq. [ml]	Yield [%]
0.5	56
1.0	57
2.0	8
3.0	5

Reaction conditions: 0.5 mmol phenylglycine, H₂O and 2.8 mol% Ni (24 mg Ni/Al₂O₃, 3.5 wt% Ni, 0.014 mmol Ni, 0.84 mg Ni) 1.0 MPa H₂, 85 °C, 20 h. The reaction mixture was filled up with H₂O to an absolute volume of 3.0 mL. GC yields of the corresponding ethyl esters using *n*-dodecane as an internal standard.

Table 6. 3: Screening of the solvent and the H₂ pressure.

c1ccc(cc1)C(=O)C(=O)O
 $\xrightarrow[\text{+ NH}_3, \text{+ H}_2, \text{- H}_2\text{O}]{\text{Ni/Al}_2\text{O}_3 \text{ cat. I}}$
c1ccc(cc1)C(N)C(=O)O

Solvent	H ₂ pressure [MPa]	Yield [%]
H ₂ O	1.0	57
H ₂ O	0.5	33
H ₂ O	0.5	92 ^[b]
H ₂ O	0.1	10 ^[a]
H ₂ O	0.1	19 ^[b]
EtOH	1.0	5
EtOH	0.5	3

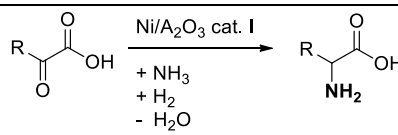
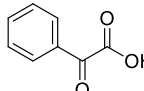
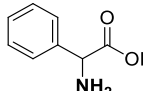
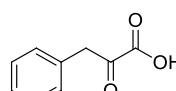
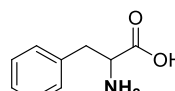
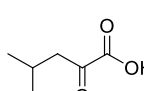
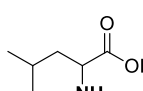
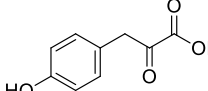
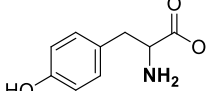
Reaction conditions: : 0.5 mmol phenylglyoxylic acid, 1.0 mL (13.36 mmol) 25% -aq. NH₃, 2.0 mL solvent, 2.9 mol% Ni (24 mg Ni/Al₂O₃, 3.5 wt% Ni, 0.014 mmol Ni, 0.84 mg Ni), 85 °C, 20 h; [a] 10 mol% Ni (84 mg Ni/Al₂O₃, 3.5 wt% Ni, 0.05 mmol Ni, 2.94 mg Ni); [b] 10 mol% Ni (84 mg Ni/Al₂O₃, 3.5 wt% Ni, 0.05 mmol Ni, 2.94 mg Ni), 48 h. GC yields of the corresponding ethyl esters using *n*-dodecane as an internal standard.

Polar solvents, such as ethanol and water, were tested for the solvent screening (see Table 6. 3). The use of water increased the yield of phenylglycine. Furthermore, the influence of water and ethanol as solvents were investigated at 1.0, 0.5 and 0.1 MPa H₂ pressure. Approximately 20 % of phenylglycine was yielded, even at 0.1 MPa H₂, with an increase of the catalyst loading (10 mol%) and of the reaction time (48 h).

A Nanostructured Earth-abundant Metal Catalyst Can Mediate the Efficient Synthesis of Amino Acids from Ammonia Dissolved in Water under Very Mild Conditions

With the optimized reaction conditions in hand (10 mol% Ni (84 mg Ni/Al₂O₃, 3.5 wt% Ni, 0.05 mmol Ni, 2.94 mg Ni), 1.0 mL (13.36 mmol) 25%-aq. NH₃, 2.0 mL H₂O, 0.5 MPa H₂, 85 °C, 48 h), we were interested in the substrate scope of our catalyst. We explored the synthesis of nonbiological, essential and nonessential amino acids via the reductive amination of the corresponding keto acids.

Table 6. 4: Substrate scope.

		
Keto acid	Amino acid	Yield [%]
Nonbiological		
		76
Essential		
		84
		73
Nonessential		
		99
		92

Reaction conditions: 0.5 mmol keto acid, 10 mol% Ni (84 mg Ni/Al₂O₃, 3.5 wt% Ni, 0.05 mmol Ni, 2.94 mg Ni), 1.0 mL (13.36 mmol) 25%-aq. NH₃, 2.0 mL H₂O, 0.5 MPa H₂, 85 °C, 48 h. Yields are of the corresponding isolated ethyl esters.

All substrates were converted to the corresponding amino acids in excellent yields. Substituents containing aromatic and aliphatic groups were tolerated.

6.3 Conclusion

In summary, we have introduced an earth-abundant metal catalyst in the reductive amination of keto acids to the corresponding amino acids. Amino acids, a subclass of primary amines, are the basic building block in proteins and played a decisive role in the origin of life. Our nanostructured nickel catalyst showed high activities in the conversion of carbonyl compounds to primary amines via reductive amination. This simple and economic synthesis could be extended and nonbiological, essential and non-

essential amino acids could be obtained in good isolated yields (0.5 MPa H₂, 85 °C). The reaction conditions applied are extremely mild and the amino acid phenylglycine could be yielded without further side products even at atmospheric H₂ pressure and 85 °C.

Acknowledgements

We thank the Deutsche Forschungsgemeinschaft for financial support (B1, SFB 840).

6.4 References

- [1] Maher, K. A. & Stevenson, D. J. Impact frustration of the origin of life. *Nature* **331**, 612 (1988).
- [2] Oparin, A. I. *The origin of life*. 2nd ed. (Dover Publications, New York, 1965).
- [3] Haldane, J. B. S. The origin of life. *Rationalist Annual*, 148–169 (1929).
- [4] Rauchfuß, H. *Chemische Evolution und der Ursprung des Lebens* (Springer, Berlin, 2005).
- [5] Wacker, A. Zur Entstehung des Lebens auf der Erde. *Angew. Chem.* **70**, 519–526 (1958).
- [6] Miller, S. L. A Production of Amino Acids Under Possible Primitive Earth Conditions. *Science*, 528–529 (1953).
- [7] Parker, E. T. *et al.* A plausible simultaneous synthesis of amino acids and simple peptides on the primordial Earth. *Angew. Chem. Int. Ed.* **53**, 8132–8136 (2014).
- [8] Harada, K. & Fox, S. W. Thermal synthesis of natural amino-acids from a postulated primitive terrestrial atmosphere. *Nature* **201**, 335–336 (1964).
- [9] Sagan, C. & Khare, B. N. Long-Wavelength Ultraviolet Photoproduction of Amino Acids on the Primitive Earth. *Science* **173**, 417–420 (1971).
- [10] Groth, W. Photochemische Bildung von Aminosäuren und anderen organischen Verbindungen aus Mischungen von H₂O, NH₃ und den eingachsten Kohlenwasserstoffen. *Angew. Chem. Int. Ed.* **69**, 681 (1957).
- [11] Groth, W. & Weysenhoff, H. Photochemische Bildung von Aminosäuren aus Mischungen einfacher Gase. *Naturwissenschaften* **44**, 510–511 (1957).
- [12] Bar-Nur, A., Bar-Nur, N., Bauer, S. H. & Sagan, C. Shock Synthesis of Amino Acids in Simulated Primitive Environments. *Science* **168**, 470–472 (1970).
- [13] Dose, K. & Rajewsky, B. Strahlenchemische Bildung von Aminen und Aminocarbonsäuren. *Biochimica et Biophysica Acta* **25**, 225–226 (1957).
- [14] Miller, S. L. & Urey, H. C. Organic compound synthesis on the primitive earth. *Science* **130**, 245–251 (1959).
- [15] Yanagawa, H. & Kobayashi, K. An experimental approach to chemical evolution in submarine hydrothermal systems. *Origin of Life and Evolution of the Biosphere* **22**, 147–159 (1992).
- [16] Oró, J., Kimball, A., Fritz, R. & Master, F. Amino acid synthesis from formaldehyde and hydroxylamine. *Archives of Biochemistry and Biophysics* **85**, 115–130 (1959)
- [17] Oró, J. & Kamat, S. S. Amino-acid Synthesis from Hydrogen Cyanide under Possible Primitive Earth Conditions. *Nature* **190**, 442–443 (1961).
- [18] Fox, S. W. Synthesis of Amino acids by the heating of formaldehyde and ammonia. *Science* **170**, 984–986 (1970).
- [19] Ferris, J. P., Wos, J. D., Ryan, T. J., Lobo, A. P. & Donner, D. B. Biomolecules from HCN. *Origin of Life* **5**, 153–157 (1974)

- [20] Danger, G., Plasson, R. & Pascal, R. Pathways for the formation and evolution of peptides in prebiotic environments. *Chem. Soc. Rev.* **41**, 5416–5429 (2012).
- [21] Kasting, J. Earth's early atmosphere. *Science* **259**, 920–926 (1993).
- [22] Aubrey, A. D., Cleaves, H. J. & Bada, J. L. The role of submarine hydrothermal systems in the synthesis of amino acids. *Origins of life and evolution of the biosphere: the journal of the International Society for the Study of the Origin of Life* **39**, 91–108 (2009).
- [23] Amend, J. P. & Shock, E. L. Energetics of amino acid synthesis in hydrothermal ecosystems. *Science* **281** (1998).
- [24] Plankensteiner, K., Reiner, H., Schranz, B. & Rode, B. M. Prebiotic formation of amino acids in a neutral atmosphere by electric discharge. *Angew. Chem. Int. Ed.* **43**, 1886–1888 (2004).
- [25] Plankensteiner, K., Reiner, H. & Rode, B. M. Amino acids on the rampant primordial Earth: electric discharges and the hot salty ocean. *Molecular diversity* **10**, 3–7 (2006).
- [26] Sojo, V., Herschy, B., Whicher, A., Camprubí, E. & Lane, N. The Origin of Life in Alkaline Hydrothermal Vents. *Astrobiology* **16**, 181–197 (2016).
- [27] Hennes, R. J.-C., Holm, N. G. & Engel, M. H. Abiotic synthesis of amino acids under hydrothermal conditions and the origin of life: A perpetual phenomenon? *Naturwissenschaften* **79**, 361–365 (1992).
- [28] Marshall, W. L. Hydrothermal synthesis of amino acids. *Geochimica et Cosmochimica Acta* **58**, 2099–2106 (1994).
- [29] Bolm, C. *et al.* Mechanochemical Activation of Iron Cyano Complexes: A Prebiotic Impact Scenario for the Synthesis of α -Amino Acid Derivatives. *Angew. Chem. Int. Ed.* **130**, 2447–2450 (2018).
- [30] Boddien, A. *et al.* Efficient Dehydrogenation of Formic Acid Using an Iron Catalyst. *Science* **333**, 1733–1736 (2011).
- [31] Tondreau, A. M. *et al.* Iron Catalysts for Selective Anti-Markovnikov Alkene Hydrosilylation Using Tertiary Silanes. *Science* **335** (2012).
- [32] Zuo, Weiwei, Lough, Alan J., Li, Y. F. & Morris, R. H. Amine(imine)diphosphine Iron Catalysts for Asymmetric Transfer Hydrogenation of Ketones and Imines. *Science* **342**, 1080–1083 (2013).
- [33] Friedfeld, M. R. *et al.* Cobalt Precursors for High-Throughput Discovery of Base Metal Asymmetric Alkene Hydrogenation Catalysts. *Science* **342**, 1076–1080 (2013).
- [34] Hoyt, J. M., Schmidt, V. A., Tondreau, A. M. & Chirik, P. J. Iron-catalyzed intermolecular [2+2] cycloadditions of unactivated alkenes. *Science* **349**, 960–963 (2015).
- [35] Korstanje, T. J., van der Vlugt, Jarl Ivar, Elsevier, C. J. & Bruin, B. de. Hydrogenation of carboxylic acids with homogeneous cobalt catalyst. *Science* **350**, 298–302 (2015).

- [36] Yu, R. P., Hesk, D., Rivera, N., Pelczer, I. & Chirik, P. J. Iron-catalysed tritiation of pharmaceuticals. *Nature* **529**, 195–199 (2016).
- [37] Friedfeld, M. R., Zhong, H., Ruck, R. T., Shevlin, M. & Chirik, P. J. Cobalt-catalyzed asymmetric hydrogenation of enamides enabled by single-electron reduction. *Science* **360**, 888–893 (2018).
- [38] Filonenko, G. A., van Putten, R., Hensen, E. J. M. & Pidko, E. A. Catalytic (de)hydrogenation promoted by non-precious metals - Co, Fe and Mn: recent advances in an emerging field. *Chem. Soc. Rev.* **47**, 1459–1483 (2018).
- [39] Kallmeier, F. & Kempe, R. Manganese Complexes for (De)Hydrogenation Catalysis: A Comparison to Cobalt and Iron Catalysts. *Angew. Chem. Int. Ed.* **57**, 46–60 (2018).
- [40] Rösler, S., Obenauf, J. & Kempe, R. A Highly Active and Easily Accessible Cobalt Catalyst for Selective Hydrogenation of C=O Bonds. *J. Am. Chem. Soc.* **137**, 7998–8001 (2015).
- [41] Rösler, S., Ertl, M., Irrgang, T. & Kempe, R. Cobalt-Catalyzed Alkylation of Aromatic Amines by Alcohols. *Angew. Chem. Int. Ed.* **54**, 15046–15050 (2015).
- [42] Deibl, N. & Kempe, R. General and Mild Cobalt-Catalyzed C-Alkylation of Unactivated Amides and Esters with Alcohols. *J. Am. Chem. Soc.* **138**, 10786–10789 (2016).
- [43] Kallmeier, F., Irrgang, T., Dietel, T. & Kempe, R. Highly Active and Selective Manganese C=O Bond Hydrogenation Catalysts: The Importance of the Multidentate Ligand, the Ancillary Ligands, and the Oxidation State. *Angew. Chem. Int. Ed.* **55**, 11806–11809 (2016).
- [44] Deibl, N. & Kempe, R. Manganese-Catalyzed Multicomponent Synthesis of Pyrimidines from Alcohols and Amidines. *Angew. Chem. Int. Ed.* **56**, 1663–1666 (2017).
- [45] Kallmeier, F., Dudzic, B., Irrgang, T. & Kempe, R. Manganese-Catalyzed Sustainable Synthesis of Pyrroles from Alcohols and Amino Alcohols. *Angew. Chem. Int. Ed.* **56**, 7261–7265 (2017).
- [46] Zhang, G., Irrgang, T., Dietel, T., Kallmeier, F. & Kempe, R. Manganese-Catalyzed Dehydrogenative Alkylation or α -Olefination of Alkyl-Substituted N-Heteroarenes with Alcohols. *Angew. Chem. Int. Ed.*, 9131–9135 (2018).
- [47] Schwob, T. & Kempe, R. A Reusable Co Catalyst for the Selective Hydrogenation of Functionalized Nitroarenes and the Direct Synthesis of Imines and Benzimidazoles from Nitroarenes and Aldehydes. *Angew. Chem. Int. Ed.* **55**, 15175–15179 (2016).
- [48] Zaheer, M. *et al.* Robust Microporous Monoliths with Integrated Catalytically Active Metal Sites Investigated by Hyperpolarized ^{129}Xe NMR. *Chem. Mater.* **24**, 3952–3963 (2012).
- [49] Zaheer, M., Hermannsdörfer, J., Kretschmer, W. P., Motz, G. & Kempe, R. Robust Heterogeneous Nickel Catalysts with Tailored Porosity for the Selective Hydrogenolysis of Aryl Ethers. *ChemCatChem* **6**, 91–95 (2014).

- [50] Hahn, G., Ewert, J.-K., Denner, C., Tilgner, D. & Kempe, R. A Reusable Mesoporous Nickel Nanocomposite Catalyst for the Selective Hydrogenation of Nitroarenes in the Presence of Sensitive Functional Groups. *ChemCatChem* **8**, 2461–2465 (2016).
- [51] Bäumlner, C. & Kempe, R. The Direct Synthesis of Imines, Benzimidazoles and Quinoxalines from Nitroarenes and Carbonyl Compounds by Selective Nitroarene Hydrogenation Employing a Reusable Iron Catalyst. *Chem. Eur. J.* **24**, 8989–8993 (2018).
- [52] Berg, J. M., Tymoczko, J. L., Stryer, L. & Gatto, G. J. *Biochemie*. 7th ed. (Springer Spektrum, Berlin, 2013).
- [53] Hahn, G., Kunas, P., Jonge, N. de & Kempe, R. General synthesis of primary amines via reductive amination employing a reusable nickel catalyst. *Nature Catalysis* **2**, 71–77 (2019).

6.5 Supporting information

6.5.1 General considerations

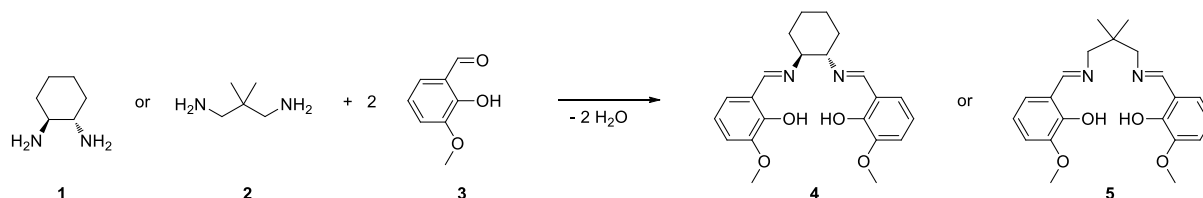
Air- and moisture sensitive reactions were carried out under dry argon or nitrogen using standard Schlenk or glove box techniques. Solvents were dried and distilled from sodium benzophenone, stored over molecular sieves (3 Å) before use or were obtained from Acros. All chemicals were purchased from commercial sources with purity over 95 % and used without further purification. γ -Al₂O₃ was purchased from Alfa Aesar and used without further purification.

NMR-Spectra were collected on Varian INOVA 300 (300 MHz for ¹H, 75 MHz for ¹³C) instruments at 298 K. Chemical shifts are reported in ppm relative to the residual solvent signal DMSO-D₆: 2.50 ppm (¹H), 39.51 ppm (¹³C)). Coupling constants (*J*) are reported in Hz (coupling patterns: d = doublet, t = triplet, q = quartet, sxt = sextet, spt = septet, m = multiplet).

GC analyses were carried out on an Agilent 6850 GC system equipped with an Optima 17 column (30 m x 0.32 mm x 0.25 μm). *N*-dodecane was used as internal standard.

GC-MS analyses were carried out on an Agilent 7890A GC system equipped with a HP-5MS column (30 m x 0.32 mm x 0.25 μm) and a 5975C inert MSD detector (EI, 70 eV).

6.5.2 Synthesis of the Metal Salen Complexes

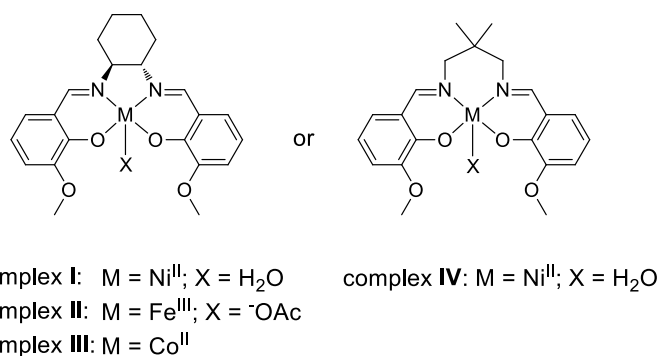


Supplementary Figure 1: Synthesis of the ligands **4** and **5**.

First, the ligands **4** and **5** were synthesized according literature.^[1] 3.04 g (20 mmol, 2 eq) *o*-vanillin (**3**) were dissolved in 50 mL ethanol and 1.32 mL (11 mmol, 1.1 eq) (±)-trans-1,2-diaminocyclohexane (**1**) were added. The solution was heated under reflux (oil bath 110 °C) for 1 h. After removal of the solvent under reduced pressure, the residue was recrystallized in methanol to yield the product as a yellow crystalline powder (3.57 g, 85 %, **4**).

Ligand **5** was synthesized with 2,2-dimethylpropane-1,3-diamine (**2**) and *o*-vanillin (**3**) in an analogous way.^[1]

For the synthesis of the Ni salen complex **I**, the ligand **4** (2.32 g, 6.0 mmol, 1 eq) was dissolved in 40 mL methanol and a methanolic solution of 1.49 g Ni(OAc)₂·4H₂O (6.0 mmol, 1 eq) in 40 mL MeOH was added. An orange-brown precipitate was formed during stirring for 2 h at room temperature, which was separated by filtration.^[2]

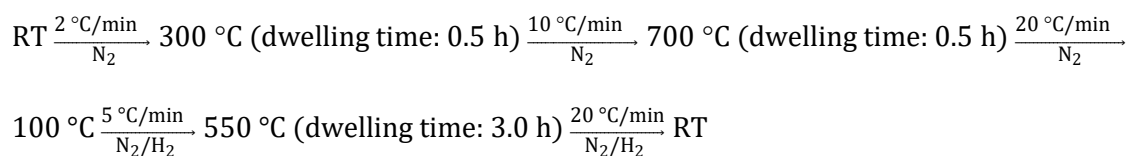


Supplementary Figure 2: Molecular structures of the complexes I–IV.

Complex II–IV were synthesized in an analogous way using Fe(OAc)₂^[3], Co(OAc)₂·4H₂O^[4] or ligand 5^[1], respectively.

6.5.3 Synthesis of the catalysts

The M/Al₂O₃ catalysts with M = Fe, Co, Ni are synthesized with 4 wt% metal supported on γ-Al₂O₃. Therefore, 81 mg (0.18 mmol) Ni complex I, 87 mg (0.18 mmol) Fe complex II, 82 mg (0.17 mmol) Co complex III or 70 mg (0.16 mmol) Ni complex IV were dissolved in 3 mL acetonitrile and 250 mg γ-Al₂O₃ were suspended. After evaporation of the solvent at 110 °C, the impregnated sample was pyrolyzed under N₂ and finally reduced by a N₂/H₂ mixture with the following program:

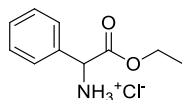


6.5.4 Reductive amination of keto acids – general procedure

A 5-mL reaction vial was charged with a magnetic stirring bar, 0.5 mmol keto acid, 1.0 mL 25% aqueous NH₃ (6.7 mmol), 2 mL H₂O and 84 mg Ni/Al₂O₃ catalyst (3.5 wt% Ni, 2.94 mg Ni, 0.05 mmol Ni, 10 mol% Ni). The vial was placed in a 250 mL high-pressure autoclave (Parr Instruments) which was flushed three times with 2 MPa hydrogen. After pressurizing the autoclave with the desired pressure of typically 0.5 MPa, the reaction was stirred for 48 h at 85 °C. The autoclave was cooled to room temperature and the hydrogen was released. The catalyst was removed by centrifugation and the aqueous layer was filtrated. The solvent was removed under reduced pressure and the product was converted to the corresponding ethyl esters. Therefore, the dry residue was dissolved in ethanol and thionyl chloride (1.5 mmol, 109 μL) was added dropwise at 0 °C. After stirring for 10 min the solution was heated under reflux for 2 h. Removing of the solvent under reduced pressure yielded the ethyl esters of the products, which were analyzed by GC with *n*-dodecane as the internal standard or by NMR.

6.5.5 Characterization of the amino acids

2-ethoxy-2-oxo-1-phenylethanaminium chloride



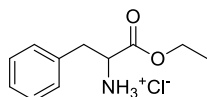
FW (C₆H₁₄ClN) = 215.68 g mol⁻¹

¹H NMR (300 MHz, DMSO-D₆): δ = 9.26 (s, 3 H), 7.43–7.55 (m, 5 H), 5.18 (s, 1 H), 4.08–4.25 (m, 2 H), 1.12 (t, *J* = 7.03 Hz, 3 H) ppm.

¹³C NMR (75 MHz, DMSO-D₆): δ = 168.27, 132.68, 129.44, 128.92, 128.28, 62.03, 55.36, 13.85 ppm.

Yield: 76% (0.38 mmol, 82 mg).

1-ethoxy-1-oxo-3-phenylpropan-2-aminium chloride



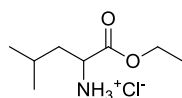
FW (C₁₁H₁₅ClNO₂) = 229.70 g mol⁻¹

¹H NMR (300 MHz, DMSO-D₆): δ = 8.86 (s, 3 H), 7.24–7.34 (m, 5 H), 4.14–4.18 (m, 1 H), 4.03–4.09 (m, 2 H), 3.24–3.30 (m, 1 H), 3.03–3.11 (m, 1 H), 1.05 (t, *J* = 7.03 Hz, 3 H) ppm.

¹³C NMR (75 MHz, DMSO-D₆): δ = 168.90, 134.86, 129.46, 128.51, 127.18, 61.50, 53.24, 35.94, 13.77 ppm.

Yield: 84 % (0.42 mmol, 96 mg).

1-ethoxy-4-methyl-1-oxopentan-2-aminium chloride



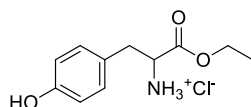
FW (C₈H₁₈ClNO₂) = 195.69 g mol⁻¹

¹H NMR (300 MHz, DMSO-D₆): δ = 8.75 (s, 3 H), 4.14–4.22 (m, 2 H), 3.85 (t, *J* = 7.03 Hz, 1 H), 1.62–1.82 (m, 3 H), 1.22 (t, *J* = 7.03 Hz), 0.88 (d, *J* = 5.86 Hz, 6 H) ppm.

¹³C NMR (75 MHz, DMSO-D₆): δ = 168.79, 61.60, 50.48, 23.75, 22.22, 21.96, 13.94 ppm.

Yield: 99 % (0.49 mmol, 67 mg).

1-ethoxy-3-(4-hydroxyphenyl)-1-oxopropan-2-aminium chloride



FW (C₁₁H₁₆ClNO₃) = 245.70 g mol⁻¹

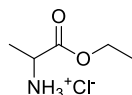
A Nanostructured Earth-abundant Metal Catalyst Can Mediate the Efficient Synthesis of Amino Acids from Ammonia Dissolved in Water under Very Mild Conditions

¹H NMR (300 MHz, DMSO-D₆): δ = 9.53 (s, 1 H), 8.71 (s, 3 H), 7.01 (d, *J* = 8.2 Hz, 2 H), 6.73 (d, *J* = 8.8 Hz, 2 H), 4.10 (m, 3 H), 2.95–3.14 (m, 2 H), 1.10 (t, *J* = 7.02 Hz, 3 H) ppm.

¹³C NMR (75 MHz, DMSO-D₆): δ = 169.47, 157.20, 130.88, 124.87, 115.82, 61.98, 53.94, 35.63, 14.31 ppm.

Yield: 99 % (0.49 mmol, 67 mg).

1-ethoxy-1-oxopropan-2-aminium chloride



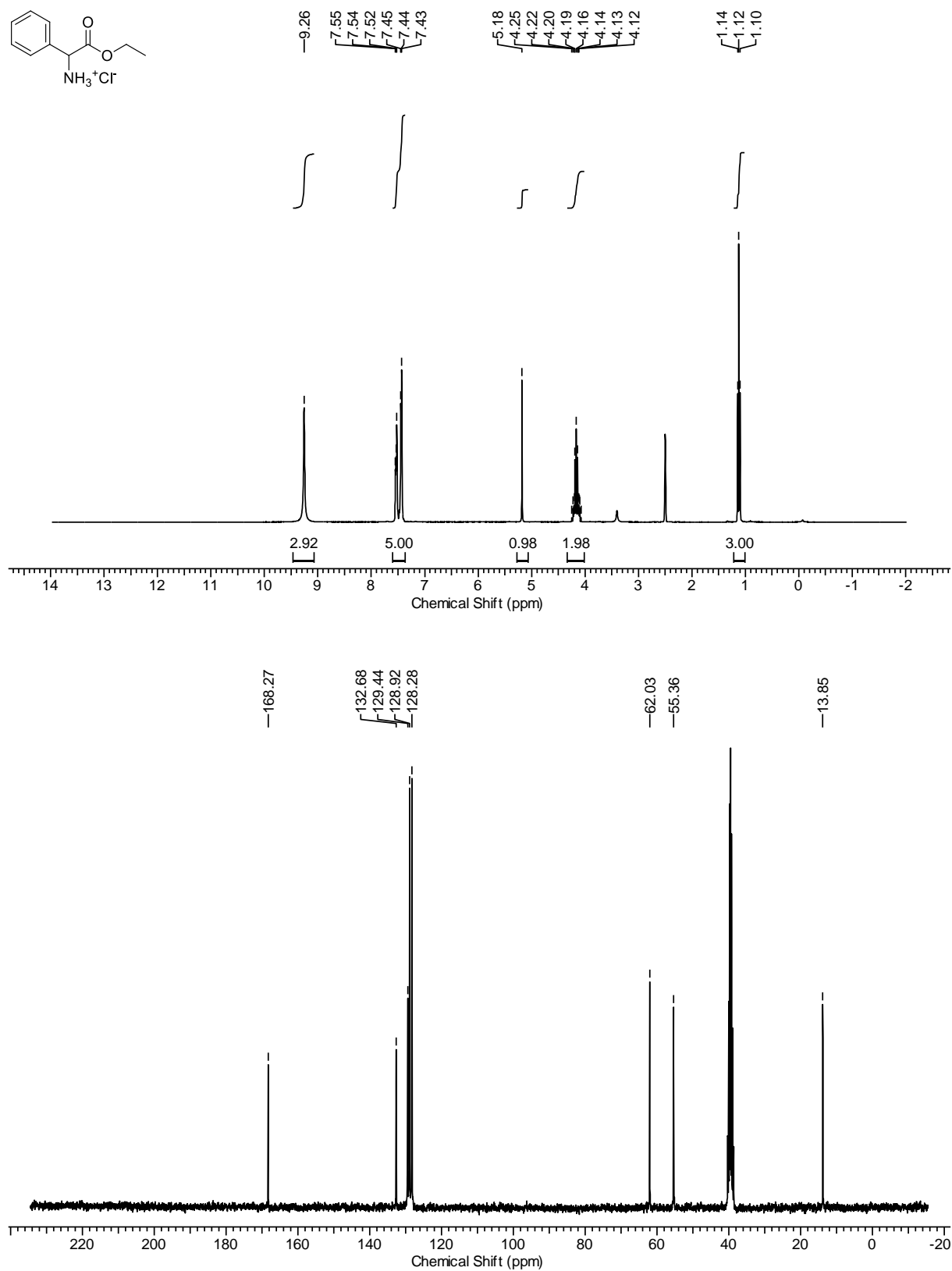
FW (C₅H₁₂ClNO₂) = 153.61 g mol⁻¹

¹H NMR (300 MHz, DMSO-D₆): δ = 8.71 (s, 3 H), 4.13–4.20 (m, 2 H), 4.00 (q, *J* = 7.03 Hz, 1 H), 1.41 (d, *J* = 7.61 Hz, 3 H), 1.20 (t, *J* = 7.03 Hz, 3 H) ppm.

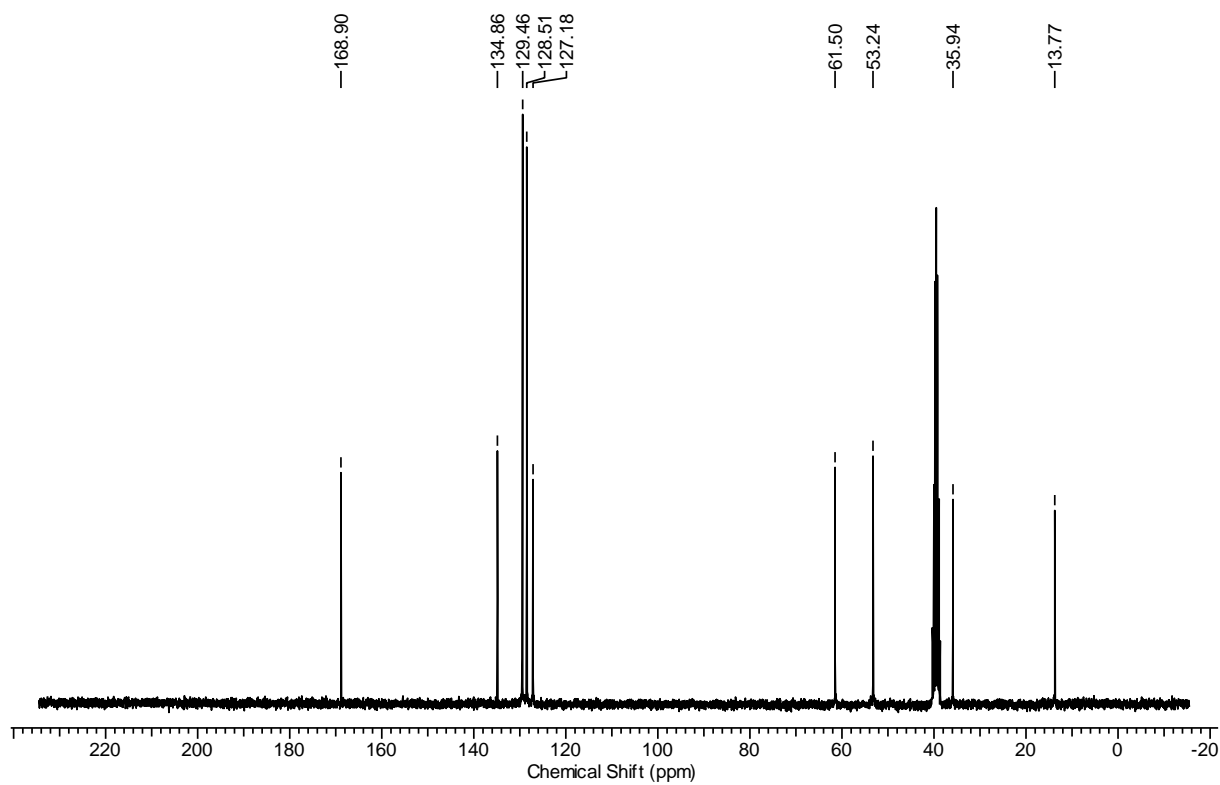
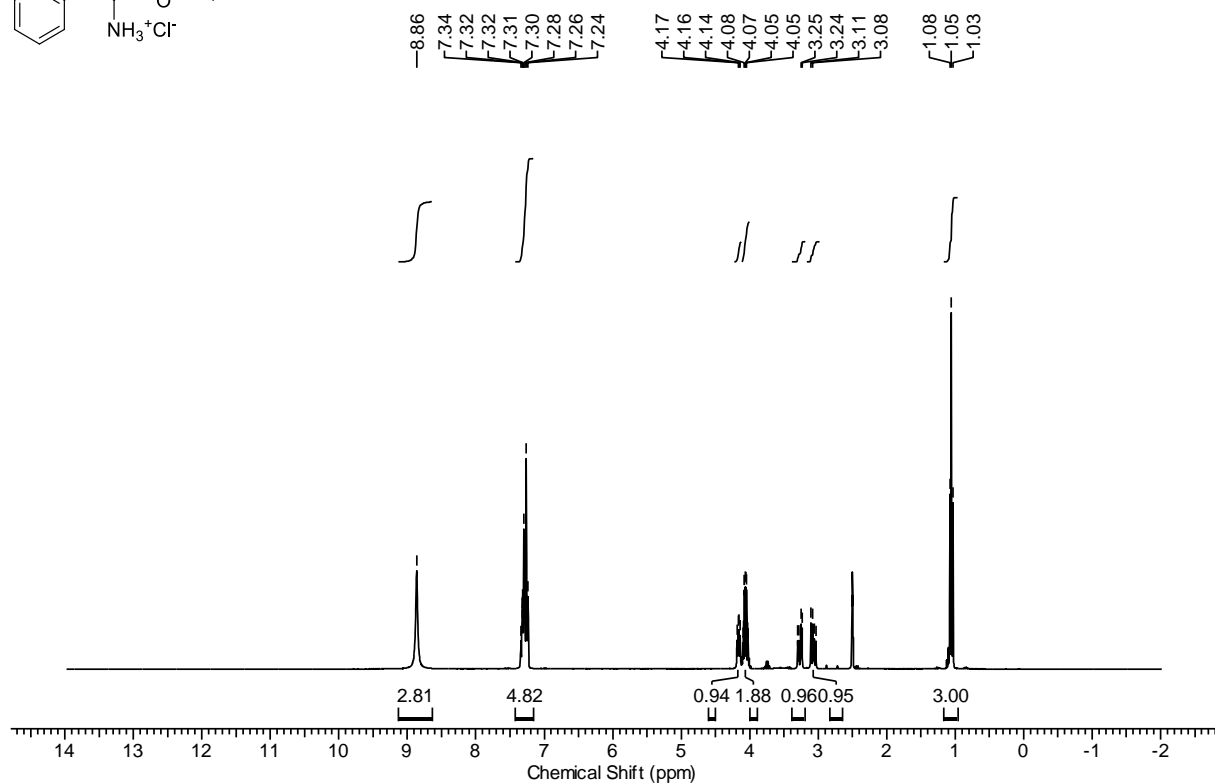
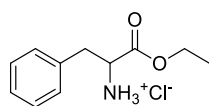
¹³C NMR (75 MHz, DMSO-D₆): δ = 169.94, 61.67, 47.84, 15.71, 13.98 ppm.

Yield: 99 % (0.49 mmol, 67 mg).

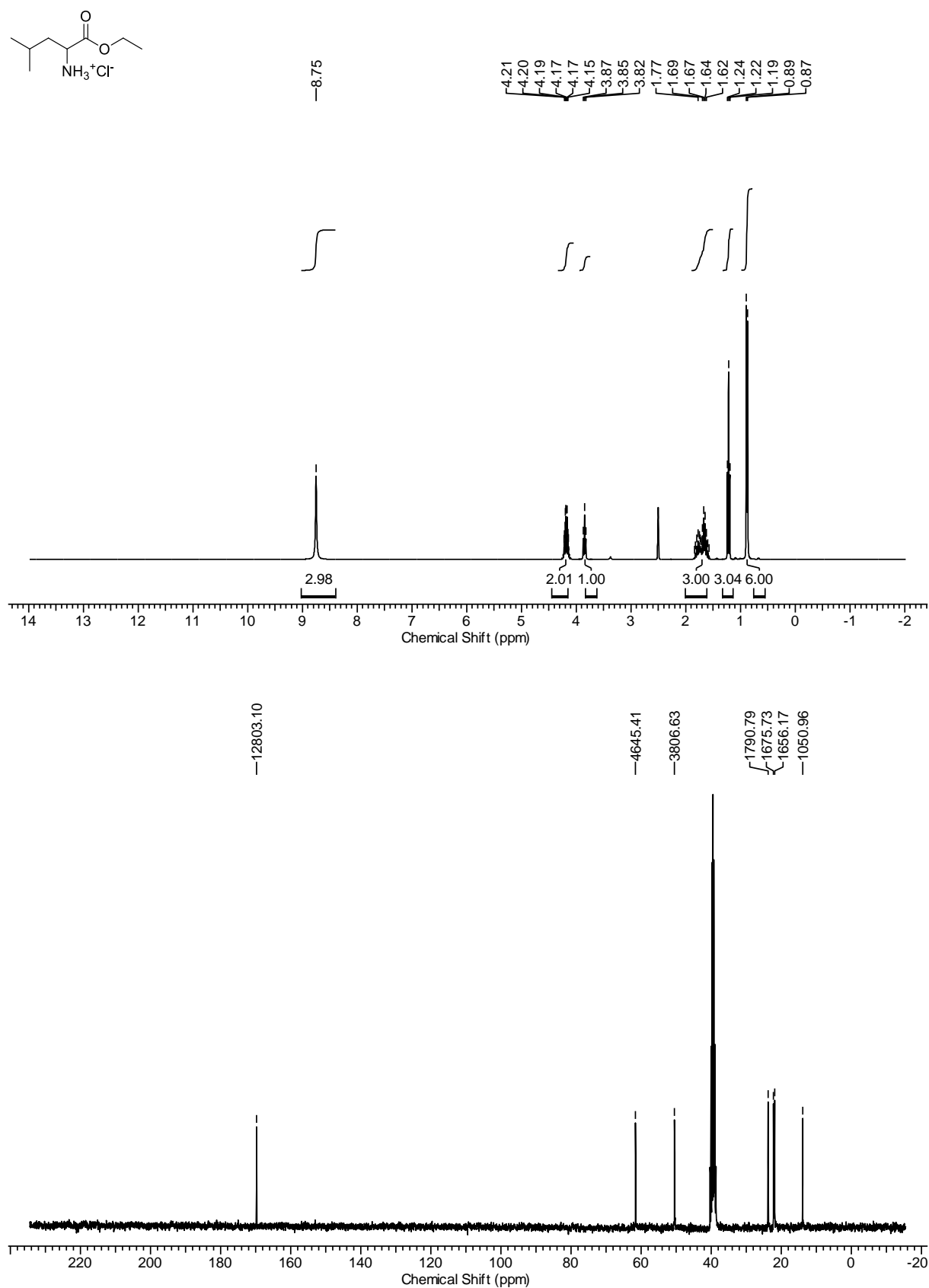
6.5.6 NMR Spectra



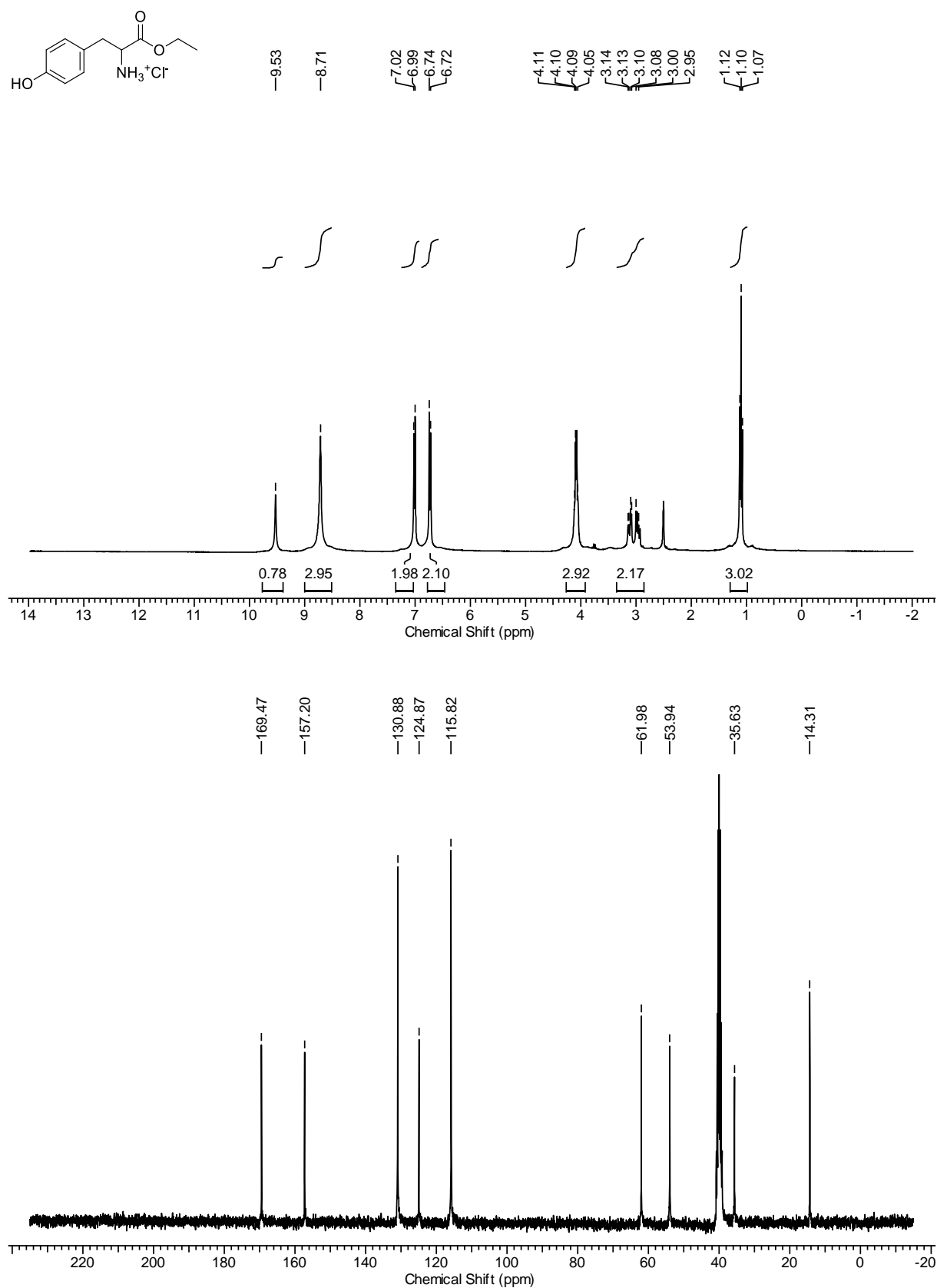
A Nanostructured Earth-abundant Metal Catalyst Can Mediate the Efficient Synthesis of Amino Acids from Ammonia Dissolved in Water under Very Mild Conditions



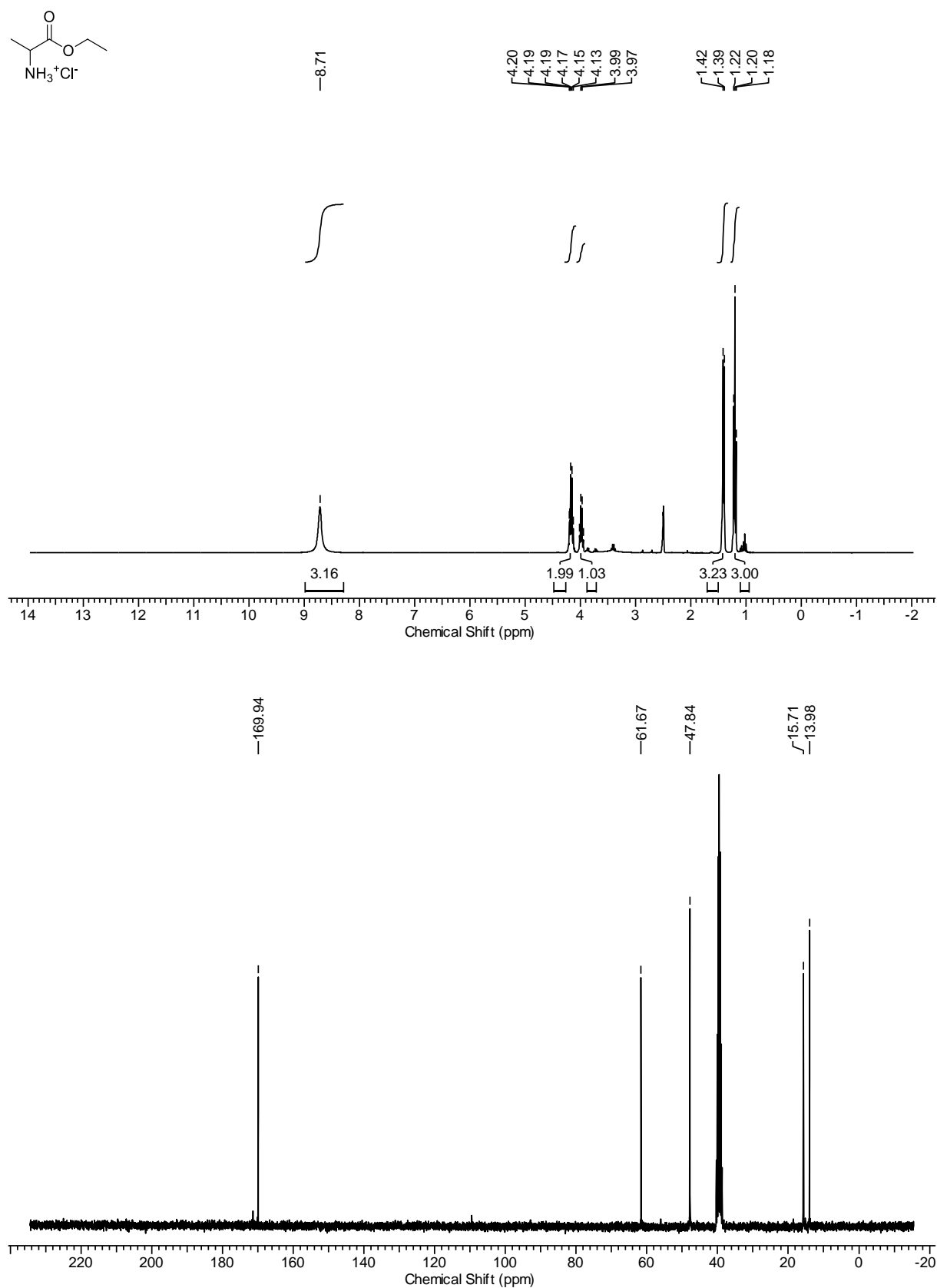
A Nanostructured Earth-abundant Metal Catalyst Can Mediate the Efficient Synthesis of Amino Acids from Ammonia Dissolved in Water under Very Mild Conditions



A Nanostructured Earth-abundant Metal Catalyst Can Mediate the Efficient Synthesis of Amino Acids from Ammonia Dissolved in Water under Very Mild Conditions



A Nanostructured Earth-abundant Metal Catalyst Can Mediate the Efficient Synthesis of Amino Acids from Ammonia Dissolved in Water under Very Mild Conditions



6.5.7 Supplementary References

- [1] Costes, J.-P. *et al.* Di- or Trinuclear 3d-4f Schiff Base Complexes. The Role of Anions. *Eur. J. Inorg. Chem.* **2008**, 5235–5244 (2008)
- [2] Wen, H.-R. *et al.* A family of nickel–lanthanide heterometallic dinuclear complexes derived from a chiral Schiff-base ligand exhibiting single-molecule magnet behaviors. *Inorg. Chim. Acta* **435**, 274–282 (2015).
- [3] Chapman, M. R., Henkelis, S. E., Kapur, N., Nguyen, B. N. & Willans, C. E. A Straightforward Electrochemical Approach to Imine- and Amine-bisphenolate Metal Complexes with Facile Control Over Metal Oxidation State. *ChemistryOpen* **5**, 351–356 (2016).
- [4] Morandi, B., Mariampillai, B. & Carreira, E. M. Enantioselective cobalt-catalyzed preparation of trifluoromethyl-substituted cyclopropanes. *Angew. Chem. Int. Ed.* **50**, 1101–1104 (2011).

7 List of Publications

The following publications were published or are to be submitted during the work on this thesis:

1. G. Hahn, J.-K. Ewert, C. Denner, D. Tilgner, R. Kempe *ChemCatChem* **2016**, 8, 2461–2465.
“A Reusable Mesoporous Nickel Nanocomposite Catalyst for the Selective Hydrogenation of Nitroarenes in the Presence of Sensitive Functional Groups”
2. G. Hahn, P. Kunnas, N. de Jonge, R. Kempe *Nature Catalysis* **2019**, 2, 71–77.
“General synthesis of primary amines via reductive amination employing a reusable nickel catalyst”
3. G. Hahn, E. Herzog, R. Kempe to be submitted.
“A Nanostructured Earth-Abundant Metal Catalyst Can Mediate the Efficient Synthesis of Amino Acids from Ammonia Dissolved in Water under Very Mild Conditions”

8 Acknowledgements/Danksagung

Acknowledgements

My very special thanks go to my academic teacher

Prof. Dr. Rhett Kempe,

for giving me the opportunity to research this very interesting topic under excellent conditions. Furthermore, I would like to thank him for his confidence, which enabled me to work under great scientific freedom, as well as for the many constructive scientific discussions.

I would like to thank Dr. Christine Denner for the excellent support of our “ceramics group”, the REM measurements and the motivating, friendly and professional support.

My big thank you goes to my lab-mates who accompanied me (partially) during my doctorate. Daniel, Sonja, Stefan, Tobias, Christoph, Mirco, Christina, Leah, Timon, Simon, Caro, Anna-Lena, Babsi, Elena, Christoph and Mirco, you have contributed not only through your willingness to discuss, but also through your friendly behavior to a great time in the laboratory with a unique working atmosphere. Furthermore, I would like to thank my colleagues Mara Klarner, Fabian Kallmeier, Robin Fertig, Frederik Freitag, Martin Schlagbauer, Andreas Gollwitzer, Alexander Goller, Patrick Wolff, Dr. Torsten Irrgang, Dr. Winfried Kretschmer, and my former colleagues Dr. Awal Noor, Dr. Dominic Tilgner, Dr. Martin Friedrich, Dr. Nicklas Deibl, Dr. Toni Hille, Dr. Sina Rösler, Thomas Dietel and especially Dr. Julia Ewert for the great time they spent with me.

Many thanks to Heidi Maisel, Sandra Kellner, Christine Fell, Anna-Maria Dietel and Marlies Schilling for their constant helpfulness in administrative things and their supporting work in the laboratory.

Furthermore, I would like to thank my students Timon Schönauer, Leah Kaiser, Carolin Wirth, Elena Herzog, Lisa Schmutzler, Phil Richter and Lisa Leitner for their hands-on support in everyday laboratory work during various internships, thesis work or HiWi time.

I am grateful for the great cooperation with Prof. Dr. Niels de Jonge and Peter Kunnas. Many thanks for the scientific discussions and the extensive help regarding the electron microscopic material characterization.

I would like to thank Dr. Dominic Tilgner and Dr. Martin Friedrich for the TEM measurements and the patient instruction on the instrument. My thanks also go to Martin Rieß and Florian Puchtler (AC I) for

the PXRD analyses, Dr. Ulrike Lacher (OC I) for the HRMS measurements, Dr. Johannes Thiessen (LCVT) for the NH₃-TPD measurements, Birgit Brunner (LCVT) for the ICP-OES measurements, Dr. Jürgen Seidel (TU Bergakademie Freiberg, Institute of Physical Chemistry) for the XPS analyses and Katja Dankhoff and Christoph Göbel for their introduction to SQUID.

I would like to thank the Graduate School (University of Bayreuth) for the financial support during the conference *EuropaCat 2017* in Florence and various further education courses. I would like to thank the research group SFB 840 for providing funds for research purposes.

Special thanks also go to my academic colleagues, who have become friends over the years. Many thanks to Julia Wollmann, Bernadette Maier, Christoph Göbel and Katja Dankhoff for the interdisciplinary and inspiring coffee breaks, which made the academic years much lighter.

Finally, I would like to thank my family, particularly my dad Lutz and my husband Daniel, for their unrestricted and unconditional support, ongoing motivation and love over the last few years.

Danksagung

Mein ganz besonderer Dank gilt meinem akademischen Lehrer

Prof. Dr. Rhett Kempe,

der mir die Möglichkeit gab, unter ausgezeichneten Arbeitsbedingungen auf diesem sehr interessanten Thema zu forschen. Des Weiteren bedanke ich mich für sein Vertrauen, das mir ermöglichte unter größter wissenschaftlicher Freiheit zu arbeiten, sowie für die Vielzahl an konstruktiven, wissenschaftlichen Diskussionen.

Für die ausgezeichnete Betreuung unserer „Keramik Gruppe“, die REM Messungen sowie die motivierende, freundliche und fachliche Unterstützung möchte ich mich recht herzlich bei Dr. Christine Denner bedanken.

Mein großer Dank gilt auch meinen Laborkollegen, die mich (abschnittsweise) während meiner Promotionszeit begleitet haben. Daniel, Sonja, Stefan, Tobias, Christoph, Mirco, Christina, Leah, Timon, Simon, Caro, Anna-Lena, Babsi, Elena, Christoph und Mirco, ihr habt mir nicht nur durch eure Diskussionsbereitschaft, sondern vielmehr durch euer freundschaftliches Verhalten eine großartige Zeit im Labor mit einer einzigartigen Arbeitsatmosphäre geschaffen. Des Weiteren möchte ich mich bei meinen Kollegen Mara Klarner, Fabian Kallmeier, Robin Fertig, Frederik Freitag, Martin Schlagbauer, Andreas Gollwitzer, Alexander Goller, Patrick Wolff, Dr. Torsten Irrgang, Dr. Winfried Kretschmer, sowie meinen ehemaligen Kollegen Dr. Awal Noor, Dr. Dominic Tilgner, Dr. Martin Friedrich, Dr. Nicklas Deibl, Dr. Toni Hille, Dr. Sina Rösler, Thomas Dietel und besonders Dr. Julia Ewert für die tolle Zeit bedanken.

Ein großer Dank gilt Heidi Maisel, Sandra Kellner, Christine Fell, Anna-Maria Dietel und Marlies Schilling für ihre stetige Hilfsbereitschaft in administrativen Angelegenheiten sowie ihre unterstützenden Arbeiten im Labor.

Weiterhin möchte ich mich auch bei meinen Studenten Timon Schönauer, Leah Kaiser, Anna-Lena Engelhardt, Carolin Wirth, Elena Herzog, Lisa Schmutzler, Phil Richter und Lisa Leitner für ihre tatkräftige Unterstützung im Laboralltag während diverser Praktika, Abschlussarbeiten oder HiWi-Stunden bedanken.

Ich bin dankbar für die großartige Kooperation mit Prof. Dr. Niels de Jonge und Peter Kunnas. Vielen Dank für die vielen wissenschaftlichen Diskussionen und die umfangreiche Hilfe bei der elektronenmikroskopischen Materialcharakterisierung.

Für die TEM Aufnahmen und die geduldige Einweisung am Gerät möchte ich mich bei Dr. Dominic Tilgner sowie Dr. Martin Friedrich bedanken. Zudem gilt mein Dank für PXRD Analysen Martin Rieß und Florian Puchtler (AC I), für HRMS Messungen Dr. Ulrike Lacher (OC I), für NH₃-TPD Messungen Dr. Johannes Thiessen (LCVT), für ICP-OES Messungen Birgit Brunner (LCVT), für XPS Analysen Dr. Jürgen Seidel (TU Bergakademie Freiberg, Institut für Physikalische Chemie) sowie Katja Dankhoff und Christoph Göbel für die Einweisung am SQUID.

Für die finanzielle Unterstützung zur Konferenz *EuropaCat 2017* in Florenz und diversen Fortbildungen möchte ich mich bei der Graduate School Uni Bayreuth bedanken. Beim Sonderforschungsbereich SFB 840 möchte ich mich für die Bereitstellung von Geldern für Forschungszwecke bedanken.

Ganz besonderer Dank gilt auch meinen Studienkollegen, die im Laufe der Zeit vielmehr zu Freunden geworden sind. Vielen Dank an Julia Wollmann, Bernadette Maier, Christoph Göbel und Katja Dankhoff für die interdisziplinären und inspirierenden Kaffeepausen, ohne die, die Jahre an der Uni, deutlich trister gewesen wären.

Abschließend möchte ich mich bei meiner Familie, im Besonderen bei meinem Papa Lutz und meinem Ehemann Daniel, für die uneingeschränkte und bedingungslose Unterstützung, die andauernde Motivation und die Liebe während der letzten Jahre bedanken.

9 Declaration/Erklärung

(Eidesstattliche) Versicherungen und Erklärungen

(§ 8 Satz 2 Nr. 3 PromO Fakultät)

Hiermit versichere ich eidesstattlich, dass ich die Arbeit selbstständig verfasst und keine anderen als die von mir angegebenen Quellen und Hilfsmittel benutzt habe (vgl. Art. 64 Abs. 1 Satz 6 BayHSchG).

(§ 8 Satz 2 Nr. 3 PromO Fakultät)

Hiermit erkläre ich, dass ich die Dissertation nicht bereits zur Erlangung eines akademischen Grades eingereicht habe und dass ich nicht bereits diese oder eine gleichartige Doktorprüfung endgültig nicht bestanden habe.

(§ 8 Satz 2 Nr. 4 PromO Fakultät)

Hiermit erkläre ich, dass ich Hilfe von gewerblichen Promotionsberatern bzw. –vermittlern oder ähnlichen Dienstleistern weder bisher in Anspruch genommen habe noch künftig in Anspruch nehmen werde.

(§ 8 Satz 2 Nr. 7 PromO Fakultät)

Hiermit erkläre ich mein Einverständnis, dass die elektronische Fassung der Dissertation unter Wahrung meiner Urheberrechte und des Datenschutzes einer gesonderten Überprüfung unterzogen werden kann.

(§ 8 Satz 2 Nr. 8 PromO Fakultät)

Hiermit erkläre ich mein Einverständnis, dass bei Verdacht wissenschaftlichen Fehlverhaltens Ermittlungen durch universitätsinterne Organe der wissenschaftlichen Selbstkontrolle stattfinden können.

Ort, Datum, Unterschrift